



SAARLAND UNIVERSITY

Optimization of
Dielectric Elastomer Actuators:
Advanced Manufacturing, Electrical Failure
Analysis, and Innovative Repair Method

Dissertation

zur Erlangung des Grades der
Doktorin der Ingenieurwissenschaften
der Naturwissenschaftlich – Technischen Fakultät
der Universität des Saarlandes

von

Bettina Fasolt

Saarbrücken

2025

Tag des Kolloquiums: 28.11.2025

Dekan: Prof. Dr.-Ing. Dirk Bähre

Berichterstatte:r: Prof. Dr. Andreas Schütze
Prof. Dr. Herbert Shea

Vorsitz: Prof. Dr.-Ing. Dirk Bähre

Akad. MitarbeiterIn: Dr.-Ing. Niklas König

Danksagung

Diese Arbeit wäre ohne die Anregung und Ermutigung meines Betreuers Prof. Stefan Seelecke nicht zustande gekommen. Nach vielen Jahren als wissenschaftliche Mitarbeiterin in seiner Arbeitsgruppe hat er mich ermutigt, doch noch eine Promotion in Angriff zu nehmen, und mich mit zahlreichen wissenschaftlichen Diskussionen begleitet und mich für das Thema begeistert. Dafür gilt ihm mein herzlicher Dank. Seinen drei W's – Was? Warum? Wie? – verdanke ich, dass aus dieser Dissertation kein tausendseitiges Werk geworden ist.

Ebenso danke ich der gesamten iMSL-Arbeitsgruppe, die mir stets mit Rat und Tat zur Seite gestanden hat und auch noch steht - sei es durch wissenschaftliche Diskussionen, Unterstützung bei elektronischen Herausforderungen, 3D-Druck, Programmierung oder bei freundschaftlichem Austausch in der Küche. Ich habe mich in der Gruppe immer sehr gut aufgehoben gefühlt. Ohne diese großartige Hilfe wären viele Untersuchungen nicht möglich gewesen. Besonders danken möchte ich dabei Tobias Willian, Daniel Bruch, Tobias Weber, Christian Müller, Johannes Feld, Julian Taffner, Felix Welsch, Ilja Naumov, Julian Kunze und Sebastian Becker.

Mein Dank gilt auch Prof. Andreas Schütze, der sich freundlicherweise bereit erklärt hat, diese Arbeit als Erstprüfer zu begleiten. Ich weiß die Zeit, die er für die Durchsicht aufgewendet hat, ebenso zu schätzen wie seine wertvollen Anmerkungen. Ebenso danke ich Prof. Herbert Shea, der sich bereit erklärt hat, das Zweitgutachten zu übernehmen.

Ganz besonderer Dank geht an meinen lieben Ehemann, der mich durch die Höhen und Tiefen dieser Arbeit begleitet und mir mit aufmunternden Worten - oder auch Gummibärchen - zur Seite gestanden hat.

Diese Danksagung wäre unvollständig, ohne auch meine Eltern zu erwähnen, die mich in all meinen Vorhaben unterstützt haben. Es schmerzt sehr, dass mein Vater die Fertigstellung dieser Arbeit nicht mehr erleben konnte.

Übersicht

Dielektrische Elastomere (DE) wurden in den letzten zwanzig Jahren als vielversprechende Technologie für neuartige Aktorsysteme identifiziert, die konventionelle elektromagnetische und hydraulische Technologien ersetzen könnten. Ihre hohe Energieeffizienz, integrierte Sensorsignale und das Potenzial für „Soft Robotics“ wurden bereits in diversen Forschungsprojekten demonstriert. Für den Schritt vom Labormaßstab zur industriellen Anwendung werden skalierbare, wirtschaftliche Herstellungsverfahren und eine optimierte Betriebszuverlässigkeit erforderlich.

Diese Dissertation präsentiert erstmals eine systematische Untersuchung des Siebdrucks zur Applikation von Elektroden auf Silikon-Dünnschichten und charakterisiert das Verfahren im Hinblick auf relevante elektro-mechanische Leistungskennwerte. Darauf aufbauend wird das elektrische Durchschlagverhalten unter Variation von Temperatur, Luftfeuchtigkeit und Vordehnung analysiert, um die Betriebsgrenzen aktuell verwendeter Silikon-Dünnschichten zu bestimmen. Der dabei erkannte starke Einfluss der Elektroden führte zu einer erweiterten Studie verschiedener Elektrodenmaterialien und Herstellungsverfahren. Alle drei Themenbereiche führten zu wissenschaftlich begutachteten Publikationen, die in kumulativer Form in diese Dissertation eingebunden sind.

Ergänzend stellt die Arbeit eine patentangemeldete Test- und Reparaturmethode vor, die die Fertigung zuverlässiger DE ermöglicht und die Einsatzgrenzen künftiger Aktorsysteme deutlich erweitert.

Abstract

Over the past twenty years, dielectric elastomers (DE) have been identified as a highly promising concept for next-generation actuators that could replace conventional electro-magnetic, pneumatic, and hydraulic systems. Their self-sensing capability, high energy efficiency, and suitability for soft robotics make them particularly attractive. To advance from lab-scale demonstrators toward industrial applications, cost-efficient and scalable manufacturing methods and improved reliability are essential.

This thesis presents the first systematic investigation of screen printing parameters for applying electrodes to silicone thin films, aiming to characterize and optimize an industry-grade process with respect to key electro-mechanical performance. It further provides a detailed study of electrical breakdown to determine operational limits of currently used silicone thin films, focusing on the influence of temperature, humidity, and pre-stretch. The analyses revealed a significant effect of electrode materials on breakdown strength, motivating an additional comparative study of various electrodes reported in literature. All three subjects resulted in peer-reviewed journal publications integrated into this thesis in a cumulative way.

A fourth, patent-pending contribution introduces a novel test and repair method for DEs during fabrication, enabling reliable operation at a defined voltage and significantly improving breakdown behavior and operability of next-generation DE actuators.

Table of contents

Danksagung	i
Übersicht	ii
Abstract	iii
Table of contents	iv
1. Introduction	1
2. Fundamentals of dielectric elastomer transducers (DET)	5
2.1 Basic structure and working principle of DET	5
2.1.1 Dielectric elastomer sensors.....	7
2.1.2 Dielectric elastomer actuators	8
2.1.3 Dielectric elastomer generators	11
2.2 DET materials	14
2.2.1 Dielectric elastomer film materials.....	14
2.2.2 Electrode materials for dielectric elastomers	16
2.3 Breakdown mechanism of silicone DET	17
2.3.1 Molecular structure and resulting macroscopic characteristics of PDMS.....	17
2.3.2 Mechanisms of electrical breakdown in PDMS	18
2.4 Experimental characterization of DET	21
2.4.1 Test setup for experimental characterization of DET	21
2.4.2 Relevant material parameter for sensor applications.....	24
2.4.3 Relevant material parameters for actuator applications	26
2.4.4 Relevant material parameters for generator applications.....	29
3. State of the Art	31
3.1 Manufacturing methods for electrodes.....	31
3.1.1 Screen-printing	31
3.1.2 Spraying DET	33
3.1.3 Inkjet printing	34
3.1.4 Pad printing	34
3.1.5 Sputter process.....	35
3.2 Breakdown test methods.....	36
3.2.1 Electrical breakdown strength tester, The Danish Polymer Center	36
3.2.2 Dielectric breakdown test stand, TU Darmstadt, I	37
3.2.3 Electrical breakdown strength tester, TU Darmstadt, II.....	37
3.2.4 Electrical breakdown strength tester, TU Darmstadt, III.....	38
3.2.5 Electrical breakdown strength tester, <i>EPFL</i>	39
4. Cumulative Part: Advanced manufacturing method and electrical failure analysis	41
4.1 Effect of screen printing parameters on sensor and actuator performance of dielectric elastomer (DE) membranes	43

4.2	Dielectric breakdown test setup for dielectric elastomers: Design and validation.....	55
4.3	Effect of actuation parameters and environment on the breakdown voltage of silicone dielectric elastomer films	67
4.4	Electrode impact on the electrical breakdown of dielectric elastomer thin films	78
5.	Innovative DEA repair method.....	99
5.1	Breakdown box and test procedure	103
5.2	Repair process.....	106
5.3	Impact of repair patch on DEA performance.....	110
5.3.1	Sample design and test procedure.....	111
5.3.2	Experimental results for actuation force and blocking force measurements.....	113
5.4	Impact of multiple repair patches on the performance of the DEA.....	116
5.5	Performance of patched DEA in practical applications	122
6.	Conclusion and Outlook	125
	References	128
	List of abbreviations	139
	Table of figures.....	139
	Author's publications.....	142
	Statement of contributions to the included publications.....	144

1. Introduction

Dielectric elastomers (DE) represent a promising concept for novel actuation systems, capable of replacing standard electro-magnetic, pneumatic, and hydraulic solutions in the future. They consist of thin dielectric polymer films and highly stretchable electrodes and offer numerous advantages such as high energy efficiency, intrinsic sensing properties, light weight, silent operation, high frequency range, large deformation capability, and they do not require rare earth or other critical materials. As smart material systems [1], DE can be used as dielectric elastomer sensors (DES) [2], and, when high voltage is applied, as dielectric elastomer actuators (DEA) and dielectric elastomer generators (DEG) [3], [4]. Their applications include but are not restricted to valves [5], [6] pumps [7], [8], switches [9], [10], soft robotics [11], [12], [13], [14], haptic devices [15], [16], [17], and smart wearables [18], [19], [20], [21].

The reliable operation of these devices depends crucially on their manufacturing process, such as printing methods for electrodes that must maintain good electrical conductivity even under large stretch conditions. In addition, the dielectric breakdown behavior of the thin polymer film limits the applicable voltage and hence the effectiveness of the actuation behavior. The objective of this work is to establish a fundamental understanding of the parameters influencing the reliable operation of dielectric elastomer actuators, by addressing both components, electrodes and thin films, through:

- investigation of the electrode application process with a particular focus on future mass-scalable production methods
- a comprehensive study of the breakdown behavior of typically used dielectric silicone thin films accounting for relevant environmental and operational parameters
- introduction of a novel patent-pending repair method for thin films to further optimize the operation of DEA systems

The work starts with a first systematic investigation of the effect of screen-printing parameters to characterize and optimize a mass-scalable DE manufacturing process in terms of relevant electro-mechanical performance. It then introduces a detailed study of electrical breakdown to determine the limits of operability for currently used silicon materials. The study particularly analyzed the effect of environmental temperature and humidity along with operational parameters such as necessary pre-stretch. It further discovered a non-negligible effect of electrodes on the electrical failure limit, which led to yet another detailed breakdown study taking previously published electrode types into account and also extending the previously considered temperature range.

All three subjects resulted in peer-reviewed journal publications and a peer-reviewed conference proceedings paper integrated into this thesis in a cumulative way. A fourth subject, which has not been published yet due to a submitted patent application, is added to introduce a novel DE repair process integrated into the manufacturing process. This method enables a significant increase of the DE actuation performance and increases the production output many times over by repairing and reusing failed DE. This method extends the limits of operability for next-generation dielectric elastomer actuators.

A standard DEA consists of a compliant dielectric elastomer membrane sandwiched between two stretchable electrodes. When a voltage is applied to the electrodes, electrostatic forces lead to a reduction of the membrane thickness along with a simultaneous lateral expansion, thus resulting in voltage-controlled motion.

Three main parameters are important for the fabrication of DEA:

- a dielectric elastomer with a high breakdown field and a high permittivity
- a highly compliant, conductive, patternable, thin (relative to film) and robust electrode, and
- a fabrication process, which can be standardized and scaled for future commercial mass-production

Various dielectric elastomer materials are available for DEA, exhibiting different material properties such as breakdown field and permittivity. Some examples are silicone [22, 23], natural rubber [24], acrylic materials [25 - 28], and polyurethane [29, 30]. This study focuses on silicone thin films, because they are commercially available, exhibit usability over a wide range of environmental conditions due to their high temperature stability and hydrophobicity, and because of the possibility to operate actuators in a high frequency range due to their compared to other dielectric elastomers low viscoelasticity [31].

Many different electrode materials are presented in the literature, such as metals, e.g. silver [32] and nickel [33], carbon black [34, 35, 36], carbon nanotubes [37, 38, 39], graphite nanoplates [40], and organic materials such as polyethylenedioxythiophene/polystyrene sulfonate (PEDOT/PSS) [41, 42, 43]. These materials are often embedded in solvent, grease, or a non-conductive base material such as polydimethylsiloxan (PDMS), which is the basic structural unit of silicone. In this thesis, with a focus on up-scalability to future mass production, electrodes are manufactured exclusively using a custom-made screen-printable ink containing highly conductive carbon black, solvents, and PDMS. Carbon black offers a cost-effective material for patternable, thin, robust, and compliant electrodes, which are conductive even under large elongations. The ink formulation has been continuously optimized and tailored to the specific DEA application, with particular emphasis on the use of materials that are non-hazardous to health [36]. In addition, the electrical breakdown studies include a range of carbon black electrode compositions and metal electrodes, developed in collaboration with partner laboratories.

Various fabrication methods can be used to apply electrodes onto dielectric films, ranging from brush applications [44] to techniques such as screen-printing [40, 45, 46], inkjet printing [10, 47, 48], pad printing [49, 50], spraying [51, 52, 53], blade casting [54, 55], and sputtering [56, 57]. Each method has its unique advantages and is suited to specific applications such as easy prototyping, miniaturization or patterning of large electrodes, reproducibility, or cost-effectiveness.

The screen-printing process is employed in this study, because it allows for versatile printing of multiple different patternable designs suitable for actuator applications and offers the advantage of being highly reproducible, making it ideal for both prototyping and large-scale production. Additionally, it offers the possibility to influence the properties of the electrode through the selection of screen-parameters. Among the techniques discussed, screen printing stands out for its capacity to achieve the highest material throughput, particularly in large-scale manufacturing.

The actuation performance of dielectric elastomers is determined by the material-specific relative permittivity of the DE and the electric field resulting from an applied voltage. As field-dependence is quadratic, higher voltage leads to more efficient actuation [58]. The limiting factor, however, is dielectric breakdown. This parameter can be measured in a breakdown test by increasing the applied voltage up to electrical breakdown.

Due to the importance of breakdown voltage for the design of a DEA system, it is crucial to gain a comprehensive understanding of the parameters influencing this breakdown voltage. Environmental conditions [59, 60], membrane thickness [61, 62], membrane stretch [63, 64], electrode materials [65 - 68], and the dielectric material itself [30, 69] are only a selection of possible parameters known

to influence the breakdown voltage. Various studies on the breakdown voltage of DE are available in the literature [70 - 73]. However, differences in selected test parameters, test setups, and procedures make a direct comparison of results challenging.

This thesis introduces a novel device for fully automated, reproducible testing, capable of evaluating films with or without electrodes. The device enables testing at multiple measurement points per sample within a climate chamber, ensuring reproducible results with statistical significance. Using the automated breakdown tester, a systematic study was conducted to examine the influence of environmental factors such as temperature and humidity, as well as water content, along with operational parameters like pre-stretch. The investigations revealed a significant effect of electrodes present on the electrical failure limit. While previous studies have observed the impact of different electrode materials, variations in test methods and materials make a direct comparison difficult. To address the aspect, this work systematically investigates the effects of various electrode materials and manufacturing techniques across a broad range of temperatures and humidity levels, establishing a framework for comparing results between different studies.

The results provide a comprehensive understanding of the factors influencing electrical breakdown, enabling the design of a DEA system that can operate reliably within the intended environment. By adjusting the operating parameters accordingly, the system can be optimized for stable performance under specific conditions.

Manufacturing of dielectric silicone thin films is still at an early stage, and, as a result, premature breakdown is sometimes observed in commercially available materials due to film inhomogeneities. These breakdowns are unpredictable and can pose significant challenges to reliable future DEA mass production. To overcome this difficulty, a test and repair process has been developed, ensuring the functionality of future DEA systems while simultaneously increasing material yield and reducing waste.

This thesis is structured into six chapters. Following the introduction in Chapter 1, Chapter 2 explains the functionality of DE transducers, provides a concise review of electrical breakdown mechanisms, and discusses parameters relevant to DET applications along with their corresponding test methods.

Chapter 3 outlines the state of the art relevant to this work by describing various fabrication methods for applying electrodes onto silicone films and introducing different setups for conducting electrical breakdown tests.

Chapter 4 constitutes the cumulative part of this thesis and includes three peer-reviewed journal publications and one conference paper.

The paper “Effect of screen printing parameters on sensor and actuator performance of dielectric elastomer (DE) membranes” (Sensors and Actuators A: Physical, 2017, IF: 4.1) is the first comprehensive work in which the influence of parameters such as screen dimensions, layer thickness, number of printed layers, and electrode material on the electromechanical properties of a DEA are systematically investigated.

The remaining three papers examine how various parameters impact the electrical breakdown behavior of DEA. Conference proceedings paper 2 “*Dielectric breakdown test setup for dielectric elastomers: design and validation*” (Proceedings of SPIE, 2018), presents a novel breakdown tester, which was specifically designed to conduct automated breakdown tests in a controlled environment within a climate chamber.

Paper 3 “*Effect of actuation parameters and environment on the breakdown voltage of silicone dielectric elastomer films*” (Smart Materials and Structures, 2019, IP: 3.7) and Paper 4 “*Electrode Impact on the Electrical Breakdown of Dielectric Elastomer Thin Films*” (MDPI Polymers, 2023, IP: 4.7) employ this breakdown tester for systematic studies on the influence of environmental conditions, i.e. temperature and humidity, as well as electrode material compositions, manufacturing methods, and film pre-stretch on the breakdown behavior of DEA. Paper 3 investigates silicone films differently pre-stretched with and without screen-printed electrodes at environmental conditions typically found in industrial facilities with temperatures between 10 °C and 50 °C and humidities between 10 % and 95 % relative humidity.

Paper 4 expands these studies to environmental conditions from 1 °C to 80 °C and humidities between 10 % and 90 % relative humidity and includes different electrode compositions manufactured via pad-printing, inkjet-printing, screen-printing, and sputtering.

The aim of this study is a thorough understanding of the influence of different electrodes and their manufacturing process on the silicone film and to present a framework for transferability of measurement results from different studies. It is conducted in collaboration of two other research groups.

Each publication is preceded by a short introduction and overview of the results. Additional results obtained after publication and relevant for the subject are also included.

Chapter 5 introduces a method for testing and repairing DEA during the manufacturing process, aimed at ensuring their functionality while minimizing waste due to early breakdown. This study focuses on commercially available silicone thin films, which may still have localized imperfections that limit their overall breakdown field and can lead to premature failure in DE actuators. Additionally, the breakdown field and quality of these films have been found to vary significantly, not only between different film types, but also across different production batches, making the development of such a method so important.

The chapter motivates the development of a repair process and emphasizes the significance of this method particularly for stacked actuators. A specially designed breakdown-tester along with a description of the testing procedure and the outlines of a repair process is then presented. These sections are followed by experimental studies that investigate the influence of repaired areas on the performance of DEA and establish the limits of multiple repairs. Examples are shown which demonstrate the proven effectiveness in the long-term operation of functioning actuators.

The thesis concludes in Chapter 6 with a comprehensive summary of the key findings and an outlook on potential next steps to further optimize the technology for enhanced applicability in future developments.

2. Fundamentals of dielectric elastomer transducers (DET)

Chapter 2 presents an overview of the fundamental principles of dielectric elastomer transducers. Section 2.1 introduces the basic design and the three primary working principles of DETs, sensors, actuators, and generators, along with examples of their applications and relevance to this work. Section 2.2 provides an overview of the materials used in DETs, while Section 2.3 focuses on manufacturing methods, specifically for the application of electrodes to dielectric elastomer films. Section 2.4 discusses the basic mechanisms of elastomer breakdown in silicones, laying the groundwork for the breakdown studies on silicone thin films presented in Chapter 4. The final section, Section 2.5, concludes with an overview of experimental characterization methods necessary for the design and optimization of DET systems.

2.1 Basic structure and working principle of DET

A basic DET consists of a compliant dielectric elastomer film which is coated on both sides with compliant electrodes. It can be simplistically described as a flexible capacitor.

A dielectric elastomer is an electrical insulator with no loosely bound or free charge carriers capable of moving through the material when an electric field is applied. Instead, under high voltage excitation, the charge carriers surrounding the atoms shift from their average equilibrium position, creating an inhomogeneous charge distribution that leads to dielectric polarization, as illustrated in Figure 2.1. This polarization generates a strong internal field that reduces the overall electric field within the material. At the same time, this polarization allows for higher charge storage in the capacitor, as the reduced electric field strength enables the material to accumulate more charge before electrical breakdown occurs.

The electric field applied to the elastomer membrane causes a reduction in elastomer thickness accompanied by a simultaneous expansion of the surface area in the lateral direction. This effect, known as shift polarization, is temporary—once the electric field is removed, the charge carriers return to their original positions. Shift polarization differs from orientational polarization, where permanent dipoles are present in the material.

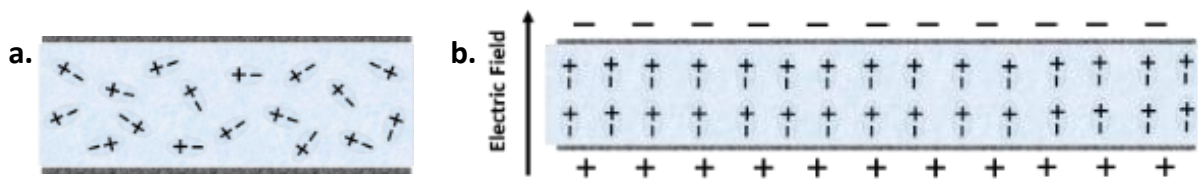


Figure 2.1. Polar molecules in dielectric elastomer without applied electric field (a.) and aligned polar molecules when electric field is applied (b.)

The near-incompressibility of polymers causes thinning to be directly associated with lateral expansion. This behavior is characterized by the Poisson's ratio, which quantifies how a material deforms laterally when stretched or compressed longitudinally. It is defined as the ratio of transverse strain (perpendicular to the applied force) to axial strain (in the direction of the applied force). A Poisson's ratio of 0.5 indicates an ideal incompressible material. Silicones and acrylic polymers, both commonly used dielectric materials in DET applications, exhibit Poisson's ratios in the range of 0.495 to 0.5 [74, 75].

The dielectric material is covered on both sides with compliant electrodes composed of an electrically conductive material, enabling uniform voltage distribution across the area to be actuated.

As early as 1876, Wilhelm Conrad Röntgen observed and described the elongation of a natural rubber band under the influence of an electric field [76]. However, it was not until the 1990s that interest in DET technology began to grow significantly, initiated by the work of Pelrine, Eckerle, and Chiba [77] on a new approach to artificial muscle actuator technology. Applications rapidly expanded to the fields of sensors and actuators, artificial muscles, soft microrobots [78, 79, 80], and energy harvesting methods [81].

Dielectric elastomer transducers are divided into three main groups, depending on their working principle:

- Dielectric elastomer sensors (DES)
- Dielectric elastomer actuators (DEA)
- Dielectric elastomer generators (DEG)

They are available in various sizes and shapes, tailored to meet the specific requirements of each application. The three primary designs are circular DE, rectangular DE, and rolled DE, see Figure 2.2.

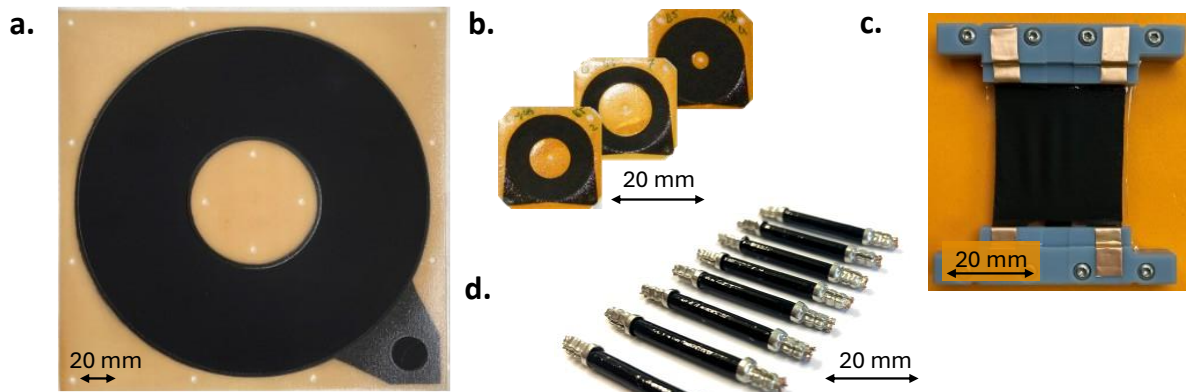


Figure 2.2. Examples of DET designs: Large circular design [82](a), small circular designs [83] (b), rectangular or strip design [84] (c), and rolled DET designs [85] (d)

Circular DET enable out-of-plane motion when pre-stretched and clamped. In addition to compact quasistatic applications such as, e.g., valve applications [83], they can also be used in systems that demand high-frequency operation, like the loudspeaker developed by Daniel Bruch, which won first prize at the EuroEAP Hardware Challenge 2018 or the haptic device by Gratz-Kelly et al. [17]. Rectangular DE are typically used for in-plane elongations and they can also be adapted for higher-frequency applications when designed for low deflection and low mass, such as the haptic feedback demonstrator for touchscreens, developed by Phillip Loew, which won third prize at the EuroEAP Hardware Challenge 2018. Rolled DE offer the advantage of a compact form factor and, depending on their design (e.g., multiple roll cycles or extended roll lengths), can achieve either high actuation forces or large strain outputs [14].

DET can be designed either as single-layer membrane structures or as multilayer configurations, commonly referred to as stacked DET. The primary advantage of multilayer DET lies in their enhanced performance: they offer significantly improved force output and energy density in actuator applications, as demonstrated by Hau et al. [23]

The principal manufacturing process for all three DETs is the same, but the electrode properties differ and must be adapted to their specific requirements during the manufacturing process. While for DES a high conductivity is the main important factor, for DEA and DEG the focus is also on compliance and a low mechanical impact of the electrode on the membrane. However, electrical breakdown behavior is relevant only for actuators and generators, as they typically operate in the kilovolt regime. While all working principles are explained in this section, the emphasis is on dielectric elastomer actuators, as they are the primary focus of this work.

2.1.1 Dielectric elastomer sensors

The operation of a dielectric elastomer sensor is based on the principle that a mechanical deformation of the elastomer induces a change in capacitance, Figure 2.3. This characteristic allows applications for force, stretch, or pressure sensors [86, 87, 88].

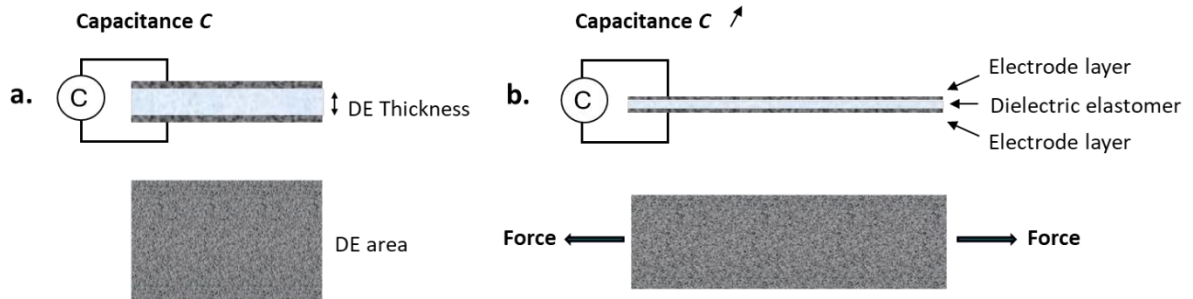


Figure 2.3. Working principle of DES in the un-stretched state (a) and stretched state (b), illustrating both the cross-section (top row) and the top view (bottom row).

When DES are mechanically stretched, the thickness of the material and thus the distance between the electrodes is reduced. The reduction in thickness is also accompanied by an increase in electrode area, leading to a corresponding rise in capacitance C . Capacitance measurements during elongation or compression allow for inferences about changes in thickness or area according to the formula for a parallel plate capacitor, Equation 1.

$$C = \epsilon_0 \epsilon_{DE} \frac{A}{z} \quad (1)$$

with:

C : capacitance

ϵ_0 : permittivity free space $\approx 8.854 \times 10^{-12} \text{ F/m}$,

ϵ_{DE} : material permittivity of DE,

z : polymer thickness

A : electrode area

Equation 1 demonstrates that the capacitance increases proportionally with the material's permittivity and the electrode area, and inversely with the thickness of the elastomer. These dependencies can be utilized for both strain and force sensing by appropriately configuring the geometry and mechanical design of the system. The overall capacitance of a DES can be further enhanced by stacking multiple DE layers, as the total capacitance is the sum of the individual layer capacitances. A higher capacitance can also help reduce the cost of the associated electronics, as low capacity is more susceptible to interference from parasitic capacitance and environmental factors.

Dielectric elastomer sensors can be implemented in various structural designs depending on the application. Strain sensors operate by detecting changes in capacitance resulting from elongation of the elastomer, while pressure sensors measure changes in capacitance caused by increases in electrode area under applied normal force, see Figure 2.4. To achieve measurable changes in capacitance, these sensors typically require a specifically designed mechanical structure that translates force or displacement into sufficient area expansion.



Figure 2.4. Stertch sensor for a respiration-monitoring functional shirt (left) and pressure sensor for gait analysis (right); kindly provided by IDEAS GmbH. Representative examples of both sensor types have been kindly provided by mateligen IDEAS GmbH.

Because the working principle of DES is based on mechanical deformation and capacitance measurements, which only require low-voltage operation, investigations about electrical breakdown behavior are not relevant. Important for a consistent performance, however, is a manufacturing process tailored to ensure low resistance is maintained over a long term under strain and various environmental conditions.

2.1.2 Dielectric elastomer actuators

The operation of a dielectric elastomer actuator relies on the principle that applying a high voltage (typically in the kilovolt range) to the membrane accumulates opposite charges on the electrodes. This results in an attractive Coulomb force that induces a compressive stretch. Due to the incompressible nature of the polymer, this compressive stretch leads to a reduction of the membrane thickness along with maximal simultaneous lateral expansion, thus resulting in controllable motion crucial for actuator applications. This principle is used in combination with a suitable biasing mechanism in applications such as valves [6, 89, 90], pumps [8], [91], or haptic components [15, 16, 18]. The basic working principle is shown in Figure 2.5.

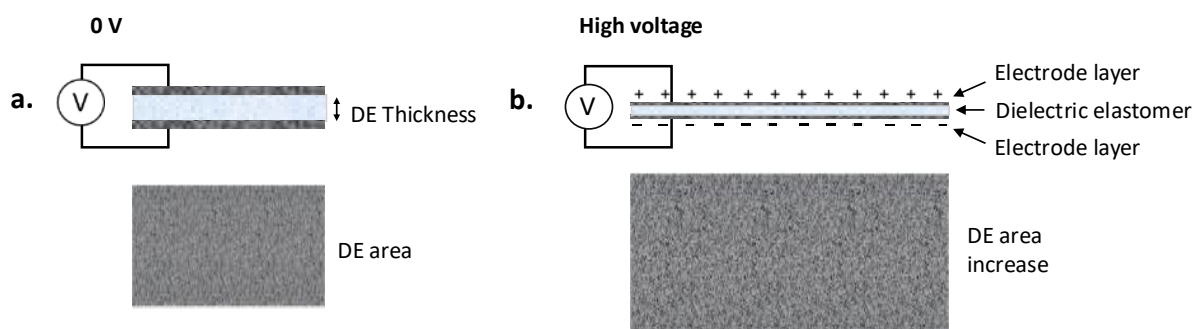


Figure 2.5. Working principle of DEA when no voltage is applied (a), and when high voltage is applied leading to area increases and simultaneous thickness decrease (b), illustrating both the cross-section (top row) and the top view (bottom row).

The induced normal stress σ_{MW} on the polymer depends on material permittivity, applied voltage, and polymer thickness, see Equation 2. It is commonly called Maxwell stress and can be calculated using the following equation for a simplified electrostatic model by Pelrine et al. [80].

$$\sigma_{MW} = \epsilon_0 \epsilon_{DE} E^2 = \epsilon_0 \epsilon_{DE} \left(\frac{V}{z} \right)^2. \quad (2)$$

with:

σ_{MW} : Maxwell stress

ϵ_0 : permittivity free space $\approx 8.854 \times 10^{-12} \text{ F/m}$,

ϵ_{DE} : relative material permittivity of DE,

E : electric field

V : voltage

z : polymer thickness

In analogy to mechanical characterization, the Maxwell stress is typically evaluated in the reference configuration using the initial polymer thickness and is then termed nominal Maxwell stress. Equation 2 shows that the nominal Maxwell stress increases linearly with higher permittivity, but quadratically with the nominal electric field, defined as voltage divided by initial polymer thickness. To enable consistent comparison, throughout this thesis, electric field values are always interpreted as nominal values.

To visualize the area expansion resulting from the Maxwell stress Figure 2.6 shows a pre-stretched DEA clamped on two sides in a fixed position and subjected to a constant voltage. The sample is pre-stretched by 75% in the y-direction, which causes a width reduction in x-axis direction due to the tensile forces - a phenomenon known as necking. When an electric field is applied, the Maxwell stress leads to an area expansion that counteracts the tensile forces and thereby compensates for the necking. At an electric field of 120 V/ μm , the area expansion fully compensates for the necking effect. However, at a field of 140 V/ μm , the area has expanded to such an extent that the clamping of the sample on two sides restricts further expansion. This results in compressive forces in the x-direction, which induce mechanical instability and leads to the formation of wrinkles.

This illustration is intended exclusively to demonstrate the area expansion behavior during actuation and should not be interpreted as a representation of an operational actuator.

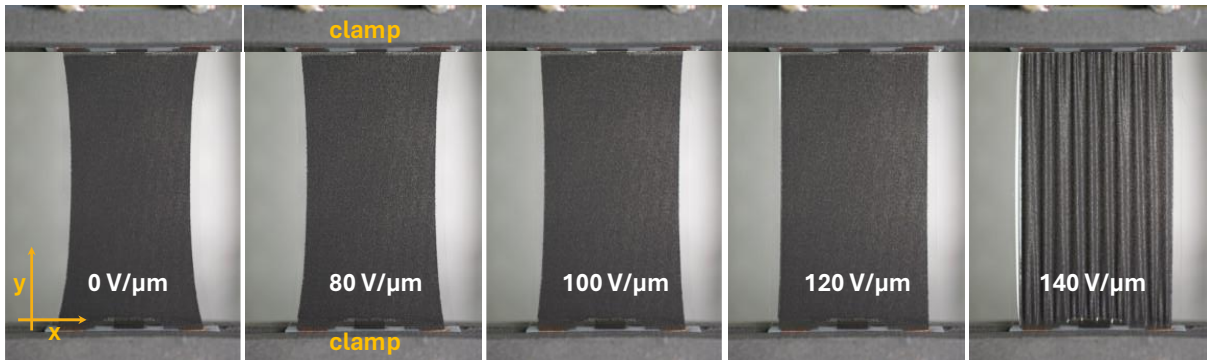


Figure 2.6. Images of a strip DEA pre-stretched by 75% and clamped on both the top and bottom edges. The sample is held in a fixed position and actuated under various constant electric fields. The photos, taken at increasing field strengths, illustrate the progressive area expansion of the membrane.

These results visualize the effect of the Maxwell stress at high electric field strengths, maximizing area expansion, which could also be interpreted as enhancing the actuator's force output. To enable operation at the highest possible electric fields over extended periods, it is hence crucial to understand the parameters that can lead to electrical breakdown and, where possible, implement measures not only to detect such breakdowns but also to prevent them.

DEA applications generally operate based on one of two main principles: exploitation of *thickness reduction* Figure 2.7 or utilization of *surface area expansion* Figure 2.8.

A single-layer DEA operating on the principle of *thickness reduction* achieves only limited displacement, typically in the micrometer range. To produce a sufficiently large stroke, multiple DEA layers must be stacked to form a so-called stack actuator. While this design allows for tuning of displacement by adjusting the number of layers, the generated force remains largely constant and cannot be scaled in the same way. Kovacs et al. [92] proposes applications for driving prosthetic limbs or robot arms.

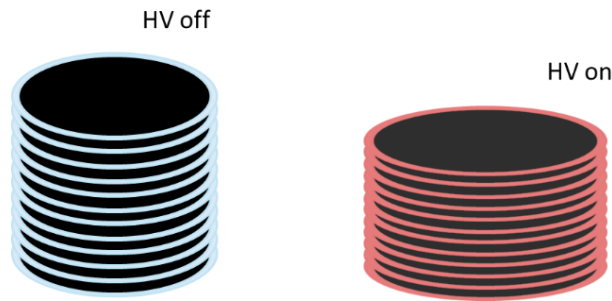


Figure 2.7. Multiple DET layers assembled in stacks that operate through thickness reduction, as proposed by Kovacs et al. [92]. High voltage and ground connections alternate between successive DEA layers.

All DEA considered in this work are based on the principle of surface *area extension*, as this principle allows for greater design flexibility. Both displacement and force can be tuned using appropriate preloading mechanisms.

DEAs utilizing surface area expansion are actuated either within the surface plane (strip design) or perpendicular to it (circular design operating out of plane). For actuator applications, these devices are typically pre-biased using mechanical elements such as springs, enabling significant strain in the higher percentage range, see Figure 2.8. In long and narrow strip configurations, the deformation approaches uniaxial conditions, resulting in large elongation with necking and relatively low actuation force.

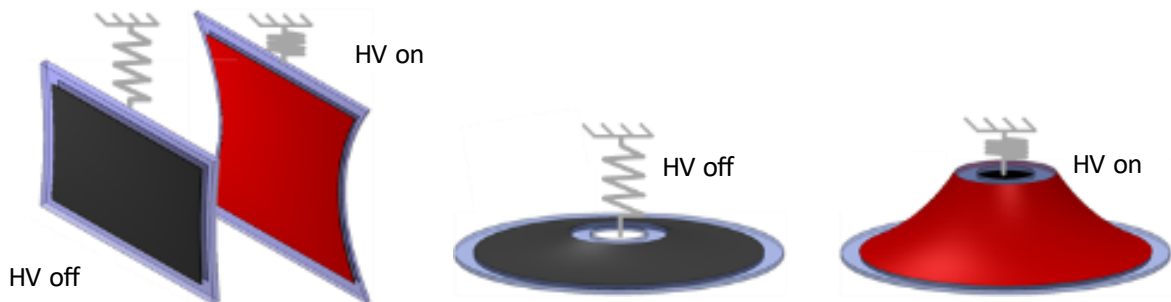


Figure 2.8. Actuation principle of typical DEA utilizing surface area expansion biased with a coil spring: in-plane strip DEA (left) and circular out of plane DEA (right). Pictures courtesy of Daniel Bruch.

In contrast, short and wide designs operate closer to pure shear conditions, producing lower deflection but higher actuation forces [93]. The same principle applies to circular out-of-plane DEA: actuators with small outer to inner radius ratio generate higher forces with lower displacements, while large outer to inner radius ratio designs allow for greater stroke at the expense of reduced actuation force.

Figure 2.9 shows two examples of DEA operation. The actuator on the left side shows a circular design operating out of plane. The DEA is designed as a high-force actuator, following the approach by Hau et al. [23], with the biasing mechanism integrated into the inner free radius of the circular DEA to minimize the overall installation space. The actuator is capable of lifting a 10 kg weight by up to 3 mm, utilizing a spring in combination with a 16-layer stacked DEA.

Figure 2.9 shows a strip actuator operating in plane. It is designed as a prototype to illustrate high stroke actuation (60 % of the initial length) using a combination of linear coil spring and non-linear biased spring. The prototype illustrates the potential for applications such as valves and pumps.

The overall force output of a DEA utilizing surface area expansion can be significantly increased by stacking multiple dielectric elastomer layers, as the total force corresponds to the sum of the forces generated by each individual layer. Although the actuation voltage remains the same for both single-layer and multilayer DEAs, the current required increases proportionally with the number of layers.

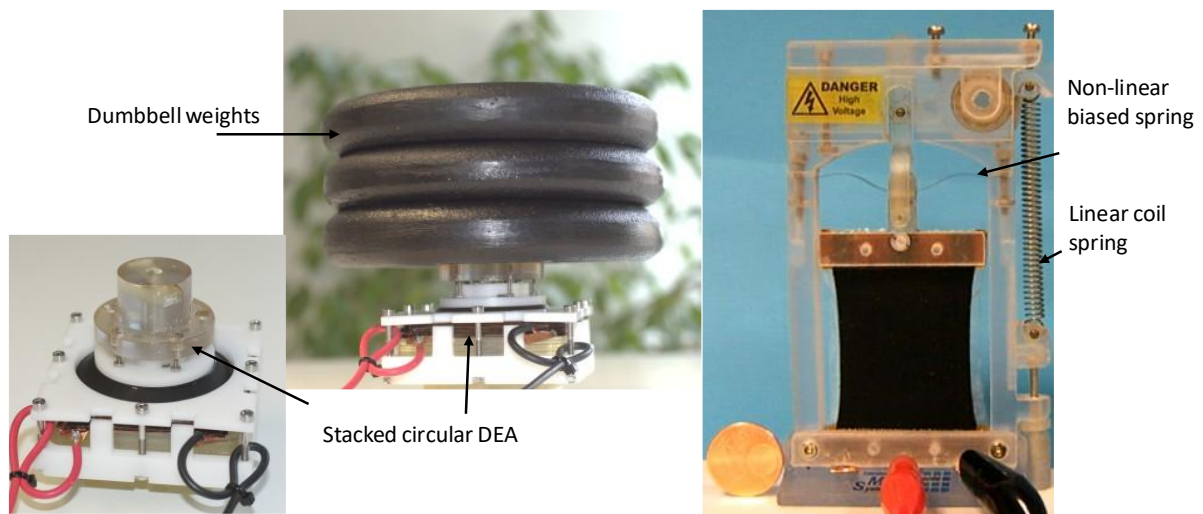


Figure 2.9. 16 DE layer high-force circular DEA (left), and biased strip in plane actuator (right), demonstrating high stroke applications.

2.1.3 Dielectric elastomer generators

The operation of a dielectric elastomer generator relies on the principle that a dielectric elastomer capacitor is cyclically deformed by external mechanical forces, leading to an increase in the electrostatic potential energy of the charges present on the electrodes [94]. DEG are especially well-suited for harvesting energy from irregular or low-frequency mechanical sources, such as ocean waves, human motion, wind-induced vibrations, or structural oscillations.

An example of a position-controlled planar DEG unit subjected to uniform stretches on the electrodes plane, driven according to a cycle with four different phases, is described by Moretti et al.[4] and illustrated in Figure 2.10.

- Phase 1: From the initial un-stretched starting position (A), where the capacitance is minimal (C_{\min}), external loads cause the DEG to expand and lead to configuration (B), where the capacitance becomes maximal (C_{\max}). No charge is present on the expanded DE.
- Phase 2: The DEG configuration is held locked, and the capacitor is charged with charge Q (C). The capacitance is still at its maximum (C_{\max}). In this phase, which is called the priming phase, an amount of electrical energy is spent to charge the device at a low voltage level.
- Phase 3: As the charge on the DEG remains constant, the external loads and DE elastic stresses perform work against the electrostatic charge, returning the DEG back to a configuration (D) with minimum capacitance (C_{\min}). During this generation phase, electrostatic energy is produced at the expanse of the work supplied by external forces and is stored in the DEG electric field. At the same time a decrease in capacitance is accompanied by an increase in voltage, according to the capacitor formula defining capacitance as electric charge divided by voltage.
- Phase 4: The DEG is held in the minimum capacitance configuration (C_{\min}) and discharged. The stored electrostatic energy can then be harvested at high voltage level.

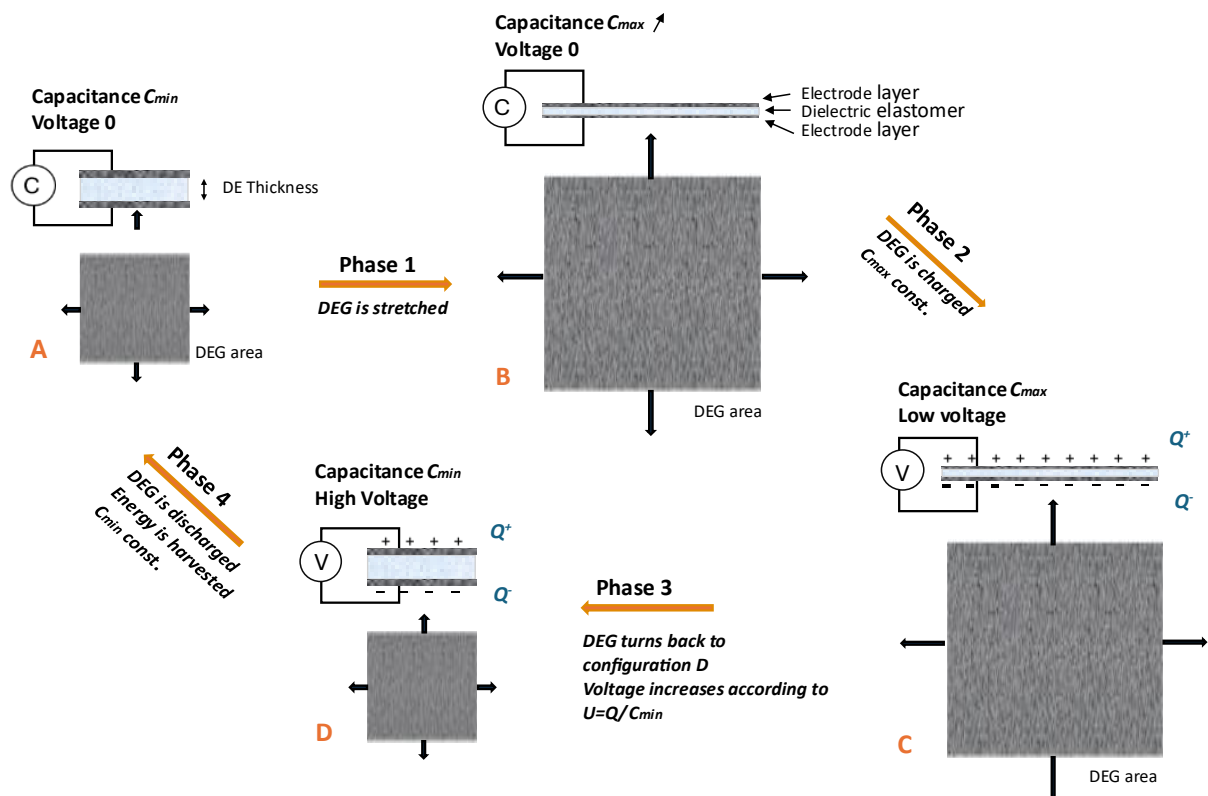


Figure 2.10. The four phases and the four configurations A, B, C, and D of the working cycle of a DE generator (Q: electric charge; C: capacitance; U: voltage), adapted from Moretti et al. [4]:

The net electrical energy generated is calculated as the difference between the energy recovered in Phase 4 and the energy expended during priming in Phase 2. A simplified expression for the electrical energy E harvested per cycle - assuming no losses due to leakage, resistance, or viscoelasticity is

$$E_{cycle} = \frac{1}{2} (C_{min} V_{max}^2 - C_{max} V_{min}^2) \quad (3)$$

with:

E_{cycle} : electrical energy harvested per cycle

C_{max} : Maximum capacitance

C_{min} : Minimum capacitance

V_{max} : Voltage at C_{min}

V_{min} : Voltage at C_{max}

The principle of DEG and the successful harvesting of wave energy have already been demonstrated in several experimental setups [4], [24], [84], [96]. The DE membranes used for wave energy harvesting are significantly larger than those used in actuator applications, in order to accommodate the large amounts of energy to make the concept economically viable. One example of such a test system - tested both in an artificial wave facility and in the ocean - is shown in Figure 2.11, photos courtesy of Giacomo Moretti.



Figure 2.11. Pilot project of DEG for wave generator harvesting: DEG setup in pool using artificial wave energy (top), and DEG setup using wave energy from the ocean. Pictures courtesy from Giacomo Moretti.

The generated energy increases with larger differences in capacitance and higher maximum electric fields, underscoring the importance of understanding electrical breakdown and the potential to operate at higher electric fields to be able to harvest energy at the highest voltage level possible. As in the case of DEA, for an efficient DEG operation it is therefore essential that DEG perform robustly under high voltages (Phase 4).

2.2 DET materials

2.2.1 Dielectric elastomer film materials

Different dielectric materials are currently available for sensor, actuator, and generator applications, including polyurethane [29, 30], natural and synthetic rubber (latex) [24], acrylic-based materials [25 - 28], and silicones [22, 23].

Efficient and reliable operation of DETs demands specific material properties [79, 94, 96 - 98], which differ among the four material classes:

- A *high relative permittivity* – defined by the dielectric constant - increases the Maxwell stresses, hereby enhancing the actuation strain or force at a given voltage. With increasing permittivity actuation at lower voltages is enabled, reducing the cost for high voltage electronics.
- A *high breakdown strength* is necessary for the DET to withstand the high electric fields required for actuation without failing to ensure long lifetime operation.
- A *low elastic modulus* results in high elastomer softness, which allows for large actuation strains under an electric field. This is especially important for large deformations.
- A *low electrical conductivity* prevents parasitic current from flowing through the material, which on the one hand increases performance losses of the DET, and on the other hand reduces the energy required to operate the DET. Furthermore, current flow through the elastomer can lead to heating of the DET during operation.
- A *low viscosity* minimizes mechanical energy dissipation during cyclic actuation. A high viscosity results in lower actuation rates and higher damping effects.
- Stability under varying environmental conditions - particularly high humidity and temperature changes - is essential to maintain consistent performance and prevent long-term degradation.

Polyurethane has the highest permittivity ($\epsilon \sim 7$) out of the four materials, good thermal stability, and high response speed. The breakdown strength is comparably high and depends on the PU composition of the films (130 - 220 V/ μm) [79]. The elastic modulus (1.4 - 3.4 MPa) is higher than that of the other three materials, making it stiffer and less deformable. It is a material that is easy to process, making it one of the most cost-effective options for dielectric elastomer applications.

However, it is not commercially available as a dielectric thin film in a quality required for DET applications. It exhibits comparatively high electrical conductivity (volume resistivity of $7 \times 10^{11} \Omega\text{cm}$) and is prone to significant creep or permanent deformation under actuation strain. Due to its polar nature, it is more sensitive to moisture than silicone [29, 74, 79].

The permittivity of **natural and synthetic rubber** ($\epsilon \sim 2.7$) is comparable to that of silicone and thus lower than the one of polyurethane and acrylic based materials such as VHB 3M. The dielectric breakdown strength of rubber is relatively high (97 V/ μm), although it decreases significantly upon exposure to moisture. Compared to silicone-based dielectric elastomers, rubber materials offer a notable cost advantage.

Films are commercially available as OPPO BAND GREEN 8003 made of natural rubber in thicknesses of 220 μm and THERABAND YELLOW 11726 made of styrenic rubber with thickness of over 290 μm [24]. These thicknesses require either a high voltage for DET applications or a very high pre-stretch to lower the overall thickness of the material. Film homogeneities vary because the film is not manufactured for DET applications.

A key limitation is their relatively high elastic stiffness (elastic modulus ≈ 2.4 MPa [99]), which may compromise performance in actuation tasks due to reduced deformability. Rubber exhibits low electrical conductivity (volume resistivity $\approx 10^{15}$ $\Omega\cdot\text{cm}$), allowing operation with minimal dielectric losses. Its viscoelastic losses are higher than those of silicone, yet lower than those of acrylic elastomers like VHB [24]. Natural and synthetic rubber remain flexible across a wide temperature range, including sub-zero conditions. Under high temperature conditions (> 80 $^{\circ}\text{C}$), however, they lose elasticity, become harder, and thermal aging is possible [74, 99 - 101].

The most common **acrylate-based rubber** for DET applications is 3M's VHB, which is an acrylic adhesive transfer tape, available with minimum thickness of 400 μm . Its relatively high permittivity ($\epsilon \sim 4.1$) compared to silicone and natural rubber materials enables larger actuation strains at lower actuation voltages at comparable film thickness. However, its moderate dielectric breakdown strength (~ 66 V/ μm) imposes a limit on the maximum applicable electric field. Due to its low elastic stiffness (elastic modulus ≈ 0.2 MPa), VHB is exceptionally soft and capable of large deformations under low mechanical stress. It is highly stretchable, accommodating strains of up to 1000%, which allows to pre-stretch the material to achieve thinner membranes for lower actuation voltages. The film features extremely low electrical conductivity (volume resistivity $\sim 10^{17}$ $\Omega\cdot\text{cm}$), making it well suited for electrically driven actuation [74, 95, 100, 102].

Despite these advantages, a major limitation of VHB in DET applications lies in its pronounced viscoelastic behavior - including creep, stress relaxation, and hysteresis - as reported by Zhao et al. [100, 101]. These time-dependent phenomena restrict the frequency range over which the material can be reliably actuated and contribute to energy losses and long-term deformation [7, 24].

Material performance is also strongly influenced by environmental conditions. At low temperatures (~ 0 $^{\circ}\text{C}$), VHB becomes stiff or brittle, while at elevated temperatures, viscoelasticity and creep effects become more pronounced. When exposed to moisture, the viscoelastic behavior is even more pronounced, and creep and relaxation increase significantly [28, 100, 101, 105].

Silicone thin films are commercially available for dielectric elastomer transducer (DET) applications exclusively from Wacker Chemie AG, and until recently, from Parker Hannifin. Wacker developed Elastosil Film 2030, offered in homogeneous thicknesses ranging from 10 μm to 400 μm , specifically tailored for DET applications. The material exhibits a relatively low permittivity ($\epsilon \approx 2.8$) compared to the other three materials, which necessitates higher actuation voltages to achieve comparable strains relative to materials with higher permittivity. The dielectric breakdown strength (~ 90 V/ μm) is slightly lower than that of rubber, but significantly higher than that of VHB. Moreover, silicone possesses low electrical conductivity (volume resistivity $\approx 10^{15}$ $\Omega\cdot\text{cm}$), allowing operation with minimal dielectric losses. With an elastic modulus of approximately 1.1 MPa, silicone films are stiffer than VHB, but more compliant than natural rubber and polyurethane, enabling moderate stretchability up to 200% [79, 106 - 108].

Even though the cost and required actuation voltages are higher than that of the other three materials, silicone offers many unique characteristics. It demonstrates low viscoelasticity, enabling low-hysteresis, energy-efficient actuation even at frequencies exceeding 2 kHz. Additionally, silicone can operate across a wide temperature range from -80 °C to +250 °C, owing to its low glass transition temperature and high thermal stability. It is inherently hydrophobic and highly resistant to environmental degradation, including oxidation, UV radiation, and moisture uptake. The influence of high humidity on actuation and breakdown behavior is low compared to the other three materials [59, 73, 79, 101].

Silicone DET exhibit significantly better long-term reliability compared to acrylate-based DET. For instance, Tang et al. 2024 [7] reports 10 million actuation cycles and Biggs et al. 2013 [79] describes actuators tested for nearly one billion cycles under both ambient and high-humidity conditions.

Given these favorable properties - particularly in terms of low viscoelasticity, environmental stability, and commercial availability - silicone was selected as the dielectric elastomer material in this thesis.

2.2.2 Electrode materials for dielectric elastomers

The electrodes, which constitute another essential component of the DET and are applied to the dielectric film, must also meet specific requirements. Ideally, an electrode should:

- Exhibit high electrical conductivity to ensure rapid charging and discharging of the dielectric capacitor.
- Maintain its conductivity under mechanical strain, without degradation or fatigue.
- Preserve strong bond to the elastomer, even during repeated stretching.
- Minimally impact the mechanical properties of the film.
- Be compatible with scalable manufacturing techniques, such as screen printing, pad printing, or blade casting.

First research efforts were based on acrylic films VHB 4910 or VHB 4905, which are available from 3M as adhesive tape. Carbon black or graphite powder electrodes were brushed or sprayed directly onto the film and adhered because of the nature of the material [109]. Under elongation, however, particle separation occurred locally, compromising uniform electrode conductivity. Therefore, in the next development step, carbon grease electrodes were applied [98], [109], [110]. These maintained conductivity even under high strain but had the drawback of smearing or rubbing off upon contact. Neither of these combinations were application-ready due to lacking robustness during handling.

Since then various electrode materials are identified for DET applications, including carbon black [34, 35, 36], carbon nanotubes [37, 38, 39], graphite nanoplates [40], metals like silver [32] and nickel [33], and organic materials such as polyethylenedioxythiophene/polystyrene sulfonate (PEDOT:PSS) [41, 42, 43]. These materials are often embedded in solvent, grease, or non-conductive base materials like polydimethylsiloxan (PDMS), which is the main component of silicone.

In the following, the term *silicone* is used to refer to the silicone film, while *PDMS* refers specifically to the silicone component within the electrode mixture.

This work focuses on DET membranes made of silicone. The surface of silicone films is hydrophobic and does not provide good adhesion for materials that are not silicone-based, see section 2.3.1. As a result, water-soluble materials such as PEDOT:PSS, despite their good conductivity, are not suitable

as electrode materials for silicone membranes. Consequently, the development of compatible electrode materials and scalable manufacturing methods remains a major challenge in this field.

The electrodes used in this thesis were developed and manufactured in the iMSL lab. The focus of electrode development was on designing electrodes that not only meet the previously defined performance requirements but are also cost-effective to manufacture and, as far as possible, composed of materials that pose no health risks, such as carcinogenic or mutagenic effects. Among the materials considered, carbon black emerged as the most affordable and well-conductive option. Carbon nanoparticles were excluded due to potential health hazards, while silver powders and carbon nanoplates were deemed unsuitable due to their high cost.

The carrier material into which carbon black is mixed consists of PDMS. The use of carbon grease - a mixture of carbon black and silicone oil - proved to be disadvantageous, as it led to swelling of the material. In subsequent developments, the addition of oil was also avoided, as it was found that the electrical resistance behavior significantly deteriorated over a period of three months [77].

The electrode composition has been continuously optimized over the past few years. The formulation used in Chapter 4, Section 4.1, is described in detail within the respective publication. The investigations in Sections 4.2 to 4.4 and Chapter 5, an oil-free electrode formulation is used, consisting of 25 wt.-% high conductive carbon black (7 wt.-% AkzoNobel-Ketjenblack EC 612D and 18 wt.-% Imerys-Timcal Ensaco350G) and 75 wt.-% PDMS (Wacker Silgel 612A/B) after solvent evaporation. Exxon Isopar M is used as a solvent to make the mixture processable for further manufacturing steps, including dispersion using a three-roll mill and manufacturing of the DET via screen-printing. A detailed description of the electrode fabrication process can be found in Willian et al., 2023 [36].

During the development of the blend, special emphasis was placed on ensuring that the materials have no harmful effects on health: carbon blacks are prepared with solvent in a glovebox, PDMS Silgel 612A/B is classified as non-hazardous, and the solvent Isopar M is classified as NFPA Health Hazard 1 out of 4, which is low compared to other solvents. The manufacturing process as well as the manufacturing of the blend are conducted in a vented and safe environment, while residue is vented and disposed of as household-type commercial waste.

2.3 Breakdown mechanism of silicone DET

A key focus of this work is to gain a comprehensive understanding of application-relevant parameters that influence the electrical breakdown behavior of silicone DEA and DEG. The primary component of silicone thin films is PDMS, and the current section provides an introduction to the molecular structure and various mechanisms leading to breakdown behavior in these materials.

2.3.1 Molecular structure and resulting macroscopic characteristics of PDMS

PDMS consists of an inorganic backbone of alternating silicon (Si) and oxygen (O) atoms, where each silicon atom is bonded to two organic methyl groups (CH_3). The chemical formula of PDMS is $((\text{CH}_3)_2\text{SiO})_n$, with n being the number of repeating units, Figure 2.12. Any number of repeating units is theoretically possible. Polmanteer reports n -values ranging from 3,000 to 5,000 units [111]. Dvornic et al. studied chain lengths spanning from 3 to 37,000 main-chain atoms (equivalent to n -values ranging from 2 to 19,000 Si-O units) and identified n -values of maximal 464 before chain entanglement and a change in the flow behavior of the polymer occurs [112].

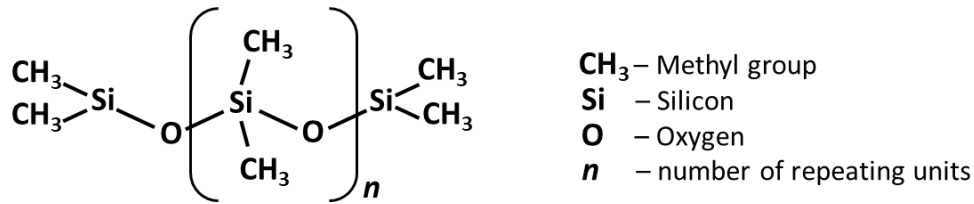


Figure 2.12 Molecular structure of PDMS

The Si-O backbone adopts a flat helical conformation. This conformation has some structural features, which makes it one of the most flexible polymer chains [107]:

The Si-O bond length is with 1.64 Å significantly longer than that of organic polymers chains (C-C bond length is 1.53 Å). The elongation is further accentuated by the large Si-O-Si bond angle of approximately 143°, which can expand up to 180° - in contrast to the usual tetrahedral angle of 110° seen in carbon compounds. The rotational energy is nearly zero, allowing the Si-O backbone to rotate freely. Additionally, the low electronegativity of silicon results in a polarized Si-O bond with high bond energy. The strength of the bond provides siloxane polymers with excellent thermal stability, making them suitable for high-temperature applications [113].

Two other structural features are important for the unique properties of PDMS. The first concerns the two methyl side groups. These are connected to the Si atom, leaving the oxygen atom unsubstituted. This allows for a free rotational movement around itself and the backbone of the PDMS and thereby shielding the backbone. This leads to chains with a very low surface free energy and is responsible for the hydrophobicity of the material [114].

The second structural feature relates to the overall arrangement of the molecules within the film. The high flexibility and helical conformation of the silicon-oxygen chain provides openings or free volumes which permit gas diffusion. These free volumes thermally form and disappear with the movement of the polymer chains. The diffusion of gas molecules is a process in which the gas molecules migrate from opening to opening [115]. A PDMS fractional free volume of 30 % was determined by Chang et al. via swelling with ethanol [116], Wang et al. obtained even fractional free volumes of 55 % due to swelling with deionized water [117]. Important for possible gas diffusion, however, is not only the fractional free volume, but also the radius of a single free opening. The average radius of a free opening is 3.9 Å and is thereby significantly larger than the average radius of a water molecule with 3 Å. These two properties allow water vapor molecules to pass through the membrane, resulting in the high water vapor permeability of PDMS [118]. On the other hand, they prohibit the passing through the membrane when water is in its aqueous state, explaining the hydrophobicity of PDMS.

The combination of the highly flexible chain, the freedom to rotate, and the substantial free volume of PDMS results in its exceptionally low glass transition temperature of -125 °C [114].

2.3.2 Mechanisms of electrical breakdown in PDMS

This chapter provides a fundamental explanation of electrical breakdown of dielectric elastomers at the molecular level to support the understanding of the breakdown investigations in Chapter 3. Electrical breakdown mechanisms have been widely discussed in the literature [119 - 125]. However, most studies focus on electrical breakdowns in cable insulators, which typically consist of millimeter-thick silicone layers designed to withstand constant voltages over long periods. In contrast, DEA

operate with micrometer-thin films and are generally exposed periodically to an electric field only when the DEA is actuated. The following section will therefore focus on breakdown mechanisms occurring within the seconds range. Continuous voltage application is also possible. It has been extensively studied by Albuquerque [73], who investigated the lifetime of DEA under DC electric fields.

Fothergill [123] and Leda [119] classify mechanisms responsible for breakdown after an electric field is applied into three main groups, depending on the time to failure: *breakdown* occurs in the first nano-seconds to seconds, *degradation* within centi-seconds to weeks, and *aging* after weeks up to years. The investigations in this thesis focus on the understanding of short-term electrical breakdown. Therefore, the explanation of breakdown mechanisms is limited to the breakdowns phase (short-term breakdown) with times to failure on the nano-seconds to centi-seconds scale. Short-term breakdown mechanisms are sub-divided into three main groups:

- Electronic breakdown
- Thermal breakdown
- Electro-mechanical breakdown

In addition to these short-term mechanisms, other mechanisms such as partial discharge and electric treeing can in theory also occur within centi-seconds. However, these phenomena are generally classified as long-term failure mechanisms that develop over hours. These effects have been extensively discussed in the literature [73, 125].

The individual breakdown mechanisms are described in the following section. However, it is likely that dielectric failure results from the superposition of several mechanisms rather than a single isolated cause. These mechanisms are influenced by multiple factors such as chemical structure, material purity, thickness, pre-stretch, voltage application mode, and environmental conditions.

Electronic breakdown

In general, electronic breakdown occurs when free charge carriers are accelerated by an electric field, gaining enough energy to ionize atoms by stripping away electrons. This process disrupts the molecular structure and leads to the reduction of the dielectric properties of the material. As the number of charge carriers increases, the material's resistance drops, causing it to become conductive, generating free radicals and triggering a chain reaction. At this point, current multiplication happens rapidly. Damage is most likely not to occur in the silicone backbone but in the methyl side chain, where bond energy is lowest [126].

Even the most ideal insulating material contains a small number of free charge carriers. This is due to two main reasons: Firstly, thermal energy at room temperature can excite a few electrons or ions into a mobile state, enabling limited electrical conduction. Secondly, material imperfections such as impurities, free volumes, grain boundaries, inherent structural disorders, or additives facilitate the provision of free electrons when a high electric field is applied. When the current flow increases to a certain level, the damage of the material is irreversible [125].

Dissado and Fothergill [123] understand *intrinsic breakdown* and *avalanche breakdown* as the two main mechanisms underlying electronic breakdown. They describe that, in terms of electron energy, there is a maximum rate at which the free-electron system can lose energy to the molecular structure through electron-phonon scattering, while the rate at which it gains energy from the field is a monotonically increasing function. Consequently, there must be a critical field and a corresponding electron energy beyond which electrons continuously gain energy faster than they can lose it, ultimately leading to breakdown. Sun et al. [127] refer to intrinsic breakdown when the electric field

will cause breakdown of a “perfect” material in a very short time, i.e., without the effects of high field aging.

Although this appears to be a mechanism which is intrinsic to the material, high-energy electrons may also lose energy by inelastic collisions with defects or scattering with other electrons, either free or trapped ones. When the bonding is very weak, perhaps after being weakened through earlier local energy-dissipating phenomena, this mechanism can lead to structural disruption.

Collisions between the high-energy electrons and trapped electrons may also lead to *avalanche breakdown*. In this process, electrons with a high energy - whether due to acceleration in the field or purely from random fluctuations - collide with trapped or bound electrons, transferring sufficient energy for both electrons to be free after the collision. In a sufficiently high field both electrons rapidly gain enough energy to generate additional free electrons. If this chain reaction continues the local concentration of high-energy electrons increases to the point where it causes the local destruction of the chain [125, 126].

Thermal breakdown

Thermal breakdown begins when an initially negligible current flows through the weaker regions of the dielectric. As the electric field strength increases, this current intensifies, leading to localized heating and the formation of point defects. These defects promote ionic conductivity, which further increases local heat production and results in a rapid rise in electrical conductivity as additional charge carriers become available. In silicone dielectric elastomers, Joule heating due to current flow is minimal, suggesting that thermal breakdown is likely to occur only in conjunction with electronic breakdown, once current flow has already been initiated [125].

Electro-mechanical breakdown

When a voltage is applied across the dielectric elastomer, electrostatic forces known as Maxwell stress act on the elastomer, compressing it in the thickness direction and expanding it laterally. This compression causes a local reduction in film thickness, which in turn increases the local electric field, defined as applied voltage divided by the thickness of the membrane. As the electric field intensifies due to continued thinning, this further promotes thinning and can cause a so-called electromechanical instability [129]. If this process continues, the local electric field can exceed the material’s dielectric breakdown strength, resulting in electro-mechanical breakdown [130].

To visualize the mechanical deformation caused by Maxwell stress under an applied electric field along with the effect of viscoelasticity, high-resolution images were taken after breakdown, when Maxwell stress was at its maximum [131]. The breakdown tests were conducted using the breakdown tester described in Chapter 4, with voltage applied via two gold contacts - one flat and one spherical - following the Standards for Dielectric Elastomer Transducers [132] and the test setup by Kollosche and Kofod [133].

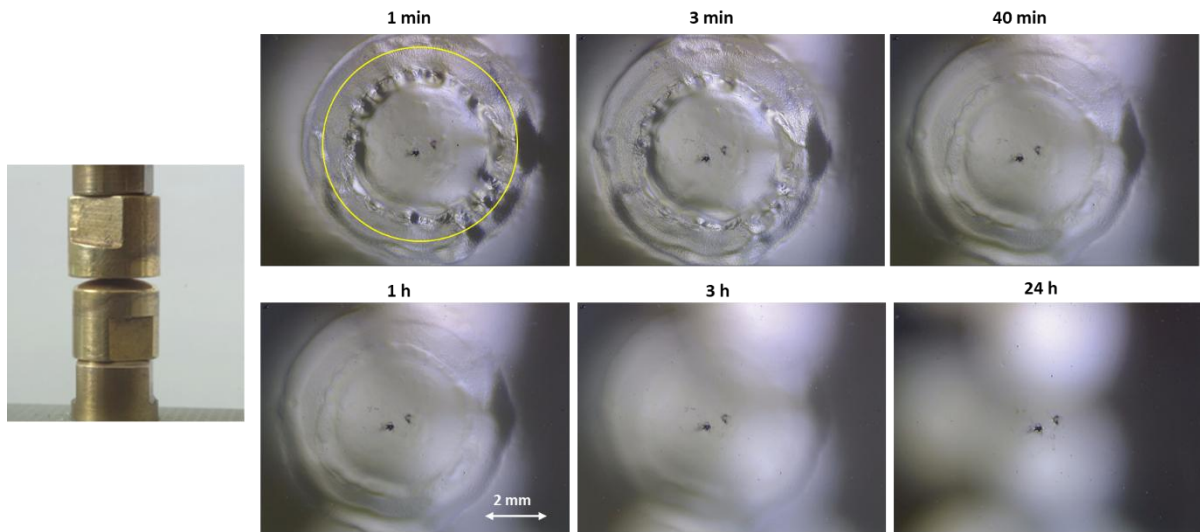


Figure 2.13. Design of gold contacts – flat and spherical - used for voltage application and images captured at intervals from 1 minute to 24 hours after breakdown, illustrating wrinkles due to Maxwell stress and return to smooth state over time. Two breakdown spots are visible in the center of the pictures. The yellow circle marks the area of the flat gold contact.

Figure 2.13 illustrates the design of the gold electrodes, the imprint left by the gold contacts, and the wrinkling of the membrane surrounding the contacts due to membrane thinning under Maxwell stress with two distinct breakdown spots. A circle marks the radius of the flat gold contact in the first image, revealing that the wrinkling extends beyond the electrode's area.

Images of the imprint were captured at intervals from 1 minute up to 24 hours. Over time, the wrinkles gradually disappeared, with the film returning to a smooth state after 24 hours. This recovery is attributed to the flexibility and constant mobility of the PDMS chains, a characteristic that defines their inherent viscoelasticity.

2.4 Experimental characterization of DET

The experimental characterization of DET is essential for subsequent design and optimization of DET systems. It involves mechanical, electrical, and electromechanical measurements, which are different for sensor, actuator, or generator applications. Section 2.4.1 introduces a universal DET test set up used in this work, while Sections 2.4.2 to 2.4.4 explain the key parameters required for a comprehensive characterization of the different DET applications.

2.4.1 Test setup for experimental characterization of DET

Micah Hodgins [134] developed an automated test rig as part of his PhD thesis, which allows to systematically test DE membranes of various geometries in a standardized manner. The following summarizes the key features and components to highlight the system's capabilities. The test rig has been used for measurements conducted throughout this thesis.

This test rig enables repeatable measurements of parameters such as resistance, capacitance, and force behavior under cyclic stretch across an extended frequency range. In addition, it allows for voltage excitation and measurements across various frequency ranges, both with and without mechanical deformation of the samples. Simultaneously, two confocal sensors measure and record

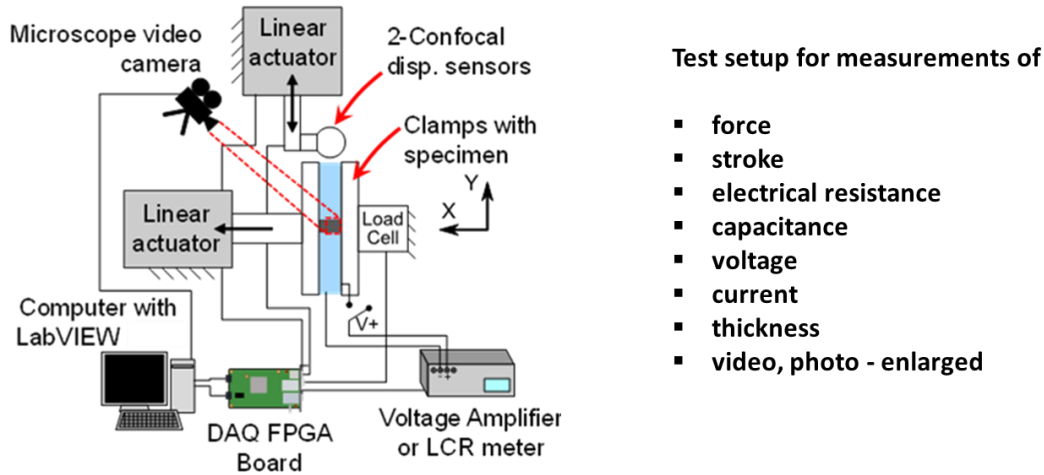


Figure 2.14. Conceptual sketch of the automated test rig including data acquisition system and user interface implemented in LabVIEW (left). Overview of the test parameters that can be measured with the test rig (right).

the thickness profiles of the samples during stretching and/or actuation, using a second independent axis for sensor movement. A conceptual sketch of the automated test rig which includes the data acquisition system and user interface implemented in LabVIEW is shown in Figure 2.14. The figure also illustrates all measurement capabilities enabled by the test rig, covering the determination of all relevant parameters required for the design of DET.

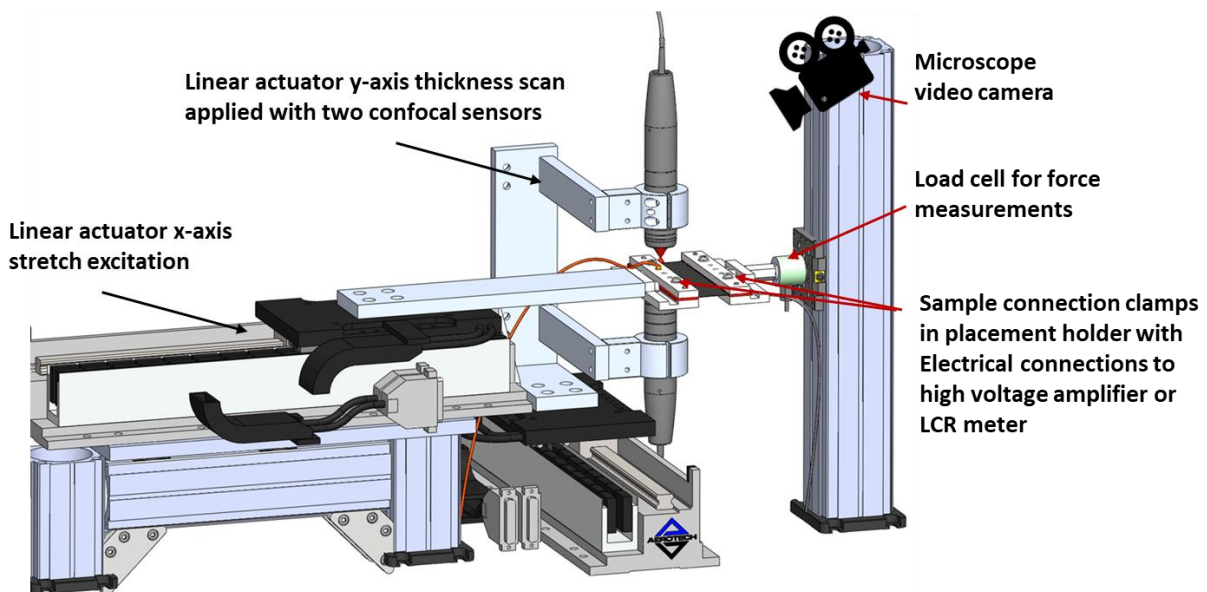


Figure 2.15. 3D model of the test rig with labeled components and sensors

The setup is mounted on a vibration-isolated optical table located within a climate-controlled cleanroom. It employs two linear servo-motor-driven actuators: the x-axis actuator is used to stretch the dielectric elastomer (DE) membrane, while the y-axis actuator holds two confocal displacement sensors for thickness measurements. A 3D model of the setup with the labeled components is shown in Figure 2.15.

The test rig includes a custom-designed sample holder that ensures precise and repeatable sample placement. This holder integrates spring-loaded, gold-plated electrical contacts for consistent electrical connection. The contacts are wired and can be connected either to an LCR meter or a high-voltage amplifier, depending on the type of measurement. Four terminals are available at the top of the clamp for four-point resistance measurements, and two terminals are available at the bottom for standard connections.

Pre-fabricated samples are mounted into the rig and characterized according to a predefined measurement protocol. Displacement of the samples is controlled and recorded using the Aerotech ACT115DL actuator system, which offers:

- 200 mm travel range
- $\pm 2 \mu\text{m}$ positioning resolution
- Maximum speed of 5 m/s
- Continuous force capacity of 105 N

For force measurements, a ME KD 40s 10N load cell with accuracy class 0.1 is used.

For resistance and capacitance measurements under zero-voltage conditions, a Hameg HM8118 LCR meter is utilized. When high-voltage excitation is required, a TREK 610E high-voltage amplifier is used. This amplifier supports:

- Output voltage: 0–10 kV
- Output current: 0–2000 μA
- Sinusoidal excitation up to 1.2 kHz

Thickness measurements are carried out using two confocal displacement sensors (Micro-Epsilon, confocalDT IFS 2405), each with:

- Resolution: 28 nm
- Linearity: 0.5 μm

The confocal sensors are arranged coaxially with overlapping measurement ranges to allow accurate profiling of the DE membrane's thickness. In the case of transparent membranes with a known refractive index, a single sensor is sufficient, as it can detect reflections through the membrane. For membranes with electrodes, however, two opposing sensors operating in displacement mode are required. For these measurements, the sensors need to be calibrated using an object of a known thickness.

Enlarged photos and videos are captured using the digital zoom microscope DI-Li 2001, with:

- Optical zoom: 20x – 120 x
- Resolution 1280 x 1024 at 1.3 M

Repeatability was ensured by preparing the samples using a standardized procedure and positioning them in a defined and reproducible manner within the test setup. The original fixture design by Hodgins [134], was replaced by an improved version developed by Willian et al. [36], enabling repeated use of the prefabricated clamps. This updated design is applied in Chapter 5. A detailed description of the alignment fixture, along with example clamps, is provided in Figure 2.16.

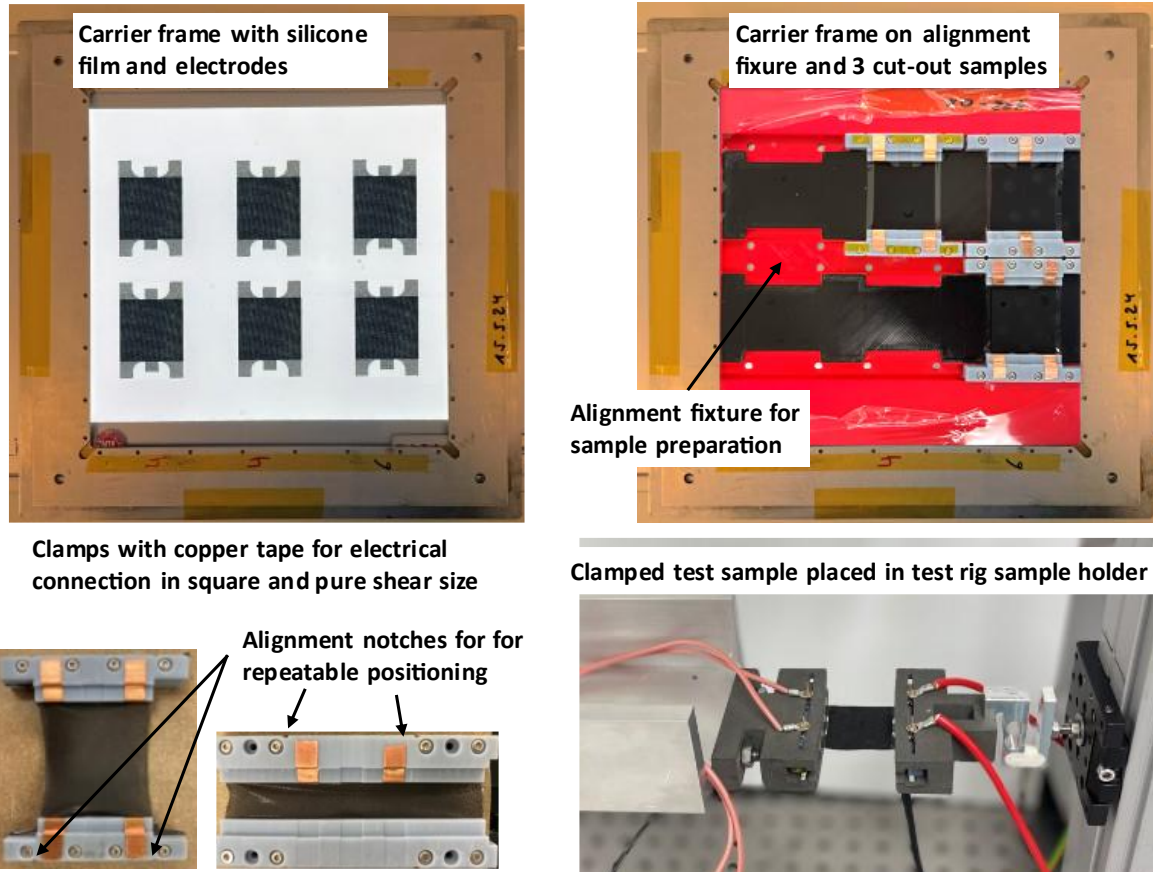


Figure 2.16. Standardized procedure for samples preparation. Screen printed electrodes on carrier frame (top left); carrier frame placed on the alignment fixture, equipped with recesses for the bottom clamps, showing three empty slots and three samples prepared for testing, each with a DE membrane clamped between bottom and top clamps (top right); DE membranes prepared for testing in various dimensions, demonstrating the versatility of the test geometries (bottom left); test sample inserted into the sample holder using alignment notches, ensuring precise and repeatable positioning (bottom right).

The test rig also allows for the performance of breakdown tests; however, due to the complex sample preparation required, it is not ideally suited for this purpose. Moreover, the size of the setup makes it difficult to place inside a climate chamber. Different breakdown test setups have specifically been developed for this purpose [60], [61], [64], [135].

2.4.2 Relevant material parameter for sensor applications

To enable application-specific sensor designs it is essential to understand their capacitance and resistance behavior - especially under mechanical deformation such as stretching or compression. This information can be obtained using special test setups, where the samples are subjected to

controlled stretching and the key parameters are continuously measured. These parameters and their relevance for DES design are:

- **Capacitance** Capacitance is the most relevant parameter for sensor design, as the sensor's displacement is determined through capacitance measurements.
- **Electrical resistance** Electrical resistance over stretch, as well as over time, is an important parameter for the design of the electronics that read and convert the capacitive signals of the sensor as it affects the signal quality. Very high resistances typically require more expensive electronics. If the resistance changes significantly over time or shows hysteretic behavior, this can also lead to issues in signal processing and stability. Since this behavior does not occur in capacitive measurements, sensors are generally designed to operate in capacitive mode
- **Elongation (stretch)** Understanding the stretch behavior is essential to enable proper calibration of the sensor to its mechanical response. Furthermore, the elongation determines the possible operating range of the sensor

Figure 2.17 shows example measurement curves that are essential for the design of a dielectric elastomer sensor. These curves include the excitation signal as well as the resulting capacitive and resistive responses over stretch and time.

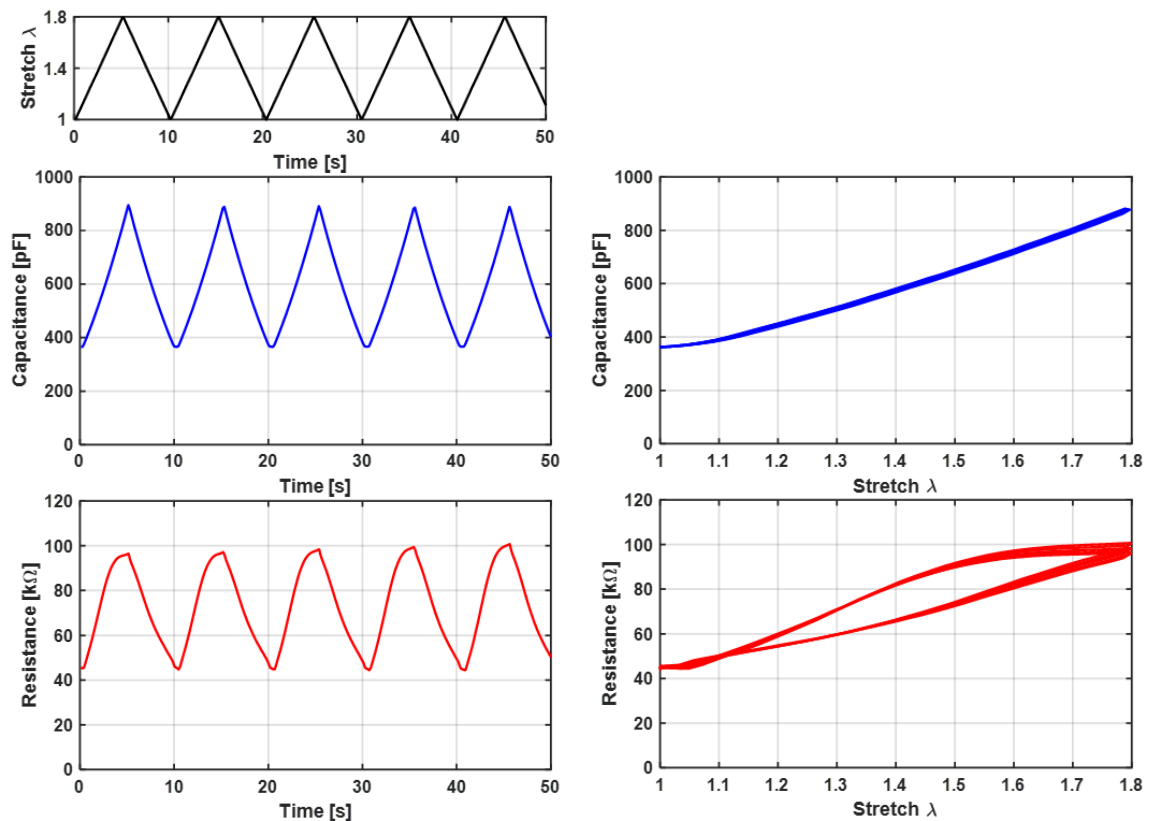


Figure 2.17. Example measurements relevant for the design of a DES: Excitation signal (top); capacitance over time and stretch (middle); electrical resistance over time and stretch (bottom)

In this example, the capacitive response exhibits an almost linear behavior, while the resistance shows a hysteresis with respect to stretch. Due to the incompressibility of the silicone film, the capacitance typically behaves linearly with uniform area expansion. The slight nonlinearity observed in the capacitance-stretch curve is attributed to lateral necking of the sample. This behavior must be taken into account when designing a sensor based on dielectric elastomers.

Additionally, information about the long-term performance of the sensor is essential, as both dielectric elastomers and electrodes may show fatigue over time or under environmental influences, potentially altering their behavior and affecting the reliability of the initial design.

2.4.3 Relevant material parameters for actuator applications

Designing a dielectric elastomer actuator (DEA) requires a broader set of parameters than sensor design, as it involves characterizing the mechanical and electrical response both in the non-actuated (voltage-off) and actuated (voltage-on) states. Critical parameters and their relevance for the design of a DEA are outlined below:

- Thickness

Information about the thickness over the area of the elastomer film gives information about the film homogeneity and are necessary to calculate the maximum breakdown field, calculated as maximum applicable voltage divided by initial film thickness.
- Force - elongation (voltage-off)

The performance of a DEA is determined by its actuation force, which is defined as the difference in mechanical force between the non-actuated and actuated states. The force-elongation behavior of the DEA in its non-actuated state provides the baseline (or ground) force response. Additionally, the measurements also reveal key mechanical characteristics such as hysteresis, Mullins effect, and pseudo-elastic behavior. These parameters are critical for actuator design, as they directly affect the design of necessary biasing mechanisms and the overall dynamic response of the system.
- Force - elongation (voltage-on)

The actuation force, defined as the difference in mechanical force between an actuated and a non-actuated DEA, is the most important parameter for DEA system design. It is typically measured during stretch cycles under constant voltage to characterize the force response of the actuator. By conducting these measurements at varying voltage levels, an optimal balance can be identified between maximal actuation force and minimal risk of electrical breakdown.
- Force - voltage at const. elongation

Blocking force measurements yield the same information as actuation force measurements, but with a different testing approach. In this method, the actuator is held at a fixed elongation, and the applied voltage is varied cyclically. The resulting change in mechanical force between the non-actuated and actuated states is recorded. This setup allows for the direct evaluation of the voltage-dependent force generation of the DEA at constant stretch, providing valuable data for applications where displacement is constrained and only force output varies with voltage.

- Electrical resistance
 - Breakdown field strength

Determining the electrical resistance as a function of stretch is particularly important for high-frequency applications, as the resistance directly influences the charging time of the capacitor. If the resistance is too high, the capacitor may not fully charge within the available time window, or it may require an impractically high current to do so.

The actuation force of a DEA is determined by material permittivity, applied voltage, and thickness of the elastomer film. As the voltage increases, the actuation force also increases. However, the limiting factor is the electrical breakdown strength of the material. It is therefore crucial to know the breakdown field strength (breakdown voltage divided by film thickness) in order to operate the actuator at the highest possible voltage while staying below the breakdown threshold. The breakdown voltage is determined by gradually increasing voltage until dielectric breakdown occurs. To obtain statistically reliable results, this test must be repeated across multiple samples. The relevance of the data is further improved by performing the tests under varying environmental conditions, such as temperature and humidity, as these factors significantly influence the dielectric breakdown behavior.

Figure 2.18 shows example measurement curves for thickness measurements along a DE membrane without electrodes to gain information about the thickness and variances in the thickness of the film. The curves depict thickness variation of over 2 μm , which is nearly 10 % of the average thickness. If the breakdown field is calculated based on the average thickness, the most likely breakdown location, however, is at the thinnest location of the film. Therefore, information about film homogeneity is highly important.

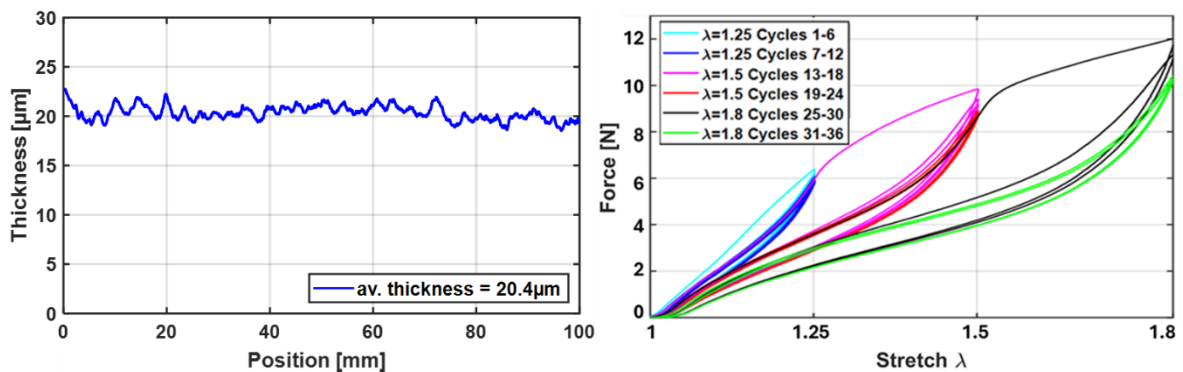


Figure 2.18. Representative measurements without applied electrodes relevant for DET design. Thickness profile across the dielectric elastomer membrane (left); force-stretch curves over multiple cycles, illustrating plastic deformation and viscoelastic effects (right).

The force-stretch curve in Figure 2.18 demonstrates two key mechanical effects typical of soft elastomers: Firstly, the initial loading cycle at each stretch rate exhibits a higher stiffness and a significantly larger hysteresis compared to subsequent cycles. This phenomenon is known as Mullins effect [136], a phenomenon observed in many polymers, in which irreversible microstructural rearrangements develop in the polymer chains the first time they are elongated. Secondly, the material still exhibits pseudo-elastic behavior, rather than purely elastic after the first cycle. The magnitude of this hysteresis is considerably smaller than during the first cycle, but it is still a critical

design consideration for DEA, as it reduces the effective actuation force between the actuated and non-actuated states, particularly under cyclic operation.

Figure 2.19 shows example measurements for the electro-mechanical characterization. These measurements require the presence of electrodes on the membrane. Important for the DEA design are force-stretch measurements, which are conducted with and without applied voltage. Understanding the force-stretch behavior is one of the most critical parameters for the design of a DEA. These tests are initially conducted without electrical excitation and then repeated under a constant voltage. To obtain meaningful results, the measurements should be repeated for various voltage levels. From these force-stretch curves, the actuation force can be determined by calculating the force difference between the actuated and non-actuated curves.

Alternatively, these measurements can be carried out by holding the actuator at a constant position while increasing the voltage from 0 V to the target voltage. This approach allows the behavior across the full voltage range to be captured in a single measurement. In this case, the measured force change is referred to as the blocking force. These measurements can be repeated under different excitation frequencies to reflect application-specific conditions. For proper interpretation of the results, it is essential that all test parameters are known and that the excitation signal is recorded and displayed alongside the force data.

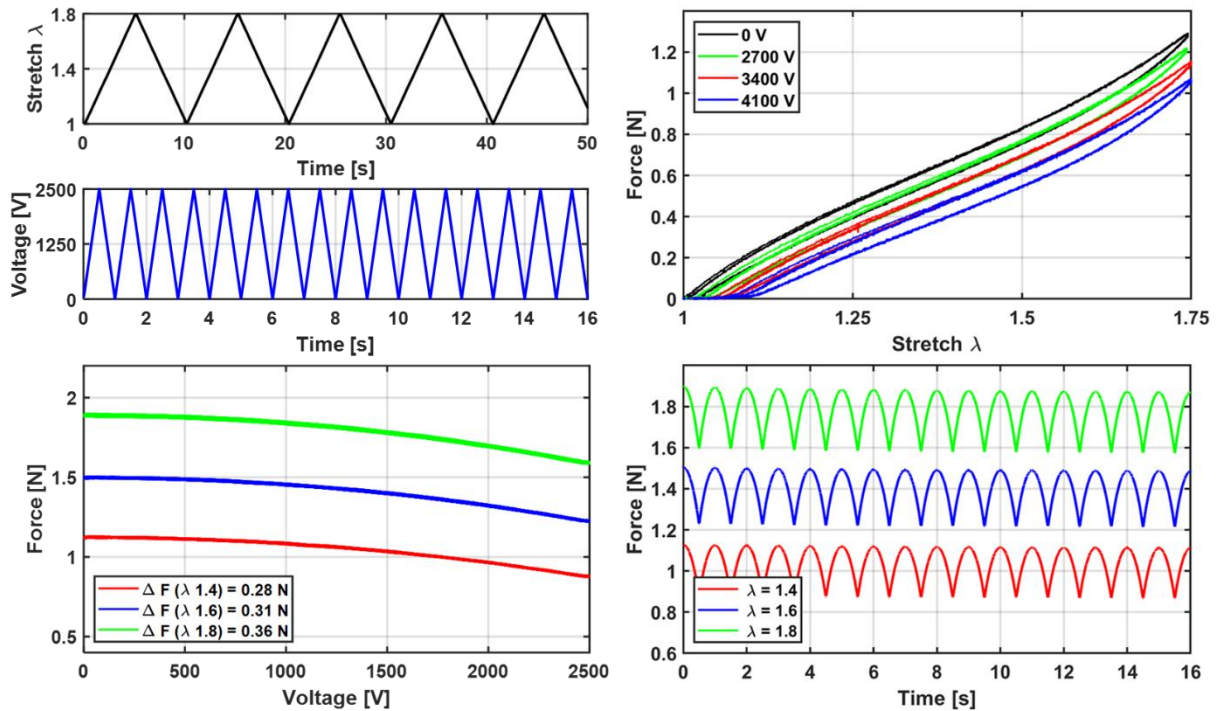


Figure 2.19. Representative measurements with applied electrodes relevant for DET design. Excitation signals (top left); force-stretch curves without voltage excitation and with constant voltage applied during elongation at different voltage levels (top right); constant-position tests at three fixed stretches with triangular voltage excitation showing resulting force responses (bottom); corresponding force-voltage relationships (left) and force-time responses (right).

As with DES, additional information about the long-term performance of the actuator as well as the operation of the DEA under different environmental conditions are essential, as both dielectric elastomers and electrodes may show fatigue over time or under environmental influences, potentially altering their behavior and affecting the reliability of the initial design.

2.4.4 Relevant material parameters for generator applications

- **Capacitance** Capacitance is the critical parameter for energy harvesting, as cyclic deformation leads to capacitance variation and subsequent harvestable voltage changes under fixed charge conditions.
- **Electrical resistance** Electrical resistance over stretch or time is an important parameter for the design of electronics that read and convert the capacitive signals of the sensor as it affects the signal quality and determines energy losses. Very high resistances typically require more expensive electronics.
- **Elongation (stretch)** The elongation determines the possible operating range of the generator. As the energy output increases with increasing capacitance change, high stretch rates are preferable.
- **Breakdown field strength** The harvested energy of a dielectric elastomer generator (DEG) depends on the change in capacitance and the maximum voltage difference applied during the energy cycle, Equation 3. Higher capacitance change and voltage yield greater energy potential. However, the limiting factor is the electrical breakdown strength of the material. It is therefore crucial to know the breakdown field strength in order to operate the generator at the highest possible voltage while staying below the breakdown threshold.

As with DES and DEA, environmental compatibility and long-term stability are critical for DEG operation. Dielectric elastomer generators may be exposed to extreme conditions, such as in wave energy harvesting applications. Both the dielectric elastomer and the electrodes may be more susceptible to fatigue under these conditions, which can impact the long-term reliability of the system. Therefore, preliminary testing under controlled environmental conditions, such as in climate chambers, is essential to evaluate durability and performance.

As previously mentioned, it is essential to investigate material parameters not only in short-term tests but also under long-term operation and varying environmental conditions. For this purpose, dedicated long-term test rigs have been developed. Long-term testers developed by Kühnel et al. [137] and Holz et al. [138] enable durability studies under different climatic conditions with dynamic voltage excitation and static pre-stretching of the samples. Systems developed by Hill [139] and Bruch [93] additionally allow dynamic mechanical stretching at different rates and velocities.

3. State of the Art

3.1 Manufacturing methods for electrodes

A variety of fabrication techniques are available for applying electrodes to dielectric elastomer films. These include simple methods such as spraying, as well as more advanced techniques like screen printing, inkjet printing, pad printing, and sputtering. Each technique offers specific advantages, making it suitable for different application requirements - ranging from rapid prototyping and miniaturization to the patterning of large-area electrodes, as well as ensuring reproducibility and acquisition cost.

Each of these methods is briefly described in the following section in respect to their applicability on silicone film, along with their respective advantages and disadvantages. As screen printing has been selected as the fabrication method for DET in this thesis - owing to its versatility and scalability for mass production - and the first paper provides a detailed analysis of how process parameters affect DET performance, this chapter places particular emphasis on this method.

3.1.1 Screen-printing

Screen printing is a versatile technique widely used across various industries, particularly for printing on textiles, paper, cardboard, metal, glass, plastics, and in the field of printable electronics. Although it is a well-established method in electronics manufacturing, its application to thin film highly stretchable silicone-based dielectric elastomer transducers has been limited due to challenges such as ink adhesion and the risk of membrane damage during printing. However, recent advancements in electrode manufacturing and parameter optimization in the iMSL lab have addressed many of these issues, making screen printing increasingly viable for DET fabrication [40, 45, 46]. The general procedure is outlined in this chapter, while detailed information on the process and the influence of manufacturing parameters on DET performance is provided in Chapter 4.

In this process, a viscous ink is applied through a mesh screen prepared with a stencil that defines the electrode pattern, allowing ink to pass only through the open areas. Mesh screens come in various thread counts and thicknesses, which determine the amount of ink deposited.

A picture of a screen printer is shown in Figure 3.1. Two squeegees (flood bar and fill bar) are operating during the print process. In a first step, the flood bar distributes the ink over the mesh. The mesh is then moved downwards until it is close to the silicone film, which is attached to a metal frame and placed in a position holder. When the mesh is in position, the fill bar presses the ink through the mesh. The mesh screen is pre-tensioned to ensure that, under downward pressure from the squeegee, it deflects just enough to make minimal contact with the silicone film, enabling precise ink transfer without the whole mesh connecting with the film. After the ink transfer is completed, the mesh moves up into the upper start position [140].

The screen-printing process requires a prefabricated mesh screen equipped with a stencil, which needs to be prepared prior to printing to define the DE electrode pattern. First, a mesh is coated with a photosensitive emulsion. Once dry, a pre-designed black pattern is placed on the screen and exposed to UV light. The areas not covered by the black electrode design are cured by UV light, while the covered regions remain uncured. These uncured areas are subsequently washed out, creating the desired stencil for printing.

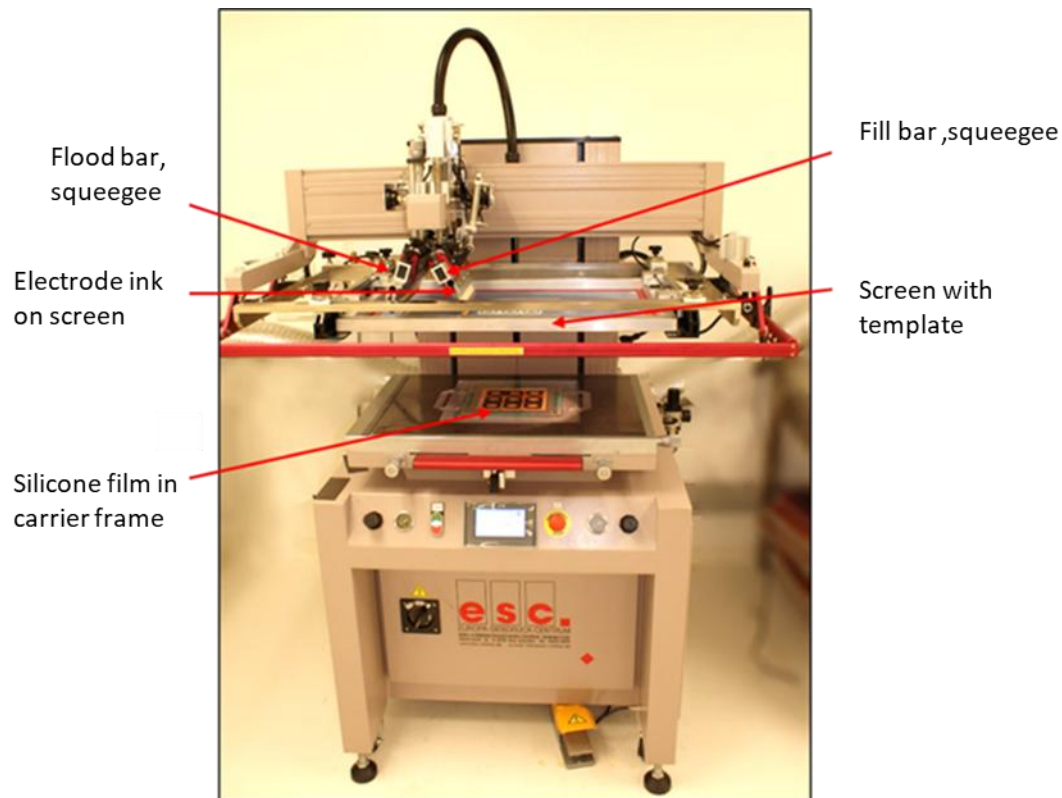


Figure 3.1. Semi- automatic screen printer setup with mesh, bars, and printed silicone film at the iMSL lab

The mesh without and with design and the proceeding print process is shown in Figure 3.2. Also shown in the figure is a carrier frame with an attached silicone film. In the iMSL lab, these carrier frames are used throughout the printing process to facilitate handling during fabrication, testing, and potential repairing. Additionally, the frame allows for easy rotation of the film, enabling electrode application on the reverse side for single-layer DEA fabrication.

Screen printing allows for precise control of the layer thickness through selection of the mesh size and amount of repetitive print layers. Design flexibility is virtually unlimited, allowing printing of small and large areas with high precision resolution. By predefining the printing parameters, the process can be repeated over thousands of cycles with consistent quality. Because the process is fast, upscaling to high quality mass production is possible. Another advantage is the printable high ink viscosity range, which allows printing of viscosities from 500 to 10,000 mPas [140]. This wide range is beneficial for the fabrication and development of new conductive materials in the field of DET.

The acquisition costs are higher than those of the spray process and are more comparable to those of inkjet printing and pad printing. Since a new screen must be fabricated for every design iteration, the method is comparatively labor-intensive for prototyping or low quantity printing. Additionally, a minimum amount of ink is required to carry out the squeegee process. This is not an issue in mass production, where the ink is continuously fed into the process. However, in small-scale production, the unused material must either be discarded or collected for future use. Due to the contact of film and screen a mechanical impact on the film is possible [141].

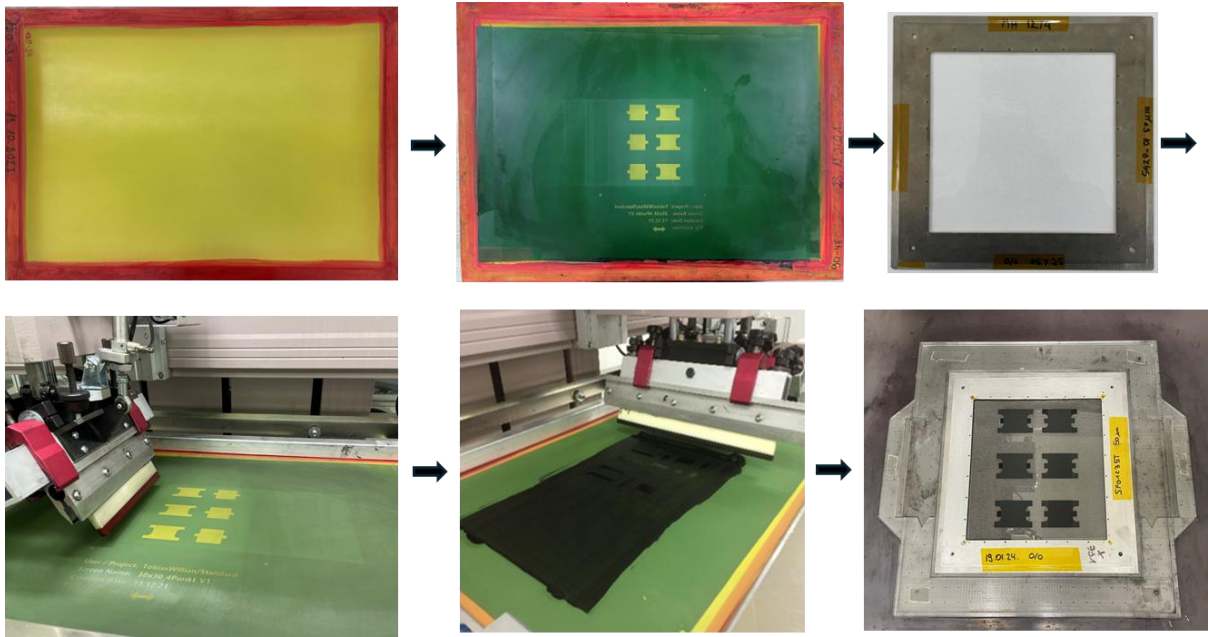


Figure 3.2. From mesh screen preparation to printed design. Top from left to right: Mesh screen, mesh screen coated with cured emulsion film and washed out electrode design, silicone film attached to carrier frame. Bottom left to right: Mesh screen in start position, flooding process, electrodes printed on both sides of the film attached to carrier frame located in a frame placement holder during the print process

Due to its scalability, near-unlimited design flexibility, broad viscosity tolerance, and robustness against clogging, screen printing was selected as the manufacturing method of choice for DEA in this thesis.

3.1.2 Spraying DET

Spraying is a well-established method for the manufacturing of DET [51, 52, 53].

Spraying or spray coating is a technique in which a liquid dispersion of conductive inks—such as carbon black, silver particles, or conductive polymers—is atomized into a fine aerosol and deposited onto the surface of a dielectric elastomer membrane. The conducted material is usually finely dispensed into a solvent, where the viscosity of the conductive ink is a critical parameter for achieving a uniform and thin layer, applicable in a viscosity range <100 mPas [142]. To maintain a well-dispersed solution the ink needs to be constantly stirred in an ultrasonic bath or on a magnetic stir plate. A simple nozzle, airbrush or automated nozzle system can be used to apply the ink. The pattern is created by placing a stencil with the defined electrode geometry onto the membrane, preventing the covered areas from being sprayed. To avoid paint or coating from seeping underneath the stencil, it is, for example, pressed down using a magnetic sheet [52]. After spraying, the solvent is evaporated in an oven or using a hot plate. The spray-coating method is a non-contact technique, however, the stencil used to define the electrode pattern must be firmly affixed to the film to prevent ink from seeping underneath.

The main advantage of spray coating lies in its low acquisition cost compared to other deposition methods. It also enables rapid prototyping, due to the ease of mask fabrication. Furthermore, spray coating offers high versatility, as it can be applied not only to flat or curved surfaces but also to complex geometries. However, the low viscosity required for spraying necessitates a high solvent

content, which makes the use of PDMS-based solutions challenging. Without a PDMS base or a comparable material, the electrodes do not adhere well to the silicone film and can be easily rubbed off. Spray nozzles are also prone to clogging, even with continuous stirring of the electrode suspension. Furthermore, unless the process is fully automated, achieving a uniform electrode thickness is difficult.

3.1.3 Inkjet printing

Inkjet printing is a non-contact, digitally controlled deposition technique that enables high-resolution and precise patterning. The process has been well established in laboratories across the dielectric elastomer research community [47, 49, 143, 144]. This section provides a brief overview of the key aspects relevant to understanding the process.

In this process, droplets of ink - for DEA fabrication conductive ink - are ejected from nozzles in a controlled manner onto the film surface. Most of the applications use the drop-on-demand-technique, in which ink droplets are generated on demand by a thermal or piezoelectric process. The positioning of the ink droplets is controlled by the digital print pattern specified in the computer-aided design file. After deposition, the printed electrodes are immediately cured through UV or thermal heating.

The conductive ink has a high solvent content to achieve the very low viscosity range between 10 and 20 mPas and small particle sizes. Nozzle clogging is the most significant issue in this process and requires frequent cleaning procedures. As with spray coating, the conductive ink must be kept in a homogeneous suspension to prevent particle settling. This can be achieved by using a combination of centrifuging and ultrasonication [145], which helps maintain a uniform dispersion of particles. Due to the high solvent content, adhesion to the film and conductivity at high stretch rates can be problematic. The print process is slow compared to the screen printing process.

The main advantage of this method lies in its flexibility. Since no screen or stencil is required, it is particularly well-suited for prototyping and low-volume production. The high printing resolution and the ability to print very fine lines allow for much smaller structures to be manufactured than with spraying, screen printing, or pad printing methods. Being a non-contact process, it eliminates mechanical stress on the film. Additionally, low ink consumption makes it especially suitable for printing with costly materials such as carbon nanotubes.

3.1.4 Pad printing

Over the last years, pad printing has been established for the fabrication of DET [49, 50, 145]

It is an indirect printing process that transfers ink from an etched plate (referred to as a *cliché*) onto a surface using a soft, flexible silicone pad. The process begins by applying ink to the etched image on the cliché. The silicone pad then presses onto the cliché, picking up the ink from the recessed areas. Next, it moves to the target surface and transfers the ink through a gentle stamping motion. Ink curing is performed in a separate step.

Thanks to the conformability of the silicone pad, pad printing is particularly well-suited for printing on irregular, curved, or textured surfaces. While slower than screen printing, it is significantly faster than inkjet printing. The method allows for the use of inks with viscosities between 1,500 and 2,000 mPas, enabling higher carbon content and lower solvent use - beneficial for highly conductive electrodes.

As a contact-based method, pad printing does impart mechanical stress on the membrane. However, due to the soft silicone pad, this impact is lower than that encountered in screen printing.

Like screen printing, which requires a screen mesh patterned with the electrode design, pad printing requires a custom-etched cliché. This makes the process less suitable for prototyping. Nonetheless, a simplified prototyping approach has been demonstrated: the ink is transferred directly to the entire surface of the silicone pad and then stamped onto a stencil-covered membrane - similar to the masking technique used in spray coating. Although this approach enables prototyping without a cliché, it significantly slows the process, as the stencil must be manually positioned for each print.

Pad printing is typically not used for large-area electrodes. However, recent work Holzer et al. [50] has notably extended the printable area, making the method more applicable for larger-scale DET applications.

3.1.5 Sputter process

Sputtering is a physical vapor deposition technique widely used to produce thin, highly conductive electrode layers deposited on DE membranes [56, 57, 146]. In this process, a target material - such as gold, silver, or nickel - is subjected to high-energy ions beams in a vacuum chamber. This causes atoms from the target to be ejected and deposited as a thin film onto the DE membrane. The method allows precise control over film thickness and uniformity, making it ideal for applications requiring high conductivity and reproducibility. However, sputtered electrodes are typically brittle and not stretchable, which limits their use to test setups where the electrodes are not subjected to mechanical strain. For this reason, sputtering is often employed in experimental studies of DETs where stretchability is not required but electrical performance and stability are critical [65]. To enable the use of this method for DETs under strain, Hubertus et al. [33] developed a process in which the electrodes are pre-stretched before sputtering and then relaxed afterward. The device is subsequently operated under strain levels that remain below the initial pre-stretch.

The advantage of this method is the manufacturing of high conductivity nanometer thin electrodes. A further processing step using laser ablation allows for microscale designs and microstructures, which even include the electrode connections to the voltage supply and measurement equipment due to the high conductivity of the electrodes. Laser ablation also has the advantage that it eliminates the need for a stencil but it requires an additional processing step.

A key disadvantage of sputtering is the high investment cost and the complexity of the process. The chamber size restricts electrode dimensions, and scaling up requires significantly more expensive equipment. Additionally, the high cost of target materials such as gold, combined with substantial energy consumption, contributes to elevated manufacturing costs. The process is slow, as achieving the required ultra-high vacuum ($\sim 10^{-6}$ bar) requires long setup times [147]. While multi-chamber systems can mitigate this, sputtering remains impractical for large-scale DET production. However, it enables the precise fabrication of high-quality electrodes for millimeter-scale DET.

3.2 Breakdown test methods

3.2.1 Electrical breakdown strength tester designed at Department of Chemical and Biochemical Engineering, The Danish Polymer Center

Yu et al. [59] presents electrical breakdown tests on an in-house-built breakdown device developed at the *Department of Chemical and Biochemical Engineering, The Danish Polymer Center, DTU, Lyngby, Denmark*. First, the film thickness is measured through optical microscopy of cross-sectional cuts, using a LEICA DM LB microscopical camera. The polymer film is tested between two spherical electrodes. The distance between the electrodes is set to a distance of 5 % less than the measured polymer thickness, which is adjusted using a micrometer stage and a gauge.

The breakdown strength is measured by stepwise increasing voltage in 50 to 100 volts per step at a rate of 0.5 to 1 step per second.

The breakdown device enclosed and the temperature within the box is adjusted using a hot air gun and a thermometer. Breakdown tests are conducted in a temperature range between 20 °C and 80 °C. Tests can be performed on unstretched and pre-stretched polymer films. The procedure consists of testing 20 measurement points per test configuration.

Figure 3.3 shows the setup for the electrical breakdown device.

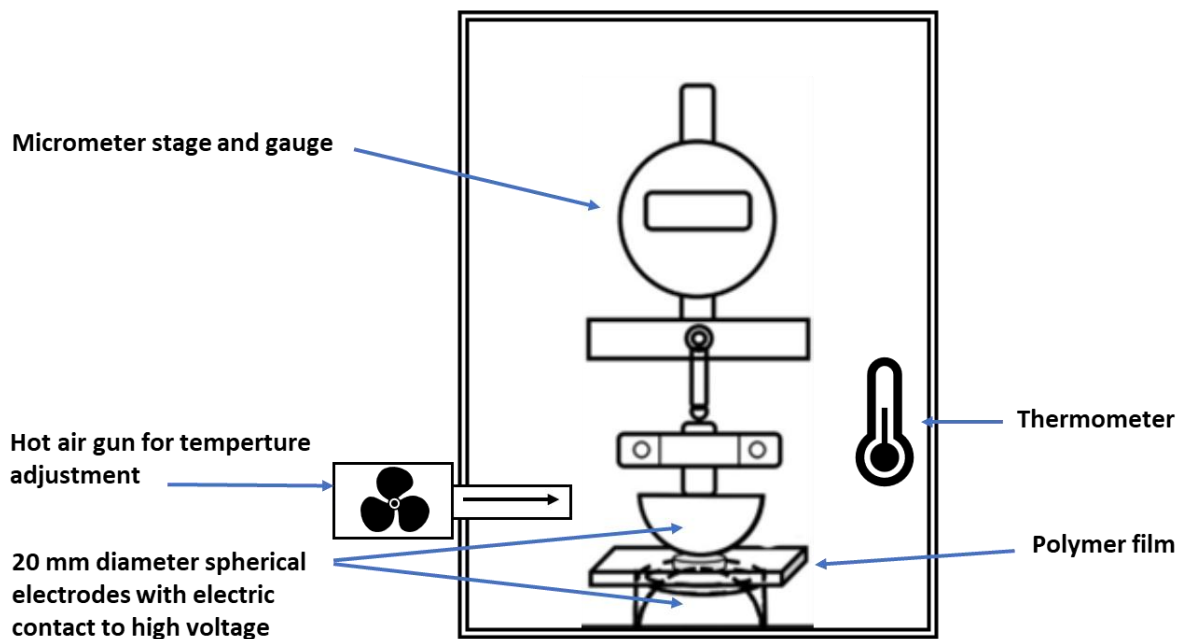


Figure 3.3. Illustration of electrical breakdown setup by Yu et al. [59]. The experimental temperatures are adjusted and measured using a hot air gun and a thermometer. The setup is located in an enclosed housing. The figure is adapted from Yu et al.

3.2.2 Dielectric breakdown test stand designed at TU Darmstadt, Mikrotechnik und Elektromechanische Systems, I

Gatti et al. [62] developed a breakdown tester at TU Darmstadt in the *Mikrotechnik und Elektromechanische Systeme* Laboratory. The tester consists of a copper plate serving as the ground electrode and a 6 mm copper cylinder, lowered onto the polymer film from above, functioning as the

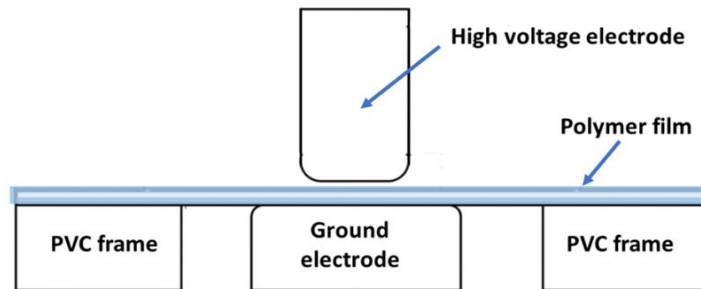


Figure 3.4. Schematic of a test stand for dielectric breakdown field strength by Gatti et al. [62], figure adapted from Gatti et al.

second electrode. The cylinder is polished and features rounded edges to minimize electric field inhomogeneities caused by sharp tips, which can lead to charge accumulation and local deformation.

The experiment is conducted by gradually increasing the voltage, supplied by an in-house 0 - 15 kV DC voltage amplifier, until the breakdown voltage is reached. The voltage is held constant for 20 seconds before being increased in 100 V increments. Breakdown is defined as the point at which a sudden, steep increase in leakage current is observed, with the breakdown voltage taken as the preceding voltage step.

The tester is used to investigate the influence of film thickness and pre-stretch on the breakdown field of the polymer films. The tests are conducted on pure films without added electrodes. The thickness of unstretched samples is measured using a Veeco Dektak 150+ surface profilometer with a stylus force of 1 mg. For stretched samples, a thickness screw gauge is used. These measurements are then used to calculate the breakdown field.

3.2.3 Electrical breakdown designed at TU Darmstadt, Mikrotechnik und Elektromechanische Systems, II

Förster-Zügel et al. [135], extended the test setup of Gatti et al. [62] at the *TU Darmstadt, Mikrotechnik und Elektromechanische Systems Lab*, to enable breakdown tests on polymer films in various ambient media, such as solids, liquids, and gases. For this purpose, a tester was designed consisting of ten cylindrical high-voltage electrodes, each equipped with a helical spring and arranged in a circular pattern, and a brass plate serving as the ground electrode, Figure 3.5. The test apparatus is enclosed in an acrylic glass cylinder that can be filled with various media. Unlike the previous setup, no air is present around the electrodes, as the cylinder is entirely filled with the chosen medium. The diameter of the high-voltage electrodes has been slightly increased from 6 mm to 8 mm, while retaining the rounded-edge design. With ten electrode connections available, it is no longer necessary to replace the film after each breakdown.

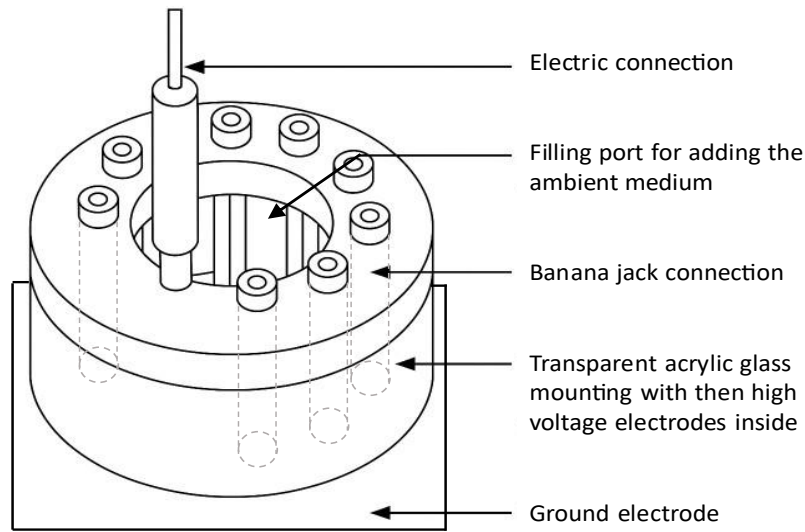


Figure 3.5 Experimental measurement setup for the characterization of the dielectric breakdown field strength of thin elastic films in various ambient media designed by Förster-Zügel et al. [135]. Figure adapted from Förster-Zügel.

The setup allows testing of elastomer films with thicknesses between 20 μm and 200 μm , either in unstretched or pre-stretched state. Each electrode is equipped with a banana jack, enabling an individual high-voltage connection to each electrode. Breakdown tests are performed sequentially for each electrode.

The thickness of the polymer samples is measured using the same measurement equipment as described in Section 3.2.2 to calculate the breakdown field.

3.2.4 Electrical breakdown strength at TU Darmstadt, Mikrotechnik und Elektromechanische Systems, III

Förster-Zügel et al. [148], from the *TU Darmstadt, Mikrotechnik und Elektromechanische Systems Lab*, also developed a breakdown test setup that enables investigations into the influence of pre-stretch and voltage excitation (AC up to 500 Hz and DC) on the electrical breakdown field of single-layer DET. In addition, the tester allows evaluation of the effect of a protective layer made of silicone material, applied to both sides of the DET, on the breakdown field.

A schematic of the test setup is shown in Figure 3.6. Silicone film is prepared with two electrodes and clamped between two PMMA frames. The electrodes overlap in the middle of the frame, forming the active part of the DET. The electrodes are equipped with connecting arms to high voltage or ground electrode outside of the frames on opposite sides. The electrode diameter is 6 mm; however, tests were also carried out with unequal electrode sizes, keeping the high-voltage electrode at 6 mm while increasing the ground electrode to 12 mm.

The thickness of the polymer samples is measured using an ATORM digital gauge before the application of the electrodes. A total of ten breakdown measurements is conducted for each sample configuration.

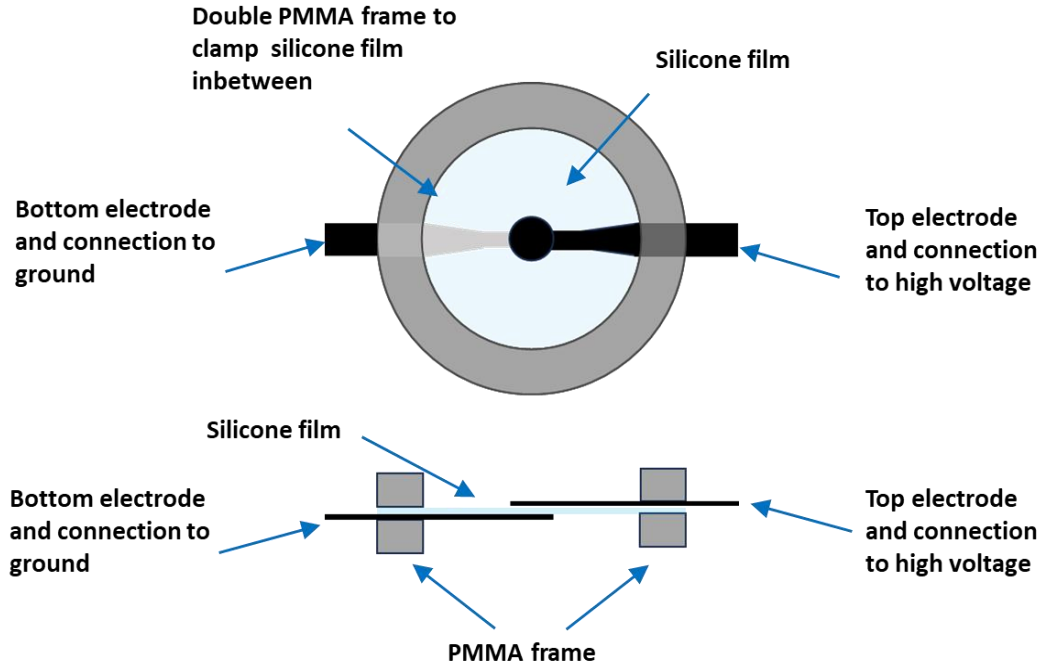


Figure 3.6. Schematic breakdown test setup for single-layer DET samples clamped between two frames by Förster-Zügel et al. [148]. Top view with circular electrodes on top and bottom (overlapping and forming the active part of the DET) and electrode connection to high voltage on top and to ground on the bottom (top). Cross section of breakdown tester (bottom). Figure adapted from Förster-Zügel et al.

3.2.5 Electrical breakdown strength tester designed at Soft Transducers Laboratory, Ecole Polytechnique Fédérale de Lausanne

Beco Albuquerque et al. [60], Soft Transducers Laboratory, Ecole Polytechnique Fédérale de Lausanne (EPFL), Neuchâtel, Switzerland, has developed a breakdown tester that allows testing of both unstretched and pre-stretched elastomer films under various climatic conditions in a climate chamber. A schematic of the breakdown tester is shown in Figure 3.7. It consists of a glass plate measuring 32 mm × 17 mm, onto which a 1 mm wide gold-sputtered electrode has been deposited along its entire length in the center, serving as the ground electrode.

An elastomer film, which is mounted on a PMMA frame, is equipped with six gold-sputtered electrodes, each consisting of a 4 mm circular contact electrode with a 1 mm wide electrode arm. It is placed on the glass plate in such a way that each electrode arm overlaps the ground electrode with an area of 1 mm².

To determine the breakdown voltage, a metal cylinder with a diameter of 4 mm is sequentially placed on the circular area of each electrode. The breakdown test is then carried out for each electrode in turn, with the activated area per electrode being 1 mm².

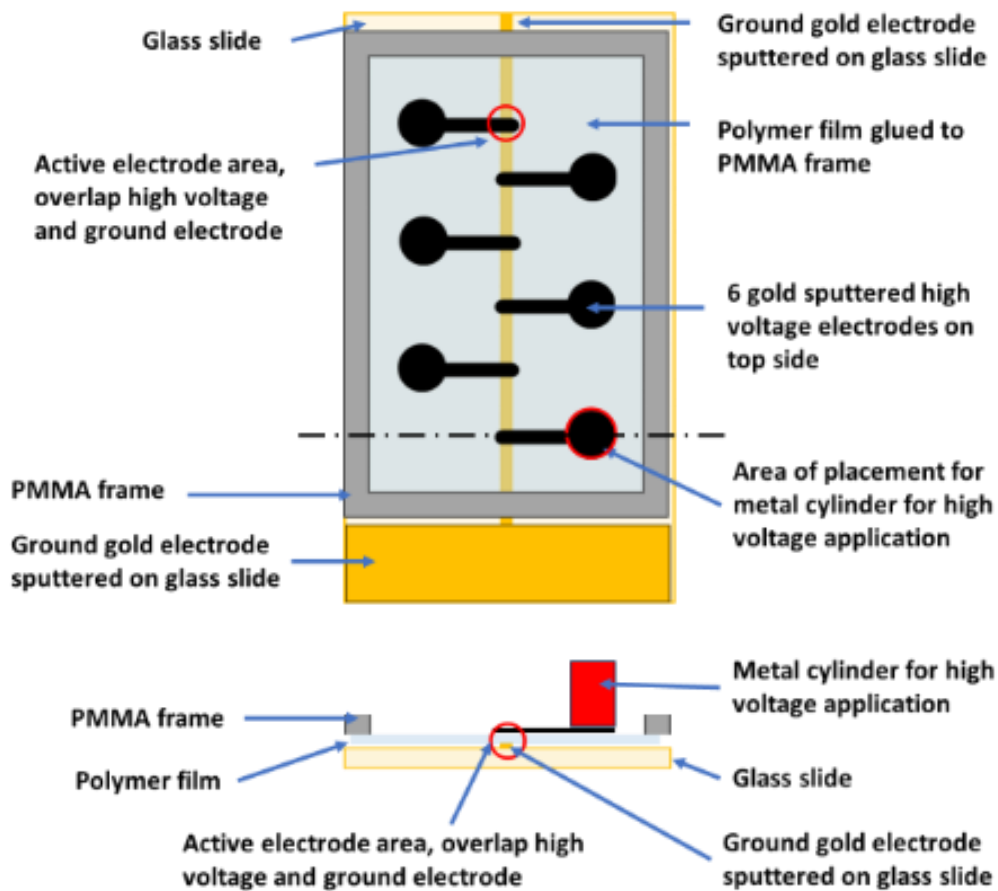


Figure 3.7. Schematic of the breakdown tester developed by Beco Albuquerque et al. [60] for breakdown tests on pre-stretched and unstretched film under varying environmental conditions. Top view (top) and cross - section (bottom) of the tester with indication of the individual components. Figure adapted from Beco Albuquerque et al.

4. Cumulative Part: Advanced manufacturing method and electrical failure analysis

The cumulative part of this thesis focuses on further developing the extensive fundamental research on DEA that has been conducted by many research groups over the past decades, with the aim of enabling large-scale industrial applicability. The objective of this work is to establish a solid scientific foundation and a fundamental understanding of the key parameters that influence the reliable operation of dielectric elastomer actuators.

Since a DEA consists of two main components—the electrode and the elastomer film—it is first necessary to develop a suitable fabrication method that allows for the electrode, which has so far often been applied manually at the laboratory scale, to be produced with high accuracy, repeatability, and throughput, while exhibiting high robustness and strong film adhesion in operation. In this thesis, silicone thin films are exclusively used for the manufacturing of DEA due to their good elastic properties, which allow applications with frequencies in the kilohertz regime, their hydrophobicity, high temperature stability (ranging from -45 °C to 200 °C), and commercial availability in a wide range of thicknesses.

Screen printing is selected as the electrode fabrication method of choice. Its high throughput, design flexibility, wide applicable viscosity range of electrode materials, and high reproducibility in accuracy make it particularly suitable for this application.

This thesis presents the first scientific study on the optimization of DE screen-printing parameters using a carbon black/polydimethylsiloxane (CB/PDMS) electrode material on silicone thin films. In particular, the effect of mesh geometries and number of printed electrode layers on various electrical and mechanical DEA performance parameters have been systematically studied and provide a basis for further optimization steps in the future.

In addition to understanding the effects of manufacturing processes on electrode properties, it is essential to identify and understand the parameters that influence the functionality of the core DEA film material. Of particular importance is its electrical breakdown strength under high voltages, specifically under varying environmental conditions such as temperature and humidity, as well as the impact of preparatory process parameters, e.g., the amount of pre-stretch prior to operation.

These objectives are addressed in Chapter 4 through four key publications which form the foundation of the cumulative part of this thesis. These publications are arranged chronologically, reflecting the thematic progression of the research. Thematically, they are divided into manufacturing, with the paper “Effect of screen printing parameters on sensor and actuator performance of dielectric elastomer (DE) membranes”, Section 4.1, and into electrical breakdown investigations. Electrical breakdown investigations contain the conference proceedings paper “Dielectric breakdown test setup for dielectric elastomers: design and validation”, Section 4.2, and two peer reviewed journal papers: “Effect of actuation parameters and environment on the breakdown voltage of silicone dielectric elastomer films”, Section 4.3, and “Electrode Impact on the Electrical Breakdown of Dielectric Elastomer Thin Films”, Section 4.4. The influence of the electrode is addressed throughout all papers, because it influences the mechanical performance addressed in Section 4.1 as well as the breakdown behavior addressed in Sections 4.3 and 4.4.

This study is based on the development of a consistent electrode manufacturing process across numerous batches over several years, providing a reliable basis for all subsequent investigations on DEA performance. Such consistency ensured that observed effects could be attributed to specific testing conditions rather than to variations in electrode properties caused by manufacturing

inconsistencies. Electrode quality in each batch is verified through visual inspection and resistance measurements.

The second section, electrical breakdown investigations, comprises of three published papers and presents a first comprehensive study on the breakdown behavior of dielectric elastomers using the same standardized test setup. This section explores key parameters influencing electrical breakdown, covering a wide range of environmental conditions, pre-stretch, manufacturing method for electrode application, and electrode composition.

The first paper “Dielectric breakdown test setup for dielectric elastomers: design and validation”, published as part of a conference proceeding, describes the development and design of a novel breakdown tester, which ensures repeatable and automated breakdown tests within a climate chamber. The design of the breakdown tester includes massive external gold plated electrodes, enabling tests of pure silicone film material as well as film material with various applied electrodes.

This breakdown tester is employed in the subsequent studies. The investigations in the paper “Effect of actuation parameters and environment on the breakdown voltage of silicone dielectric elastomer films” cover a climatic range that is present in industrial facilities where many technical applications of DEA, e.g. pumps and valves, are present (10 °C to 50 °C and 20 % to 95 % relative humidity).

The first set of experiments investigates 50 µm silicone thin films without applied electrodes, examining their breakdown without pre-stretch and under different levels of pre-stretch under the ambient conditions listed above. Since technical applications require the presence of electrodes on the film, these experiments were subsequently repeated using the same film and screen-printed carbon black electrodes applied to the membrane.

A significant influence of the electrodes on the breakdown field was observed, raising the question of whether this effect stemmed from the electrode material itself or the manufacturing process. While many breakdown studies exist in the literature [70 - 73]. However, direct comparison is challenging due to differences in test setups, experimental conditions, film material and thickness, membrane pre-stretch, and electrodes application method.

This challenge motivated the concept of a collaborative study, in which multiple electrodes - manufactured using different methods but applied to the same film material with identical pre-stretch - were tested using the same breakdown tester (Section 4.2) within a controlled climate chamber. Three different research groups participated and provided DEA manufactured with different electrodes. The results of this investigation are summarized in the paper “Electrode Impact on the Electrical Breakdown of Dielectric Elastomer Thin Films” (Section 4.4) and provide an important contribution to understanding the influence of electrodes on DEA breakdown behavior.

4.1 Effect of screen printing parameters on sensor and actuator performance of dielectric elastomer (DE) membranes

Bettina Fasolt¹, Micah Hodgins², Gianluca Rizzello², Stefan Seelecke^{1,2}

- ¹ Center for Mechatronics and Automation Technologies (ZeMA), Saarbrücken, Germany
- ² Department of Systems Engineering, Department of Materials Science & Engineering, Saarland University, Saarbrücken, Germany

Publication: Sensors and Actuators A: Physical

Publisher: Elsevier

October 1, 2017

Citations: 110

Impact Factor: 4.1

DOI: 10.1016/j.sna.2017.08.028

Journal Author Rights Elsevier: The author retains the right to include publication in a thesis or dissertation provided it is cited and not published commercially. Permission is not required.

The paper provides a systematic study of the effect of screen-printing parameters on the electromechanical performance of DEA. It particularly highlights two important parameters of the screen-printing process: screen dimensions and number of printed layers and discusses the influence of these two parameters on the print image, electrode thickness, electrical resistance, capacitance, and actuation force in detail.

The conceptualization of the paper was developed by Bettina Fasolt, who also conducted the investigations, manufactured the samples via screen printing, prepared the samples, and wrote the majority of the paper. She performed the experimental investigations on a test rig, which was designed and built by Micah Hodgins, who also programmed the test setup and implemented the required test routines.

The selection of the screen, also known as mesh, significantly influences the properties of the screen-printed product. A mesh is defined by its thread count per centimeter as well as the thread thickness. These factors determine the mesh opening degree, which affects the amount of material that can pass through during printing. Three mesh sizes were selected, ranging from fine (120 threads/cm), over medium (60 threads/cm) to coarse (27 threads/cm), with each step doubling the thread count while halving the thread thickness. Another key parameter influencing the properties is the number of repeated printed layers, with one, two, and three layers considered for each mesh size.

Enlarged photos reveal the printing pattern for each configuration. Interestingly, these patterns differ from the expected ones, where the ink typically follows the mesh openings, and the threads should be as thin as possible to maintain conductivity—such as in silver-printed electronics. Instead, the carbon black ink on the silicone film exhibits an imprint of the threads, significantly influencing mesh selection for screen printing DETs. Contrary to conventional expectations, a thicker thread is now preferable. When multiple layers are printed, each subsequent layer adheres to the crosslinked ink on the film, progressively emphasizing the mesh opening pattern with each additional layer.

The electrode layer thickness increases with each additional print pass, effectively adding the thickness for each additional layer. As a result, a three-layer print using a fine mesh (120 threads/cm) achieves a similar thickness to a single-layer print using a coarse mesh (27 threads/cm). However, the electrical resistance during deflection is consistently lower with the fine mesh multi-layer print. This is because subsequent layers not only reinforce the areas initially covered by the mesh threads but also progressively fill in regions left uncovered in the first pass, resulting in a more uniform and conductive electrode surface.

The thickness of the electrode also determines the hysteretic mechanical behavior of the DET, which is true for both cases, when voltage is applied and without voltage. With increasing thickness, the DEA becomes stiffer and the hysteresis larger. The actuation force, however, is not affected. It is also important to note that while a very thin electrode has minimal stiffening effects, its high resistance prevents a DEA from operating at high frequencies. Additionally, such high resistance makes certain electronic measurements, such as capacitance and resistance measurements using an LCR meter, no longer feasible.

The results suggest that, for sensor applications, a coarser mesh or a two- to three-layer print with minimal electrical resistance is preferable. For actuator applications, however, the mesh and printing parameters must be tailored to the specific DEA configuration. A thin electrode layer minimizes mechanical hysteresis and stiffening of the DEA, yet its higher resistance can be disadvantageous in high-frequency applications, where rapid charging and low current flow are critical. In such cases, multi-layer printing is the more suitable approach.



Effect of screen printing parameters on sensor and actuator performance of dielectric elastomer (DE) membranes

Bettina Fasolt^{a,*}, Micah Hodgins^b, Gianluca Rizzello^b, Stefan Seelecke^{a,b}

^a Center for Mechatronics and Automation Technologies (ZeMA), Saarbrücken, Germany

^b Department of Systems Engineering, Department of Materials Science & Engineering, Saarland University, Saarbrücken, Germany

ARTICLE INFO

Article history:

Received 31 January 2017

Received in revised form 14 August 2017

Accepted 15 August 2017

Available online 19 August 2017

Keywords:

Dielectric elastomers

Actuators and sensors

Sheet resistance

Compliant electrodes

Screen printing

Electromechanical characterization

ABSTRACT

Screen printing represents an effective way for applying stretchable electrodes on silicone thin films for the fabrication of dielectric elastomer transducers (DET). Screen printing allows to manufacture a multitude of patternable designs for actuator and sensor applications, in such a way the same methodology can be used for prototyping as well as for large-scale production. The fabrication of DETs does not only require the development of a flexible, highly conductive electrode material, which adheres to a stretched and un-stretched silicone film, but also calls for a thorough understanding of the effects of the different printing parameters. This work studies the influence of screen dimensions (open area, mesh thickness) as well as the influence of multiple-layer-printing on the electrode stiffness, electrical resistance and capacitance as well as actuator performance. The investigation is conducted in a custom-built testing device, which enables electro-mechanical characterization of the DET, performing simultaneous measurements of parameters such as strain, voltage, force, sheet resistance, capacitance, and membrane thickness. Magnified pictures of the electrodes additionally illustrate the effects of the different printing parameters.

© 2017 Elsevier B.V. All rights reserved.

1. Introduction

In recent years, interest in applications for dielectric elastomer transducers (DETs) as actuators, sensors, or generators is increasing in the research community as well as in industry [1–4]. A standard DET simply consists of a compliant dielectric elastomer sandwiched between two stretchable electrodes. When a voltage is applied to the electrodes, electrostatic forces lead to a reduction of the membrane thickness along with a simultaneous lateral expansion, thus resulting in controllable motion. Applications such as valves [5], [6], sensors [7], and tactile devices [8] are ready for marketing or are already on the market. It is remarked how three main parameters are important for the fabrication of DETs: a dielectric elastomer with a high breakdown field and a high permittivity [9], a highly compliant, conductive, patternable, thin (relative to film) and robust electrode [10], and a fabrication process, which has to be standardized and scalable for future commercial mass-production.

Investigations of available dielectric elastomer materials and their improvements for DET applications are conducted in ongoing studies [11–14]. At the same time, various potential electrode materials have been investigated [15]. Metals, e.g., silver, are stiff but have excellent conductivity for strains less than 12% [16]. Organic materials such as polyethylenedioxythiophene/polystyrene sulfonate (PEDOT/PSS) are flexible and conductive [17], but the material is expensive and does not adhere to the silicone DE without pre-conditioning. The preferred electrode material has primarily been carbon based (such as carbon black), because it is low-priced and is easily dispersed into an elastomer matrix. Alternative conductive filler materials which are also used include graphite powder [18,19], and carbon nanotubes [20]. Carbon black dispensed into oil/grease is easily applied by hand [21], but the electrodes remain wet for some time before drying out and losing conductivity [10]. Alternatively, two-component silicone elastomer mixes can be filled with conductive particles and cured with heat or UV to serve as conductive and compliant electrodes [22]. Preliminary investigation of the influence of the electrode on DET performance has been performed in [23].

For the study proposed in this paper, the electrode material consists of carbon black, polydimethylsiloxane (PDMS), silicone oil, and different solvents. The composition of the electrode (size and concentration of carbon black particles in the matrix) impacts

* Corresponding author.

E-mail addresses: b.fasolt@zema.de (B. Fasolt), micah.hodgins@imsl.uni-saarland.de (M. Hodgins), gianluca.rizzello@imsl.uni-saarland.de (G. Rizzello), stefan.seelecke@imsl.uni-saarland.de (S. Seelecke).

the stiffness and conductivity of the printed layer. Not only carbon black and PDMS content play a role, but also solvents, mixing, and curing/aging can impact film and electrode electromechanical behavior. Different fabrication methods are used for applying the electrode, such as pad-printing [24,25], screen printing [26], spin-coating, spraying, and blade casting with laser ablation [27]. While each method has advantages and disadvantages, the authors chose screen printing as the preferred method in this study. Screen printing is a well-established process for patterning thin layers on a variety of substrates. It can be used for prototyping as well as for large-scale production. While screen printing of flexible electronics is an established technology, e.g., [28–30], printing on stretchable silicone thin film is challenging, since the electrode material has to adhere to the film while stretching up to 100%, and at the same time it needs to ensure electrical conductivity without a significant impact on the film mechanical behavior [31]. Screen printing process parameters, like mesh, size and number of printed layers, also affect the device performance. Since these parameters influence the thickness of the electrodes, it can directly impact not only the electrical but also the mechanical response of DETs. Therefore, in this study, systematic electromechanical measurements are performed to understand the influence of electrode thickness and layering on quantities like sheet resistance and force generation of in-plane membrane DETs. These results will factor into the selection of appropriate parameters for actuator and/or sensor applications.

2. Experimental setup and procedure

2.1. Materials, specimen design and fabrication

A Wacker Elastasil 2030, 50 μm silicone film, is used in this paper as dielectric elastomer material. The protective cover is removed from the film, and then the film is clamped between two carrier frames without pre-stretch. The frame is utilized to handle the film during the printing process. For the electrode material, a Wacker RTV-2, polydimethylsiloxane is mixed with Orion Printex XE2 carbon black, and Wacker AK 100 K silicone oil. Solvent, Coats Screen Inks VD 60, and additive, Coats Screen Inks VM1, are added to obtain screen printability. The electrode material is processed in an EXAKT 3-roll-mill and a Thinky planetary mixer to homogenize the material. The composition of the mixture after curing (without solvents) consists of 20 wt% carbon black, 30 wt% silicone oil and 50 wt% PDMS.

Three different mesh sizes of Sefar PET 1500 monofilament polyester screens with a plain weave 1:1 are used to investigate the influence of screen dimensions: 27/70–120W, 61/156–64Y and 120/305–34Y. The mesh size 27/70–120W refers to a mesh with 27 threads per cm (70 threads per inch), a thread diameter of 120 μm , with a thread color W-white (Y-yellow, respectively).

Each screen is coated with an UV-sensitive photo emulsion film. The emulsion film is adjusted to the mesh size. An 80 μm emulsion film is used for Mesh27, 40 μm film for Mesh60, and 20 μm film for Mesh120. An image is printed in black on transparent overlay (shadow mask) with two different test designs. The overlay is then placed on the screen and exposed to UV light with 350–420 nm spectrum. The emulsion film areas not exposed to UV light are dissolved with water and washed away.

The electrodes are subsequently printed with a semi-automatic screen printer (ESC-AT 60P). Samples are prepared with one layer, two layers, and three layers prints for each mesh size, see Table 1. After one electrode layer is printed, the carrier frame is placed in a ventilated oven at 150 $^{\circ}\text{C}$ for 15 min to cure the electrode. After the last layer is printed, the electrodes are heat cured for an additional two hours. After the printing and curing process, two monolithic 3D-printed reinforcement frames are applied to sandwich the film. These frames are designed in a way that the whole unit (which

Table 1
The 9 print configurations

No. of layers	mesh size (threads/cm)		
	27	60	120
1	x	x	x
2	x	x	x
3	x	x	x

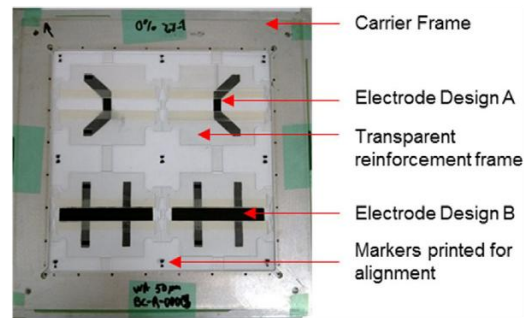


Fig. 1. Carrier frame with printed electrodes (two different designs) and reinforcement frames, showing the exact positioning using connected spacers for alignment.

forms four test specimens with two different designs) is aligned precisely in the opening of the carrier frame via the connected offset spacers, see Fig. 1. The two different designs A and B are described in Section 2.2.

2.2. Specimen design

Two different pure-shear test designs are prepared. One design is used to study the stretch-resistance relationship and to acquire enlarged pictures and videos (design A), while the second design (design B) is used to study the impact of the electrodes on membrane stiffness and actuation. The stretchable area of the DE film for both designs is 75 mm \times 10 mm. For design A, an electrode is printed only on one side of the film with an active testing area of 6 mm \times 10 mm. (Fig. 2(a)). Design B is prepared similarly to the previous one, but with electrodes covering 70 mm \times 10 mm of the active area on both sides of the film (Fig. 2(b)). The aspect ratio of 7–1 is chosen in accordance with the standard recommended in [32] to obtain approximately pure-shear conditions. A 2.5 mm passive region is left at the edges to prevent shorting across electrodes. Electrodes to link to the contact points in the un-stretchable area are printed on both designs, and then covered with a reinforcement frame. The DE film is sandwiched between thin monolithic reinforcement frames, for handling and defined positioning in the test rig clamps. Once adjusted in a test rig, the sacrificial connection spacers are cut and the test initiated.

2.3. Test rig design

The test rig is a custom designed tensile tester, as detailed explained in [33]. The test device is designed to obtain test results for a variety of different samples under repeatable conditions. The reinforcement frame ensures that the test samples are always placed in the tester in the exact same location and under identical conditions. In this way, alignment and/or specimen geometry errors are minimized and valid comparisons can be made between specimens.

Fig. 3 shows a photo and a drawing of the tester and setup.

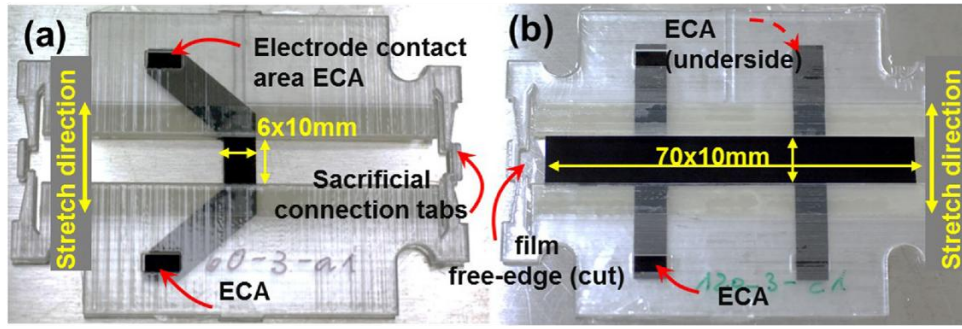


Fig. 2. Photo (a) shows a resistive specimen design A with the electrode pattern on one side only. Photo (b) shows an actuator specimen with electrodes patterned on both sides, design B.

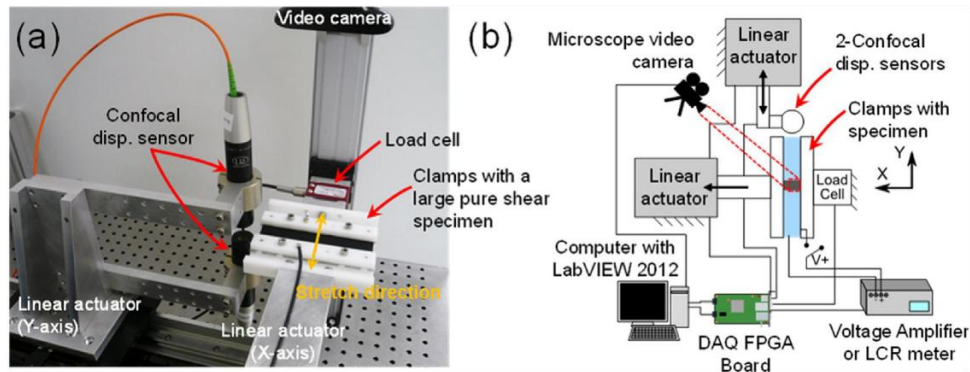


Fig. 3. Photo (a) and drawing (b) of the test setup.

Table 2

Overview of the tests performed with samples form design A and design B.

Design A, Fig. 2(a)	Design B, Fig. 2(a)
<ul style="list-style-type: none"> $\lambda = 1$: Thickness measurement, resistance and magnified photo with microscope, @0 V $\lambda = 1$ to $\lambda = 1.7$, 1.2 mm/s (0.1 Hz): Tensile test electrode resistance vs. stretch response, 6 cycles @0 V $\lambda = 1.7$ Film thickness measurement, resistance and magnified photo @0 V 	<ul style="list-style-type: none"> $\lambda = 1$: Thickness measurement, resistance, capacitance $\lambda = 1$ to $\lambda = 1.7$, 1.2 mm/s: Tensile test electrode resistance vs. stretch response, 6 cycles @0 V $\lambda = 1$ to $\lambda = 1.7$, 0.1 Hz: Tensile test @2700 V (max. 93 V/μm) $\lambda = 1.6$: Constant position, voltage 0 V to 2700 V at 0.1 Hz, 1 Hz, 10 Hz

2.4. Test procedure

Systematic tests are performed for each specimen at different stretches λ with voltages ranging from 0 V to 2700 V. An overview of the tests is shown in Table 2.

3. Results

The purpose of the investigation presented in this section is the electromechanical analysis of silicone membrane DETs, which are manufactured using screen printing with three different screen

dimensions and one, two, and three print layers to predicate the optimal printing parameters for sensor and actuator applications. Firstly, we detail the findings about the resistance/stretch behavior on one-sided electrode samples and support the findings by visual illustration from microscopic photographs, showing features of the printed electrode structure resulting from the screen-printing process, design A. Then we discuss the electrical properties, such as resistance and capacitance, as well as the effect of printing parameters on the force and stiffness characteristics of the DETs for two-sided electrodes, design B.

3.1. Design A: resistance specimens

For the characterization of the electrodes' resistive behavior, a specimen is manufactured with only one electrode printed on the top surface of the specimen, see Fig. 2a. This allows us to take photographs enhanced by a translucent light source revealing the printing patterns. Even though the experiments are conducted with three mesh sizes, for clarity only the coarse and fine mesh are depicted in the photographs and thickness scans.

Fig. 4 shows optical photographs of the printing patterns resulting from usage of coarse (top) and fine (bottom) meshes, displayed in the rightmost column. For one layer, we clearly recognize the mesh structure in the unstretched state ($\lambda=1.0$, first and third row). For two layers this is increasingly homogenized, and for three layers the electrode area is almost fully covered. The second and fourth rows show the same electrodes under a stretch of $\lambda=1.7$ in the horizontal direction, leading to a very noticeable deformation of the electrode grid. At $\lambda=1.7$, large areas of the surface printed with the fine mesh and a 1-layer-print are only covered with very little electrode material.

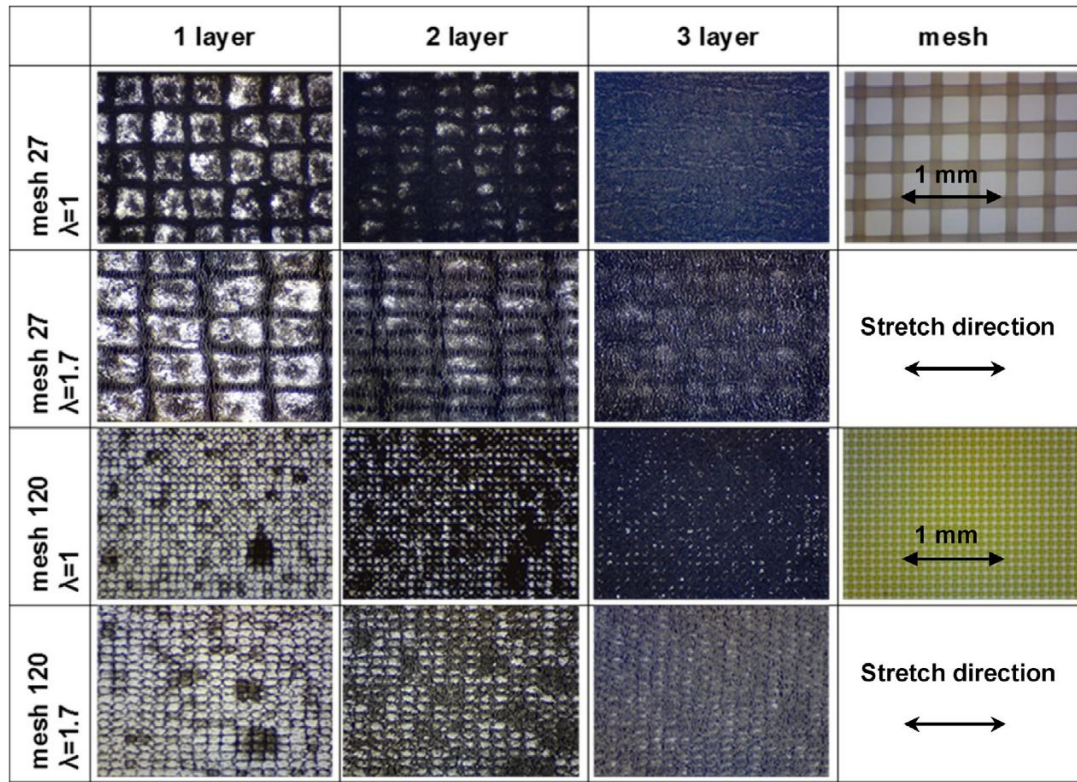


Fig. 4. Optical photographs, enlarged, of printing pattern with and without stretch for coarse and fine mesh.

Interestingly, the 1-layer-prints show the pattern of the mesh and not the pattern of the free mesh area. This is due to the fact that the surface tension of the silicone film is very low, and requires the contact pressure of the thread for adhesion. The 3-layer-prints depict the expected pattern of the free mesh area, because the silicone film is already covered with electrode material with a higher surface tension. It is important to point out that a different electrode material, e.g., consisting of a higher percentage or different type of PDMS, can show a different print pattern. The electrode material used in this study is designed for low mechanical impact on the silicone film.

3.1.1. Thickness measurement

Printing electrodes with coarse (27 threads/cm) and fine (120 threads/cm) screens results in very different surface structures, see Fig. 4. Figs. 5 depicts the thickness measurements along the measurement path marked with a red line in the picture in Fig. 5a. The measurement path covers the length of 3 mm silicone film without electrode, 6 mm with electrode, and again 3 mm without electrode at $\lambda=1$. The thickness of the silicone film ranges between 46 μm and 48 μm , and is therefore in the range of $\pm 5\%$ specified in [34]. In the case of the Mesh27 screen, we observe an average electrode layer thickness of $\sim 3 \mu\text{m}$ with strong local variations, while the layer thickness for the Mesh120 screen is only $\sim 1 \mu\text{m}$ with noticeably reduced local variations.

Fig. 6 shows the average electrode thickness for the print configurations. As it can be readily seen from the figure, the electrode thickness increases linearly with each added layer. Even though the surface tension of the film for the first layer is lower than the surface tension for the second and third layers, showing a different printing pattern, the amount of electrode material disposed on the film is the same for each layer. The quantity of the disposed mate-

rial is a function of the mesh thickness, the free mesh area, and the amount of solvents evaporating during heat curing.

3.1.2. Resistance measurements

The resistance measurements are reported as surface (or sheet) resistance R_{\square} to facilitate comparison with resistance results in the literature. This unit is used for thin films with a nominally uniform thickness, assuming the current to be along the sheet and not perpendicular to it. It is given in Ω/sq (Ohm per square).

The resistance in a three dimensional bulk conductor is

$$R_{\text{meas}} = \frac{\rho}{t} \frac{l}{w} = R_{\square} \frac{l}{w},$$

which yields the sheet resistance

$$R_{\square} = R_{\text{meas}} \frac{w}{l}.$$

The results for the sheet resistance measurements account for the electrode area consisting of a passive electrode area (electrode underneath reinforcement frame with connection to electrode contact area EAC) and a freely stretchable electrode area, see Fig. 2 (a). The area of the free electrode changes while stretched. It is assumed that the width is constant during stretch and only the length changes; changes in electrode thickness are neglected. The sheet resistance is calculated using Eq. (3) and reported in $\text{k}\Omega/\text{sq}$

$$R_{\square} = R_{\text{meas}} \left(\frac{w_{\text{free}}}{l_{\text{free}} \lambda} + \frac{w_{\text{passiv}}}{l_{\text{passiv}}} \right),$$

where:

- R_{meas} : Resistance measured;
- ρ : Resistivity;
- t : Thickness of electrode
- w : Width of electrode area;

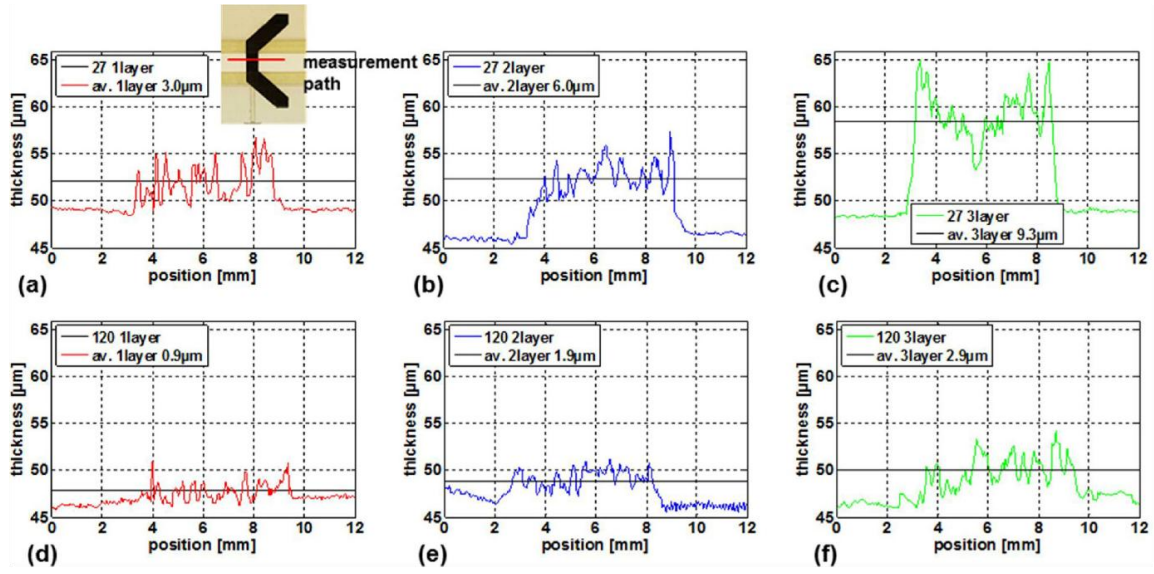


Fig. 5. Thickness profiles of silicone film samples with electrodes printed with coarse (27, a-c) and fine (120, d-f) meshes and one to three layers (left to right).

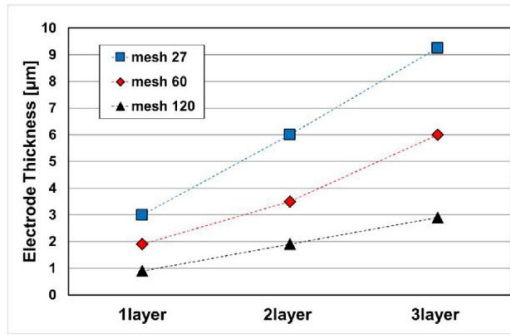


Fig. 6. Average electrode layer thickness for 3 meshes at $\lambda=1$.

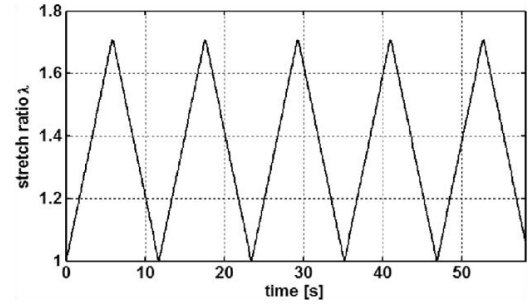


Fig. 7. Stretch vs. time input for electrical measurements, 1.2 mm/s, 0.1 Hz.

w_{free} : Width of free electrode area;
 w_{passiv} : width of passiv electrode area;
 l : length of electrode area;
 l_{free} : length of free electrode area;
 l_{passiv} : length of passiv electrode area;
 λ : stretch ratio

The resistance changes reflect only the contributions from the deformable area which is not blocked by the clamps and the reinforcement frame, and not the total resistance. The time-resolved deformation input can be seen in Fig. 7.

Fig. 8 shows stretch-dependent sheet resistance values for different mesh sizes. The upper row gives results for one-layer-printing, while the bottom row covers the three-layer-case. Each case displays a resistance increase with increasing deformation, thereby following the stretch input in a non-linear and hysteretic fashion, similarly to the results reported in [35,36]. The hysteresis effect is dependent on the mesh size, and is largest with the finest mesh (Fig. 8b). Comparing top row to bottom, the increase from one to three layers also decreases the resistance change by nearly a factor of ten. Finally, we observe that while the 27- and 60-meshes produce relatively similar resistance values, the fine 120-mesh exhibits significantly larger values. This is in accordance with the results of Fig. 4, where the picture for the 120-mesh, $\lambda=1.7$, shows that large areas of the surface are only covered with very

little electrode material. If the electrode layer is intermittent, the conductivity is reduced and the resistance becomes higher.

3.2. Design B: actuator specimens

While the above resistance measurements are performed with a single electrode printed onto the silicone film, measurements for sensor or actuator applications require a top and a bottom electrode, realized in a second specimen type, see Fig. 2b.

3.2.1. Capacitance measurements

While ideally one would not expect the electrodes to have an impact on the capacitance measurements, Fig. 9 indicates that this might indeed be the case. As the left picture shows capacitance results following the stretch input as to Fig. 7, the capacitance of the 27- and 60-mesh is consistent, whereas the one-layer fine mesh shows a strongly deteriorated measurement signal. The reason is the excessively large value for the resistance, in the range of $\sim 1 M\Omega$, which causes a breakdown in the LCR meter measurements leading to inaccurate capacitance values. The deteriorated measurements are therefore a result of the limitation of the LCR meter method and not of actual material behavior. Increasing the number of layers to two, right picture, reduces the resistance down to $\sim 250 k\Omega$, which reproduces the result from the coarse mesh case and is within the measurement range of the LCR meter.

An alternative option to measure the capacitance is by measuring the current and using a self-sensing algorithms as presented in,

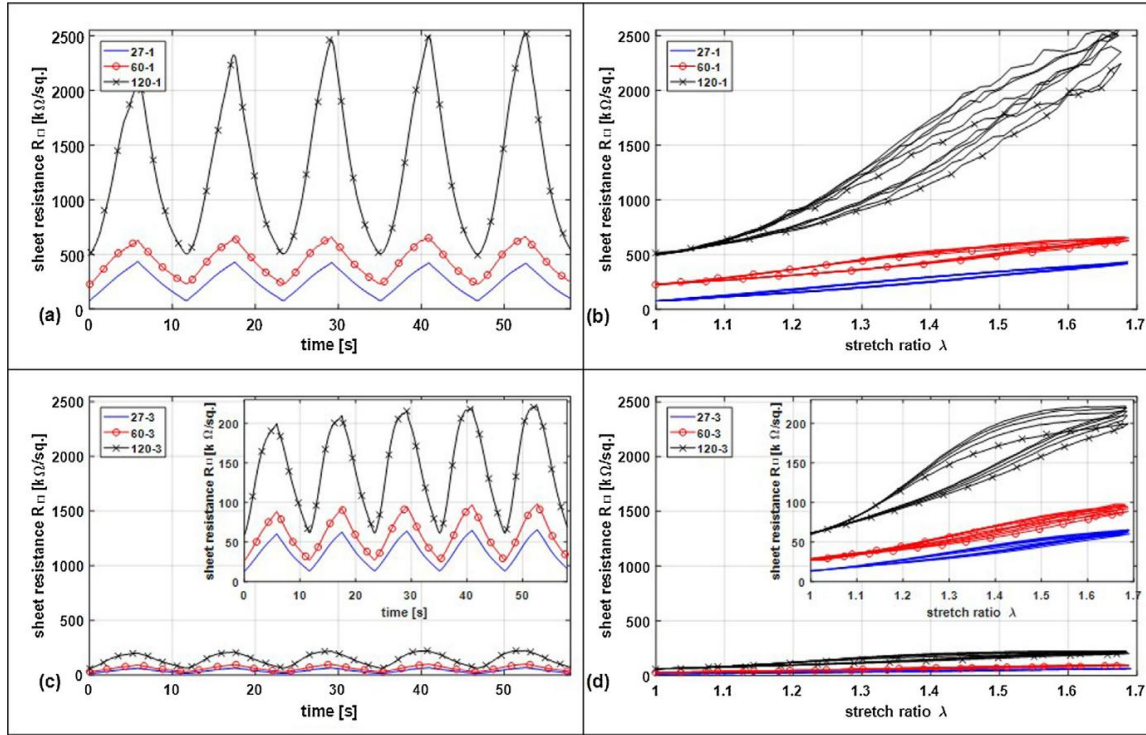


Fig. 8. Sheet resistance values comparing one- and three-layer-electrodes for the three meshes.

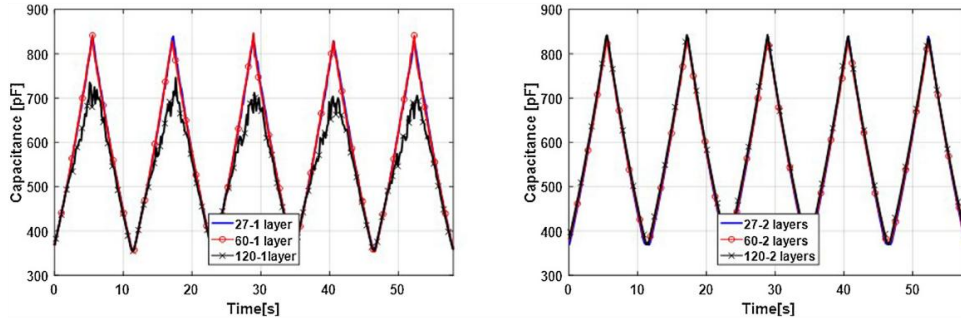


Fig. 9. Capacitance values for the three mesh sizes for 1-layer (left) and 2-layers (right) at $\lambda = 1$ to 1.7 as per Fig. 7.

e.g., [32,33]. An additional advantage using these algorithms is the possibility to obtain results for resistance and capacitance while the drive voltage is applied. However, this method had not been implemented into the current experimental setup due to lack of reliable current measurements. Nevertheless, it will be available in the future.

3.2.2. Force-displacement measurements w/o voltage

One specimen is prepared without electrodes and tested in the same manner as those with electrodes to observe the stiffening effect of the electrodes. The stretch input is shown in Fig. 7. Fig. 10 (a)–(c) shows that the electrodes stiffen the membrane slightly. One exception is the 1-layer print on the fine Mesh120, where no stiffening effect is observed. The thicker the electrode layer the stiffer the membrane is. At the highest extensions, the effect is most visible.

Fig. 10 (d) shows the electrode thickness (top plus bottom electrode) for each print configuration in unstretched state and at

$\lambda = 1.7$. The thickness ratio Te/f is used to indicate the proportion from electrode layer thickness to silicone film thickness

$$Te/f = 100 \frac{d_{top} + d_{bottom}}{d_{siliconefilm}}, \quad (4)$$

with:

d_{top} : thickness top electrode;

d_{bottom} : thickness bottom electrode;

$d_{siliconefilm}$: thickness silicone film.

At a ratio $Te/f \approx 3.7$, i.e., the ratio for a 1-layer print with a Mesh120, the electrode has no mechanical stiffening effect. At $Te/f \approx 8$, the electrode has a slight stiffening effect, the force is about 10% higher than without electrode. At $Te/f \approx 38$ the stiffening effect is significant, and the force is about 25% higher with electrodes than without. Even though the 1-layer print with Mesh120 shows no stiffening effect, a ratio of about 8 (2-layer Mesh120 or 1-layer Mesh60) is preferable considering the results in Fig. 10 (a), (b) and (d).

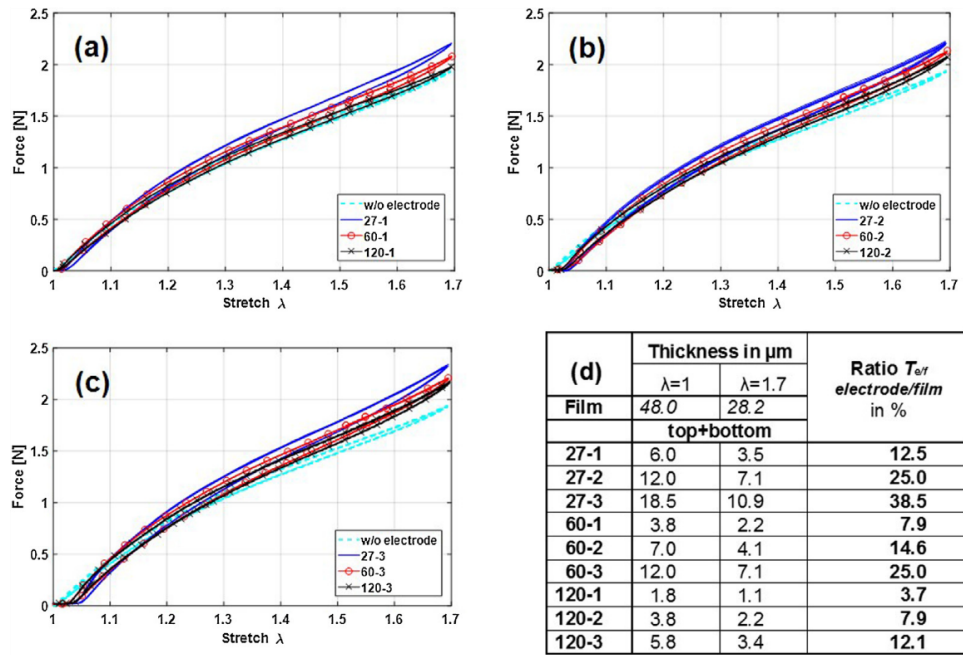


Fig. 10. (a)–(c) Force-displacement response to the stretch for 1, 2, and 3-layer prints; (d) electrode and film thickness for all configurations and ratio of electrodes to film.

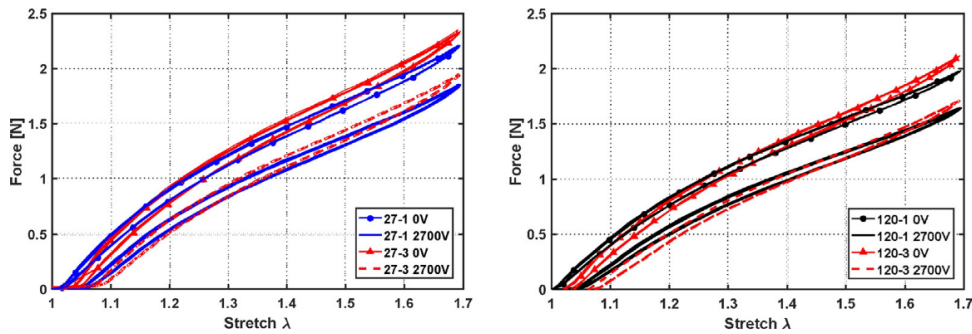


Fig. 11. Force vs displacement tests for linear ramp (1.2 mm/s, 0.1 Hz) @ 0 V and 2.7 kV, electrodes printed with Mesh27 (left) and Mesh120 (right) with one and three layers.

3.2.3. Force-displacement measurements with constant voltage

High voltage is applied to the specimens to observe the softening effect on the membrane due to the Maxwell stress. Fig. 11 shows force vs. stretch for the coarse and very fine mesh at a constant voltage of 0 V and 2700 V for 1-layer and 3-layer electrodes. The stretch input is shown in Fig. 7. The overall force during stretch is higher for the coarse mesh as well as for the 3-layer prints due to the electrode thickness as discussed in Fig. 12. However, the force difference $\Delta F_{\text{max}@0V-2700V}$ at $\lambda=1.7$, calculated with the force at 0 V, $\lambda=1.7$, subtracted with the force at 2700 V, $\lambda=1.7$, is the same for the print configurations 27-3 layer (0.38 N), 27-1 layer (0.376 N), and 120-3 layer (0.382 N). The print configuration 120 1-layer shows a slightly lower ΔF_{max} (0.363 N), which is a result of the thin electrode, which covers large areas with only very little electrode material. Aside from this case, the layer thickness seems not to influence the ΔF output of the force measured between 0 V and 2700 V, but only to have an influence of the overall stiffening effect.

3.2.4. Force measurements with constant position

The force-displacement measurements at constant voltage, Section 3.2.3, are conducted at a displacement speed of 1.2 mm/s

(0.1 Hz). To further investigate the influence of the mesh size and electrode thickness on the actuation performance, experiments are carried out at higher frequencies. The linear actuator used to stretch the samples mechanically is not able to perform at a displacement speed of 120 mm/s (10 Hz). Therefore, in this section the samples are tested at a constant stretch $\lambda=1.6$ with a voltage ramping from 0 V to 2700 V at frequencies of 0.1 Hz, 1 Hz and 10 Hz. All tests are conducted on 1-layer electrode prints. The voltage inputs are depicted in Fig. 12.

Fig. 13 shows voltage over normalized force for the coarse and fine mesh at the three different frequencies. The force is normalized with the initial force measured at $\lambda=1.6$, 0 V.

As it can be seen in Fig. 13, at a voltage ramp of 0.1 Hz, ΔF shows no hysteresis effect in the coarse and fine mesh case. At 1 Hz, no hysteresis can be observed with the coarse mesh and only negligible hysteresis effect is visible for the tests conducted with the fine mesh. However, if the voltage is applied at high frequency (10 Hz), hysteresis can be observed for both mesh sizes, with a significant larger hysteresis in the fine mesh case.

Fig. 14 shows the isometric response for all three mesh sizes at a voltage applied with 10 Hz. Fig. 14 shows that the hysteresis

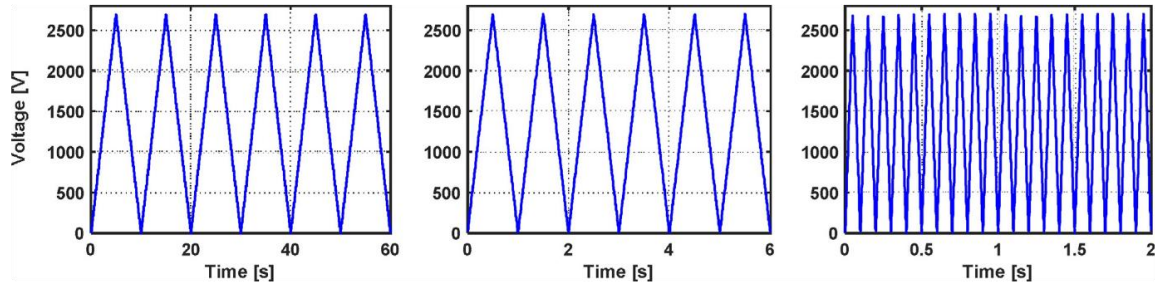


Fig. 12. Voltage input at 0.1 Hz (left), 1 Hz (middle), 10 Hz (right) for constant position tests.

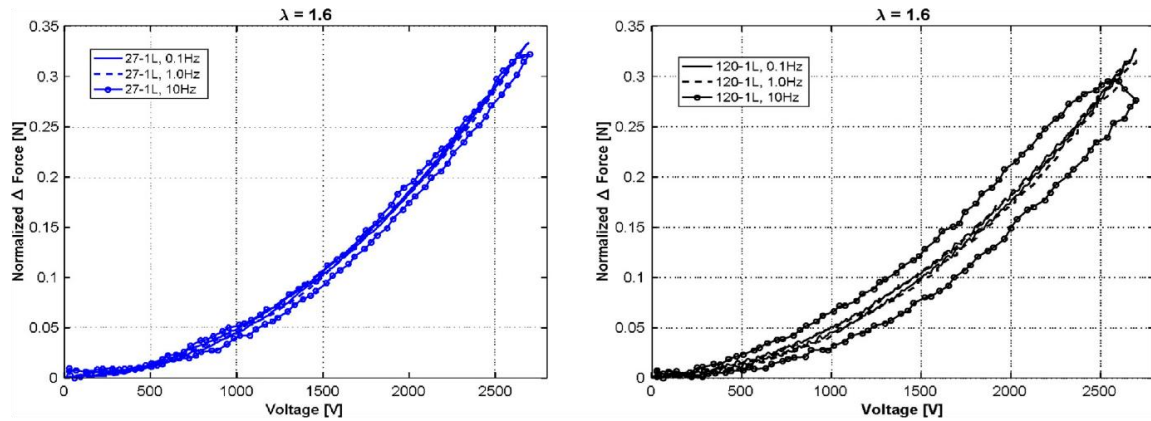


Fig. 13. Isometric response to voltage at 0.1 Hz, 1 Hz, 10 Hz for coarse (left) and fine (right) mesh.

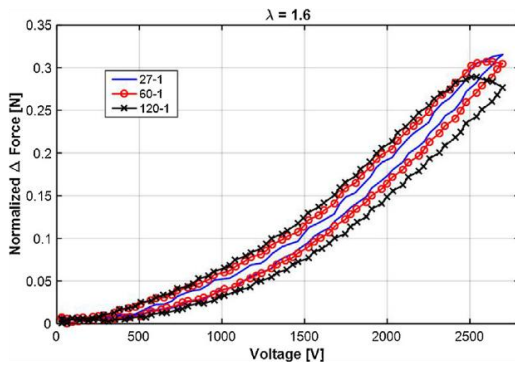


Fig. 14. Isometric response to voltage at 10 Hz for Mesh27, Mesh60, and Mesh120.

effect increases with finer mesh sizes and therefore with decreasing electrode thickness.

The observed hysteresis is zero in quasi-static conditions, and it increases as the frequency increases. It is reasonable to assume that such a rate-dependent hysteresis is due to the dynamic behavior of the material, which is mainly determined by DE electrical dynamics and viscoelasticity [37]. Since we are performing constant position tests, it is reasonable to assume that the material viscoelasticity has no effects on the response, thus the observed hysteresis has to be related to a change in the electrical impedance of the DE, i.e., a change in electrical resistance.

The electrical dynamics of a DE is typically described by means of RC series circuits. In particular, the relationship between applied voltage and voltage seen by the DE membrane, which is directly converted into force due to Maxwell stress, follows a first-order low-pass dynamics. Since the excitation we are using is periodical,

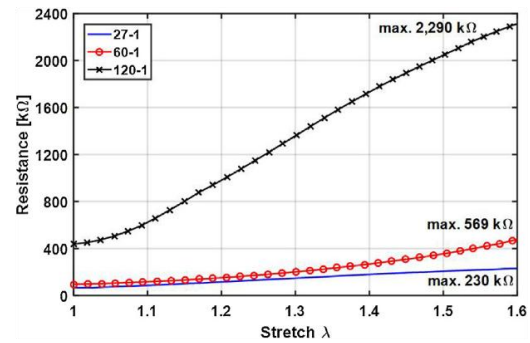


Fig. 15. Resistance vs. stretch at 0.1 Hz 0 V, 1 layer, Mesh27, Mesh60, and Mesh120.

the study of this phenomenon is carried out based on frequency domain analysis. In particular, the cut-off frequency of the RC low-pass filter is given as follows [37],

$$f_c = \frac{1}{2\pi RC}, \quad (5)$$

with R being the resistance of the electrodes in Ω and C the capacitance of the silicone film in F. The resistance dependency on the stretch is shown in Fig. 15 for all three mesh sizes. For obtaining those curves, the resistance is recorded at a stretch rate of 0.1 Hz, compatibly with the sampling time of the used LCR-meter. The cut-off frequency f_c is calculated according to (5) using the values for the silicone film capacitance and resistance values at $\lambda=1.6$ (Fig. 9 and Fig. 15, respectively). Numerical values of resistance, capacitance, and corresponding cut-off frequency at $\lambda=1.6$ are shown in Table 3 for different meshes. If the resistance increases, the cut-off frequency f_c tends to decrease, and consequently we expect a higher attenuation and phase delay in the output signal. Both these

Table 3

Resistance, capacitance and total time necessary to charge the DE to 99%.

	R [k]	C [pF]	f_c [Hz]
mesh 27	230	760	910.5
mesh 60	469	760	446.5
mesh 120	2290	760	91.4

effects result in a dynamic hysteresis having smaller final value and larger area, in agreement with Fig. 14.

For the largest resistance (mesh 120), we obtain a cut-of frequency of 91.4 Hz, about 10 times lower than for the case of smallest resistance (mesh 27). From this significant change in resistance, we can also explain the very large change in dynamic response of the membrane.

Since both capacitance and resistance depend on the material stretch, the resulting f_c and associated hysteresis also depend on the current state of deformation of the membrane. Further investigation of relationship between f_c and stretch, however, goes beyond the scope of this paper, and a more in-depth analysis will be performed in future research work.

4. Conclusions

This paper has presented the experimental investigation of the impact of screen printing parameters on the performance of membrane DETs. The screen mesh size has been varied in three steps from coarse to fine mesh, and these three mesh sizes have been used to print one, two, and three layer electrodes, resulting in a total of 9 different configurations. The samples have been investigated in a test rig in which electrode thickness, sheet resistance, capacitance and force have been measured for a stretch range from $\lambda=1$ to $\lambda=1.7$ at 0 V and 2.7 kV. Enlarged photos have been taken for each configuration at a stretch rate $\lambda=1$ and $\lambda=1.7$. Additionally, isometric response measurements have been conducted at $\lambda=1.6$ and electrical frequencies of 0.1 Hz, 1 Hz, and 10 Hz.

The photos have shown different mesh patterns on the silicone film along with the deformation of these patterns during stretching. One-layer prints show the printing pattern of the mesh thread with the silicone film only intermittently covered with electrode material. In the three-layer case, the film area is completely covered with electrode material and no clear pattern is visible any more.

The experiments show that with increasing mesh size (from fine to coarse) the sheet resistance decreases, also resulting in stable capacitance measurements using a standard LCR meter. The resistance in one-layer electrodes printed with the fine mesh size (120 threads per cm) increases during the stretching process to magnitudes that made LCR meter capacitance measurements no longer possible. The hysteretic behavior of the resistance measured on the prints with one-layer fine mesh is significant. A two-layer print with fine mesh resulted, once again, in stable capacitance measurements. The mesh size influences the film stiffness (compared to a film without electrodes) in a way that a coarser mesh stiffens the material while a fine mesh has almost no influence. The overall stiffening effect of a one-layer print is low in all three cases.

The tests conducted with high voltage (2700 V) show that the mesh sizes appeared to have no impact on the electrical force at low frequencies. At high frequencies, however, the mesh size has a significant impact on the hysteretic behavior. Tests conducted on samples at constant position with 60% stretch and with a 10 Hz triangle signal from 0 to 2700 V exhibited increasing hysteresis force from coarse to fine mesh.

In summary, the conclusion of our experimental investigation is that the mesh size and the amount of layers have a significant impact on the resistance and, in some cases, depending on the measurement method, also capacitance measurements. The results

indicate that for sensor applications a coarser mesh or a two- or three-layer print is advisable. For actuator applications, the impact of the mesh size is negligible at low frequencies for the electrode material under investigation. However, if higher frequencies are needed, a thicker electrode layer (coarser mesh or 2-layer print) is recommended, even though it stiffens the material slightly.

Acknowledgement

We gratefully acknowledge the support from WACKER Chemie AG, who supplied Elastosil 2030 film and other chemicals, as well as ORION Engineered Carbons GmbH for providing carbon blacks used for this investigation.

References

- [1] K. Danielmeier, D. Schapeler, et al., Elektroaktive polymere: entwicklungen und perspektiven dielektrischer elastomere, *Angewandte Chemie* 125 (2015) 2–17.
- [2] S. Hau, A. York, S. Seelecke, High-Force dielectric electroactive polymer (DEAP) membrane actuator, Las Vegas, in: Conference: Proc. SPIE 9798, Electroactive Polymer Actuators and Devices (EAPAD), 9798, 2016, <http://dx.doi.org/10.1117/12.2220775>.
- [3] G. Hau, M. Rizzello, A. York, S. Seelecke, Design and Control of a High-Speed Positioning System Based on Dielectric Elastomer Membrane Actuators, *IEEE/ASME Transactions on Mechatronics* (2017), Under review.
- [4] S. Rosset, H. Shea, Small, fast and tough: shrinking down integrated elastomer transducers, *Appl. Phys. Rev.* 3 (3) (2016) 31105, <http://dx.doi.org/10.1063/1.4963164>.
- [5] M. Giousouf, G. Kovacs, Dielectric elastomer actuators used for pneumatic valve technology, *Smart Mater. Struct.* 22 (10) (2013) 104010.
- [6] A.H. Muir, S.J. Biggs, R.N. Hitchcock, U.S. Patent Application No. 14/912,960, (2014).
- [7] A. York, J. Dunn, S. Seelecke, Systematic approach to development of pressure sensors using dielectric electro-active polymer membranes, *Smart Mater. Struct.* 22 (9) (2013) 094015.
- [8] Y. S. Kim, K. U. Kyung, S. Park et al., U.S. Patent No. 9,323,328. Washington, DC: U.S. Patent and Trademark Office, (2016).
- [9] F. Carpi, D. De Rossi, R. Kornbluh, et al. (Eds.), *Dielectric Elastomers as Electromechanical Transducers: Fundamentals, Materials, Devices, Models and Applications of an Emerging Electroactive Polymer Technology*, Elsevier, 2011, 2017.
- [10] S. Rosset, H.R. Shea, Flexible and stretchable electrodes for dielectric elastomer actuators, *Appl. Phys. A* 110 (February (2)) (2013) 281–307.
- [11] L.J. Romasanta, M.A. Lopez-Manchado, R. Verdejo, Increasing the performance of dielectric elastomer actuators: a review from the materials perspective, *Prog. Polym. Sci.* 51 (2015) 188–211.
- [12] M. Molberg, D. Crespy, P. Rupper, et al., High breakdown field dielectric elastomer actuators using encapsulated polyaniline as high dielectric constant filler, *Adv. Funct. Mater.* 20 (19) (2010) 3280–3291.
- [13] S. Hunt, T.G. McKay, I.A. Anderson, A self-healing dielectric elastomer actuator, *Appl. Phys. Lett.* 104 (11) (2014) 113701.
- [14] F.B. Madsen, A.E. Dugaard, S. Hvilsted, A.L. Skov, The current state of silicone-based dielectric elastomer transducers, *Macromol. Rapid Commun.* 37 (2016) 378–413.
- [15] D. McCoul, W. Hu, M. Gao, et al., Recent advances in stretchable and transparent electronic materials, *Adv. Electron. Mater.* 2 (5) (2017) 1500407, <http://dx.doi.org/10.1002/aelm.201500407>.
- [16] F. Habrard, J. Patscheider, G. Kovacs, Super-compliant Metallic Electrodes for Electroactive Polymer Actuators, in: *SPIE Smart Structures and Materials+ Nondestructive Evaluation and Health Monitoring*, International Society for Optics and Photonics, 2012, 2017.
- [17] R. Giesen, M. Adam, H.-P. Heim, Dielectric electroactive polymers (dEAP) based on thermoplastic elastomers (TPE), *J. Plast. Technol.* 10 (2014) 29–48.
- [18] P. Lotz, M. Matysek, H.F. Schlaak, Fabrication and application of miniaturized dielectric elastomer stack actuators, *IEEE/ASME Trans. Mechatronics* 16 (1) (2011) 58–66.
- [19] F. Carpi, P. Chiarelli, A. Mazzoldi, D. De Rossi, Electromechanical characterisation of dielectric elastomer planar actuators: comparative evaluation of different electrode materials and different counterloads, *Sens. Actuators A Phys.* 107 (no. 1) (2003) 85–95.
- [20] E. Cakmak, X. Fang, O. Yildiz, et al., Carbon nanotube sheet electrodes for anisotropic actuation of dielectric elastomers, *Carbon* 89 (2015) 113–120.
- [21] B.M. O'Brien, E.P. Calius, T. Inamura, et al., Dielectric elastomer switches for smart artificial muscles, *Appl. Phys. A* 100 (no. 2) (2010) 385–389.
- [22] M. Kujawski, J.D. Pearce, E. Smela, Elastomers filled with exfoliated graphite as compliant electrodes, *Carbon N. Y.* 48 (no. 9) (2010) 2409–2417.
- [23] A. Tröls, A. Kogler, R. Baumgartner, et al., Stretch dependence of the electrical breakdown strength and dielectric constant of dielectric elastomers, *Smart Mater. Struct.* 22 (10) (2013) 104012.

- [24] A. Poulin, S. Rosset, H. Shea, Fully printed 3 microns thick dielectric elastomer actuator, in: *SPIE Smart Structures and Materials+ Nondestructive Evaluation and Health Monitoring*, April 2016, International Society for Optics and Photonics, 2016, p. 97980L.
- [25] S. Araromi, P. Romano, S. Rosset, J. Perruisseau-Carrier, H. Shea, A tunable millimeter-wave phase shifter driven by dielectric elastomer actuators, *Proc. SPIE* vol. 9056 (2014) 90562M.
- [26] B. Fasolt, M. Hodgins, S. Seelecke, Characterization of screen-printed electrodes for Dielectric Elastomer (DE) membranes: influence of screen dimensions and electrode thickness on actuator performance, in: *SPIE Smart Structures and Materials+ Nondestructive Evaluation and Health Monitoring*, April 2016, International Society for Optics and Photonics, 2017, p. 97983E.
- [27] O.A. Araromi, S. Rosset, H. Shea, High-resolution, large-area fabrication of compliant electrodes via laser ablation for robust, stretchable dielectric elastomer actuators and sensors, *ACS Appl. Mater. Interfaces* (2015) (p 150722072212009).
- [28] T.-W. Lee, H.-H. Park, The effect of MWCNTs on the electrical properties of a stretchable carbon composite electrode, *Compos. Sci. Technol.* 114 (2015) 11–16.
- [29] W.J. Hyun, E.B. Secor, M.C. Hersam, C.D. Frisbie, L.F. Francis, High-resolution patterning of graphene by screen printing with a silicon stencil for highly flexible printed electronics, *Adv. Mater.* 27 (no. 1) (2015) 109–115.
- [30] L.L. Wang, B.K. Tay, K.Y. See, Z. Sun, L.K. Tan, D. Lua, Electromagnetic interference shielding effectiveness of carbon-based materials prepared by screen printing, *Carbon N. Y.* 47 (no. 8) (2009) 1905–1910.
- [31] M. Hodgins, S. Seelecke, Systematic experimental study of pure shear type dielectric elastomer membranes with different electrode and film thicknesses, *Smart Mater. Struct.* 25 (9) (2016) 095001.
- [32] F. Carpi, I. Anderson, S. Bauer, et al., Standards for dielectric elastomer transducers, *Smart Mater. Struct.* 24 (10) (2015) 105025.
- [33] M. Hodgins, A. York, S. Seelecke, Systematic experimental investigation of dielectric elastomer membranes using a custom-built tensile test rig, *J. Intell. Mater. Syst. Struct.* (2017).
- [34] Wacker Chemie, AG Datasheet Neue Perspektiven Und Innovative Anwendungen Mit Elastosil® Film, 2014.
- [35] G. Rizzello, D. Naso, A. York, S. Seelecke, A self-Sensing approach for dielectric elastomer actuators based on online estimation algorithms, *IEEE/ASME Transac. Mech.* (2017) (accepted for publication).
- [36] G. Rizzello, M. Hodgins, S. Seelecke, D. Naso, Self-Sensing at low sampling-To-Signal frequency ratio: an improved algorithm for dielectric elastomer actuators, *The 12th IEEE/ASME International Conference on Mechatronic and Embedded Systems and Applications* (2016) 7587146.
- [37] G. Rizzello, M. Hodgins, D. Naso, A. York, S. Seelecke, Modeling of the effects of the electrical dynamics on the electromechanical response of a DEAP circular actuator with a mass-spring load, *Smart Mater. Struct.* 24 (August 9) (2015) 094003.

4.2 Dielectric breakdown test setup for dielectric elastomers: Design and validation

Felix Welsch¹, Bettina Fasolt², Stefan Seelecke^{1,2}

¹ Intelligent Materials Systems lab, Department of Systems Engineering,
Department of Materials Science and Engineering, Saarland University,
Saarbruecken, Germany

² Intelligent Materials Systems Lab, Center for Mechatronics and Automation
Technologies (ZeMA) gGmbH, Saarbruecken, Germany

Published in Proceedings of SPIE 10594

Electroactive Polymer Actuators and Devices (EAPAD) XX

Event: SPIE Smart Structures and Materials + Nondestructive Evaluation and Health Monitoring
2018

Denver, Colorado, United States

March 27, 2018

DOI: 10.1117/12.2296995

© SPIE, Journal Author Rights: Permission under SPIE Copyright.

This conference paper presents the development of a scientific breakdown test setup designed for multiple repetitive DEA breakdown tests under controlled environmental conditions within a climate chamber. The system enables automated consecutive measurements without opening the chamber, preserving climatic conditions for measuring a minimum of eleven measurement points on pure film as well as film with applied electrodes during one test procedure. Designed and built by Felix Welsh, the tester is used by Bettina Fasolt to investigate breakdown behavior, validate the test procedure, and assess the potential influence of gold contact weight on the test film.

The tester is configured to accommodate prepared samples consisting of a polymer film clamped between two metal frames. The frames contain recesses that ensure reproducible alignment and are lined with polyimide tape to enhance film adhesion. The sample assembly is secured onto a movable sample stage in a predefined position. During operation, the stage positions the sample above a fixed ground electrode. Contact from the high-voltage electrode is established via a pivoting arm, with the applied force adjustable through a movable counterweight.

A voltage is applied in a ramped manner until electrical breakdown occurs. Subsequently, the pivoting arm carrying the high-voltage electrode is released, and the sample is moved to the next test position, where the procedure is repeated.

The potential influence of high voltage contact weight on the test film is investigated by varying the load applied by the pivoting arm with the high-voltage electrode. This is achieved by adjusting the counterbalance and by applying additional external weights. Weights from 0.5 gram to 30 grams are applied to the film and breakdown tests performed.

The setup operates successfully, demonstrating that the contact force-induced stress from gold contacts is negligible compared to Maxwell stress when voltage is applied.

The breakdown holes are visible to the naked eye. Figure 4.1 presents magnified images of two representative breakdown spots, each shown under reflected light and under transmitted light.

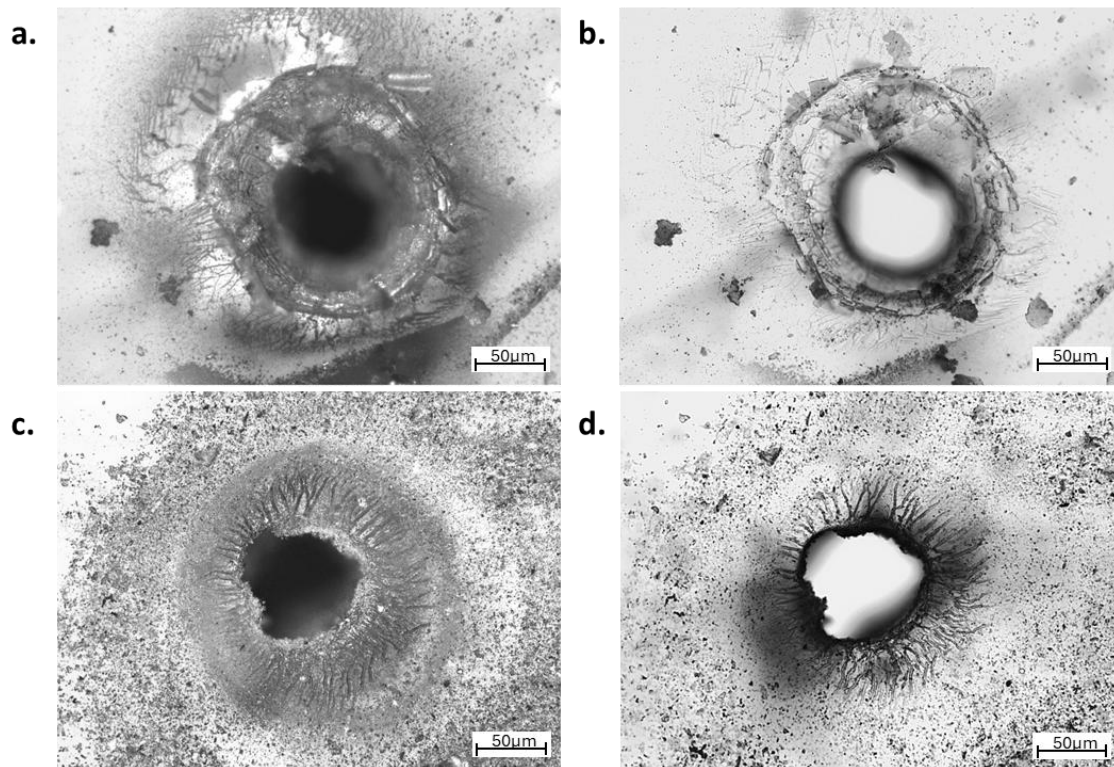


Figure 4.1. Example of two breakdown spots formed during electrical breakdown on Wacker Elastasil 2030 film. Images (a) and (b) depict the first breakdown spot under reflected light (a) and transmitted light (b). Similarly, images (c) and (d) show the second breakdown spot under the same lightening conditions.

PROCEEDINGS OF SPIE

SPIDigitalLibrary.org/conference-proceedings-of-spie

Dielectric breakdown test setup for dielectric elastomers: design and validation

Felix Welsch, Bettina Fasolt, Stefan Seelecke

Felix Welsch, Bettina Fasolt, Stefan Seelecke, "Dielectric breakdown test setup for dielectric elastomers: design and validation," Proc. SPIE 10594, Electroactive Polymer Actuators and Devices (EAPAD) XX, 105941A (27 March 2018); doi: 10.1117/12.2296995

SPIE.

Event: SPIE Smart Structures and Materials + Nondestructive Evaluation and Health Monitoring, 2018, Denver, Colorado, United States

Dielectric breakdown test setup for dielectric elastomers: Design and validation

Felix Welsch ^{*a}, Bettina Fasolt ^b, Stefan Seelecke ^a

^a Intelligent Materials Systems Lab, Department of Systems Engineering, Department of Materials Science and Engineering, Saarland University, Saarbruecken, Germany

^b Intelligent Materials Systems Lab, Center for Mechatronics and Automation Technologies (ZeMA) gGmbH, Saarbruecken, Germany

ABSTRACT

Dielectric Elastomers (DE) represent an attractive technology in the field of electromechanical transducers for the realization of low cost actuators and sensors. These devices consist of a thin DE membrane with flexible electrodes resulting in a stretchable capacitor. An electrical field, applied by the electrodes causes a thickness reduction due to the dielectric forces in the membrane resulting in a mechanical output. The actuator performance strongly depends on the material properties of the membrane, especially permittivity and breakdown field strength. To characterize the enhanced materials developed by current researches a reproducible testing method is needed. This work presents the development, realization and validation of a scientific test stand to investigate the electrical breakdown in dielectric elastomer films under different environmental conditions. The presented test setup allows the study of various film thicknesses at comparable conditions. Exchangeable electrode tips allow the research of different electrical field distribution induced by the electrode geometry. A fine adjustable contact pressure ensures a defined mechanical contact with the film surface while creating minimal film thickness deformation in a repeatable manner. Furthermore, this enables to research the influence of the contact pressure on the electrical breakdown field strength. An exchangeable specimen frame offers easy film preparation with different pre-stretch strains and spatial resolved thickness measurements in preparation of the breakdown test. To allow the characterization of the film under different ambient conditions the test stand is placed in a climate chamber controlling ambient temperature and humidity. A remote-controlled servo motor allows spatial resolved breakdown voltage measurements resulting in combination with the local thickness measurements in a breakdown field strength.

Keywords: Dielectric Elastomer, Membrane Actuator, Dielectric Breakdown Test, Dielectric Withstand Test, Breakdown Voltage, Breakdown Field Strength

1. INTRODUCTION

Dielectric Elastomers (DEs) represent a promising new technology which enables the realization of lightweight, energy efficient, fast responding, silent and scalable mechatronic systems.¹ A DE consists of an elastomer film which is sandwiched between two compliant electrodes, resulting in a flexible capacitor, illustrated in Figure 1 (a). Commonly used elastomers are silicone, acrylic, polyurethane, or natural rubber.^{2,3} DE transducers can be used in several applications, such as energy harvesting, sensing and actuation.⁴ They can be operated as actuators and sensors simultaneously, by exploiting the so-called self-sensing feature of the material.⁵

Voltages between 1 kV and 10 kV are typically used during actuation to achieve a reasonable compressive stress onto the elastomer. The Coulomb forces acting between the charges on the electrodes generate a thickness reduction of the membrane. Since the used elastomers are almost incompressible, the thickness reduction causes an increase of area perpendicular to the thickness direction, which can be used as a drive mechanism as shown in Figure 1 (b).

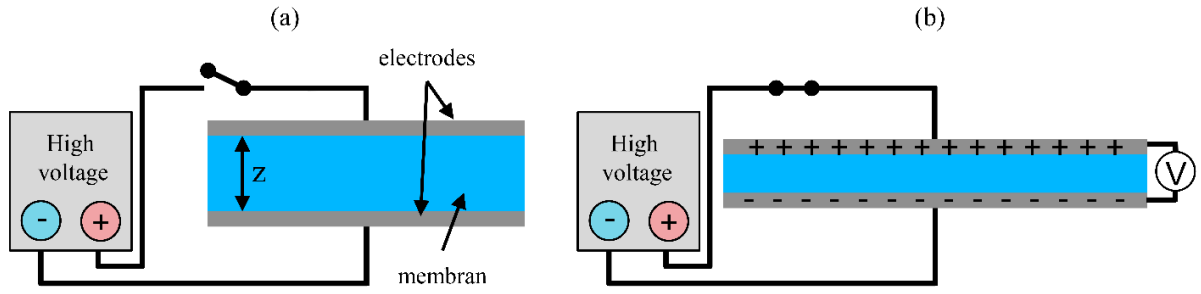


Figure 1. DE actuation principle: (a) Initial state (b) Activated state at applied high voltage.

The physical mechanism behind the actuation of DEs is the so-called Maxwell stress and is given by equation **Error! Reference source not found.**(1), with the void permittivity ε_0 , the DE's relative permittivity ε_r , and the applied electric field E .⁶

$$\sigma_{MW} = \varepsilon_0 \cdot \varepsilon_r \cdot E^2 \quad (1)$$

The actuator performance strongly depends on the electromechanical behavior of the membrane, which is influenced by the permittivity and breakdown field strength.

$$E_{krit} = \frac{V_{krit}}{z} \quad (2)$$

The breakdown field strength represents the maximum value of the electrical field E_{krit} which can be withstand by the membrane, limiting the maximum actuator potential of the DE. This parameter can be measured in a breakdown test by increasing the applied voltage up to the breakdown event at V_{krit} and is calculated with equation (2) using the film thickness z . Common values for the dielectric breakdown field strength of typical DE materials are in the range of 10 V/ μm to 100 V/ μm .⁷ The sample's thickness has a significant impact on dielectric breakdown field strength as it appears in the literature^{8,9}. While the physical reasons for such behavior are not currently completely understood, at least a contribution is likely to come from the fact that samples with a different thickness from a given material might require different processing methods with different curing conditions introducing different types of defects.⁷ To gain a better understanding of this effects a characterization of different film thicknesses and sizes is required, demanding a test setup with a thickness range from a few microns to several hundred microns.

Carpi et al.⁷ present a definition of standards and guidelines on how to assess and compare performance of DE transducer materials and devices. Different test stands for material and performance characterization in the field of Des are presented in literature.^{10,11}

The meaningful investigation and optimization of the DE especially study on the breakdown field strength requires a fully automated reproducible testing setup which covers all influence parameters.

2. DEVELOPMENT

2.1 Requirements

Development of the dielectric breakdown test setup starts by determining the needed requirements. The dielectric breakdown strength depends on extrinsic factors, such as humidity, temperature, the rate and duration of the electrical stimulation, as well as the stiffness, geometry, size, surface properties and contact force of the electrodes. The dielectric strength typically varies also with the material elastic modulus¹⁰, the sample thickness^{8,9} and the applied pre-stretch^{8,9,12,13,14}. In addition, the dielectric strength relates to the threshold value of the current that has been set to define a breakdown event. Therefore, meaningful dielectric breakdown strength values always need to be accompanied by detailed information about the test conditions.

To cover a wide range of potential industrial DE actuator and sensor application a minimal temperature range for the dielectric breakdown test setup is defined as 0 °C to 150 °C. Negative temperatures down to -70 °C are optional due to potential problems with surface freezing on the DE or test electrodes. A stated relative humidity range of 10 % to 95 % includes most environmental conditions omitting total surface wetting.

The electrical field between the two electrodes strongly depends on the electrode tip geometry. A flat electrode face creates a uniform electrical field, comparable to a parallel-plate capacitor, and an even mechanical contact pressure. However, a not perfectly polished edge on the flat electrode may potentially harm the elastomer by cutting or induce high electric field concentrations at sharp imperfections. An alternative hemispheric or elliptical electrode tip geometry generates a smooth electric field by the lack of edges, but inhomogeneous distribution due to the nonparallel electrode surfaces. Additionally, the pointwise mechanical contact, creating a high contact pressure, may significantly influence the samples thickness and thereby the resulting breakdown field strength. Since there are advantages and drawbacks for each electrode geometry no concluding specification for the electrode is possible, an experimental investigation is required. Hence the test setup should allow an easy adaptation of the various electrode tip geometries.

The sample thickness z strongly influence the induced electrical field at an applied voltage V as mentioned in equation (2). Since the contact force influences the sample thickness, its value needs to be precisely adjustable and repeatable. A simple position controlled approach tends to be insufficient as slight thickness deviations in combination with a relative high compression stiffness of the elastomer leads to large contact force variations. Therefore, the test setup requires a force-controlled electrode approach independent of the samples thickness in a range from 0.1 gF to 30 gF.

Considering the strong dependency of the breakdown field strength from the sample thickness and the local material condition the breakdown test must be combined with a spatial resolved thickness measurement. The specimen frame should be exchangeable with a reproducible positioning system.

Since the dielectric breakdown is a statistic event depending on local defects, a single measurement is not meaningful. To obtain a representative value a multitude of test points need to be evaluated. The analysis of the measurements can be performed by using the Weibull distribution¹⁵ as mentioned by Kollosche and Kofod¹⁰ which combine their measurements in a statistical value.

To obtain repeatable and accurate test results a fully automated test procedure for positioning and applying the electrodes is needed. In addition, no manual user interaction during tests in the climate chamber with closed doors is possible to ensure consistent climate conditions.

2.2 Design

Figure 2 presents a novel mechanical setup to perform advanced breakdown test on membranes. The mechanism provides a specimen fixture, movable electrodes with adjustable contact force and a scanning system for multiple test points on one sample.

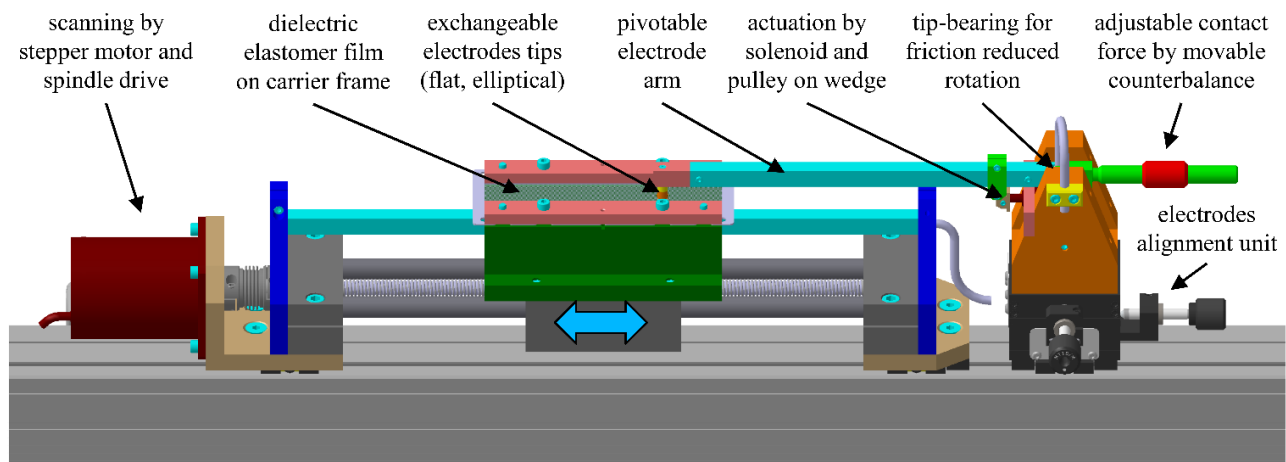


Figure 2. Schematic view of the novel advanced dielectric breakdown test setup.

For the investigation of the dielectric breakdown, an electrical field has to be induced in the membrane, therefore the film needs to be in contact with the electrodes connected to a high voltage source. To enable multiple test points on one sample at least one electrodes is needed to be movable.

The movable electrode is attached to a pivoting arm, like a record player, allowing to be switched between in contact with the elastomer film or being vacant. The arm is suspended on a tip-bearing consisting of a hardened sharp both-sided cone in two spherical calottes resulting in a very low friction bearing with negligible play and high temperature

resistance. On the right-hand side, a counterbalance mounted on a fine-pitched thread is balancing the torque of the electrode's and arm's weight. The thread offers a precise positioning of the counterbalance allowing to adjust the contact force with a repeatable resolution of 0.01 gF. To measure the currently set contact force, a scale with an adapted frame is placed beneath the electrode instead of the elastomer film. The electrode is parted in a fixed body mounted isolated on the arm and an electrode tip attached to the body by an internal thread enabling a simple exchange of the electrode tip thus geometry. Downwards pivoting of the arm to touch the elastomer film is done automatically by the adjusted contact force, to move up the arm during repositioning a mechanism is needed. A spring-loaded wedge pushes the arm up during standby, while measurement a solenoid retracts the wedge allowing the arm to move freely generating the contact force. The second electrode is fixed stationary beneath the elastomer film with a small gap. Applying the contact force of the upper electrode deflects the soft film slightly downwards closing the gap and fixing the film between the two electrodes. After retraction of the upper electrode the tension in the elastomer separates the film again from der lower electrode. To ensure a precise alignment of both electrodes the upper one is placed on a two-dimensional positioning stage allowing manual adjustments.

During separation of both electrodes the elastomer is freely movable. A positioning stage consisting of a high temperature linear bearing with a threaded spindle and stepper motor allows position-controlled movement in a temperature range from $-20\text{ }^{\circ}\text{C}$ to $+180\text{ }^{\circ}\text{C}$. In preparation to the experiment the elastomer film is placed with adjustable pre-strain on a lab-specific standardized stainless-steel frame to enable a simple sample transport between various experiment setups ensuring reproducible positioning. The standardized frame is mounted in a clamping system attached to the linear bearing and positioned by locator pins to enable the transfer of position related measurements. In preparation to the dielectric breakdown voltage test at multiple positions along the samples centerline, a film thickness measurement along the centerline is carried out using another test setup. For the calculation of the breakdown field strength from the measured breakdown voltage and film thickness a precise correlation of the measurement positions is crucial. A step-edge on the standardized frame defines the reference position allowing the detection in the thickness profile and providing a stop edge as reference for linear bearing.

The high voltage generation is provided by a commercial available HypotMAX 7710¹⁶. This device offers a dielectric withstand test mode generating up to 12 kV with adjustable ramp-up time and a resolution of 10 V. The detection of the dielectric breakdown is realized by a current threshold, adjustable in a range from $0\text{ }\mu\text{A}$ to $9999\text{ }\mu\text{A}$. To generate different environment conditions, a CTS Climatic Chamber C-70/350¹⁷ is used, offering a sufficiently large test chamber with temperature range of -70 to $+180\text{ }^{\circ}\text{C}$ and a relative humidity range of 10 to 98 %.

2.3 Realization

Figure 3 shows the realization of the completely assembled test setup with the linear guiding in the mounting position, a freshly installed $50\text{ }\mu\text{m}$ elastomer film and flat electrode tips.

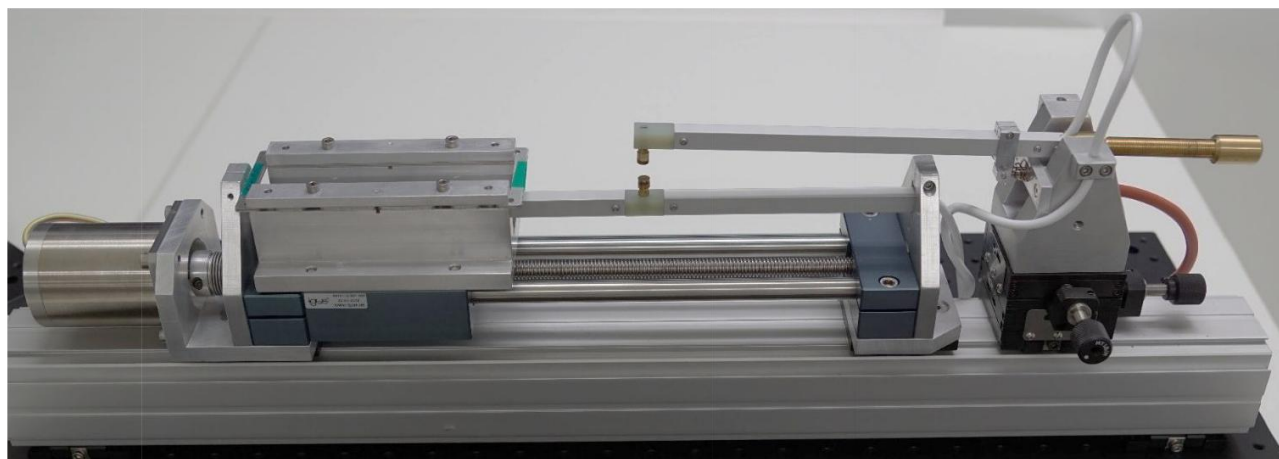


Figure 3. Realization of the novel advanced dielectric breakdown test setup.

To allow the characterization of the membrane under different ambient conditions the test stand is placed in a climate chamber controlling ambient temperature and humidity. Additionally, a multiplicity of samples needs to be processed for

statistical investigations, requiring the utilization of an automated test setup with minimum manual physical interaction. Since all components, like dielectric withstand tester, climate chamber, stepper motor and solenoid, are remote controllable via various interfaces, the setup is automated using LabVIEW. Figure 4 gives a schematic overview of the complete test setup. All electrical connections made by temperature resistant wiring pass through an insulated port to the surrounding where the components with lower temperature rating are placed.

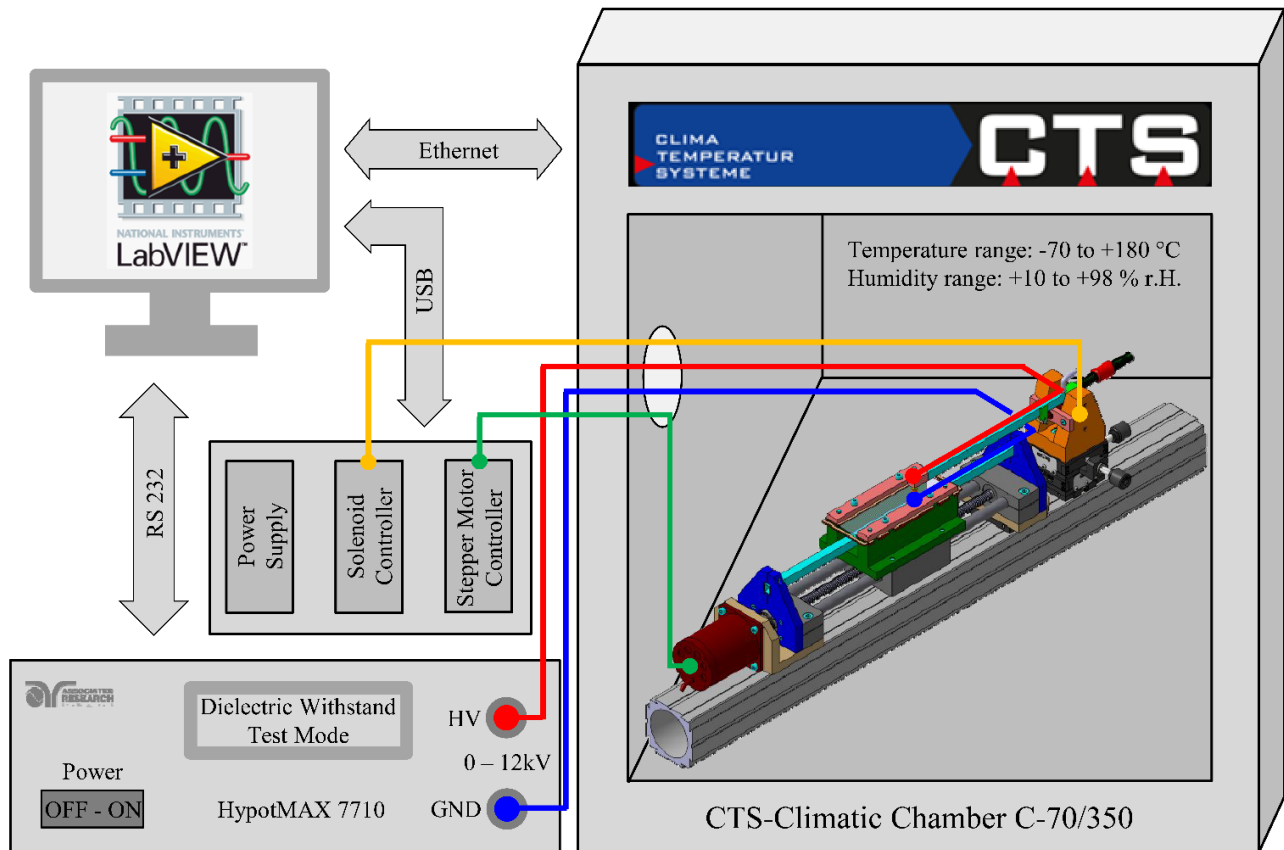


Figure 4. Schematic view of the dielectric breakdown test setup inside the climate chamber including all mechanical, electrical and control elements.

The high voltage generation (HypotMAX 7710) holds a serial RS232 interface providing full control over test parameters like voltage ramp and current threshold for breakdown detection. In addition, a real-time readout of voltage, current and failure mode is possible.

The stepper motor and solenoid controller are connected via USB, allowing position real-time readout and sending of motion tasks. Communication with the climate chamber via ethernet network offers receiving current temperature and humidity values as well as sending new setpoints for both quantities. The implemented LabVIEW program interacts with all four components and guides the user with a simple user interface through the experiment sequence. Starting by sending new setpoints to the climate chamber and waiting for stationary conditions, followed by finding the reference position on the standardized frame and finally executing multiple breakdown tests along the samples centerline with prior given parameters. These parameters include the position of the first and last test point related to the reference edge as well as the number of test points. The measured breakdown voltage for each test point and its position are stored in a CSV file for further processing to calculate the breakdown field strength by utilizing the thickness profile. The actual breakdown test sequence consists of moving to the requested test position, lowering the electrode arm by energizing the solenoid, waiting for the arm to settle, requesting a breakdown test, waiting for the breakdown event, collecting the result and finally lifting the arm again.

3. FIRST RESULTS

After the completion of the test setup with its mechanical and electronical components, first tests are conducted to validate its capabilities.

3.1 Test parameter

To simplify the test procedure, this first measurements are taken outside the climate chamber at a room temperature of 22 °C and a relative humidity of 35 %. All test and preparations are conducted under cleanroom conditions (ISO 7) to prevent damage of the film surface by dust particles. The specimens are fabricated at zero pre-stain using ELASTOSIL 2030 250/50¹⁸, a 50 µm thick silicone film produced by Wacker for DE applications.

Figure 5 shows the film after the breakdown test. The standardized test frame offers an accessible centerline length of 130 mm on the sample. To prevent arcing to the metal frame a symmetric safety margin of 15 mm on both sides is used, leaving a test range of 100 mm. Using flat electrodes with a uniform electrical field distribution a breakdown event can occur at any point of the electrode surface due to local weak points in the film. During a breakdown event a tiny carbonized tube connecting top and bottom layer is generated. To minimize the influence of recent breakdown events, a sufficient spacing of 10 mm between neighboring test points for an electrode diameter of 6 mm is chosen.



Figure 5. Dielectric elastomer film after dielectric breakdown test with circular flat electrode at eleven positions.

3.2 Contact force variation

The first step in the validation process of test setup is a systematic variation of the electrode contact force to investigate its influence on the breakdown voltage using a flat electrode geometry. A total of eighteen samples is prepared to test contact forces in the range of 0.5 gF to 30 gF in six steps. To reach a statistical significant number of test points three samples per force step are used resulting in 33 test points per force step.

Figure 6 shows a table of selected plots presenting the results of three force steps. A row represents a force step and exhibits the breakdown voltage over sample position for all 33 test points. Each plot reports the median value as a red line and the average value as turquoise line. The average breakdown voltage at a contact force of 0.5 gF is 5600 V resulting in a breakdown field strength of 112 V/µm. Overall the experiments (a) to (c) show very little mean variation and no outliers confirming the repeatability of the test setup. The second row depicts the results for a contact force of 9.0 gF with a slightly reduced average breakdown voltage of 5532 V and just as little mean variation. In the last row a contact force of 30.0 gF is applied resulting in a still high average breakdown voltage of 5523 V including the two outliers in plot (g).

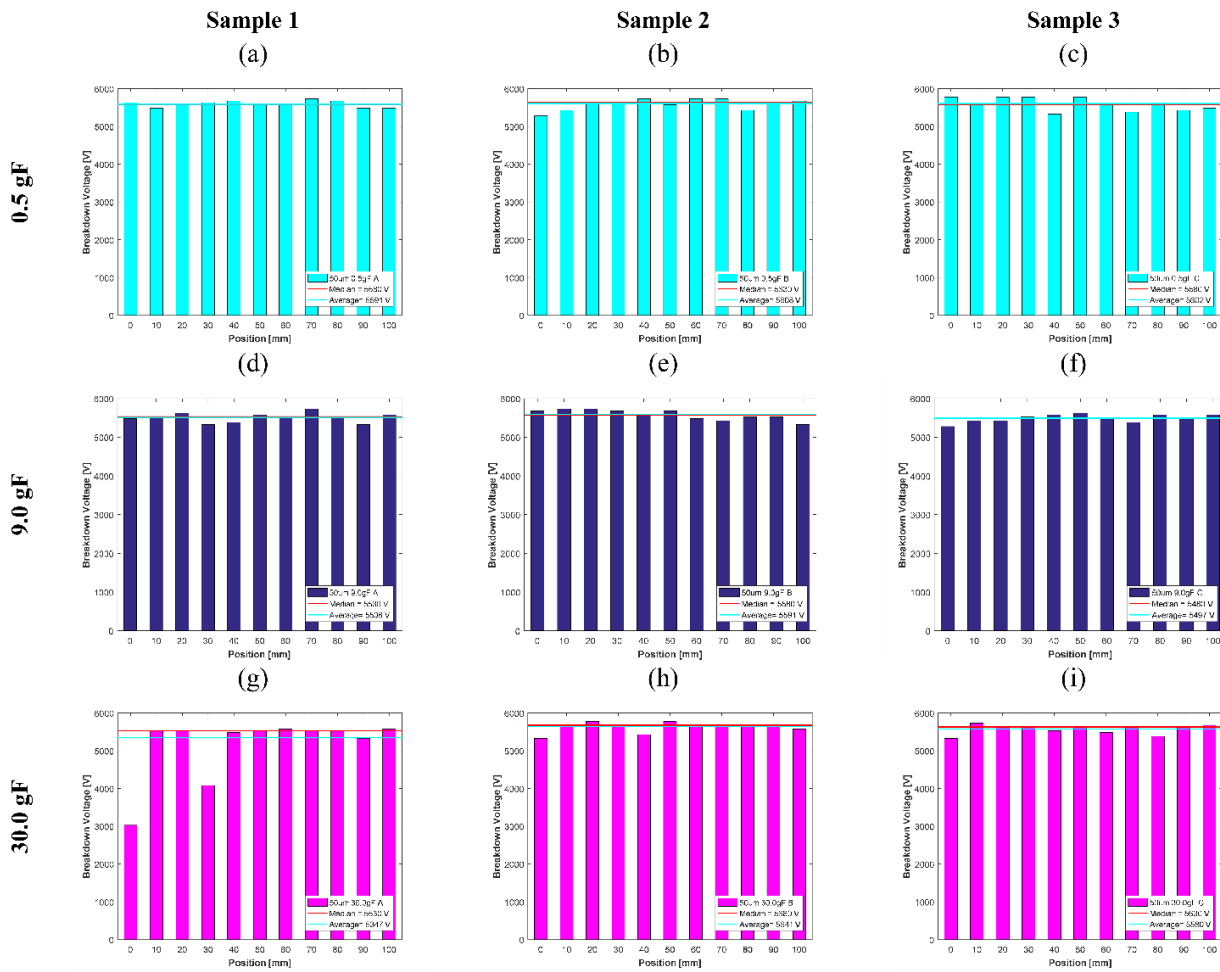


Figure 6. Experimental breakdown test results for flat electrodes with different electrode contact forces using three samples for each force level and eleven test positions per sample, using 50 μm silicone film ELASTOSIL 2030 by Wacker¹⁸.

To gain a better understanding of the contact force influence on the statistical breakdown voltage distribution, a condensed representation of the results is shown in Figure 7. This plot reveals all seven force steps as abscissa and the breakdown voltage as ordinate. The red lines represent the median value for all 33 test points in each force step. An indicator for the 25th and 75th percentiles is given by the top and bottom edges of the blue boxes. Breakdown voltages deviating more than 1.5 times the distance between the 25th and 75th percentiles from the median are treated as outliers and marked with red crosses. The black whiskers extend to the most extreme data points not including outliers.

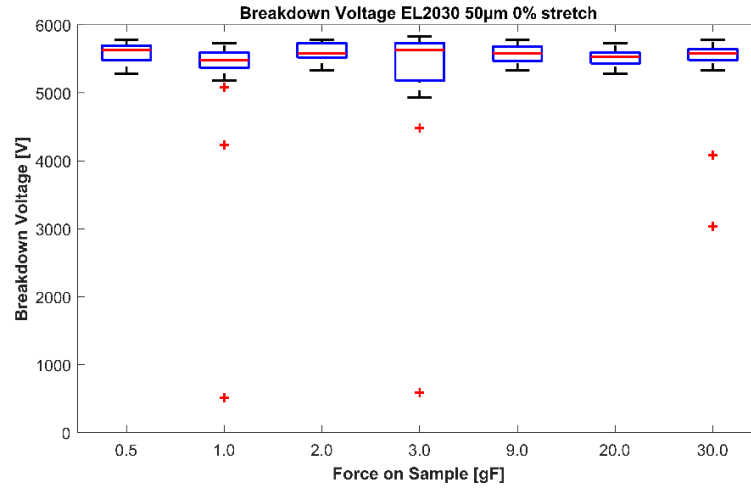


Figure 7. Condensed statistical results for flat electrodes with different contact forces, using the 50 μm silicone film ELASTOSIL 2030 by Wacker¹⁸: Red line is median, Blue box indicates the 25th and 75th percentiles, Black whiskers represents extreme values without outliers, Red cross is outlier.

Asides from a somewhat larger variance for the experiments with a contact force of 3.0 gF and the seven outliers in a total of 231 test points, the test setup generates consistent measurements. The median breakdown voltage appears rather independent of the contact force showing a steady value of around 5550 V. This contrasts with the expected behavior that an increasing contact force reduces the film thickness leading to a premature breakdown. A feasible explanation may be that the contact force applied by the arm is negligible in comparison to the Coulomb forces generated by the charges on the electrode surface. The charge induces compressive Maxwell stress σ_{MW} is calculated for an applied voltage of 5550 V and a film thickness of 50 μm by the simplified electrostatic model from Pelrine et al.⁶ with equation (3).

$$\sigma_{\text{MW}} = \epsilon_0 \cdot \epsilon_r \cdot \left(\frac{V}{z}\right)^2 = 8.854 \cdot 10^{-12} \frac{\text{F}}{\text{m}} \cdot 2.8 \cdot \left(\frac{5550 \text{ V}}{50 \mu\text{m}}\right)^2 = 305 \text{ kPa} \quad (3)$$

The compressive stress $\sigma_{\text{m,el}}$ introduced by the contact force F_{el} of the electrode is calculated in equation (4) for the maximal applied contact force of 30.0 gF.

$$\sigma_{\text{m,el}} = \frac{F_{\text{el}}}{A_{\text{el}}} = \frac{m_{\text{el}} \cdot g}{A_{\text{el}}} = \frac{30 \text{ g} \cdot 9.81 \text{ N/kg}}{(6.3 \text{ mm})^2 \cdot \pi/4} = 9.44 \text{ kPa} \quad (4)$$

Comparing the Maxwell stress with the contact force induced stress, exhibits a 32 times larger influence of the Maxwell stress and a negligible impact of the contact force in the range from 0.5 gF to 30.0 gF. To generate a measurably effect of the contact force on the breakdown voltage either a higher contact force in the range of 1000 gF or a smaller contact area is needed. The contact area can be reduced by using smaller diameter electrodes or applying a hemispheric/elliptical electrode tip geometry resulting in an almost pointwise contact. However, these results illustrate a very low intrinsic measurement uncertainty of the setup, allowing further investigations on the influencing factors of the dielectric breakdown field strength.

4. CONCLUSION

The development, realization and validation of a fully automated scientific test stand is presented, allowing the investigation of the dielectric breakdown in DE films under different environmental conditions. The test setup offers the study of various film thicknesses at comparable conditions. Exchangeable electrode tips allow the research of different electrical field distribution induced by the electrode geometry. A fine adjustable contact force ensures a defined mechanical contact with the film surface while creating minimal film thickness deformation in a repeatable manner. Furthermore, this enables to investigate the influence of the contact pressure on the electrical breakdown field strength. An exchangeable specimen frame offers easy film preparation with different pre-stretch strains and spatial resolved thickness measurements in preparation of the breakdown test. To allow the characterization of the film under different

ambient conditions the test stand is placed inside a climate chamber controlling ambient temperature and humidity. A remote-controlled servo motor allows spatial resolved breakdown voltage measurements resulting in combination with the local thickness measurements in a breakdown field strength. Additionally, the fully automated setup allows statistical investigations using numerous samples and thereby a meaningful investigation of the breakdown field strength. Finally, first test results with variation of the contact force are conducted and discussed.

REFERENCES

- [1] York, A. and Seelecke, S., "Towards Self-Sensing of DEAP Actuators: Capacitive Sensing Experimental Analysis," ASME 2010 Conf. Smart Mater. Adapt. Struct. Intell. Syst. Vol. 1, 307–314, ASME (2010).
- [2] Shankar, R., Ghosh, T. K. and Spontak, R. J., "Dielectric elastomers as next-generation polymeric actuators," *Soft Matter* **3**(9), 1116 (2007).
- [3] Koh, S. J. A., Keplinger, C., Li, T., Bauer, S. and Suo, Z., "Dielectric Elastomer Generators: How Much Energy Can Be Converted?," *IEEE/ASME Trans. Mechatronics* **16**(1), 33–41 (2011).
- [4] Carpi, F., De Rossi, D., Kornbluh, R., Pelrine, R. and Sommer-Larsen, P., [Dielectric elastomers as electromechanical transducers: Fundamentals, Materials, Devices, Models and Applications of an Emerging Electroactive Polymer Technology] (2008).
- [5] Rizzello, G., Naso, D., York, A. and Seelecke, S., "A Self-Sensing Approach for Dielectric Elastomer Actuators Based on Online Estimation Algorithms," *IEEE/ASME Trans. Mechatronics* **22**(2), 728–738 (2017).
- [6] Pelrine, R., Kornbluh, R., Joseph, J., Heydt, R., Pei, Q. and Chiba, S., "High-field deformation of elastomeric dielectrics for actuators," *Mater. Sci. Eng. C* **11**(2), 89–100 (2000).
- [7] Carpi, F., Anderson, I., Bauer, S., Frediani, G., Gallone, G., Gei, M., Graaf, C., Jean-Mistral, C., Kaal, W., Kofod, G., Kollosche, M., Kornbluh, R., Lassen, B., Matysek, M., Michel, S., Nowak, S., O'Brien, B., Pei, Q., Pelrine, R., et al., "Standards for dielectric elastomer transducers," *Smart Mater. Struct.* **24**(10), 25pp (2015).
- [8] Huang, J., Shian, S., Diebold, R. M., Suo, Z. and Clarke, D. R., "The thickness and stretch dependence of the electrical breakdown strength of an acrylic dielectric elastomer," *Appl. Phys. Lett.* **101**, 122905 (2012).
- [9] Gatti, D., Haus, H., Matysek, M., Frohnapfel, B., Tropea, C. and Schlaak, H. F., "The dielectric breakdown limit of silicone dielectric elastomer actuators," *Appl. Phys. Lett.* **104**, 52905 (2014).
- [10] Kollosche, M. and Kofod, G., "Electrical failure in blends of chemically identical, soft thermoplastic elastomers with different elastic stiffness," *Appl. Phys. Lett.* **96**, 71904 (2010).
- [11] ASTM International., "Standard Test Method for Dielectric Breakdown Voltage and Dielectric Strength of Solid Electrical Insulating Materials at Commercial Power Frequencies" (2013).
- [12] Kofod, G., Sommer-Larsen, P., Kornbluh, R. and Pelrine, R., "Actuation response of polyacrylate dielectric elastomers," *J. Intell. Mater. Syst. Struct.* **14**(12), 787–793 (2003).
- [13] Choi, H. R., Jung, K., Chuc, N. H., Jung, M., Koo, I., Koo, J., Lee, J., Lee, J., Nam, J., Cho, M. and Lee, Y., "Effects of prestrain on behavior of dielectric elastomer actuator," *Smart Struct. Mater. 2005 Electroact. Polym. Actuators Devices*, Y. Bar-Cohen, Ed., 283 (2005).
- [14] Tröls, A., Kogler, A., Baumgartner, R., Kaltseis, R., Keplinger, C., Schwödiauer, R., Graz, I. and Bauer, S., "Stretch dependence of the electrical breakdown strength and dielectric constant of dielectric elastomers," *Smart Mater. Struct.* **22**(10), 5 (2013).
- [15] Weibull, W., "A statistical distribution function of wide applicability," *J. Appl. Mech.* **18**, 293–297 (1951).
- [16] Associated Research Inc., "HypotMAX 7710 Manual" (2016).
- [17] CTS GmbH., "Climatic Test Chamber C-70/350 Specification" (2000).
- [18] Wacker Chemie AG., "ELASTOSIL® Film 2030 250/50," 2016, <http://sdb.wacker.com/pf/e/result/report.jsp?P_LANGU=D&P_SYS=2&P_SSN=6653&P_REP=00000000000000000002&P_RES=8586&P_SPEC=R>.

4.3 Effect of actuation parameters and environment on the breakdown voltage of silicone dielectric elastomer films

Bettina Fasolt¹, Felix Welsch², Marius Jank², Stefan Seelecke^{1,2}

- ¹ Intelligent Materials Systems Lab, Center for Mechatronics and Automation Technologies (ZeMA) gGmbH, Saarbrücken, Germany
- ² Intelligent Materials Systems Lab, Department of Systems Engineering, Department of Materials Science & Engineering, Saarland University, Saarbrücken, Germany

Publication: Smart Materials and Structures

Publisher: IOP Publishing

August 2019

Citations: 29

Impact Factor: 3.7

<https://doi.org/10.1088/1361-665X/ab2f34>

Author Rights Policy IOPscience: The author retains the right to include publication in a thesis or dissertation provided it is cited and not published commercially. Permission is not required.

The paper presents a comprehensive study of the electrical breakdown behavior of DEA within a temperature range from 10 °C to 50 °C and relative humidities from 20 % to 95 % relative humidity. This range corresponds to the environmental conditions typically encountered in industrial systems, where DEAs may be employed as pumps or valves. The influence of these conditions is examined on pure silicone thin film, pre-stretched uniaxially between 0 % and 100 %. To ensure consistently homogeneous stretching, a newly developed automated stretcher, designed and built by Marius Jank, is introduced in this paper. Jank programmed the stretcher, adapted the program throughout the study, and prepared pre-stretched samples.

Because DEA applications require not only dielectric material but also an electrode, the influence of the indoor environmental conditions on the breakdown behavior of a DEA are repeated using the same silicone thin films but applied with screen printed carbon black electrodes to assess whether the applied electrodes cause different behavior under varying environmental conditions. These investigations are carried out on unstretched films.

The scope of the work was defined by Bettina Fasolt, who also manufactured and prepared the samples, conducted the experiments, and wrote the paper.

The experimental setup utilizes the breakdown tester described in Section 4.2, which was designed and built by Felix Welsch and enables multiple consecutive tests within the climate chamber without

interruption. This allows for a high number of measurement points, with 66 measurements conducted on films without screen printed electrodes and 55 on films with applied electrodes.

The results indicate a slight increase in breakdown voltage across all sample types with rising temperature. This trend is observed in both electrode-free and electrode-equipped samples, as well as in pre-stretched films. No significant influence of relative humidity or moisture content on breakdown voltage is detected. However, a subsequent study by Albuquerque and Shea [60], published after this paper was presented, suggests that a broader temperature range may be necessary to reveal such effects.

Pre-stretched samples exhibit a significant increase in breakdown field strength, which correlates with the increasing stretch ratio. In contrast, samples with screen printed electrodes exhibit breakdown field values approximately 20 % lower than those without electrodes. As electrodes are essential for DEA functionality, this reduction highlights the need for further investigation into electrode-related performance impacts.

Effect of actuation parameters and environment on the breakdown voltage of silicone dielectric elastomer films

Bettina Fasolt¹ , Felix Welsch², Marius Jank² and Stefan Seelecke^{1,2}

¹ Intelligent Materials Systems Lab, Center for Mechatronics and Automation Technologies (ZeMA) gGmbH, Saarbruecken, Germany

² Intelligent Materials Systems Lab, Department of Systems Engineering, Department of Materials Science and Engineering, Saarland University, Saarbruecken, Germany

E-mail: b.fasolt@zema.de

Received 7 February 2019, revised 31 May 2019

Accepted for publication 1 July 2019

Published 2 August 2019



CrossMark

Abstract

This paper presents results on dielectric breakdown studies for silicone dielectric elastomer (DE) membranes. Dielectric breakdown is a crucial property for the characterization of DE actuator behaviour. Here, we particularly focus on the effect of environmental parameters on the breakdown field, using a recently designed novel test stand for automatic testing of multiple measurement points per sample in a climate chamber. We present an extensive study about the influence of temperature, humidity, and water content on the breakdown field of DEs under indoor environmental conditions. Additionally, the effect of actuation parameters, such as various stretch-ratios, as well as the influence of screen-printed carbon black electrodes, is systematically investigated. The study indicates slightly higher breakdown fields with increasing temperatures but negligible influence of humidity and water content changes. Samples with printed electrodes show significantly lower breakdown fields whereas the increase of stretch ratio resulted in significantly higher breakdown fields.

Keywords: dielectric breakdown test, silicone films, environmental conditions, stretch, electrodes, temperature, humidity

(Some figures may appear in colour only in the online journal)

1. Introduction

The last years have seen an increasing interest in applications for dielectric elastomer transducers (DETs) as actuators, sensors, and generators in the research community as well as in industry [1–4]. A standard DET typically consists of a compliant dielectric elastomer (DE) membrane sandwiched between two stretchable electrodes. When a voltage is applied to the electrodes, electrostatic forces lead to a reduction of the membrane thickness along with a simultaneous lateral expansion, thus resulting in controllable motion. A large number of applications can be derived from this mechanism, such as valves [5–7], pumps, switches [8, 9], wearables [10–12], haptic devices [13, 14], and soft robotics applications [15–17]. Development of fast and cheap high voltage

electronics [18, 19] as well as DET applications with high force [20] and high stroke [21] expand application fields.

DE actuator performance strongly depends on the electromechanical behaviour of the membrane, which is influenced by the permittivity and the breakdown field strength. The breakdown field strength represents the maximum value of the electrical field, which can be withstood by the membrane, limiting the maximum actuator potential of the DE. This parameter can be measured in a breakdown test by increasing the applied voltage up to the breakdown point. Carpi *et al* [22] present a definition of standards and guidelines on how to assess and compare the performance of DE materials and devices. Different test stands for material and performance characterization are presented in the literature [23–25].

A number of studies have been performed to document the effect of various parameters on the dielectric breakdown of silicone materials. The effect of environmental conditions on bulk silicone used for electrical insulation has been reported in [26, 27], membrane stretch has also been shown to influence breakdown [25, 28–31], as well as film production quality [32], electrode properties [33] or different ambient media [34]. Welsch *et al* [35] recently developed a device for automatic testing of multiple measurement points per sample in a climate chamber, thus allowing for high-throughput reproducible measurements for statistically relevant results. This test stand, for which first test results were shown in [36], was utilized in the following study.

This paper presents a comprehensive investigation of the influence of environmental conditions, e.g. temperature and relative humidity/water content, on the breakdown strength of silicone DE membrane actuators. Wacker ELASTOSIL 2030/50 silicone film [37] has been selected for this study, as it is at present the only commercial silicone film available in large quantities for technical applications, and comprehensive results on the material have not been published to date. The focus of the study was on the investigation under typical conditions within industrial buildings in which DE systems will most likely be operated, with temperatures between 10 °C and 50 °C and relative humidities between 20% and 90%.

Additionally, the effect of various stretch-ratios was investigated under different environmental conditions. Sample pre-stretched uni-axially from $\lambda = 1$ to $\lambda = 2$ were studied to simulate stretch conditions in actuator systems. Finally, the influence of printed carbon black electrodes on the membrane was analyzed under three different temperatures and varying relative humidities. The electrodes in this paper were manufactured using the screen-printing method described in [38]. Information about the influence of the electrodes on the breakdown voltage is essential, because almost all DE applications require flexible electrodes attached to the membranes. Here, not only the influence of the application method and parameters are important, but also the electrode material [33]. Due to the variety of electrode materials and parameters for the application, this investigation is an ongoing process.

2. Experimental setup and procedure

2.1. Materials and sample preparation

Wacker Elastosil 2030/50 50 μm silicone film is used as DE material in this paper. The influence of environmental conditions on the breakdown field of the DE film was investigated on (a) samples at $\lambda = 1$, (b) pre-stretched samples $\lambda = 1$ to $\lambda = 2$, and (c) samples at $\lambda = 1$ with screen-printed electrode dots. These different types of tests require three different types of sample preparation.

2.1.1. Preparation samples (a) at $\lambda = 1$. Each sample is composed of silicone film sandwiched between two test frames equipped with sticky tape. Shown in figure 1, left side,

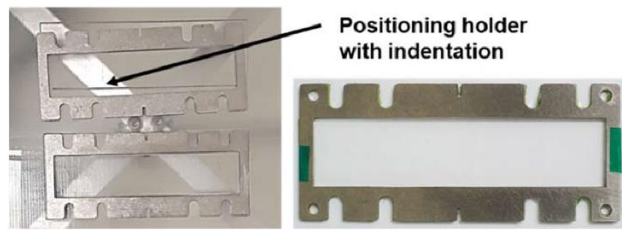


Figure 1. Positioning holder (transparent) with test frames (left). Upper frame is not aligned to show indentation. Fully prepared sample (right).

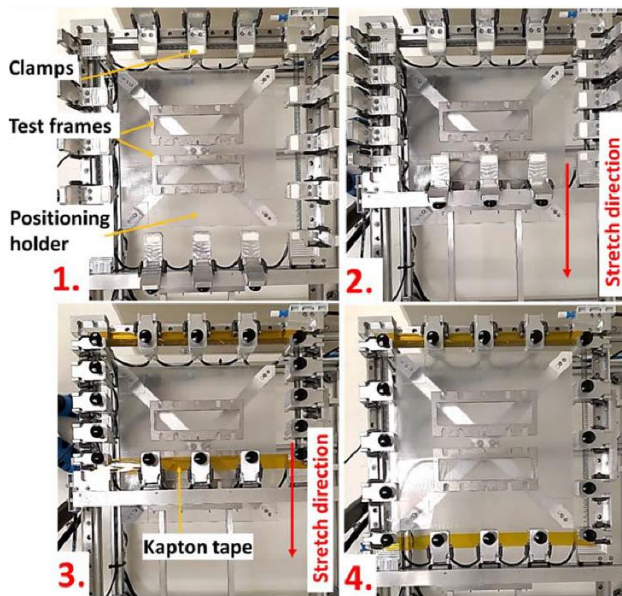


Figure 2. Preparation steps for pre-stretched samples in automated stretcher, uni-axial stretch. Pictures showing home position with placement holder and frames (1), start position before stretch (2), start position with silicone film (3), and end position with stretched film (4).

two frames were placed in a 3D-printed positioning holder containing two indentations for exact positioning in the centre of the stretcher. Wacker Elastosil 2030 film was placed on the frames and the carrier was removed. Two frames were then placed on top of the film. Excess material was trimmed from the edges, the frames taken out of the holder and top and bottom frame taped together on the small side of the frame, figure 1, right side.

2.1.2. Preparation samples (b) pre-stretched $\lambda = 1$ to $\lambda = 2$.

The preparation process for the uni-axially pre-stretched samples is shown in figure 2, step 1 (left) to 4 (right). An automated stretcher, consisting of two separately controlled stepper motors and vacuum clamps for the fixation of the DE film was used for the stretching process. Step 1 shows the positioning holder and test frames with double-sided sticky tape with the stretcher in home position. In Step 2, the start position before stretch can be seen, after entering input parameters (stretch ratio, frame size) into the stretcher control system. In Step 3, the silicone film is cut to fit into the clamps

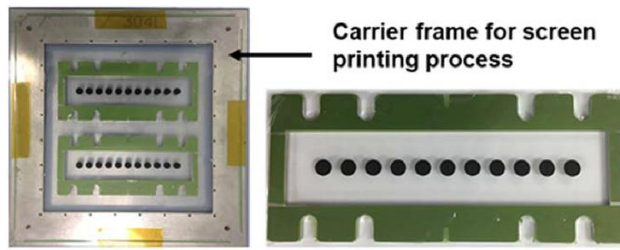


Figure 3. Carrier frame with screen-printed electrodes and test frames (left), finished sample for testing (right).

at start position. The clamps contain porous vacuum areas, which are activated before placing the film into the clamps and removing the carrier. For stretches $\lambda > 1.25$, Kapton tape is attached to the film to avoid necking, realizing an uni-axial in plane stretch. The film is then stretched to the desired ratio (Step 4). After stretch, the positioning holder with the test frames moves up automatically until film contact. A second test frame with sticky tape is placed on top of the film. The test frame is then cut out, and top and bottom frame are taped together. The stretcher allows different stretch ratios in each direction. However, only uni-axial stretch was used in this paper. The parameters stretch ratio, stretch direction, and sample size are controlled via LabVIEW interface. Twelve frames each were prepared with stretch ratios $\lambda = 1, 1.25, 1.5, 1.75$, and 2.0 .

2.1.3. Preparation samples (c) with printed electrodes. The electrodes on the samples investigated in this paper were applied via a screen-printing method. The preparation of the samples with printed electrodes required a more complex preparation process. The film was first transferred to a carrier frame at $\lambda = 1$, using the stretcher for holding and positioning the film and carrier frame, figure 3, left. The carrier frame is necessary for the screen-printing process. The electrode material was manufactured using a mixture of carbon black, PDMS and solvents. After heat curing, the electrodes consisted of 16% carbon black and 84% PDMS. The Carbon black/PDMS electrode dots were then screen-printed on both sides of the DE film in locations, where breakdown tests were conducted later. The electrodes were printed in a one-layer process using a *Sefar PET 1500 90/230* mesh. A description of the screen-printing process as well as the utilized material is presented in [38]. The diameter of the electrode dots coincided with the diameter of the electrodes of the breakdown tester used in the experiments. Finally, the film was transferred to the test frames in the same manner as described in 2.1.1, figure 3.

2.2. Test setup

The breakdown tests were conducted using an automated electrical breakdown tester, which allows reproducible electrical breakdown measurements under varying environmental conditions. A detailed description of the development, design, and first measurement results is provided in [32]. A picture of the tester is shown in figure 4.

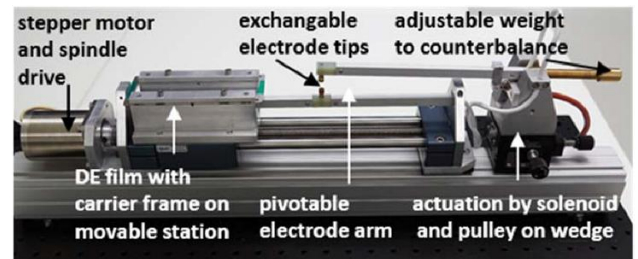


Figure 4. Automated dielectric breakdown tester.

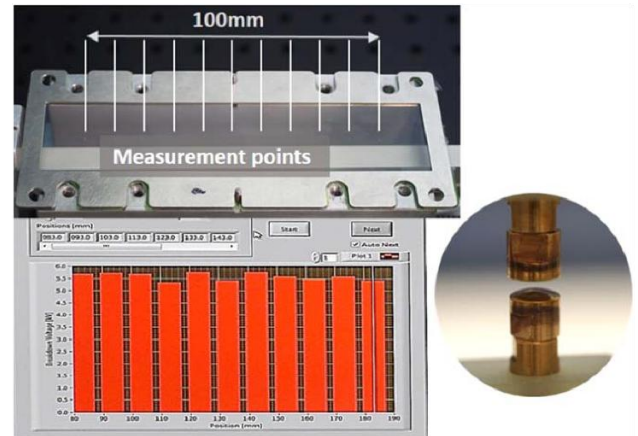


Figure 5. Position of 11 measurement points per sample sheet (top), example of test results (bottom left) and gold plated electrodes (right).

During the tests, two gold plated electrodes, one movable on a pivoting arm and one fixed, come in contact with the film and voltage is applied at a rate of 0.5 kV s^{-1} until breakdown or a maximum of 12 kV . The electrodes have a diameter of 6.3 mm . The movable top electrode is flat and the bottom electrode has a round shape, which is compatible with standardization suggestion from Carpi *et al* [22] and has also been selected due to minimal membrane interaction during spot positioning, figure 5, right. After breakdown, the electrodes disconnect and the tester automatically moves to the next position. The maximum size of the silicone test sheet used in the breakdown tester was $130 \text{ mm} \times 30 \text{ mm}$. On this sheet, a total of 11 positions per sample are tested, the locations are shown in figure 5, left. To ensure a sufficient number of measurements for statistic evaluation, five or six test sheets were used, respectively, resulting in a total of 66 measurement points for the samples without electrodes and 55 for the samples with electrodes for each environmental condition.

2.3. Test procedure

To allow for the characterization of the membrane under different ambient conditions the test stand was placed in a climate chamber controlling ambient temperature and humidity, figure 6. The prepared samples were placed onto the movable station of the breakdown tester and fixed into position using four screws. The respective ambient conditions were adjusted, and the samples were tested when the required



Figure 6. Placement of breakdown tester in climate chamber and outlet with connection to high voltage withstand tester, control unit and computer.

Table 1. Water content (g m^{-3}) depending on temperature and relative humidity. Grey areas show conditions not achievable in climate chamber within reasonable time, boxes with yellow border show example values for constant water content.

	Rel. humidity (%)								
	95	85	75	65	55	45	35	25	20
10	8.9	8.0	7.1	6.1	5.2	4.2	3.3	2.4	1.9
15	12.2	10.9	9.6	8.3	7.1	5.8	4.5	3.2	2.6
20	16.4	15.6	13.0	11.2	9.5	7.8	6.1	4.3	3.5
25	20.0	17.9	15.8	13.7	11.6	9.5	7.4	5.3	4.2
30	28.8	25.8	22.8	19.7	16.7	13.7	10.6	7.6	6.1
35	37.6	33.7	29.7	25.7	21.8	17.8	13.9	9.9	7.9
40	48.6	43.5	38.4	33.2	28.1	23.0	17.9	12.8	10.2
45	62.1	55.6	49.1	42.5	36.0	29.4	22.9	16.4	13.1
50	78.9	70.6	62.3	54.0	45.6	37.3	29.1	20.8	16.6

environmental conditions had been stable for at least 30 min. Since the stepper motor, pivoting arm with electrodes, solenoid, and the dielectric withstand tester are remotely controllable, the setup of the programme is automated using LabVIEW. After starting the programme, the movable station drives into position for the first measurement point and the electrodes on the pivoting arm make contact with the film. After breakdown, the electrodes disconnect and the carrier moves to the next position. This process is repeated until all 11 measurement points are tested.

All samples tested for one specific ambient condition were stored on a rack in the climate chamber for maximum exposure time. After opening the climate chamber door to exchange test frames, stable ambient condition were again ensured before the next test. Six test frames were prepared for each environmental condition (a) and (b), resulting in 66 measurement points. For the samples with screen-printed electrodes (c), five test frames were prepared, resulting in 55 measurement points per respective condition.

3. Results

This study focuses on the influence of environmental conditions on the breakdown behaviour of DE membranes, including also the additional influence of membranes under pre-stretch as well as membranes with pre-printed electrodes. Therefore, this section is subdivided into three parts. Section 3.1 shows the results of the tests conducted on un-stretched samples, section 3.2 shows the results achieved on pre-stretched samples, and section 3.3 illustrates the test results on samples with screen-printed electrodes on both sides of the membrane.

The environmental conditions investigated in this paper were restricted to indoor ambient conditions with temperatures between 10 °C and 50 °C and a relative humidity between 20% and 90%. Standard environmental conditions were established at a temperature of 20 °C and 55% rel. humidity. For a comprehensive study, each parameter temperature, relative humidity, and water content, was investigated separately.

Table 1 shows the water content (actual vapour density) depending on temperature and relative humidity. The relative humidity at a certain temperature is defined as

$$\text{Rel. humidity} = \frac{\text{Actual vapor density}}{\text{Saturation vapor density}} \times 100.$$

The values for the saturation vapour density were determined using the table and graph depicted in [39]. As seen in table 1, an increase in temperature causes a significant increase in water content. It was therefore not possible in this study, to keep the water content constant over a wide temperature range. The areas marked with a yellow box show an example of constant water content for different temperature and relative humidity values. The areas in grey show the conditions, which can not be achieved in the climate chamber within a reasonable amount of time. The table illustrates that a constant water content could only be achieved in the climate chamber over a ~ 25 °C temperature range.

3.1. Influence of water content, relative humidity, and temperature on breakdown voltage of un-stretched samples

The influence of water content, relative humidity, and temperature is shown in figure 7 (left). The possible influence of each parameter is separately discussed. To gain a better understanding of the statistical breakdown voltage distribution, a condensed representation of the results is shown in the form of a box plot. This plot reveals all eight ambient conditions as abscissa and the breakdown voltage as ordinate. The red lines represent the median value for the 66 test points (six frames) for each individual condition. An indicator for the 25- and 75-percentiles is given by the top and bottom edges of the blue boxes. Breakdown voltages deviating less than 1.5 times distance between the 25- and 75-percentiles from the median are within the range of the black whiskers, breakdown voltages deviation more than this are treated as outliers and marked with red crosses. An explanation for the reading of a box plot can be seen in figure 7 (right).

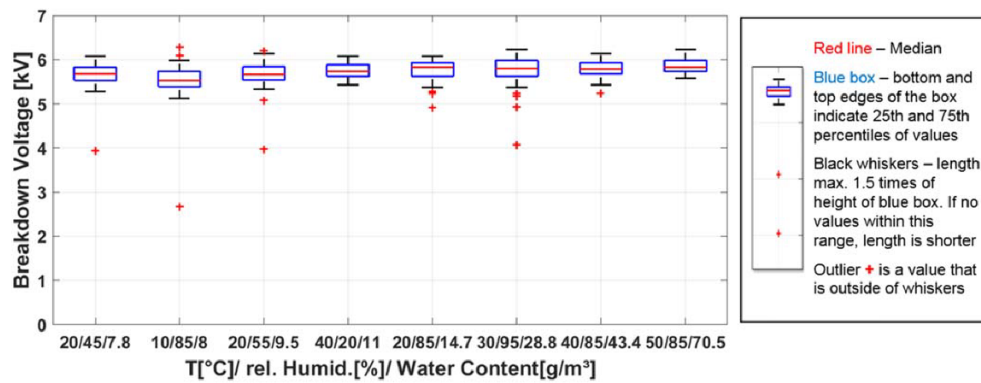


Figure 7. Influence of water content on breakdown voltage with lowest to highest water content from left to right (left). Bottom axis shows environmental condition 20/45/7.8: 20 °C/45% relative humidity/7.8 g H₂O. Explanation for reading a box plot (right).

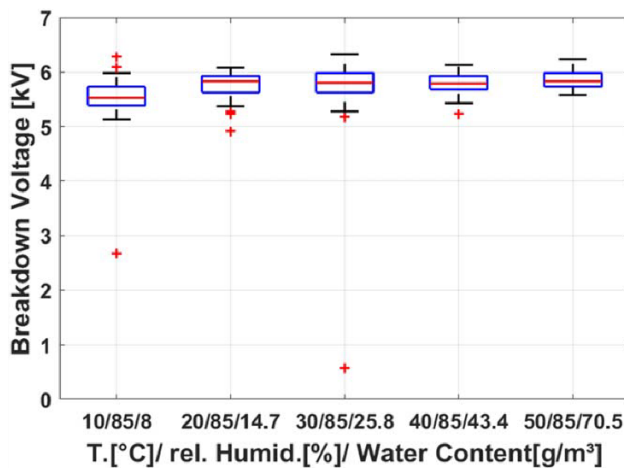


Figure 8. Influence of temperature on breakdown voltage @ const. relative humidity.

The diagram shows eight different environmental conditions increasing from lowest water content, 7.8 g m⁻³ to the highest water content, 70.5 g m⁻³ with temperatures between 10 °C and 50 °C. As illustrated in table 1, allowing for a reasonable stabilization time in the climate chamber (~30 min), constant water content was only achievable within a temperature range of 25 °C, because little changes in temperature and relative humidity have a great impact on the water content. Even though breakdown voltages vary slightly within the diagram, no indication of an influence of changing water content is visible. Slight changes of breakdown voltages are more likely due to the statistically limited number of samples, therefore inhomogeneities within the film having a higher impact.

The relative humidity also indicates to have no influence on the breakdown voltage. Figure 7 shows equal breakdown voltages for three different relative humidities at 20 °C (45%, 55%, and 85%) and two different relative humidities at 40 °C (20% and 85%).

To evaluate the influence of temperature on the breakdown voltage, the relative humidity was kept constant at 85% and the temperatures varied from 10 °C to 50 °C. As

established above, changing water content had no influence on the breakdown voltage under these conditions. The influence of temperature on the breakdown voltage is depicted in figure 8. Within this temperature range, a slight increase in breakdown voltage with increasing temperature is observed. This effect is probably due to the higher mobility and possible rearrangement of dipoles to an electrically more favourable position on the silicone chains at higher temperatures. A similar behaviour was observed by Du *et al* [40], who studied temperature effects on pre-breakdown formation of electrical pathways in bulk silicone. A more pronounced effect is expected at larger temperature changes, e.g. 0 °C–100 °C.

3.2. Influence of pre-stretch under varying environmental conditions on breakdown voltage

DEs operated as actuator run through a continuous process of membrane stretch and release. Therefore, knowledge about the influence of stretch on the breakdown behaviour is crucial for the operation of an actuator. Because the setup for the breakdown tests presented in this paper only allowed static membrane conditions, the influence of stretch was investigated on samples with a pre-stretched membrane. Five different uni-axial stretch ratios were investigated ($\lambda = 1.0$, $\lambda = 1.25$, $\lambda = 1.5$, $\lambda = 1.75$, and $\lambda = 2.0$). The samples were tested at two different environmental conditions, one condition being the standard condition and the second condition at higher temperature and relative humidity (40 °C, 85% rel. humidity). Six frames with a total of 66 measurement points were tested for each stretch ratio and environmental condition.

The breakdown results versus stretch ratio are shown in figure 9 depicting both environmental conditions.

The measurement results show a decrease of breakdown voltage with increasing stretch ratio. This is not astonishing, because the thickness of the membrane decreases with increasing stretch. The initial thickness of the Wacker Elastosil 2030/50 in un-stretched state ($\lambda = 1.0$) is 50 μ m. When the film is stretched to $\lambda = 2.0$, the film thickness decreases to 25 μ m, assuming uni-axial in-plane stretch and incompressibility. Therefore, an additional illustration of the results is necessary,

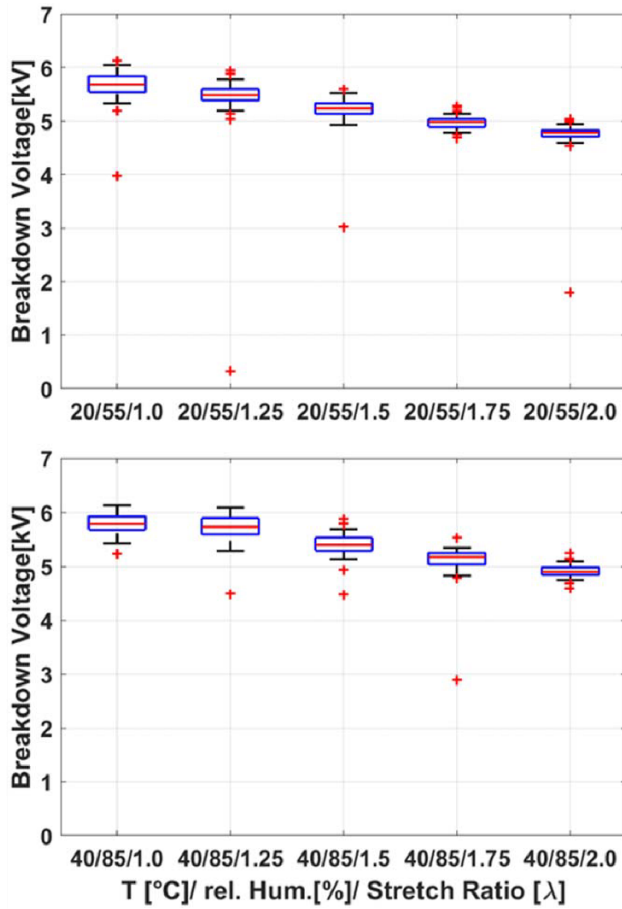


Figure 9. Breakdown voltage over stretch ratio λ from $\lambda = 1$ to $\lambda = 2$ at 20 °C (top) and 40 °C (bottom). Bottom axis shows environmental condition 40/85/1.25: 40 °C/85% relative humidity/Stretch ratio 1.25.

taking into account the change of thickness of the membranes over the different stretch ratios, figure 10. However, the result of figure 9 is important for the design of an actuator, when knowledge of the maximum applicable voltage for a defined deflection is required. Figure 10 shows the same test results as figure 9, but the breakdown voltage is divided by the respective membrane thicknesses, depicting breakdown field versus stretch ratio. As seen in figure 10, higher pre-stretch results in significantly higher breakdown field ($115 \text{ V } \mu\text{m}^{-1}$ @ $\lambda = 1.0$ – $180 \text{ V } \mu\text{m}^{-1}$ @ $\lambda = 2.0$). The phenomenon is likely due to the fact that a higher pre-stretch decreases the distance between neighbouring polymer chains, thus increasing attractive forces. In addition, most polymers exhibit stiffer mechanical behaviour for larger strains and are able to better withstand the electrically induced compression. The same behaviour was also observed by Vaicekauskaitė *et al* [28], while conducting breakdown tests on bi-axially stretched samples.

The tests were conducted using two different environmental conditions. Comparing the results, again a higher temperature consistently shows a slightly higher breakdown voltage. The relative humidity was also higher at 40 °C, but the influence of humidity was seen to be negligible in the previous investigation.

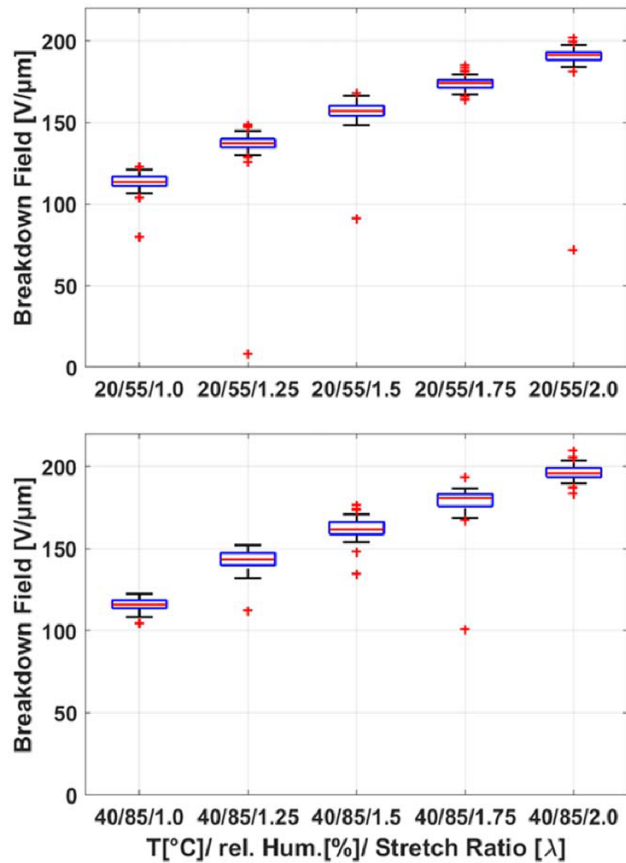


Figure 10. Breakdown field over stretch ratio λ from $\lambda = 1$ to $\lambda = 2$ at 20 °C (top) and 40 °C (bottom) considering the thinning of membrane due to stretch.

3.3. Influence of screen-printed electrodes under varying environmental conditions on breakdown voltage

The operation of DEs for actuator and sensor applications requires a flexible electrode attached to the membrane. Knowledge about the influence of the electrode on the breakdown behaviour of the DE as well as influence of environmental conditions on the membrane with electrodes are essential for the operational design. In this paper, the electrodes were printed via the screen-printing method.

Figure 11 shows the placement of the test frame with the printed electrode dots in the breakdown tester. The area where the gold-plated electrodes from the breakdown tester are positioned above the first electrode dots is enlarged. The picture was taken before the electrodes made contact and the sample was secured to the breakdown tester with a frame holder. In the upper left-hand corner, prepared test frames are visible, stored in a rack in the climate chamber. As explained in 2.3 Test procedure, the whole batch of samples is stored in the climate chamber for acclimatization before testing.

Results for the breakdown tests conducted on DE membranes with screen-printed electrodes are shown in figure 12. Noticeable in the figure are homogeneous breakdown voltages for each environmental condition, visible in the low height of the blue box. The three boxes on the left hand side in figure 12 document breakdown results from tests

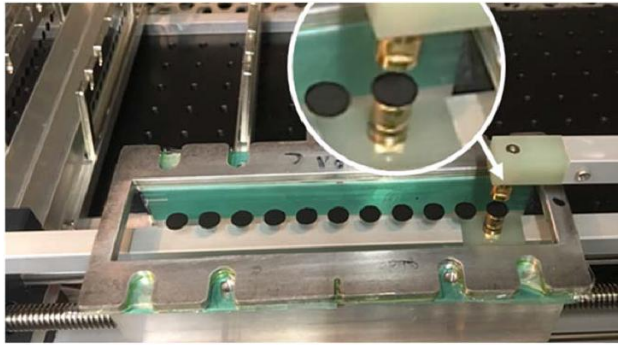


Figure 11. Test frame with electrode dots in breakdown tester; enlargement depicts electrode dots before connection and high voltage application. Left upper corner shows already prepared frames for acclimatization stored in climate chamber.

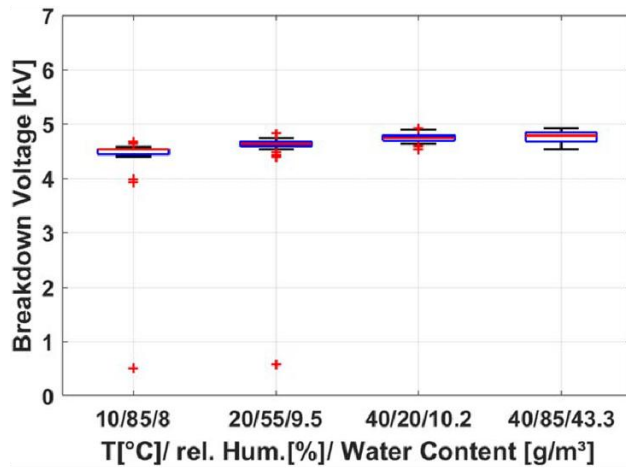


Figure 12. Breakdown voltage of samples with screen-printed electrodes for three different temperatures and similar water content (leftmost three boxes) and the same temperature but different water content (rightmost two boxes).

conducted at three different temperatures (10 °C, 20 °C, and 40 °C) and similar water contents (between 8.0 and 10.2 g m⁻³). The two boxes on the right hand side of the figure show results for tests operated at one temperature, 40 °C, but different water contents (10.2 and 43.3 g m⁻³). Figure 13 combines the results from figure 12 (different temperatures but similar water content) with results from samples without electrodes at the same environmental conditions, see also figure 7. The results indicate the same trend in breakdown behaviour for samples with and without printed electrodes, showing slightly increasing breakdown voltages with increasing temperatures. Comparing the results for different relative humidities at 40 °C, the water content also seems to have no impact on samples with printed electrodes as was shown for samples without electrodes in section 3.1.

The different breakdown behaviour between samples with electrodes and samples without electrodes is clearly visible in the height of the blue boxes, showing homogeneous results for samples with electrodes and higher variances in samples without electrodes. With voltage application, immediate homogeneous voltage distribution occurs within

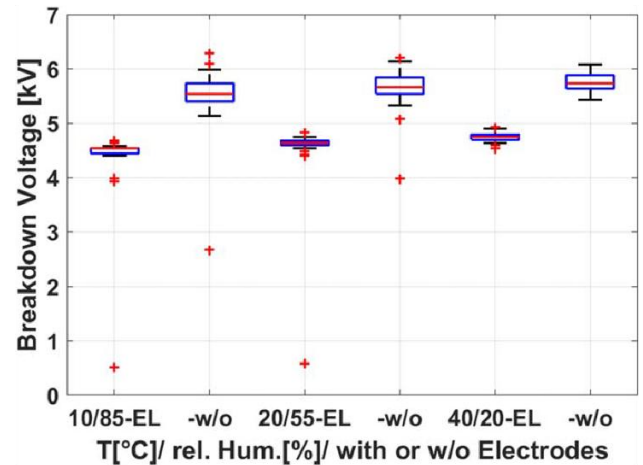


Figure 13. Comparison of breakdown voltage of samples with electrodes (-EL) and without electrodes (-w/o) at three different temperatures and similar water content.

pre-printed electrodes. Samples without electrodes, however, where voltage is applied with gold plated electrodes, do not immediately see a homogeneous voltage distribution over the contact area, probably due to either the shape of the electrodes (round and flat) or due to non-uniform membrane surfaces. Fasolt *et al* [36] investigated the influence of electrode shapes on breakdown behaviour and also found a more homogeneous but only slightly lower breakdown voltage using flat/flat compared to round/flat electrodes.

Also noticeable is the disparity of the breakdown voltages. The breakdown voltage for samples with pre-printed electrodes is consistently and significantly lower (by @900 V) than the voltages for samples without electrodes. Homogeneous voltage distribution in the pre-printed electrodes does not account for such a disparity in breakdown voltages. Rather printing method and/or electrode material seem to affect the breakdown voltage and should be investigated further.

4. Conclusions

Optimal application design of actuator systems for DE membranes requires a comprehensive knowledge of breakdown behaviour and breakdown-influencing parameters. This study presented the influence of parameters such as indoor environmental conditions (temperature, relative humidity, and water content), stretch ratio, and pre-printed electrodes via screen-printing method.

Out of the environmental parameters only the temperature was shown to have an influence on the breakdown behaviour, indicating slightly higher breakdown voltages with increasing temperature. The temperature range in this study incorporated only indoor temperatures from 10 °C to 50 °C, a considerably more visible influence in tests conducted at a greater temperature range is expected, however. Depending on DE applications, additional studies within such a greater temperature range could be meaningful. An influence of water

content and humidity on the breakdown behaviour was not observed.

Tests conducted on pre-stretched samples showed significantly higher breakdown fields in stretched samples compared to un-stretched samples with breakdown fields increasing from $115 \text{ V } \mu\text{m}^{-1}$ @ $\lambda = 1.0$ – $180 \text{ V } \mu\text{m}^{-1}$ @ $\lambda = 2.0$. The influence of environmental conditions was identical to the ones observed above.

Pre-printed electrodes on the DE membranes had a significant impact on the breakdown behaviour. Firstly, the tests showed homogeneous breakdown voltages in samples with electrodes compared to higher variances without electrodes. Responsible is an immediate homogeneous voltage distribution within pre-printed electrodes, whereas in samples without electrodes the voltage distribution through the flat/round gold plated electrodes is time-delayed and depends on the coupled electro-mechanical deformation during voltage application. Secondly, and most importantly, the breakdown voltage of samples with pre-printed electrodes (@4600V) was significantly lower than the breakdown voltage of samples without electrodes (@5500V) for silicone membranes with $50 \mu\text{m}$ thickness. This phenomenon is most likely not due the influence of environmental parameters—these showing the same influence in samples with and without electrodes—but most likely due to the application method and the electrode material. Further investigations on the influence of these parameters are in progress.

Acknowledgments

We gratefully acknowledge the support from WACKER Chemie AG, who sponsored the development of the breakdown tester and the subsequent studies as well as provided the *Elastosil 2030* film and other chemicals.

ORCID iDs

Bettina Fasolt  <https://orcid.org/0000-0002-7117-4839>

References

- [1] Pelrine R, Pei Q and Kornbluh R 2018 Dielectric elastomers: past, present, and potential future *Proc. SPIE* **10594** 1059406
- [2] Rosset S and Shea H 2016 Small, fast and tough: shrinking down integrated elastomer transducers *Appl. Phys. Rev.* **3** 31105
- [3] Madsen F B, Daugaard A E, Hvilsted S and Skov A L 2016 The current state of silicone-based dielectric elastomer transducers *Macromol. Rapid Commun.* **37** 378–413
- [4] Motzki P, Hau S, Schmidt M and Seelecke S 2018 Künstliche muskeln und nerven in industrie 4.0 konzepten *Ind. 4.0 Manage.* **2018** 38–41
- [5] Hill M, Rizzello G and Seelecke S 2017 Development and experimental characterization of a pneumatic valve actuated by a dielectric elastomer membrane *Smart Mater. Struct.* **26** 085023
- [6] Giousoufand M and Kovacs G G 2013 Dielectric elastomer actuators used for pneumatic valve technology *Smart Mater. Struct.* **22** 104010
- [7] Muir A H, Biggs S J and Hitchcock R N 2014 *US Patent Application No.* 14/912,960
- [8] Wilson K E, Henke E F M, Slipper G A and Anderson I A 2016 Rubbery logic gates *Extreme Mech. Lett.* **9** 188–94
- [9] Linnebach P, Simone F, Rizzello G and Seelecke S 2018 Development, manufacturing, and validation of a dielectric elastomer membrane actuator-driven contactor *J. Intell. Mater. Syst. Struct.* **30** 636–48
- [10] Böse H, Thuy M and Stier S 2018 Wearable operation device with different types of dielectric elastomer sensors *Proc. SPIE* **10594** 105940X
- [11] Lidka M, Price A D and Trejos A L 2018 Development and evaluation of dielectric elastomer actuators for assistive wearable devices *2018 IEEE Canadian Conf. on Electrical & Computer Engineering (CCECE)* (Piscataway, NJ: IEEE) pp 1–4
- [12] Gratz-Kelly S, Hau S, Motzki P and Seelecke S 2018 Intelligente Handschuhe zur Werkerunterstützung in der digitalisierten Produktion *Technische Unterstützungssysteme, die die Menschen wirklich wollen* p 59
- [13] Pyo D, Ryu S, Kyung K U, Yun S and Kwon D S 2018 High-pressure endurable flexible tactile actuator based on microstructured dielectric elastomer *Appl. Phys. Lett.* **112** 061902
- [14] <http://euroeap.eu/index.php/past-edition-winners#ed2018>
- [15] Henke E F M, Schlatter S and Anderson I A 2017 Soft dielectric elastomer oscillators driving bioinspired robots *Soft Robot.* **4** 353–66
- [16] Shintake J, Caccuciolo V, Shea H and Floreano D 2018 Soft biomimetic fish robot made of dielectric elastomer actuators *Soft Robot.* **5** 466–74
- [17] Li W B, Zhang W M, Zou H X, Peng Z K and Meng G 2018 Multisegment annular dielectric elastomer actuators for soft robots *Smart Mater. Struct.* **27** 115024
- [18] Lenz S, Holz B, Hau S and Seelecke S 2018 Development of a high voltage source for dielectric elastomer actuators (DEA) *ACTUATOR 2018; 16th Int. Conf. on New Actuators* pp 1–4 (VDE)
- [19] Hoffstadt T and Maas J 2016 Sensorless BCM control for a bidirectional flyback-converter *Industrial Electronics Society, IECON 2016—42nd Annual Conf. of the IEEE* (Piscataway, NJ: IEEE) pp 3600–5
- [20] Hau S, Rizzello G and Seelecke S 2018 A novel dielectric elastomer membrane actuator concept for high-force applications *Extreme Mech. Lett.* **23** 24–8
- [21] Linnebach P, Hau S, Rizzello G, Motzki P and Seelecke S 2018 Stroke magnification in dielectric elastomer actuators with dynamic excitation *ACTUATOR 2018; 16th Int. Conf. on New Actuators* pp 1–5 (VDE)
- [22] Carpi F, Anderson I, Bauer S, Frediani G, Gallone G, Gei M and Kollrosche M 2015 Standards for dielectric elastomer transducers *Smart Mater. Struct.* **24** 105025
- [23] ASTM International 2013 Standard Test Method for Dielectric Breakdown Voltage and Dielectric Strength of Solid electrical Insulating Materials at Commercial Power Frequencies
- [24] Gatti D, Haus H, Matysek M, Frohnepfel B, Tropea C and Schlaak H F 2014 The dielectric breakdown limit of silicone dielectric elastomer actuators *Appl. Phys. Lett.* **104** 052905
- [25] Chen B, Kollrosche M, Stewart M, Busfield J and Carpi F 2016 Electrical breakdown of dielectric elastomers: influence of compression, electrode's curvature and environmental humidity *Proc. SPIE* **9798** 97980Q
- [26] Shen R, Tu Y, Zhang C and Xu S 2016 Influence of electric field on the moisture absorption characteristic of silicone

- rubber material *2016 IEEE Int. Conf. on High Voltage Engineering and Application (ICHVE)* (Piscataway, NJ: IEEE) pp 1–4
- [27] Haddad G, Wong K L and Gupta R K 2014 Dielectric breakdown characteristics of HTV silicone rubber under multiple stress conditions *Proc. 2014 Int. Symp. on Electrical Insulating Materials (ISEIM)* (Piscataway, NJ: IEEE) pp 276–9
- [28] Vaicekauskaitė J, Mayurek P, Yu L and Skov A L 2018 Insight into the dielectric breakdown of elastomers *Proc. EuroEAP2018* (Lyon: Poster) 1.4.1
- [29] Zakaria S, Morshuis P H, Benslimane M Y, Yu L and Skov A L 2015 The electrical breakdown strength of pre-stretched elastomers, with and without sample volume conservation *Smart Mater. Struct.* **24** 055009
- [30] Li B, Chen H, Qiang J, Hu S, Zhu Z and Wang Y 2011 Effect of mechanical pre-stretch on the stabilization of dielectric elastomer actuation *J. Phys. D: Appl. Phys.* **44** 155301
- [31] Kofod G 2008 The static actuation of dielectric elastomer actuators: how does pre-stretch improve actuation? *J. Phys. D: Appl. Phys.* **41** 215405
- [32] Silau H, Stabell N B, Petersen F R, Pham M, Yu L and Skov A L 2018 Weibull analysis of electrical breakdown strength as an effective means of evaluating elastomer thin film quality *Adv. Eng. Mater.* **20** 1800241
- [33] de Saint-Aubin C A, Rosset S, Schlatter S and Shea H 2018 High-cycle electromechanical aging of dielectric elastomer actuators with carbon-based electrodes *Smart Mater. Struct.* **27** 074002
- [34] Förster-Zügel F, Braisz L and Schlaak H F 2016 Characterization of the dielectric breakdown strength of thin elastic films in various ambient media *2016 IEEE Int. Conf. on Dielectrics (ICD)* vol 1 (Piscataway, NJ: IEEE) pp 569–72
- [35] Welsch F, Fasolt B and Seelecke S 2018 Dielectric breakdown test setup for dielectric elastomers: design and validation *Proc. SPIE* **10594** 105941A
- [36] Fasolt B, Welsch F and Seelecke S 2018 DE electrical breakdown test setup for varying environmental conditions *Proc. EuroEAP2018* (Lyon: Poster) 1.4.13
- [37] Wacker Chemie AG datasheet 2016 Neue Perspektiven und innovative Anwendungen mit Elastosil® Film
- [38] Fasolt B, Hodgins M, Rizzello G and Seelecke S 2017 Effect of screen-printing parameters on sensor and actuator performance of dielectric elastomer (DE) membranes *Sensors Actuators A* **265** 10–9
- [39] Müller I and Müller W I 2009 Moist air *Fundamentals of Thermodynamics and Applications: with Historical Annotations and Many Citations from Avogadro to Zermelo* (Berlin: Springer) ch 10, p 287
- [40] Du B X, Ma Z L, Gao Y and Han T 2011 Effect of ambient temperature on electrical treeing characteristics in silicone rubber *IEEE Trans. Dielectr. Electr. Insul.* **18** 401–7

4.4 Electrode impact on the electrical breakdown of dielectric elastomer thin films

Bettina Fasolt^{1,2}, Fabio Beco Albuquerque³, Jonas Hubertus⁴, Günter Schultes⁴,
Herbert Shea³, and Stefan Seelecke²

- ¹ Intelligent Materials Systems Lab, Center for Mechatronics and Automation Technologies (ZeMA) gGmbH, Saarbrücken, Germany
- ² Intelligent Materials Systems Lab, Department of Systems Engineering, Department of Materials Science & Engineering, Saarland University, Saarbrücken, Germany
- ³ LMTS Soft Transducers Laboratory, EPFL Ecole Polytechnique Fédérale de Lausanne, Neuchâtel, Switzerland
- ⁴ Sensors and Thin Film Group, University of Applied Sciences, Saarbrücken, Germany

Publication: Polymers

Publisher: MDPI

October 2023

Citations: 14

Impact Factor: 4.7

<https://doi.org/10.3390/polym15204071>

Copyright © 2023 by the authors. Articles are licensed under an open access Creative Commons CC by 4.0 license

The work done in Section 4.3 left two key questions unanswered: Was the investigated temperature range too narrow to detect an influence of humidity or water content? And is the reduction in breakdown field observed with screen printed carbon black electrodes a general effect of electrode application on DEA membranes or is it specific to screen printing? While numerous breakdown studies exist in the literature, direct comparisons are challenging due to variations in test setups, experimental conditions, film material and thickness, membrane pre-stretch, and electrode application methods, motivating the systematic and consistent approach in this paper.

In a first step, the temperature range is extended from 1 °C to 80 °C, with relative humidity levels ranging from 10 % to 90 %. Additionally, to enable at least one direct comparison with existing literature, the study by Albuquerque and Shea [60] was selected. Their research examined the influence of humidity, temperature, and pre-stretch on the breakdown strength of various silicone elastomer membranes using sputtered gold electrodes. For consistency, the same film material (Wacker Elastosil 2030/20µm) and one of their investigated pre-stretch conditions (bi-axial 30%) are used in the present tests. The breakdown tester is operated within a climate chamber, and the electrode dimensions of the tester's gold contacts are used as a reference for comparing pure film with film containing applied electrodes.

Given the critical importance of understanding both the influence of environmental conditions and the impact of electrode design on the breakdown behavior of DEAs for ensuring reliable operation, a collaborative study was initiated. In this study, multiple institutions contributed DEAs fabricated using their respective manufacturing methods and electrode formulations - but all manufactured on the same silicone film and subjected to identical pre-stretching conditions. These standardized samples were then tested at the iMSL lab using the same test setup, breakdown tester, and climate chamber employed in the investigations described in Sections 4.2 and 4.3.

Three research groups collaborated to provide test samples prepared on pre-stretched films with electrodes using different manufacturing methods and compositions. Fabio Beco Albuquerque (LMTS Soft Transducers Laboratory) supplied sputtered gold electrodes, inkjet printed carbon black electrodes, and pad printed carbon black electrodes. Jonas Hubertus (Sensors and Thin Film Group) contributed sputtered nickel electrodes, while Bettina Fasolt (Intelligent Materials Systems Lab) provided screen printed electrodes and pre-stretched film without electrodes. Fasolt conducted all investigations and prepared additional samples that emerged during the course of the study, including those for solvent tests and carbon black granularity tests.

The study confirms the influence of temperature on the electric breakdown behavior when the temperature range is increased and also reveals a significant influence of humidity as observed by Albuquerque and Shea [60]. While breakdown voltage increases with rising temperature, it decreases as humidity increases. This phenomenon is observed in electrode-free samples as well as those with all electrode types.

Also confirmed is the decrease of the breakdown voltage described in Section 4.3 when electrodes are applied to the film. Although this effect occurs across all configurations, its magnitude varies. While sputtered metal electrodes cause only a slight decrease in breakdown voltage, carbon black electrodes - regardless of the application method - result in a significantly greater reduction.

To understand the differences in breakdown behavior, both electrode stiffness and composition are examined. To assess the stiffening effect, films with no electrodes, sputtered gold electrodes, screen printed carbon black electrodes, and electrodes made from finely milled carbon black powder are compared. The higher breakdown field observed in metal electrodes is attributed to their higher stiffness compared to those of carbon black electrodes. The higher stiffness coupled with the incompressibility of polymers result in a smaller thickness reduction when actuated, which leads to a smaller electric field at an identical voltage.

The sputtering process constitutes a non-contact technique in which the mechanical impact during electrode deposition is negligible. Consequently, the possibility that the increased breakdown voltage arises from this mechanically less invasive manufacturing method must be considered. This influence, however, can be excluded, as the inkjet process is likewise a non-contact technique yet yields breakdown fields comparable to those obtained with screen and pad printing, see Section 3.1.

Although sputtered electrodes exhibit higher breakdown field strengths, they are unsuitable for DEA operation without additional pre-stretching and relaxation treatment, as they lose conductivity under strain. Consequently, subsequent investigations into the influence of electrode composition on breakdown behavior are limited to carbon black-based electrodes. For this study, each component of carbon black electrodes - solvent, PDMS, and carbon black - is investigated separately.




Since each manufacturing method utilizes different solvents, their influence on breakdown voltage is first tested by applying pure solvent to the film and repeating these tests with the solvent-carbon black blend. No significant influence of solvents is detected when applied alone; however, when blended with carbon black, all three tested solvents produced the same effect of a reduced breakdown voltage.

The effect of PDMS on the breakdown behavior is investigated by varying its concentration from 0 % to 90 % within the carbon black-based electrode mixture. Both PDMS and carbon black are key components of the screen printed electrodes. Additionally, the influence of carbon black is examined by comparing particle sizes, ranging from finely milled to coarsely ground grades. The results indicate that breakdown voltage increases with higher PDMS content and when carbon black is as finely milled as possible.

The higher breakdown field observed at increased PDMS content is most likely attributable to the insulating effect of the PDMS, which both encapsulates the potentially sharp-edged carbon black particles - thereby reducing their penetration into the silicone membrane - and distributes the charge concentration at the interface. Furthermore, a reduction in particle size decreases the likelihood that larger, sharp-edged particles at the film/electrode interface penetrate more deeply into the film when a voltage is applied and Maxwell stresses are exerted.

Article

Electrode Impact on the Electrical Breakdown of Dielectric Elastomer Thin Films

Bettina Fasolt ^{1,2,*} , Fabio Beco Albuquerque ³, Jonas Hubertus ⁴, Günter Schultes ⁴, Herbert Shea ³  and Stefan Seelecke ² 

- ¹ Intelligent Material Systems Lab, Center for Mechatronics and Automation Technology, ZcMA gGmbH, DE-66121 Saarbrücken, Germany
- ² Intelligent Material Systems Lab, Department of Systems Engineering, Department of Materials Science and Engineering, Saarland University, DE-66121 Saarbrücken, Germany; stefan.seelecke@ims.uni-saarland.de
- ³ LMTS Soft Transducers Laboratory, EPFL Ecole Polytechnique Fédérale de Lausanne, CH-2002 Neuchâtel, Switzerland; herbert.shea@epfl.ch (H.S.)
- ⁴ Sensors and Thin Film Group, University of Applied Sciences, DE-66117 Saarbrücken, Germany; jonas.hubertus@htwsaar.de (J.H.); guenter.schultes@htwsaar.de (G.S.)
- * Correspondence: b.fasolt@zema.de

Abstract: Dielectric Elastomer Actuators (DEAs) enable the realization of energy-efficient and compact actuator systems. DEAs operate at the kilovolt range with typically microampere-level currents and hence minimize thermal losses in comparison to low voltage/high current actuators such as shape memory alloys or solenoids. The main limiting factor for reaching high energy density in high voltage applications is dielectric breakdown. In previous investigations on silicone-based thin films, we reported that not only do environmental conditions and film parameters such as pre-stretch play an important role but that electrode composition also has a significant impact on the breakdown behavior. In this paper, we present a comprehensive study of electrical breakdown on thin silicone films coated with electrodes manufactured by five different methods: screen printing, inkjet printing, pad printing, gold sputtering, and nickel sputtering. For each method, breakdown was studied under environmental conditions ranging from 1 °C to 80 °C and 10% to 90% relative humidity. The effect of different manufacturing methods was analyzed as was the influence of parameters such as solvents, silicone content, and the particle processing method. The breakdown field increases with increasing temperature and decreases with increasing humidity for all electrode types. The stiffer metal electrodes have a higher breakdown field than the carbon-based electrodes, for which particle size also plays a large role.

Keywords: dielectric breakdown test; electrode manufacturing methods; influence electrodes; silicone films; carbon black; environmental conditions



Citation: Fasolt, B.; Albuquerque, F.B.; Hubertus, J.; Schultes, G.; Shea, H.; Seelecke, S. Electrode Impact on the Electrical Breakdown of Dielectric Elastomer Thin Films. *Polymers* **2023**, *15*, 4071. <https://doi.org/10.3390/polym15204071>

Academic Editor: Md Najib Alam

Received: 23 August 2023

Revised: 26 September 2023

Accepted: 4 October 2023

Published: 12 October 2023



Copyright: © 2023 by the authors. Licensee MDPI, Basel, Switzerland. This article is an open access article distributed under the terms and conditions of the Creative Commons Attribution (CC BY) license (<https://creativecommons.org/licenses/by/4.0/>).

1. Introduction

The utilization of DEAs as electromechanical transducers is attractive for a number of different applications such as valves [1,2], pumps [3], and switches [4,5], as well as in haptic devices [6,7], wearables [8,9], and soft robotics applications [10–14]. DEAs are lightweight and offer silent, energy-efficient actuation without the use of rare earth materials. Additionally, the actuators' self-sensing properties enable smart applications without the need for external sensors.

A standard DEA typically consists of a compliant dielectric elastomer membrane sandwiched between two stretchable electrodes [15,16]. When a voltage is applied to the electrodes, electrostatic forces lead to a reduction of the membrane thickness along with a simultaneous lateral expansion, thus resulting in voltage-controlled motion.

An important limiting factor for high voltage applications is dielectric breakdown. The breakdown field strength E_{BD} represents the maximum value of the electrical field

which can be withstood by the membrane. The Maxwell pressure scales as E_{BD}^2 while the elastic energy density scales as E_{BD}^4 [17]. It is thus essential to be able to operate DEAs at high electric fields and to understand on which parameters the maximal breakdown field depends. Environmental conditions such as temperature and humidity, as well as the pre-stretch of the membrane, and the dielectric material itself are only a selection of possible parameters known to have an influence on the breakdown voltage [18–24]. In a previous breakdown study by Fasolt et al. conducted on pure silicone film and film with screen-printed carbon black (CB) electrodes, it was discovered that in addition to the above parameters the electrode also had a significant impact on the breakdown, lowering the breakdown field by up to 20% [25]. To validate the influence of electrodes on the breakdown behavior, the results were compared with a study conducted by Albuquerque and Shea [16], which tested silicone film with sputtered gold electrodes under various environmental conditions. The results of the breakdown fields varied significantly but because the film thickness, pre-stretch, and electrode material were also different, a direct comparison was not possible. Other published studies about breakdown behavior of silicone thin film used yet different electrode materials: Förster-Zügel et al. used graphite powder and a shadow mask [26], Stoyanov et al. sprayed carbon nanotubes [27], Jiang et al. applied conductive carbon grease [28], Albuquerque and Shea applied CB electrodes by pad printing [29], and Zakaria et al. sputtered silver electrodes [30]. In order to establish a framework for transferability of measured results between different studies, the current paper systematically investigates the effect of different electrode materials and electrode manufacturing methods over a wide temperature and humidity range.

Specifically, this study provides a comprehensive breakdown investigation conducted on electrodes applied by four different manufacturing methods, using the same test setup and environmental conditions, ranging from 1 °C to 80 °C and 10% to 90% relative humidity. Three research groups collaborated on this project and provided different electrodes manufactured with application methods used in their labs: screen printing, inkjet printing, pad printing, gold sputtering, and nickel sputtering. The electrodes were applied on the same 20 µm-thick silicone dielectric material, Wacker Elastosil 2030/20 µm, and the same bi-axial pre-stretch of the film was used for all samples.

Each manufacturing method has its unique application scope, shown in Table 1. Manufacturing methods such as spraying, spin coating, blade casting, or 3D printing are also possible but were not included in this study [31–33]. Sputtered metal electrodes have a high conductivity and nanometer-scale thicknesses but usually lose conductivity when stretched. Hubertus et al. [34–36] describe a method where electrodes are sputtered on a pre-stretched film and subsequently released so that they exhibit a strongly wrinkled configuration, enabling subsequent stretching within the pre-stretch range and even above. Carbon black electrodes are attractive low-cost materials and can be applied by high-throughput and scalable processes such as screen printing, pad printing, or inkjet printing. These electrodes can remain conductive even at large deformations and hence are a widely used material for soft actuator and sensor applications. Other printable electrode materials such as carbon nanotubes, silver, and graphenes are not included in the study.

The breakdown behavior of the different manufacturing methods is systematically analyzed in this paper and possible breakdown-affecting parameters are discussed. As a reference, experiments were also conducted on samples without applied electrodes. The investigations conducted in this paper are divided into three main sections. The focus of the first group is the influence of environmental conditions such as temperature and humidity on the breakdown behavior. The results are shown for all different types of electrodes. Sections 3.1–3.3 focus on the differences in breakdown behavior for the different types of electrodes. Influencing parameters such as the mechanical effect of the manufacturing method and stiffness (pull-in effect) are discussed. Sections 3.4–3.6 examine possible influencing parameters for the carbon black-based electrodes such as solvents, carbon black processing (mixing and milling), and silicone content. The experiments of Section 3.3,

Sections 3.4–3.6 were conducted under standard environmental conditions (20 °C/55% rel. humidity).

Table 1. Application range of electrode manufacturing methods for DEAs used in this study and associated advantages/disadvantages.

	Advantage	Disadvantage
Screen-printing	<ul style="list-style-type: none"> • Very fast process, ready up-scaling to mass production • Printing of small and large areas • High acceptable range of ink viscosity (500–10,000 mPas) 	<ul style="list-style-type: none"> • New screen for each design → not ideal for prototyping • Material waste for prototyping due to large minimum amount of ink needed for first print • Can only print on flat or rounded surfaces • Mechanical impact of screen on DE film
Pad-printing	<ul style="list-style-type: none"> • Printing on irregular shaped surfaces possible • Fast process • Medium range of acceptable ink viscosity (1500–2000 mPas) 	<ul style="list-style-type: none"> • Stencil necessary → not ideal for prototyping • Cannot print on large areas • Mechanical impact of soft pad on DE film
Inkjet-printing	<ul style="list-style-type: none"> • No screen or stencil necessary • Ideal for prototyping • Contactless process—no mechanical impact 	<ul style="list-style-type: none"> • Very low range of acceptable ink viscosity (10–20 mPas) • Ink needs high solvent content • Clogging of nozzle requires frequent cleaning procedures • Slow process, poorly suited for mass production
Sputtering	<ul style="list-style-type: none"> • Nanometer-thick high-conductivity electrodes • Microscale actuator designs possible with subsequent laser ablation • Ideal for micro-structures incl. connections using laser ablation 	<ul style="list-style-type: none"> • Slow and complex process for laboratory sputtering systems, involving a vacuum step • Pre-stretch of film required for sputtering and subsequently releasing to avoid cracks → DE operation preferable within pre-stretched range • High investment cost for mass production

2. Experimental Setup and Procedure

2.1. Test Setup

The breakdown tests were conducted using a custom-built automated electrical breakdown test setup. A detailed description of the development and design is given in [37]. During the tests, two gold-plated electrodes, subsequently denoted measurement electrodes, with a diameter of 6.3 mm, one moveable on a pivoting arm and one fixed, make contact with the silicone film and voltage is applied at a rate of 0.5 kV/s until breakdown. The breakdown voltage is defined as the voltage when the current flow through the material reached a value of 150 µA. A LabVIEW test software automatically stops the voltage application and records the breakdown value when the admissible current flow is detected by the HypotMAX 7710 Dielectric Withstand Tester (Associated Research, Lake Forest, IL, USA). The movable top electrode is flat, and the bottom electrode has a convex shape with a radius of curvature of 26 mm. The geometry configuration flat top and flat bottom was also investigated for the same film and pre-stretch, but only a negligible difference in the breakdown field was detected. Therefore, the flat/convex shape, also compatible with standardization suggestions from Carpi et al. [38], was chosen for the measurement electrodes, as it also features minimal membrane interactions during spot positioning. After breakdown, the electrodes separate, and the tester automatically moves to the next position. The test setup was placed in a climate chamber Vötsch CLIMEEVENT C/600/40/3 to be able to conduct all breakdown tests in a controlled environment. The tester design allows for consecutive testing without the need to open the climate chamber. Figure 1

shows a schematic illustration of the breakdown tester and the steps carried out for each measurement point.

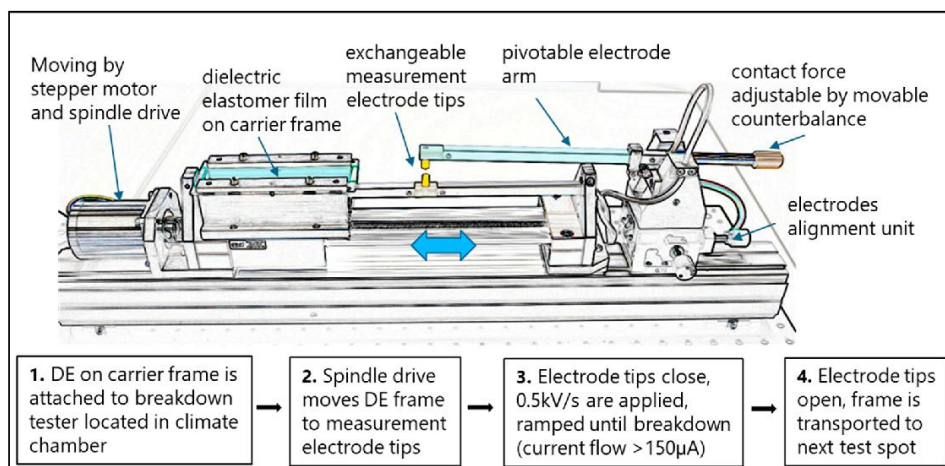


Figure 1. Schematic sketch (top) and diagram (bottom) of the breakdown tester and measurement steps.

The tests were conducted on pure film and film with applied electrodes. To compare these results, all manufactured electrodes had the same diameter as the measurement electrodes. Two different test frames were used. The frames for the screen-printed, nickel-sputtered, and pure film were prepared at the iMSL lab on a metal frame with eleven measurement points, and the gold-sputtered, pad-printed, and inkjet-printed electrodes were prepared at the EPFL lab on plastic frames with three measurement points each. Figure 2 shows a picture of the automated tester with the measurement electrodes and an example of the screen-printed and gold-sputtered electrode samples located in the tester as well as the placement of the tester in the climate chamber.



Figure 2. Left: Automated breakdown tester with measurement electrodes (convex/flat design for voltage application) and example of screen-printed and gold-sputtered electrodes. Right: Test setup in climate chamber CLIMEEVENT C/600/40/3, Fa. Vötsch.

2.2. Materials and Sample Preparation

Wacker Elastosil 2030/20 μm, pre-stretched bi-axially by $\lambda_1 = \lambda_2 = 1.3$, is used as a dielectric film for all samples. The average sample thickness after stretching is 11.8 μm. The samples without electrodes, with screen-printed electrodes, and with nickel-sputtered

electrodes are pre-stretched using an automated stretcher, consisting of two separately controlled stepper motors and vacuum clamps for the fixation of the DE film. Screen-printed samples are first transferred onto special printer frames to allow for the printing of two designs at the same time and are subsequently transferred onto the test frames. The nickel-sputtered samples and the samples used for tests without electrodes are directly transferred to the test frames used in the breakdown tester. This procedure is described in more detail in [37]. The gold-sputtered, inkjet-printed, and pad-printed samples are pre-stretched using a circular stretcher and transferred to PMMA frames coated with a pressure-sensitive adhesive (Adhesives Research ArClear). The thickness is controlled using a white light transmission interferometer, as described in [39].

2.2.1. Gold-Sputtered Samples

The gold electrodes (≈ 20 nm thick) are applied over a mask using a Jeol JFC-1200 gold coater, Jeol USA, Inc., Peabody, MA, USA (Argon, 8 Pa, 140 s at 20 mA), as described in [40]. The coating is carried out on both sides, leading to circular 6.3 mm diameter electrodes.

2.2.2. Nickel-Sputtered Samples

Ten nm-thick nickel electrodes are deposited by a DC magnetron sputter process in a laboratory vacuum chamber. At the beginning of the process, the samples, covered with a shadow mask, are inserted into the vacuum chamber and placed on a movable sample holder. The pumping process is started until a background pressure of less than 1×10^{-5} mbar is reached. Prior to sputtering, three pump-purge cycles are executed, where Argon is let into the chamber up to a pressure of 1×10^{-1} mbar and pumped out again. A constant gas flow of 15 sccm Argon in combination with an appropriate position of a downstream throttle then leads to a constant sputter pressure of 1.5×10^{-3} mbar. The sputtering process is started by first pre-sputtering the magnetron target for 1.5 min, while the sample is still located outside the influence of the target. After that, the sample is transferred under the target and coated with a 10 nm-thick nickel thin film. A total of 300 W is applied to the target and held constant during the whole process. With a target-to-substrate distance of 4.5 cm, a 10 nm-thick nickel thin film is manufactured in 5 s. The geometry of the deposited thin film is realized by using a shadow mask, lasering 11 circles with a diameter of 6.3 mm and a distance of 10 mm between the centers of the circles out of a 50 μm -thick metal foil.

2.2.3. Screen-Printed Samples

A screen-printing process requires electrode materials for printing and a screen provided with the desired sample design [41]. The electrode material is prepared using a mixture of 83 wt.% solvent (50% Coats screen VD60, 50% Wacker Belsil DM 1 Plus), 3.8 wt.% carbon black, and 13.2 wt.% PDMS. The solvent is added to achieve the viscosity necessary for screen printing. The preparation of the electrode material is carried out in multiple steps. First, the carbon black and solvents are blended in a planetary mixer. This mixture is subsequently ground in a three-roll mill and, after adding PDMS, again blended in the planetary mixer. A screen with two sets of eleven dots, each with a diameter of 6.3 mm, is prepared, and the electrode material is screen printed onto the pre-stretched film, achieving a thickness of 3 μm . After heat curing at 150 $^{\circ}\text{C}$ for 10 min, the electrodes are screen printed onto the other side of the film and heat cured for another 60 min at 150 $^{\circ}\text{C}$. The film is then transferred onto two test frames consisting of 11 electrode dots designed for testing in a breakdown tester. After curing, the solvents are evaporated, and the mixture consists of 25 wt.% carbon black and 75 wt.% silicone.

2.2.4. Pad-Printed Samples

The carbon black-PDMS composite electrode is a 4 ± 1 μm -thick pad-printed electrode comprising 0.8 g of carbon black (Ketjenblack EC-300J, Nouryon, Amsterdam, Netherlands) dispersed in 8 g of silicone elastomer (Silbione LSR 4305, Elkem, Oslo, Norway) of A:B ratio

1:1 and 32 g of a mixture of 50% isopropanol and 50% iso-octan, prepared following Rosset et al. [39] using a planetary mixer. After pad printing, the samples with the pad-printed electrodes are cured at 80 °C for 1 h. The pad-printing process is repeated on the opposite membrane side, leading to 6.3 mm diameter electrodes.

2.2.5. Inkjet-Printed Samples

The inkjet-printed electrodes ($3 \pm 1 \mu\text{m}$ thick) contain carbon black (Ketjenblack EC-300J), a dispersant (Wacker Belsil SPG 128 VP, WACKER Chemie AG, Munic, Germany), and a solvent (DOWSIL OS2, Dow Chemical Company, Midland, MI, USA) and were applied following the process described in Schlatter et al. [42]. Circular electrodes of 6.3 mm were directly printed on the membrane.

2.3. Test Procedure

For characterization under well-defined environmental conditions, the breakdown tester is placed in a climate chamber. The samples are tested at six different environmental conditions, covering a wide range of possible conditions from low via medium to high temperatures with low, medium, and high humidities, Table 2. The difference in water content between low and high humidity at 1 °C is only 4 g/m³, which is outside of the adjustable range of the climate chamber.

Table 2. Temperatures and relative humidities of test conditions.

Temperature and % RH		
1 °C—undefined % RH	20 °C 10% RH	80 °C 10% RH
	20 °C 55% RH—defined as standard environmental condition	
	20 °C 90% RH	80 °C 90% RH

The respective conditions are adjusted, and when stable, an additional 30 min remain before the test samples are placed into the chamber. One test sample is immediately fixed onto the movable station of the breakdown tester and five more samples are placed on a storage rack located above the tester. After 60 min, thermal equilibrium is reached in the test samples, and the tests are conducted on all test points consecutively (eleven electrodes on the large frames and three on the small frames). The tested frame is removed and replaced with a sample from the storage rack, which will then be re-stocked with samples from outside the climate chamber so that the minimum dwell time for each sample is 1 h. When conditions are stable again after replacement, another 10 min remain before the next test is conducted. This procedure is repeated until results for 15 measurement points per condition are available.

3. Results

The motivation of this study was to understand how different electrode materials and their manufacturing methods influence dielectric breakdown behavior in thin silicone films. First, the influence of six different environmental conditions is discussed in Section 3.1. Then, Sections 3.2 and 3.3 discuss the mechanical effects associated with the different electrode materials. This includes the mechanical impact due to the manufacturing method as well as the different stiffnesses of the metal and non-metal electrodes. These experiments are conducted at defined standard condition (20 °C/55% RH). In Sections 3.4–3.6, the focus is on the carbon black-based electrodes, which are of particular relevance as they are not only used for lab breakdown measurements but also in applications with dielectric elastomer actuator devices. Here, parameters important for manufacturing, i.e., solvents, carbon black processing, and silicone content, and their impact on the breakdown behavior are systematically studied.

Results from the breakdown measurements performed for each test case typically lead to plots such as the one shown in Figure 3, displaying breakdown results for all electrode types at standard conditions. Each test point is consecutively tested by connecting the setup electrodes of the breakdown tester to the manufactured top and bottom electrode and applying a voltage. The voltage is ramped with 500 V/s until breakdown, which is defined by a current flow of $>150 \mu\text{A}$ through the dielectric material. The breakdown voltage is recorded for each breakdown point in the tested sequence until 15 points are tested. The results in Figure 3 indicate significant differences between the breakdown voltages for metal-sputtered electrodes and carbon black (CB) electrodes, showing an average of more than 400 volts ($>20\%$) higher for the sputtered electrodes than the CB electrodes. The samples without electrodes are tested as a reference and are consistently higher than for all the samples with applied electrodes.

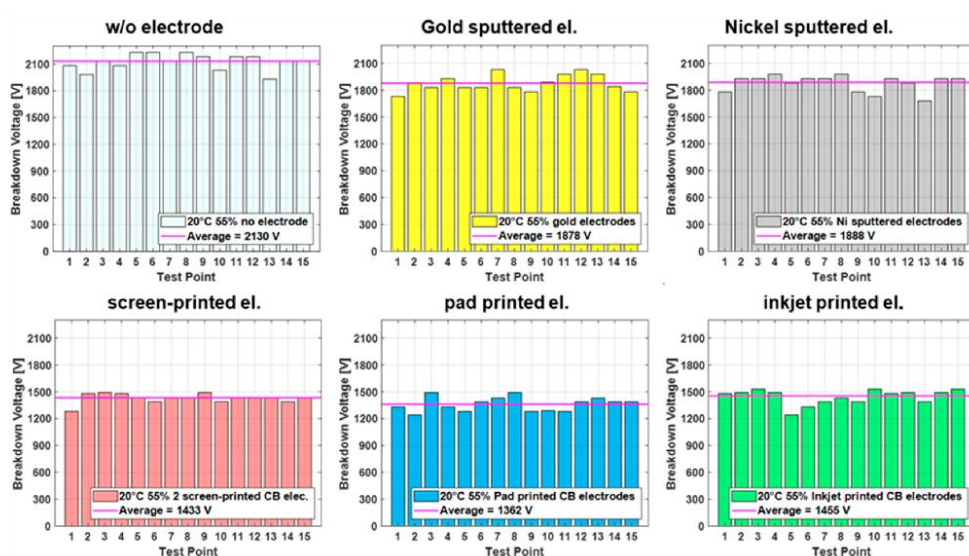


Figure 3. Breakdown voltage of Elastosil 2030/20 at 20 °C 55% RH for all electrode types, with 15 measurement points per sample.

However, to compare the different conditions and electrodes, a bar graph illustration is impractical. Therefore, for the remaining figures in this paper, a boxplot design is used, which allows for a compact comparison and interpretation of the different cases. For example, the breakdown of single spots (depicted as red cross) due to imperfections in the film are easily identified through outliers, while additionally the margin of the breakdown values is visible by the width of the box, including the value for the median.

Furthermore, the breakdown field, defined as the breakdown voltage divided by the initial film thickness, rather than the breakdown voltage, is introduced, because it allows for a better comparison with published measurements conducted on samples with different membrane thicknesses. The small thickness change when the voltage is applied is not taken into account for the calculation of the electric field.

Figure 4 gives a comprehensive overview of the test results for each electrode type under all of the environmental conditions. The experiments were conducted at low, ambient, and high temperatures: 1 °C, 20 °C, and 80 °C. The ambient and high temperatures are tested each at low relative humidity (10% RH) and high relative humidity (90% RH). The difference in water content between the low and high humidity at 1 °C is only 4 g/m^3 , which is outside of the range adjustable in the climate chamber. Therefore, the results in Figure 4 for 1 °C are shown with an unspecified relative humidity.

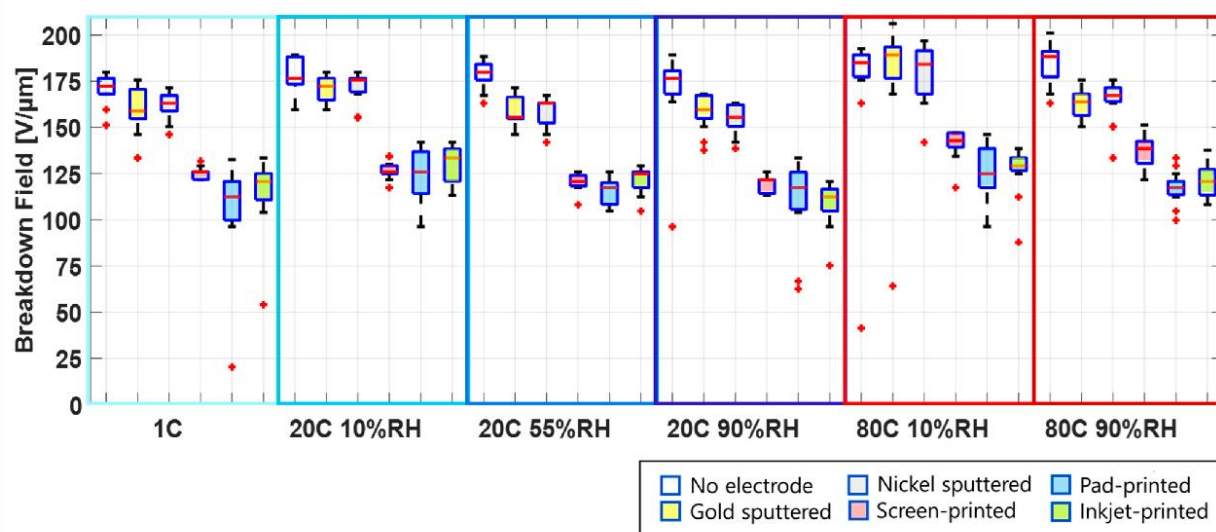


Figure 4. Breakdown field of Elastosil 2030/20 at different environmental conditions for pure silicone film (no electrode) and for film with electrodes applied using different manufacturing methods.

Depending on the environmental conditions and the manufacturing method of the electrodes, breakdown fields ranging from 100 V/μm to 200 V/μm are measured. It is important to point out that the samples are pre-stretched bi-axially by 30%, and therefore the breakdown field is higher than what is expected for un-stretched samples. The influence of pre-stretching on the breakdown field is reported in different studies [25,43–45].

From Figure 4, one sees that the breakdown field for films without electrodes as well as films with sputtered electrodes is significantly higher than for samples with carbon black electrodes, for all environmental conditions.

3.1. Influence of Temperature and Humidity on Breakdown Behavior

Even though breakdown fields vary between electrode materials and deposition methods, two trends are apparent for all electrode types: the breakdown field increases with an increasing temperature and decreases with increasing humidity. This is shown in Figure 5, where two temperatures at low and high humidity are displayed for a metal and a carbon black electrode. These two observations will be discussed in the following sections.

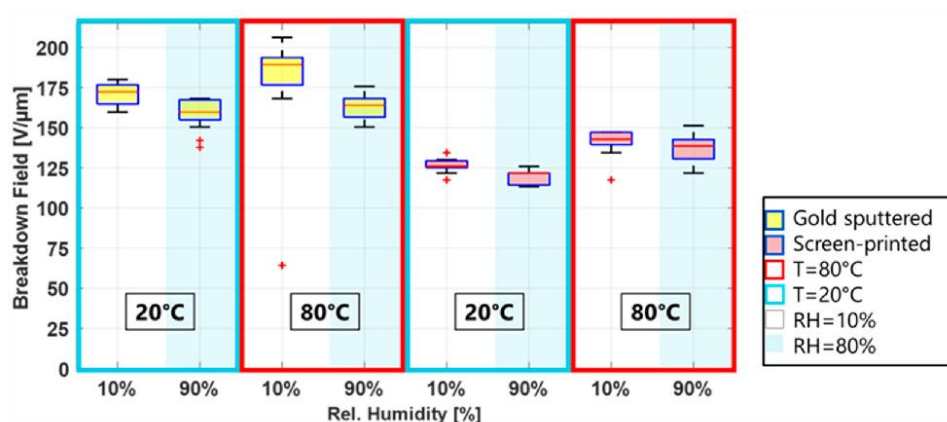


Figure 5. Influence of temperature (red and blue box) and relative humidity (light blue background) on the breakdown field of silicone film Elastosil 2030/20 for gold electrodes and screen-printed carbon black electrodes.

3.1.1. Increase of Breakdown Field with Increasing Temperature

The exact composition of Elastosil 2030 is not known to the authors, but it is assumed that it mainly consists of polydimethylsiloxan (PDMS). PDMS is a silicone polymer with a long backbone of alternating units of silicon and oxygen (Si-O) and two side chains of methyl on each silicon. The silicone molecule is helical, and intermolecular forces are low, hence easy rotational movements along the backbone are possible. The tetrahedral structure of the silicon in the chains prevents tight packing, thus the free volume in PDMS is high. Additionally, the methyl groups can rotate freely around the backbone [46,47], allowing for even more flexibility. How this composition is affected by temperature change can be explained using the free energy F of the system, defined in Equation (1), with U : Internal Energy, T : temperature, and S : the entropy [48].

$$F = U - TS \quad (1)$$

The most stable condition is when the free energy is minimized. Silicone elastomers behave nearly entropy elastic above the glass transition temperature ($-126\text{ }^{\circ}\text{C}$ for Elastosil 2030), and therefore the contribution of the internal energy to the free energy can be neglected in our tested temperature range. From Equation (1), an increase in temperature and entropy will be more energetically favorable. An increasing temperature causes the PDMS molecules to move and rotate more freely and increase in entropy. This state has two consequences for the breakdown behavior. One is a stiffening effect and hence increase in Young's modulus [49]. The other one is a prolonged breakdown through the membrane due to the high activity of the chains, which was observed by Du et al. in their investigation about the treeing characteristics at different temperatures [50].

A different influence of the temperature on the breakdown behavior for different electrode materials was not observed.

3.1.2. Decrease of Breakdown Field with Increasing Relative Humidity

With increasing humidity at a constant temperature, a reduction in the breakdown field was observed for all electrodes. The high water vapor permeability of $3000\text{ g/m}^2/24\text{ h}$ for Elastosil 2030/20 μm , [51], a result of the high free volume, allows for the water vapor to rapidly diffuse into and through the membrane. The free volume is a function of the temperature, and when the temperature increases, the free volume and the permeability increase as well [52]. Furthermore, the polymer chains become more mobile, and the diffusion of the water molecules is favored. The mobility of the water vapor molecules significantly depends on the temperature as well. Thus, higher temperatures mean higher gas mobility which subsequently results in a higher gas diffusivity and permeability [53].

Depending on the temperature and humidity, the membrane can absorb 0.1 to 0.25 wt.% of water [54,55]. The absorbed water molecules in the membrane lower the dielectric properties of the material because the water introduces additional charge carriers and thus breakdown takes place at lower breakdown fields.

Figure 5 shows the breakdown fields for metal (gold) electrodes and carbon black (screen-printed) electrodes for two temperatures, at low and high humidity. The lower breakdown field for higher humidities is clearly visible for both electrodes. However, while the median difference (calculated by subtracting the medial breakdown at 90% RH from 10% RH and divided by the 10% RH value times 100) for the CB electrodes is around 3% for both temperatures, it is significantly higher, 13.5%, for the gold electrodes at $80\text{ }^{\circ}\text{C}$ and 90% RH.

3.2. Effect of Electrode Manufacturing-Induced Mechanical Actions on Breakdown Behavior

Section 3.1 illustrated the influence of the environmental conditions on the breakdown field and reported how the breakdown field is different for different electrode types for a given environmental condition. This difference can either be due to processes during manufacturing or due to specific electrode properties and their influence on the film. This

section explores whether the manufacturing process is responsible for a mechanical change of the film. Figure 6 shows a breakdown plot for all electrode types, combining data from all temperatures and humidities in one box for each electrode type (90 data points per electrode).

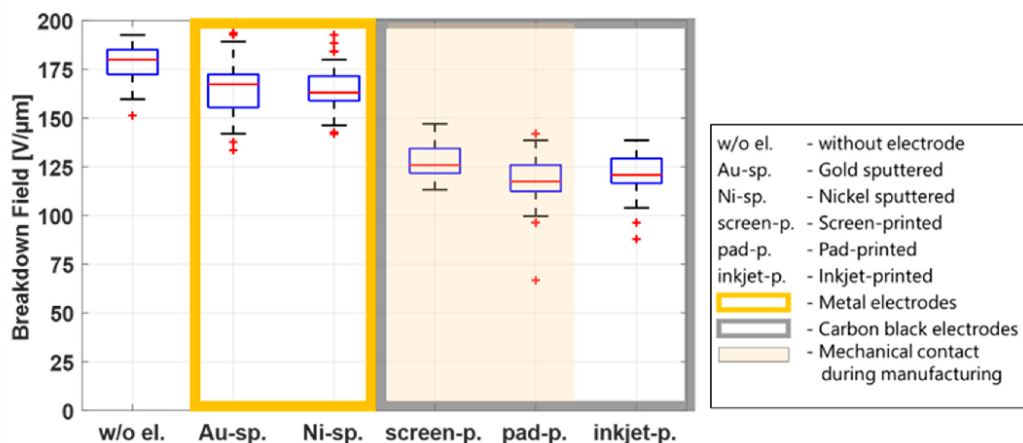


Figure 6. Summarized breakdown field results from all temperature and humidity tests conducted in Figure 4 subdivided into samples without electrodes, metal electrodes, and CB electrodes.

The sputtering process and the inkjet-printing process are non-contact manufacturing methods. During screen printing and pad printing, direct mechanical contact with the film is necessary. In the screen-printing process, the mesh touches the film, and a squeegee applies the electrode material through the mesh. In the pad-printing process, the pad, which transfers the electrode material onto the film, stamps the electrode material directly onto the film. Figure 6 shows higher breakdown fields for the sputtered electrodes, but the results for the inkjet-printing electrodes are in the same order of magnitude as for the contact processes screen printing and inkjet printing, indicating that the mechanical impact is not a decisive parameter that influences the breakdown behavior. Because a breakdown field reduction is observed whenever electrodes are applied—compared to the reference samples without electrodes—other parameters responsible for this phenomenon are discussed in the following sections.

3.3. Influence of Electrode Stiffness

Figure 6 shows that the breakdown field of the samples with metal electrodes (gold and nickel) is significantly higher than that of the samples with CB electrodes, regardless of temperature or humidity. Therefore, the following investigations of possible parameters influencing the breakdown behavior of the film will only be discussed under standard environmental conditions (20 °C and 55% RH).

An important difference between metal and CB electrodes is the stiffness of the material. When a voltage is applied, the Maxwell stress induces a thinning of the membrane and subsequently an increase in the electric field. In an ideal silicone film, where incompressibility is assumed, the thinning of the membrane will result in an area extension of the film.

Two parameters generate an electric field increase: the thinning of the dielectric membrane due to the Maxwell stress and the voltage increase due to the experimental procedure. While soft CB electrodes allow for both of these mechanisms to occur, gold electrodes are extremely stiff and hence impede the area extension. Because of the membrane's incompressibility, this subsequently strongly suppresses the thinning of the material under the application of a voltage. In this way, the electric field in the gold electrode case only increases due to the voltage increase and is thus lower than the electric field, resulting from

the same voltage with soft CB electrodes. To confirm this theory, two limiting cases are investigated. One case is a very soft electrode, consisting only of finely milled CB powder. The other is a rigid electrode. Here, the external measurement electrodes are used, which adhere to the pure film when voltage is applied, thus restricting expansion. For this case, the highest breakdown field is expected. The CB powder adds nearly no stiffness to the film; thus, the lowest breakdown field is expected. Figure 7 shows the breakdown field for the four discussed configurations. The results confirm the theory that with an increasing rigidity of the electrode, the breakdown field will also increase.

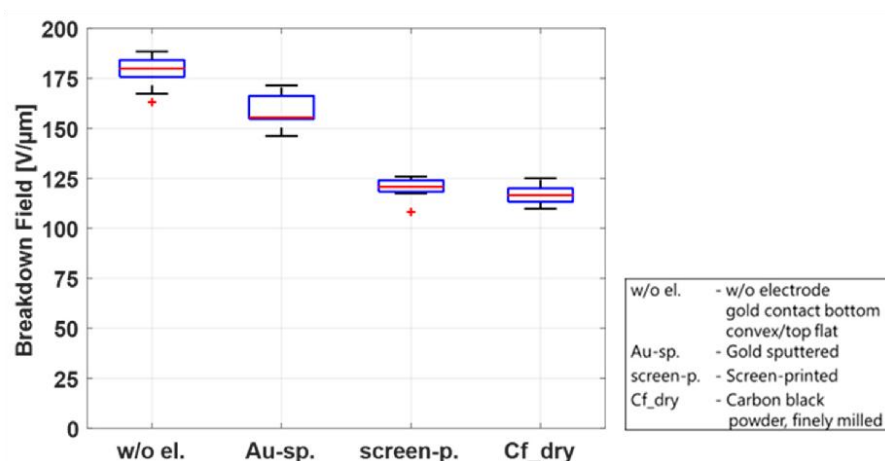


Figure 7. Comparison of electrodes with different stiffnesses (external-measurement electrodes, sputtered gold electrodes, screen-printed CB/PDMS electrodes, and finely milled CB powder) and their influence on the breakdown field at 20 °C/55% RH.

Another possible mechanism for the higher breakdown voltage in the case with only measurement electrodes might be the fact that the contact surface is reduced in comparison to sputtered electrodes due to surface roughness and potential micro-sized air bubbles.

The previous sections explained the factors that are mainly responsible for the different breakdown behavior of metal and carbon black electrodes. The following sections will focus on the material parameters of carbon black electrodes and their possible influence on the breakdown behavior. Metal electrodes are not included in these sections.

3.4. Carbon Black Electrodes: Influence of Solvents with and without Carbon Black

During the manufacturing process of carbon black electrodes via screen printing, pad printing, and inkjet printing, solvents are necessary to provide the electrode material with the viscosity required for the respective process. Even though the solvents are fully evaporated when the electrodes are cured, an influence on the breakdown during the manufacturing is possible. This section will investigate a possible influence of solvents on the breakdown behavior of the DE membrane under standard environmental conditions.

First, the breakdown effect of the three solvent mixtures used for screen printing, S1 (50% Belsil/50% VD60), pad printing, S2 (50% Iso-octane/50% Isopropanol), and inkjet printing, S3 (OS2), was studied. These tests were conducted on twelve test frames, four for each mixture, pre-stretched with Elastosil 2030/20 μm, identical to the frames prepared in the sections above. A total of 0.2 mL of each solvent mixture per test frame was applied by a syringe along the length of the frame and immediately distributed over an area of 110 mm × 20 mm using a spatula. Immediately after application, mixtures S1 and S3 led to significant swelling of the membrane, whereas less swelling but the formation of micro bubbles on the surface of the film was observed using mixture S2. To determine if these phenomena influence the breakdown behavior and also if they are dwell-time dependent, two samples of each mixture were heat cured immediately and two samples

were first stored for 24 h before heat curing at 150 °C for one hour. The samples were then tested in the breakdown tester, and the results are shown in Figure 8. For comparison, the results of untreated samples are also included in this figure. No significant differences in the breakdown fields are observed between solvent mixtures, regardless of whether the solvents remained on the sample before curing or were heat cured immediately. Compared to the breakdown field of the untreated samples, only a slightly lower breakdown field (~ 10 V/ μm between medians) is visible. This indicates that the swelling of the membrane after application and heat curing is only temporary and has no major impact on the membrane. The solvent by itself is therefore not the sole parameter responsible for the different breakdown behavior of sputtered metal electrodes and carbon black electrodes, but it may have an influence when carbon black is added to the mixture.

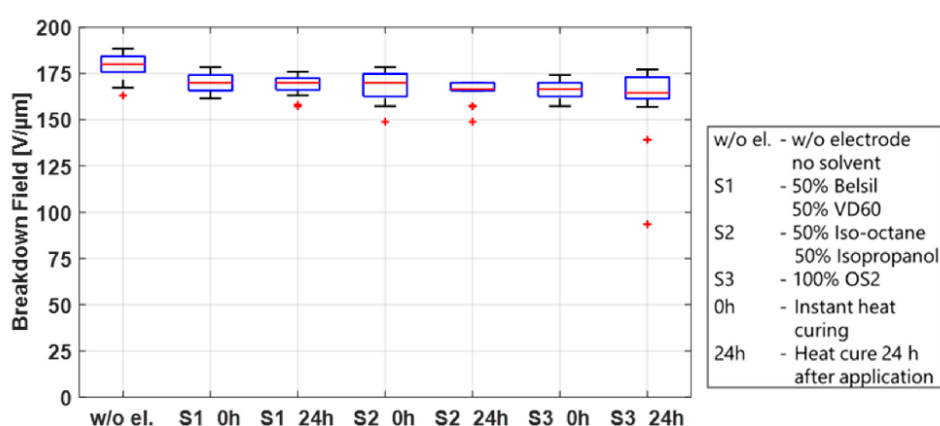


Figure 8. Influence of different solvents and their dwell time before heat curing at 150 °C on the breakdown field of Elastosil 2030/20 μm .

To investigate the influence of the solvent mixtures in the presence of carbon black, 0.5 g of CB was added to 6 g of each solvent mixture and processed in a planetary mixer. A planetary mixer was chosen because the different volatilities of the solvents would result in different evaporation rates when processed in a three-roll mill. The CB/solvent mixtures were manually applied using a stencil and a spatula. As in the test conducted above, two frames of each mixture were immediately heat cured, and two frames were stored 24 h before heat curing at 150 °C for 1 h. A picture of the electrode dots on the film as well as the breakdown results are shown in Figure 9. The addition of CB to the solvents has a significant impact on the breakdown field, regardless of the solvent mixture or dwell time, lowering the breakdown field by 40%. This phenomenon can be explained by two different mechanisms. On the one hand, the soft electrode layer covers the entire surface and thus detects all irregularities and changes in the thickness of the film, which are specified by the data sheet to $\pm 5\%$. The breakdown field will therefore always be determined by the thinnest spot of the film. Second, as discussed above, when solvents are applied to the membrane, swelling of the membrane or the forming of small bubbles on the surface are observed. When CB particles are present, it allows the particles to embed into the membrane, effectively thinning the dielectric layer. A calculation of the thickness reduction of the dielectric layer based on the difference in the breakdown field of the pure film (median 180 V/ μm) and the film with the CB/solvent electrodes (median 110 V/ μm) results in a reduction of 4.5 μm , or a 2.25 μm layer of embedded CB particles on each side. Even though the primary aggregate size of conductive carbon blacks is in the nanometer range, conglomerates > 150 nm up to micrometer structures form when solvents are added [56,57].

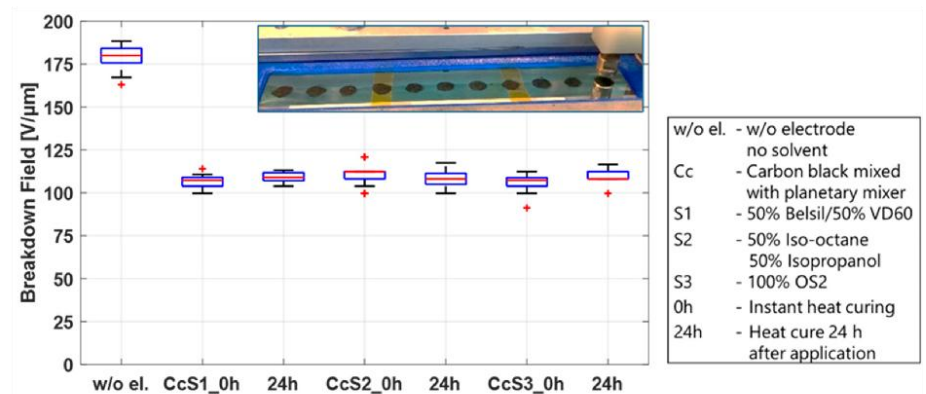


Figure 9. Influence of different solvents mixed with CB powder (without milling), dwelling time before heat curing on the breakdown behavior, and a picture with electrodes applied by hand using a stencil.

The results of Figure 9 are now compared to the results at the standard environmental conditions of Figure 4 to determine whether the lower breakdown field of the manufactured CB electrodes is solely a function of the solvent/CB mixtures, or if additional material parameters influence the breakdown behavior as well. Therefore, each solvent mixture is compared to the respective manufacturing method using this solvent. The results are shown in Figure 10, where the CB/solvent and manufacturing method for each solvent are combined in one box for better comparability. It is clearly visible that the breakdown field of all three manufactured electrodes is considerably higher than that of the CB/solvent mixture, indicating that not only do carbon black and solvents have an impact on the breakdown behavior but also that other manufacturing or material parameters are relevant as well. Two additional parameters possibly influencing the breakdown are (i) the fineness of the carbon black particles used in the process and (ii) the amount of PDMS added to the electrode material. Both will be investigated in the next sections.

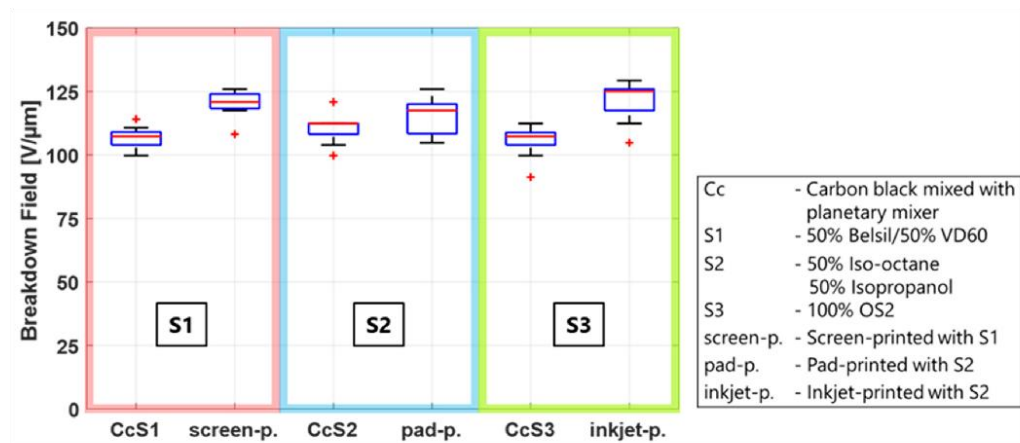


Figure 10. Influence of three solvent mixtures in CB powder and processed in their respective manufacturing method on the breakdown behavior.

3.5. Influence of Carbon Black Processing

Section 3.4 discussed the importance of investigating a possible impact of the fineness of the CB particles in the applied electrodes on the breakdown behavior. Because CB particles agglomerate when blended with most liquids, a grinding process is necessary to break down the agglomerates to smaller sizes. The grinding process was different in the

three manufacturing methods. Though the process is explained in Section 2.1 and in the references, a short comparison is necessary for a better understanding: the CB/solvent electrodes used in Section 3.4 were mixed using a planetary mixer; the CB for pad printing was also mixed using a planetary mixer, but steel balls were added to increase grinding. The CB in the screen-printing electrodes was first mixed in a planetary mixer and subsequently milled in a three-roll mill. Lastly, the CB for the inkjet formulation was first ground in a three-roll mill and subsequently sonicated in an ultrasound bath, with a 10 min waiting period for the larger particles to settle down before decanting. The fineness of the CB mixtures increases from CB/solvent to inkjet formulation in the order above.

The experiments were conducted on electrodes consisting of carbon black, and the solvent with the lowest vapor pressure, S1, was processed with the planetary mixer as an example of a coarser blend and a three-roll mill as an example for a finer blend. To investigate the influence on the membrane when no swelling from the solvents occurs, the experiments were additionally conducted with a CB/distilled water mixture. Both sample sets were prepared in the same way and heat cured at 150 °C for 1 h.

The results in Figure 11 show a higher breakdown field when the carbon black is more finely milled than in the coarser samples. While this effect is only small in the electrodes with solvents, it is considerably more pronounced in the electrodes without solvents. A possible explanation could be that due to the swelling of the membrane, when in contact with solvents, CB particles can be embedded in the surface layer of the PDMS membrane, and the difference between very fine and coarser particles will not be as pronounced. Without solvents and no swelling, however, the particles will stay on the surface of the membrane. Larger particles could damage the film more when an electric field is applied, probably due to the sharp edges and higher imprint. If the CB powder is very fine, the damaging effect on the film is likely reduced and a higher breakdown field than for the fine CB particles and solvents is achieved. The presence as well as the processing of the carbon black is an important parameter to influence the breakdown behavior of a DE.

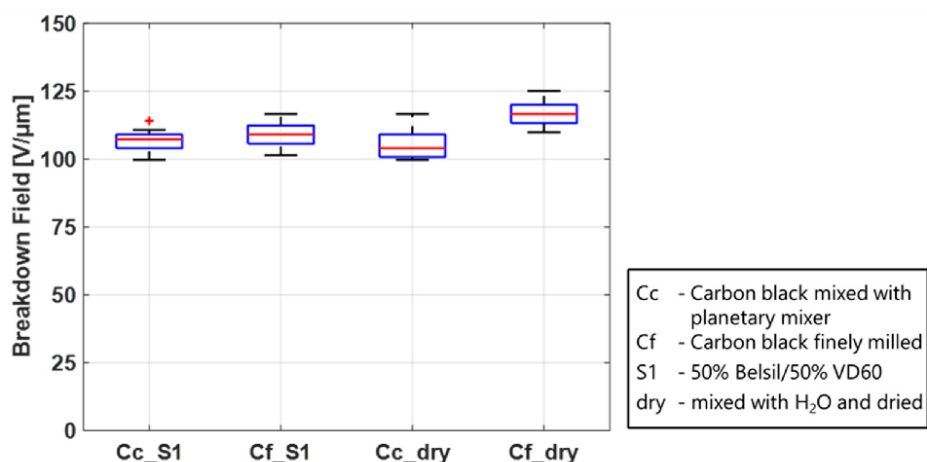


Figure 11. Influence of carbon black particle fineness on the breakdown behavior of Elastosil 2030/20. Particles were either mixed in a three-roll mill for a very fine homogeneous distribution or mixed using a planetary mixer, obtaining a slightly coarser structure.

3.6. Influence of Silicone Content (PDMS)

The influence of solvent and carbon black has been investigated, and the last important material parameter to study is the silicone content. The silicone content in the electrode mixtures varies depending on the manufacturing method. The highest PDMS content—90 wt.% after curing—is used in pad printing. The screen-printed electrodes consist of 75 wt.% PDMS, and the inkjet electrode material is not mixed with PDMS at all but with a silicone polyglucoside dispersant (~60 wt.% after solvent removal).

The study in this section was conducted on mixtures containing four different PDMS concentrations—0 wt.%, 45 wt.%, 75 wt.%, and 90 wt.%—after curing (without solvents). A stock mixture of CB and PDMS was prepared using a planetary mixer and was subsequently milled in a three-roll mill. The required test concentrations were then blended with PDMS using the planetary mixer. The electrode dots containing PDMS were applied using the screen-printing method. The electrodes without silicone were not processable in a screen printer and were applied as described above using a stencil. All the samples were cured at 150 °C for one hour. The results are depicted in Figure 12 and show a significant impact of the PDMS content in the electrodes on the breakdown behavior.

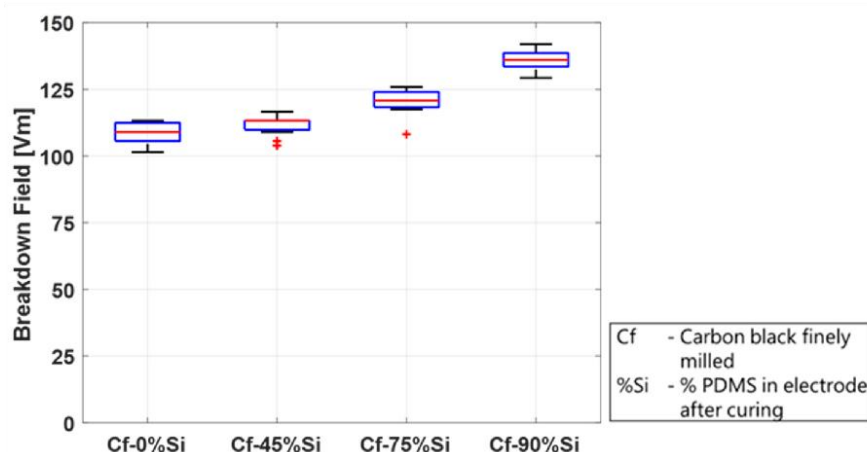


Figure 12. Influence of silicone content in the electrode matrix on the breakdown behavior of Elastosil 2030/20 at 20 °C/55% rel. humidity in wt.%. All electrodes except Cf-0%Si are applied by the screen-printing method.

The breakdown field increases with an increasing PDMS content, from a median of 109 V/μm without silicone to 136 V/μm in the mixture with 90 wt.% silicone. This could be explained by the fact that the higher the silicone content, the more the particles are embedded in the silicone structure, and damage due to sharp particles is reduced. Furthermore, less CB particles are directly located on the surface but are enclosed in the dielectric matrix. This proposed explanation is in agreement with the results of Section 3.5, where finely milled CB dust present on the top of the film and not embedded in the silicone also leads to lower breakdown fields. It should be mentioned, however, that this is only an observation regarding the breakdown field. A higher PDMS/carbon black ratio has not only the advantage of the higher breakdown field and better attachment to the film but also the disadvantage of a lower electrical resistance, as discussed in detail by Willian et al. [58].

4. Conclusions

This paper presented results on the dielectric breakdown of silicone-based electroactive polymer actuators to give a comprehensive understanding about breakdown-influencing parameters. A particular focus was on the effects of electrode composition and electrode manufacturing. These results will allow for a comparison and interpretation of results from different published studies, using these results to better design given applications. As previous work [19] indicated a significant impact of the presence of electrodes on the PDMS membrane, it is important to understand which parameters influence the electric breakdown behavior. This paper focused on a systematic study of different electrodes including gold- and nickel-sputtered electrodes as well as carbon black-based electrodes applied by widely used manufacturing methods such as screen printing, pad printing, or inkjet printing. In addition to a systematic comparison of the different materials, the present work also studied the effect of environmental parameters, such as temperature and humidity, on the breakdown behavior.

We found that adding electrodes lowers the breakdown field compared to films without electrodes. The effect, however, is low for sputtered metal electrodes but significant when carbon black electrodes are applied, reducing the breakdown field by up to 30%. Possible parameters responsible are identified as the mechanical impact during manufacturing, the stiffness of the electrode, and material parameters. Material parameters include the used solvent, carbon black processing, and the silicone content. They were investigated and discussed in detail.

The mechanical impact due to direct contact with the membrane during screen printing and pad printing has no effect on the breakdown behavior compared to inkjet printing, where no direct contact is present. The influence of the electrode stiffness is clearly visible, showing that breakdown tests using stiff metal electrodes yielded a higher breakdown field.

Further investigations should focus on material parameters used for carbon black electrode manufacturing, because these electrodes are common for actuator and sensor applications and are applied by fast and scalable processes. Different manufacturing methods require different solvents, thus the solvent mixtures used during the three manufacturing methods were investigated separately. The data indicate only a minor influence of the solvents on the breakdown field, regardless of the dwelling time on the film before curing. When carbon black is added to the solvents, however, the breakdown field is reduced by up to 40%. This effect is slightly improved when the fineness of the carbon black particles is increased, e.g., through processing in a three-roll mill. Another important parameter influencing the breakdown behavior is the silicone content in the electrode material. The breakdown field is significantly increased when silicone is added to the electrode material and increases with increasing silicone content.

The study on the influence of various environmental conditions was carried out for all types of electrodes with temperatures between 1 °C and 80 °C and humidities ranging from 10%RH to 90%RH. An increasing breakdown behavior with an increasing temperature and decreasing humidity was observed for all electrode types.

Author Contributions: Conceptualization, B.F. and S.S.; methodology, B.F., S.S., H.S. and G.S.; software, B.F.; validation, B.F.; formal analysis, B.F., F.B.A. and J.H.; investigation, B.F.; resources, B.F., F.B.A. and J.H.; writing—original draft preparation, B.F.; writing—review and editing, B.F., H.S., F.B.A., J.H., G.S. and S.S.; visualization, B.F.; supervision, S.S.; project administration, B.F. All authors have read and agreed to the published version of the manuscript.

Funding: This research received no external funding.

Institutional Review Board Statement: Not applicable.

Data Availability Statement: The data presented in this study are available on request from the corresponding author.

Acknowledgments: We gratefully acknowledge the support from WACKER Chemie AG, who supplied the Elastosil 2030 film and other chemicals necessary for the tests.

Conflicts of Interest: Author Bettina Fasolt was employed by the company Intelligent Material Systems Lab, Center for Mechatronics and Automation Technology, ZeMA gGmbH, Saarbrücken, Germany. All authors declare that the research was conducted in the absence of any commercial or financial relationships that could be construed as a potential conflict of interest.

References

1. Hill, M.; Rizzello, G.; Seelecke, S. Development and experimental characterization of a pneumatic valve actuated by a dielectric elastomer membrane. *Smart Mater. Struct.* **2017**, *26*, 085023. [\[CrossRef\]](#)
2. Giousouf, M.; Kovacs, G. Dielectric elastomer actuators used for pneumatic valve technology. *Smart Mater. Struct.* **2013**, *22*, 104010. [\[CrossRef\]](#)
3. Cao, C.; Gao, X.; Conn, A.T. A Magnetically Coupled Dielectric Elastomer Pump for Soft Robotics. *Adv. Mater. Technol.* **2019**, *4*. [\[CrossRef\]](#)
4. Ciarella, L.; Richter, A.; Henke, E.F.M. Digital electronics using dielectric elastomer structures as transistors. *Appl. Phys. Lett.* **2021**, *119*, 261901. [\[CrossRef\]](#)

5. Pniak, L.; Almanza, M.; Civet, Y.; Perriard, Y. Ultrahigh-Voltage Switch for Bidirectional DC-DC Converter Driving Dielectric Elastomer Actuator. *IEEE Trans Power Electron.* **2020**, *35*, 13172–13181. [\[CrossRef\]](#)
6. Gratz-Kelly, S.; Krüger, T.; Rizzello, G.; Seelecke, S.; Moretti, G. An audio-tactile interface based on dielectric elastomer actuators. *Smart Mater. Struct.* **2023**, *32*, 034005. [\[CrossRef\]](#)
7. Ji, X.; Liu, X.; Cacucciolo, V.; Civet, Y.; El Haitami, A.; Cantin, S.; Perriard, Y.; Shea, H. Untethered Feel-Through Haptics Using 18- μ m Thick Dielectric Elastomer Actuators. *Adv. Funct. Mater.* **2021**, *31*, 2006639. [\[CrossRef\]](#)
8. Zhao, H.; Hussain, A.M.; Israr, A.; Vogt, D.M.; Duduta, M.; Clarke, D.R.; Wood, R.J. A Wearable Soft Haptic Communicator Based on Dielectric Elastomer Actuators. *Soft Robot.* **2020**, *7*, 451–461. [\[CrossRef\]](#)
9. Bolzmacher, C.; Biggs, J.; Srinivasan, M. Flexible dielectric elastomer actuators for wearable human-machine interfaces. In Proceedings of the Smart Structures and Materials 2006: Electroactive Polymer Actuators and Devices (EAPAD), SPIE, San Diego, CA, USA, 26 February–2 March 2006; Volume 6168, p. 616804. [\[CrossRef\]](#)
10. Henke, E.F.M.; Schlatter, S.; Anderson, I.A. Soft Dielectric Elastomer Oscillators Driving Bioinspired Robots. *Soft Robot.* **2017**, *4*, 353–366. [\[CrossRef\]](#)
11. Li, W.B.; Zhang, W.M.; Zou, H.X.; Peng, Z.K.; Meng, G. Multisegment annular dielectric elastomer actuators for soft robots. *Smart Mater. Struct.* **2018**, *27*. [\[CrossRef\]](#)
12. Guo, Y.; Liu, L.; Liu, Y.; Leng, J. Review of Dielectric Elastomer Actuators and Their Applications in Soft Robots. *Adv. Intell. Syst.* **2021**, *3*, 2000282. [\[CrossRef\]](#)
13. Mahmoudinezhad, M.H.; Anderson, I.; Rosset, S. A Skin-Like Soft Compression Sensor for Robotic Applications. *Soft Robot.* **2023**, *10*, 687–700. [\[CrossRef\]](#) [\[PubMed\]](#)
14. Ji, X.; Liu, X.; Cacucciolo, V.; Imboden, M.; Civet, Y.; El Haitami, A.; Cantin, S.; Perriard, Y.; Shea, H. An Autonomous Untethered Fast Soft Robotic Insect Driven by Low-Voltage Dielectric Elastomer Actuators. *Sci. Robot.* **2019**, *4*, eaaz6451. [\[CrossRef\]](#) [\[PubMed\]](#)
15. Hajiesmaili, E.; Clarke, D.R. Dielectric elastomer actuators. *J. Appl. Phys.* **2021**, *129*, 151102. [\[CrossRef\]](#)
16. Pelrine, R.; Kornbluh, R.; Pei, Q.; Joseph, J. High-Speed Electrically Actuated Elastomers with Strain Greater Than 100%. *Science* **2000**, *287*, 836–839. [\[CrossRef\]](#)
17. Duduta, M.; Hajiesmaili, E.; Zhao, H.; Wood, R.J.; Clarke, D.R. Realizing the potential of dielectric elastomer artificial muscles. *Proc. Natl. Acad. Sci. USA* **2019**, *116*, 2476–2481. [\[CrossRef\]](#)
18. Haddad, G.; Wong, K.L.; Gupta, R.K. Dielectric Breakdown Characteristics of HTV Silicone Rubber under Multiple Stress Conditions. In Proceedings of the 2014 International Symposium on Electrical Insulating Materials, Niigata, Japan, 1–5 June 2014.
19. Gatti, D.; Haus, H.; Matysek, M.; Frohnäpfel, B.; Tropea, C.; Schlaak, H.F. The dielectric breakdown limit of silicone dielectric elastomer actuators. *Appl. Phys. Lett.* **2014**, *104*, 052905. [\[CrossRef\]](#)
20. Yu, L.; Vudayagiri, S.; Jensen, L.A.; Skov, A.L. Temperature dependence of dielectric breakdown of silicone-based dielectric elastomers. *Int. J. Smart Nano Mater.* **2020**, *11*, 129–146. [\[CrossRef\]](#)
21. Albuquerque, F.B.; Shea, H. Influence of humidity, temperature and prestretch on the dielectric breakdown strength of silicone elastomer membranes for DEAs. *Smart Mater. Struct.* **2020**, *29*, 105024. [\[CrossRef\]](#)
22. Gerratt, A.P.; Bergbreiter, S. Dielectric breakdown of PDMS thin films. *J. Micromech. Microeng.* **2013**, *23*. [\[CrossRef\]](#)
23. Taine, E.; Andritsch, T.; Saeedi, I.A.; Morshuis, P.H.F. Size effect and electrical ageing of PDMS dielectric elastomer with competing failure modes. *Smart Mater. Struct.* **2023**, *32*, 105021. [\[CrossRef\]](#)
24. Prakash Prabhakar, O.; Sahu, R.K. Effects of Soft and Hard Fillers on Electromechanical Properties and Performance of Polydimethylsiloxane Elastomer for Actuator Applications. 2023. Available online: <https://doi.org/10.21203/rs.3.rs-2559565/v2> (accessed on 26 September 2023).
25. Fasolt, B.; Welsch, F.; Jank, M.; Seelecke, S. Effect of actuation parameters and environment on the breakdown voltage of silicone dielectric elastomer films. *Smart Mater. Struct.* **2019**, *28*, 094002. [\[CrossRef\]](#)
26. Förster-Zügel, F.; Solano-Arana, S.; Klug, F.; Schlaak, H.F. Dielectric breakdown strength measurements with silicone-based single-layer dielectric elastomer transducers. *Smart Mater. Struct.* **2019**, *28*, 075042. [\[CrossRef\]](#)
27. Stoyanov, H.; Brochu, P.; Niu, X.; Lai, C.; Yun, S.; Pei, Q. Long lifetime, fault-tolerant freestanding actuators based on a silicone dielectric elastomer and self-clearing carbon nanotube compliant electrodes. *RSC Adv.* **2013**, *3*, 2272–2278. [\[CrossRef\]](#)
28. Jiang, L.; Betts, A.; Kennedy, D.; Jerrams, S. Investigation into the electromechanical properties of dielectric elastomers subjected to pre-stressing. *Mater. Sci. Eng. C* **2015**, *49*, 754–760. [\[CrossRef\]](#)
29. Albuquerque, F.B.; Shea, H. Influence of electric field, temperature, humidity, elastomer material, and encapsulation on the lifetime of dielectric elastomer actuators (DEAs) under DC actuation. *Smart Mater. Struct.* **2021**, *30*, 125022. [\[CrossRef\]](#)
30. Zakaria, S.; Morshuis, P.H.F.; Benslimane, M.Y.; Yu, L.; Skov, A.L. The electrical breakdown strength of pre-stretched elastomers, with and without sample volume conservation. *Smart Mater. Struct.* **2015**, *24*, 055009. [\[CrossRef\]](#)
31. Chortos, A.; Hajiesmaili, E.; Morales, J.; Clarke, D.R.; Lewis, J.A. 3D Printing of Interdigitated Dielectric Elastomer Actuators. *Adv. Funct. Mater.* **2020**, *30*, 1907375. [\[CrossRef\]](#)
32. Cohen, A.J.; Kolloosche, M.; Yuen, M.C.; Lee, D.Y.; Clarke, D.R.; Wood, R.J. Batch-Sprayed and Stamp-Transferred Electrodes: A New Paradigm for Scalable Fabrication of Multilayer Dielectric Elastomer Actuators. *Adv. Funct. Mater.* **2022**, *32*, 2205394. [\[CrossRef\]](#)
33. Krüger, T.S.; Çabuk, O.; Maas, J. Manufacturing Process for Multilayer Dielectric Elastomer Transducers Based on Sheet-to-Sheet Lamination and Contactless Electrode Application. *Actuators* **2023**, *12*, 95. [\[CrossRef\]](#)

34. Hubertus, J.; Fasolt, B.; Linnebach, P.; Seelecke, S.; Schultes, G. Electromechanical evaluation of sub-micron NiCr-carbon thin films as highly conductive and compliant electrodes for dielectric elastomers. *Sens. Actuators A Phys.* **2020**, *315*, 112243. [\[CrossRef\]](#)
35. Hubertus, J.; Croce, S.; Neu, J.; Seelecke, S.; Rizzello, G.; Schultes, G. Laser Structuring of Thin Metal Films of Compliant Electrodes on Dielectric Elastomers. *Adv. Funct. Mater.* **2023**, *33*, 2214176. [\[CrossRef\]](#)
36. Hubertus, J.; Neu, J.; Croce, S.; Rizzello, G.; Seelecke, S.; Schultes, G. Nanoscale Nickel-Based Thin Films as Highly Conductive Electrodes for Dielectric Elastomer Applications with Extremely High Stretchability up to 200%. *ACS Appl. Mater. Interfaces* **2021**, *13*, 39894–39904. [\[CrossRef\]](#)
37. Welsch, F.; Fasolt, B.; Seelecke, S. Dielectric breakdown test setup for dielectric elastomers: Design and validation. In Proceedings of the SPIE Smart Structures and Materials + Nondestructive Evaluation and Health Monitoring, Denver, CO, USA, 5–6 March 2018; Volume 10594, p. 43. [\[CrossRef\]](#)
38. Carpi, F.; Anderson, I.; Bauer, S.; Frediani, G.; Gallone, G.; Gei, M.; Graaf, C.; Jean-Mistral, C.; Kaal, W.; Kofod, G.; et al. Standards for dielectric elastomer transducers. *Smart Mater. Struct.* **2015**, *24*, 105025. [\[CrossRef\]](#)
39. Rosset, S.; Ararom, O.A.; Schlatter, S.; Shea, H.R. Fabrication process of silicone-based dielectric elastomer actuators. *J. Vis. Exp.* **2016**, *108*, e53423. [\[CrossRef\]](#)
40. Albuquerque, F.B. *Lifetime of Dielectric Elastomer Actuators under DC Electric Fields*; EPFL: Lausanne, Switzerland, 2022. [\[CrossRef\]](#)
41. Fasolt, B.; Hodgins, M.; Rizzello, G.; Seelecke, S. Effect of screen printing parameters on sensor and actuator performance of dielectric elastomer (DE) membranes. *Sens. Actuators A Phys.* **2017**, *265*, 10–19. [\[CrossRef\]](#)
42. Schlatter, S.; Grasso, G.; Rosset, S.; Shea, H. Inkjet Printing of Complex Soft Machines with Densely Integrated Electrostatic Actuators. *Adv. Intell. Syst.* **2020**, *2*, 2000136. [\[CrossRef\]](#)
43. Iannarelli, A.; Niasar, M.G.; Ross, R. The effects of static pre-stretching on the short and long-term reliability of dielectric elastomer actuators. *Smart Mater. Struct.* **2019**, *28*, 125014. [\[CrossRef\]](#)
44. Zakaria, S.; Yu, L.; Kofod, G.; Skov, A.L. The influence of static pre-stretching on the mechanical ageing of filled silicone rubbers for dielectric elastomer applications. *Mater. Today Commun.* **2015**, *4*, 204–213. [\[CrossRef\]](#)
45. Kofod, G. Dielectric Elastomer Actuators. Ph.D. Thesis, Technical University of Denmark, Lyngby, Denmark, 2001.
46. Mazurek, P.; Vudayagiri, S.; Skov, A.L. How to tailor flexible silicone elastomers with mechanical integrity: A tutorial review. *Chem. Soc. Rev.* **2019**, *48*, 1448–1464. [\[CrossRef\]](#)
47. Shin-Etsu Silicone Chemical Co., Ltd. Characteristic Properties of Silicone Rubber Compounds. Available online: https://www.shinetsusilicone-global.com/catalog/pdf/rubber_e.pdf (accessed on 23 June 2023).
48. Polmanteer, K.E. Current Perspectives on Silicone Rubber Technology. *Rubber Chem. Technol.* **1981**, *54*, 1051–1080. [\[CrossRef\]](#)
49. Rey, T.; Chagnon, G.; Le Cam, J.B.; Favier, D. Influence of the temperature on the mechanical behaviour of filled and unfilled silicone rubbers. *Polym. Test.* **2013**, *32*, 492–501. [\[CrossRef\]](#)
50. Du, B.X.; Ma, Z.L.; Gao, Y.; Han, T. Effect of Ambient Temperature on Electrical Treeing Characteristics in Silicone Rubber. *Trans. Dielectr. Electr. Insul.* **2011**, *18*, 401–407. [\[CrossRef\]](#)
51. Wacker Chemical Corporation. Datenblätter Elastosil Film 2030 250/20. 2016. Available online: <https://www.wacker.com> (accessed on 10 March 2021).
52. Chang, K.S.; Chung, Y.C.; Yang, T.H.; Lue, S.J.; Tung, K.L.; Lin, Y.F. Free volume and alcohol transport properties of PDMS membranes: Insights of nano-structure and interfacial affinity from molecular modeling. *J. Memb. Sci.* **2012**, *417–418*, 119–130. [\[CrossRef\]](#)
53. Zhang, H.; Cloud, A. The Permeability characteristics of silicone Rubber. In Proceedings of the Sampe Fall Technical Conference, Global Advances in Material and Process Engineering, Dallas, TX, USA, 6–9 November 2006.
54. Gong, B.; Tu, Y.; Zhou, Y.; Li, R.; Zhang, F.; Xu, Z.; Liang, D. Moisture Absorption Characteristics of Silicone Rubber and Its Effect on Dielectric Properties. In Proceedings of the 2013 Annual Report Conference on Electrical Insulation and Dielectric Phenomena, Chenzhen, China, 20–23 October 2013.
55. Hillborgl, H.; Gedde, U.W. Hydrophobicity Changes in Silicone Rubbers. *IEEE Trans. Dielectr. Electr. Insul.* **1999**, *6*, 703–717. [\[CrossRef\]](#)
56. Neffati, R.; Brokken-Zijp, J.M.C. Structure and porosity of conductive carbon blacks. *Mater. Chem. Phys.* **2021**, *260*, 124177. [\[CrossRef\]](#)
57. Ketjenblack®. Available online: <https://www.fuelcellstore.com/spec-sheets/ketjenblack-ec-300j-fact-sheet.pdf> (accessed on 19 July 2023).
58. Willian, T.P.; Fasolt, B.; Motzki, P.; Rizzello, G.; Seelecke, S. Effects of Electrode Materials and Compositions on the Resistance Behavior of Dielectric Elastomer Transducers. *Polymers* **2023**, *15*, 310. [\[CrossRef\]](#)

Disclaimer/Publisher’s Note: The statements, opinions and data contained in all publications are solely those of the individual author(s) and contributor(s) and not of MDPI and/or the editor(s). MDPI and/or the editor(s) disclaim responsibility for any injury to people or property resulting from any ideas, methods, instructions or products referred to in the content.

5. Innovative DEA repair method

Chapter 4 examined the impact of climatic conditions, manufacturing processes, pre-stretch, and electrode composition on the dielectric breakdown behavior of DEA. The findings from these investigations provide valuable guidelines for ensuring reliable DEA operation, provided that parameters and operating conditions are appropriately adjusted, and thereby successfully address the research question. However, in addition to these adjustments, a reliable operation also relies on the silicone film quality. Given the complex nature of current manufacturing processes, even commercially available thin films may still exhibit local imperfections, which can limit the overall breakdown field and, in some cases, lead to premature failure of DE actuators. This issue becomes particularly critical when producing large-scale or multi-layer actuators, where an early breakdown at a single location or within one layer can result in the failure of the entire actuator system. Achieving process capability will require additional measures to resolve this problem.

This chapter introduces an innovative patent-pending DEA repair method (Patent PCT/EP2024/063804, 17-05-2023, Verfahren zum Reparieren von dielektrischen Elastomeren nach elektrischem Durchschlag oder mechanischer Beschädigung) that will ensure reliable operation up to a pre-defined electric field level. This chapter focusses on the repair method for DEA, however, it is also applicable for DEG applications. Figure 5.1 explains the main process steps for this method, beginning with the testing of DEA up to a voltage slightly higher than the voltage required for the application, a repair process, and a subsequent quality control, which ensures reliable and robust operation.

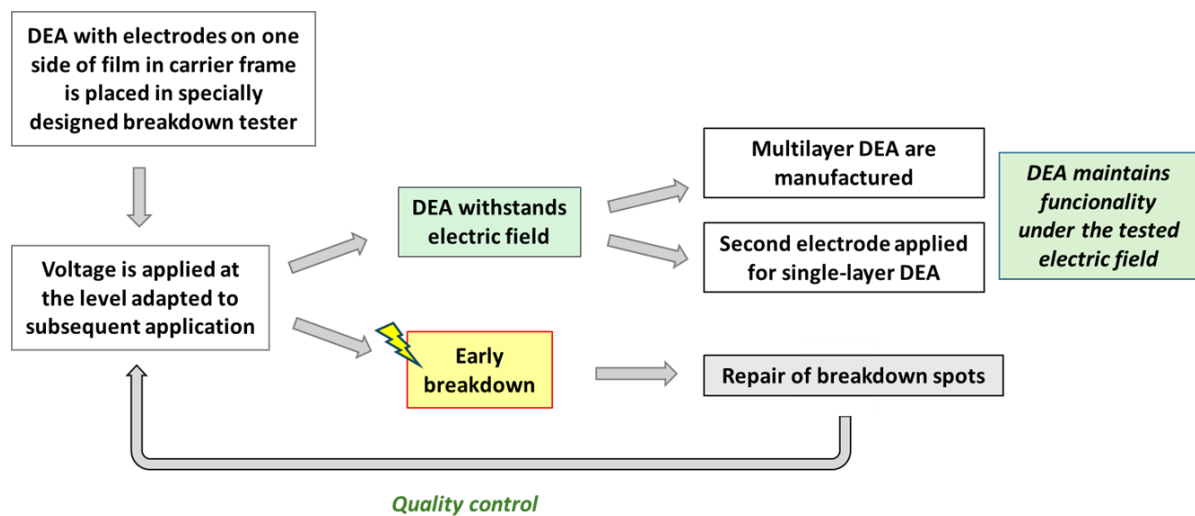


Figure 5.1. Main process steps for repair method and quality control

Film imperfections are particularly problematic in applications involving actuators with large electrode areas or in multilayer DEA configurations. Applying this method enables the operation of even large-diameter actuators, such as the examples shown in Figure 5.2. Due to their large surface area, these would be highly probable to exhibit imperfections leading to breakdown if not properly repaired.

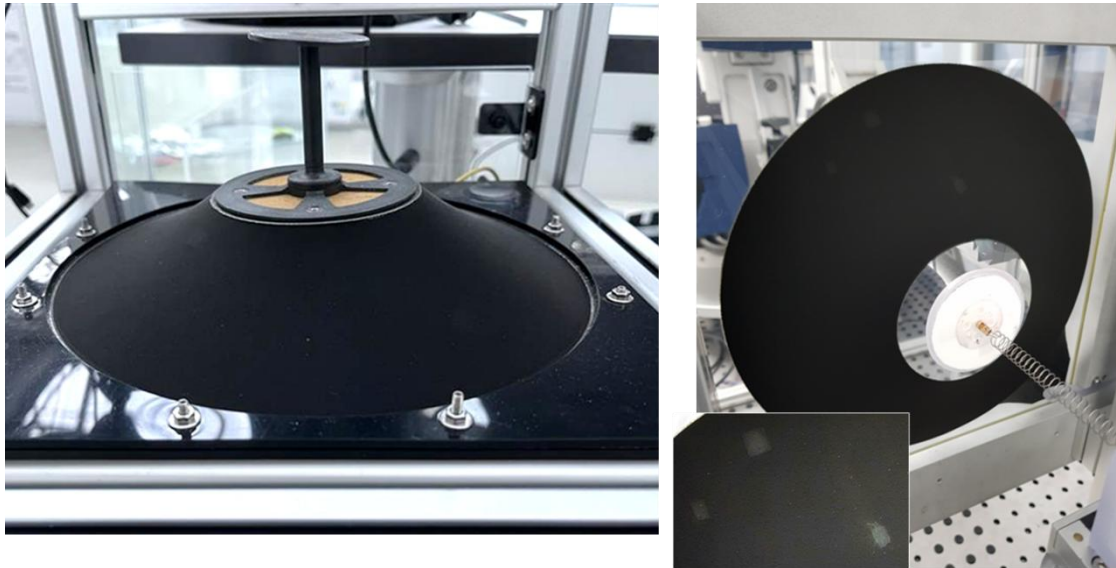


Figure 5.2. 300 mm repaired circular DEA used for large-stroke actuation (left), and investigation of vibration modes in loudspeaker applications (right).

Additionally, this approach enables the fabrication and operation of multi-layer DEA, in which multiple single DEA membranes are stacked. A sketch of the setup for a multilayer design is shown in Figure 5.3. Multilayers are used when the actuation force of a single layer is insufficient for the specific application. By stacking individual layers, the actuation force of a single layer is multiplied by the number of layers, while the deflection for the stack remains unchanged. The figure shows a photograph of a DEA in which three seven layer stacks are combined. It also schematically illustrates the electrode design and a side view of a seven-layer stack.

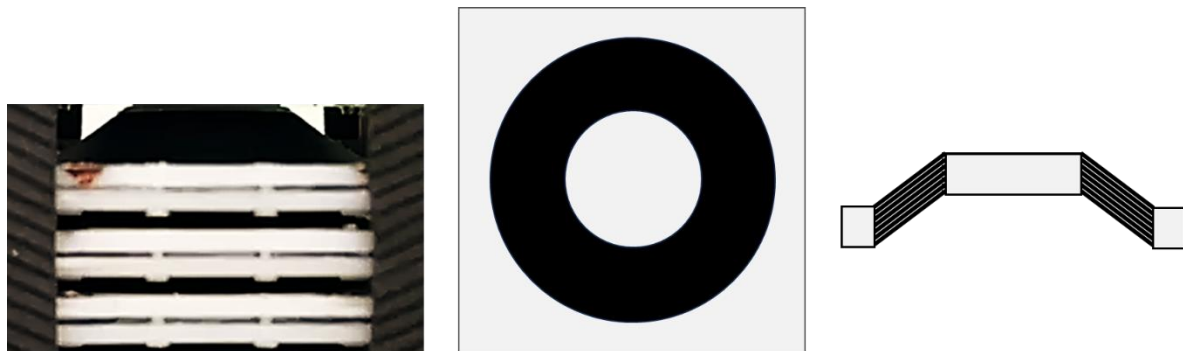


Figure 5.3. Photograph of a deflected multilayer DEA consisting of three stacks of seven single-layer DEAs each (left); electrode design used for the stack (middle), and cross-section of the deflected seven-layer stack (right).

As previously described, DEA manufactured at the iMSL lab remain attached to a carrier frame throughout the entire manufacturing process, with multiple electrodes screen printed on each membrane. The stacking process is carried out using these carrier frames, and the individual DEAs are only separated after stacking is complete. During the stacking process, it is crucial to ensure that electrode connection points with differing voltage potentials do not overlap, as overlapping in the voltage application area has been identified in the iMSL lab as a common location for the initial occurrence of electrical breakdown. Figure 5.4 illustrates the stacking process using a three-layer example; however, up to 17 layers are typically stacked in a single process. Once the layers are

stacked, the individual DEAs are clamped in a way that allows them to be separated and addressed individually.

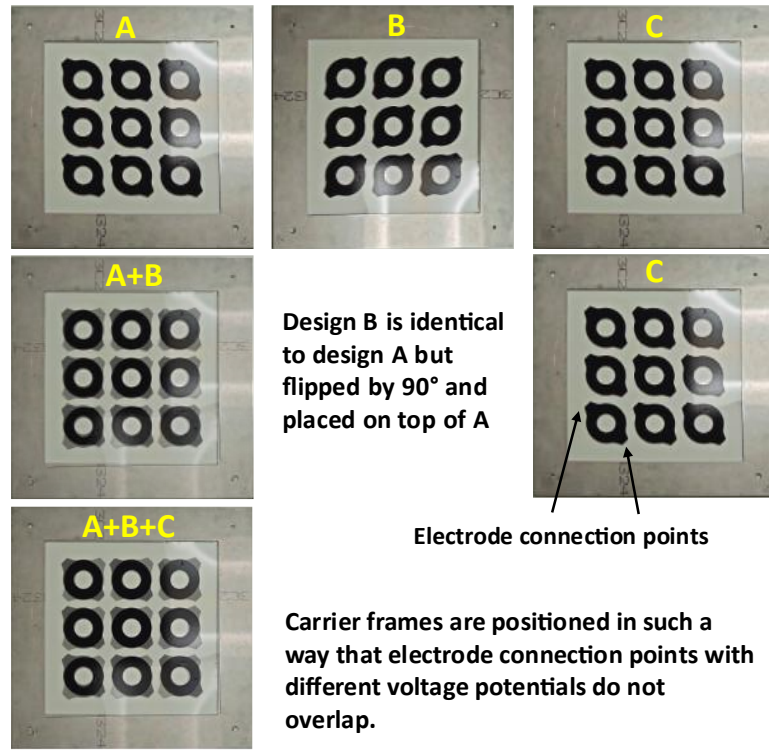


Figure 5.4. Example of carrier frame placement when frames are stacked. Three single layer frames (top); Frame B rotated 90° and placed on top of Frame A (middle); Frames A, B, and C are stacked.

Figure 5.5 illustrates a representative failure analysis of four single-layer DEAs and highlights the influence of individual layer failure on the overall performance of the stacked actuator. This specific design has been used repeatedly for demonstrator devices in the iMSL lab, and the observed failure pattern is representative of multiple four-layer DEA assemblies.

Each 200 mm × 200 mm silicone film, mounted on a carrier frame, contains nine screen-printed DEA. These frames were tested in the breakdown tester described in Section 5.1, using the target operating voltage intended for the final application. The results showed that, for each frame, one to three DEA typically experienced dielectric breakdown before reaching the desired voltage threshold. Due to the fixed electrode configuration in the stacking process, defective DEA cannot be excluded once the layers are assembled. Consequently, after stacking four layers, only three out of nine multilayer stacks remained operational. This underscores the importance of incorporating a robust testing and repair procedure prior to or during the stacking process.

Premature breakdown has been extensively discussed in Chapter 4, Sections 4.3 and 4.4, and various strategies have been discussed in the literature to either maintain operation after breakdowns or to identify and repair weak spots through inspection and restoration of the DEA [149, 150]. The development of self-healing or self-repairing DEA has been proposed in [151, 152, 153]. But even though the approach is promising, these self-healing materials are not commercially available.

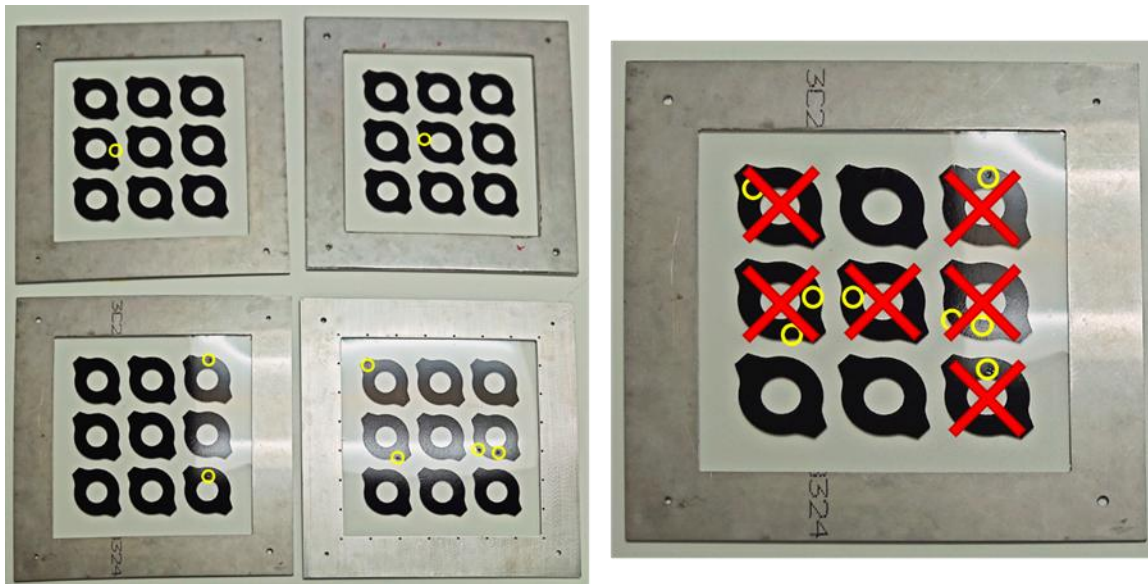


Figure 5.5. Premature breakdown spots in four single-layer frames with nine DEA each (left) and the number of failed DEA when the four frames are stacked (right)

Hunt et al. [154] propose a solution combining DEA with an open-cell silicone sponge saturated with silicone oil, allowing the oil to flow back into voids and restore the dielectric structure. Another effective approach, presented by Kim et al. [155], involves eliminating electrical shorting through self-clearing, where current flow thermally degrades local electrical connectivity, or through a laser-assisted repair method that removes electrode material around the breakdown site, effectively isolating the damaged area to enable continued operation. However, the amount of electrode material that must be removed to prevent short circuits increases with voltage, potentially limiting this method to applications in the lower kilovolt range.

Two solutions are already patented. Patent JP 2019169659A [150] describes a method in which an uncoated dielectric elastomer (DE) film is placed on a conductive plate and scanned by two flexible rollers with an applied voltage, systematically rolling over the film until all areas have been assessed. If a difference in electric potential is detected at any location, the affected area is reinforced using repair patches or liquid gel. Additionally, optical inspection devices identify potential breakdown sites, which are similarly reinforced. Following these procedures, an electrode is applied to the film. The method detects and reinforces potential weak spots, which might not be the ones to cause electrical breakdown. The influence of the electrode on the electrical breakdown is not evaluated, because it is applied after reinforcement.

Patent WO 2020/064872 A1 [156] describes the repair process for stacked DE in DE wave energy generator applications, where each layer is tested before stacking. The size of each individual layer and the layer thickness are not specified in the patent. A single-side coated or uncoated film is placed on a conductive surface, with the uncoated side facing up. A flexible roller, charged with the target voltage, is rolled over the film. If a breakdown occurs, it is temporarily covered with a non-conductive material to allow uninterrupted testing. Afterward, self-adhesive removable stickers (25 to 50 mm rings with a 10 mm central opening) replace the temporary covers. An electrode is then applied across the membrane, and the stickers are removed, leaving breakdown sites electrode-covered but electrically isolated. This method ensures the film withstands the target voltage post-electrode application. This method electrically isolates breakdown spots. The patent justifies the isolated area size of 25 mm to 50 mm by stating that this range ensures reliable high-voltage application.

While the size of the electrically isolated area is suitable for wave energy generator applications, in which electrode areas are known to be large [4], it is impractical for DEA applications, where the actuator areas are significantly smaller, often comparable in size to the isolated region, making actuation impossible.

The method presented in this work is specifically developed for DEA applications, with the objective of producing actuators capable of withstanding the electric field required for reliable operation. To achieve this, electrodes are printed on one side of the film, and the DEA is subsequently tested in a custom-designed breakdown box at a field slightly higher than that of the intended application. Testing the samples at a voltage 5% higher than the application voltage has proven to be resulting in more reliable DEA performance without breakdown than when tested at the nominal application. It provides a safety margin without reaching voltage levels that would result in an unnecessary high breakdown rate. If the DEA successfully endures this test, it proceeds to the next manufacturing steps. However, if breakdown occurs below the required field, the DEA is removed from the breakdown box and repaired using a silicone patch applied to the non-electrode side. The actuator is then retested, and the process is repeated until all DEA withstand the required field. Multiple repair cycles may be necessary. The procedure always concludes with a final breakdown test to ensure reliable operation under the specified conditions.

The process is designed as a batch operation, with DEA manufactured attached to a metal frame that remains in use throughout electrode screen printing, testing, and repair. This integrated approach ensures consistency and enables scalability for future mass production.

Chapter 5 is divided into three main sections. The first part, Section 5.1 and Section 5.2, outlines the design of a breakdown box and the test and repair procedure. Additionally, it examines the mechanical effects of materials used for the repair process. The second part, Section 5.3 and Section 5.4, examines the impact of repair patches on the mechanical and electro-mechanical properties of the DEA. The section first presents results of single repairs and then expands these investigations to multiple repairs. Furthermore, it discusses up to how many repeated cycles continue to enhance actuator performance. Finally, the third part, Section 5.5, presents three examples of repaired multilayer applications and their operation cycles.

5.1 Breakdown box and test procedure

The breakdown box is specifically designed to test dielectric elastomer actuators under applied voltage up to the breakdown level required for the respective application, in a controlled and safe manner. The breakdown box consists of a conductive metal plate, which is connected to the ground electrode, and a flexible connection pad, which is linked to the voltage source supply. A safety enclosure with a control unit and an emergency stop switch guarantees that operation is only possible when the lid is closed. A control unit ensures that the charge on the DEA is discharged before the lid is reopened. A TREK Model 610E high voltage amplifier allows voltage application up to 10 kV and a maximal current of 2 mA.

The setup for the breakdown experiments and a test frame positioned in the breakdown box are shown in Figure 5.6. The test frame consists of a silicone thin film with six CB/PDMS electrodes, which are screen-printed onto the upper side of the film. The film is attached to a metal frame and placed on a brass plate functioning as ground electrode. The upper CB electrodes are connected via connecting arms to a high voltage amplifier. To avoid breakdown at the location where voltage is applied, additional electrical insulation to the ground plate is provided using polyimide tape underneath the connection points.

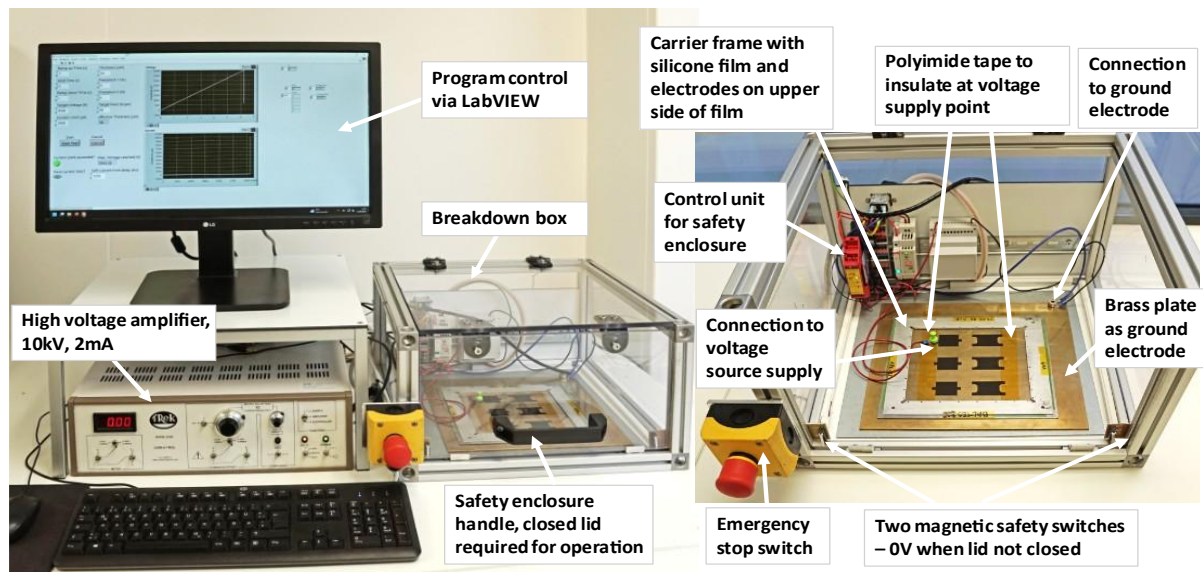


Figure 5.6. Test setup for breakdown experiments (left) and breakdown box (lid open) with test frame (right)

The measurement process is controlled via LabVIEW, which provides an interface for setting input parameters such as film thickness, pre-stretch, breakdown field or maximum voltage, voltage ramp time, and hold time. Additionally, electrical current limit for shut-off at breakdown as well as current hold time before shut-off are parameters that can be adjusted as needed, since both have an impact on the size of the breakdown spots.

The magnitude of the breakdown voltage is defined as the voltage applied at the time when the current flow through the material reaches $1000 \mu\text{A}$. Since the subsequent repair process requires visually identifying the breakdown spot, immediate electrical shut-off after breakdown is not always ideal. To address this, the LabVIEW program allows current flow to continue for a set duration, improving spot visibility. In this study, the current hold time before shut-off was set to $250 \mu\text{s}$.

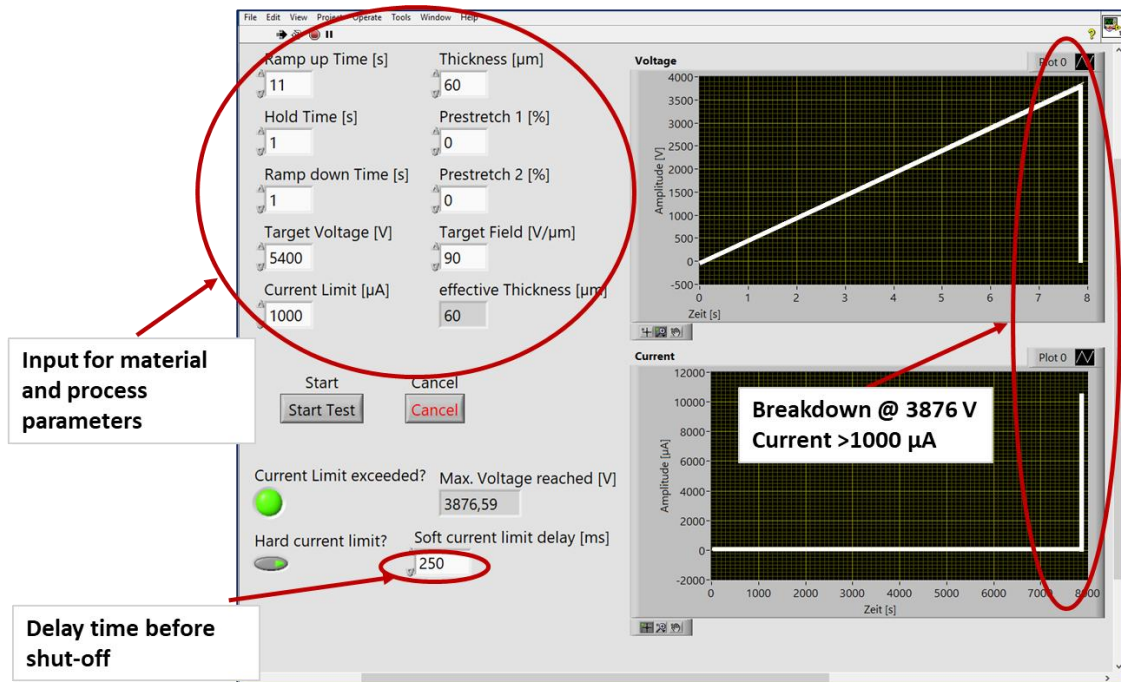


Figure 5.7. Illustration of the LabVIEW program interface, enabling input parameters such as film thickness, pre-stretch, target breakdown field, voltage, and current threshold for defining electrical breakdown. This example displays an early breakdown at 3876 V.

The breakdown test procedure consists of six consecutive steps:

1. Insulating tape is attached to the metal ground electrode plate to avoid breakdown at supply points in areas where the connection pad is located.
2. The test frame is placed electrode side up onto the metal ground electrode in a way that at least one connecting arm is placed on the insulating tape. The connection pad for voltage source supply is placed onto the connecting arm.
3. The safety lid is closed.
4. Parameters such as required voltage and electrical current for shut-off at breakdown are entered into the LabVIEW program, Figure 7, and the program started.
5. After the test, the safety lid is opened and the connection pad is connected to the next electrode, until all electrodes are tested.
6. The frame is removed, and when electrodes with early breakdown are present on the film, it is transferred to the repair station.

Once testing on a frame's electrodes is complete, the frame is removed, and breakdown spots are repaired. After repair, the frame undergoes retesting in the breakdown box. If all DEA withstand the required field, the frame advances to the next manufacturing stage. If breakdown recurs, the process is repeated until all DEA meet the required field strength.

5.2 Repair process

When early electrical breakdown occurs during testing, the repair process is initiated. Repairs are carried out in an enclosed workstation equipped with a fume extraction system, which draws vapors through perforations in the bottom plate. Figure 5.8 illustrates the setup of the repair station, while Figure 5.9 outlines the step-by-step repair procedure, accompanied by corresponding images.

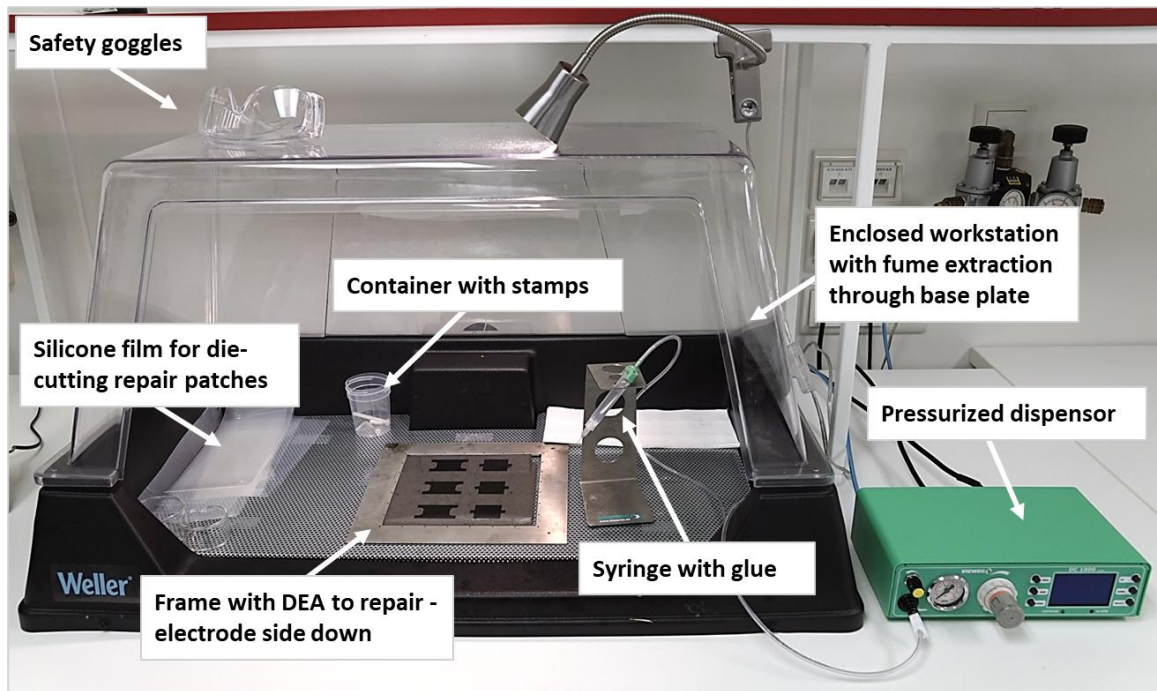


Figure 5.8. Illustration of a repair station enclosed on three sides, featuring a perforated base plate for fume extraction, and a pressurized dispenser for adhesive application located outside the station.

The first crucial step is to visually identify the breakdown spot on the membrane's non-electrode side. To facilitate localization, the test frame is placed electrode-side down onto a black mat, enhancing contrast. The visibility and size of the breakdown spot can be adjusted by controlling the current flow and shut-off timing, as detailed in Section 5.1. Once identified, the breakdown spot is repaired using a patch made from the same material as the DE membrane, which is then affixed with an appropriate adhesive.

The adhesive is applied using a pressurized syringe, which ensures application of the same amount of glue for each patch. The glue is then levelled with a glue-repellent stamp (e.g. Teflon) in the same diameter as the patch to distribute the glue evenly before the patch is attached to the film. A circular 3.5 mm repair patch is die-cut and applied with tweezers to the glue. This procedure is repeated until all breakdown spots on one frame are repaired and the frame then transferred to a vented oven for heat curing.

The repair process is carried out on films with electrodes applied to one side of the film. Following repair, the films can be stacked, as only one electrode per film is necessary - the electrode of the adjacent film serves as the counter-electrode. In a stacked configuration, one of the outer layers lacks a second electrode and thus functions as an electrical insulation layer. For single-layer DEA, the second electrode is screen-printed after the repair process. When the second electrode is applied, repairing of the DEA is no longer possible.

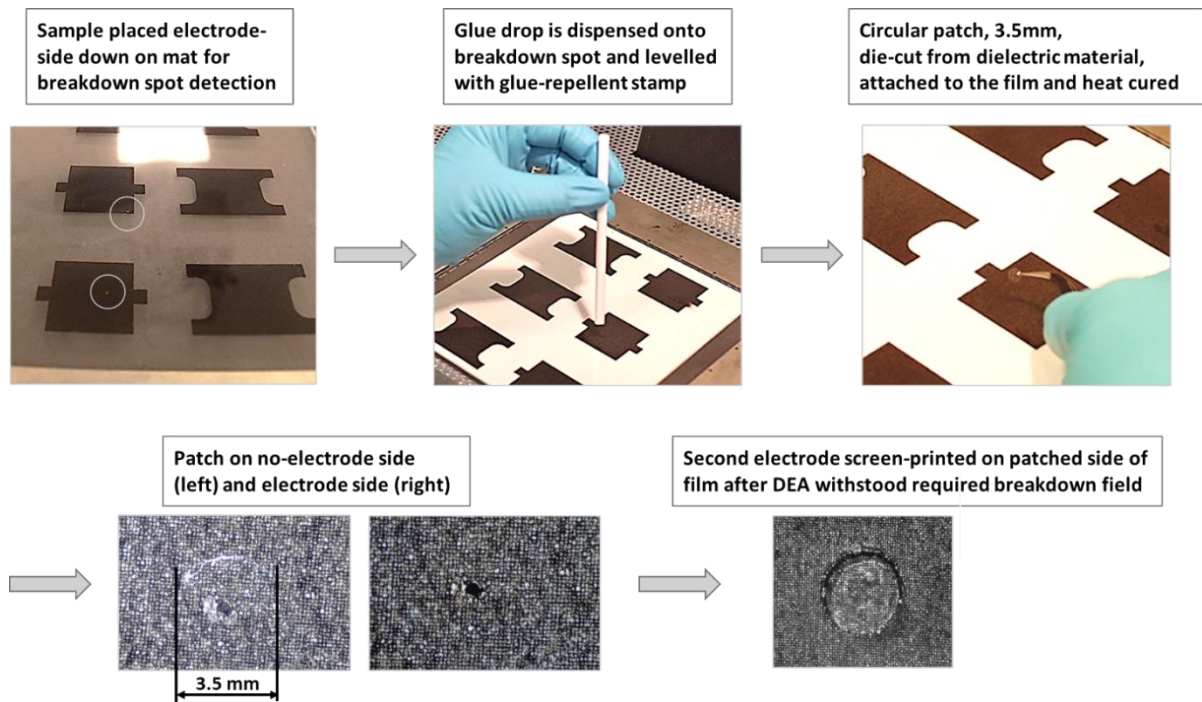


Figure 5.9. Repair procedure after DEA breakdown

The experiments described in the following sections use single-layer DEA to evaluate the performance impact of the repair procedure. A photo of a repaired patch with screen-printed electrodes on both sides is shown in Figure 5.9.

Material requirements for repair procedure

To ensure an optimal repair process, both the adhesive and the material of the repair patch must meet specific performance and compatibility requirements:

Important properties for the adhesive:

- Chemical, electrical, and mechanical properties compatible with dielectric film to ensure adhesion with minimal electrical and mechanical impact during stretch and actuation
- Elasticity to avoid stiffening of repair spot
- Good adhesion properties even under elongation
- Low viscosity to manufacture thin layers
- Fast curing
- Applicability by dispenser and/or stamp

Important properties for the repair patch:

- Same dielectric constant or higher than dielectric film
- Mechanical properties like that of dielectric film
- Mechanical impact on film as low as possible (hysteresis, stretch)
- Ideally be made from the same material as the dielectric film to ensure matching mechanical properties and dielectric constant

Adhesives are used either as single-component systems (1K), or as two-component systems (2K), where two parts must be combined prior to use. Single-component materials offer the advantage of a shorter preparation time and a significantly longer pot life - that is the usable working time after preparation - compared to two-component alternatives.

To identify a suitable adhesive for the repair process, various materials were evaluated based on the requirements outlined above. They were selected by their shore hardness, aiming for materials with a hardness close to the shore hardness A 27 of the silicone thin film. The adhesives were grouped into three categories according to their crosslinking mechanisms, with representative materials tested within each group.

Room temperature cured

- CHT AS1603, 1K, Shore A 33

UV cured

- Dow Dowsil SE9169, 1 K, Shore A 38
- Henkel Loctite SI5091, 1K, Shore A 31

Heat cured

- CHT AS1402, 1K, Shore A 30
- Wacker Silgel 612 A/B, 2K, Shore A 32
- SunChemical TP 253L/TP219L, 2K, Shore A 38

With the exception of CHT AS1402, all tested adhesives demonstrated strong bonding between the silicone film and the patch, which is manufactured from the same film material, even at a stretch ratio of $\lambda = 2$, once fully cured. However, curing times varied considerably. Since the repair process is intended to be integrated into the manufacturing process, short curing times—ideally within seconds to a few minutes—are essential.

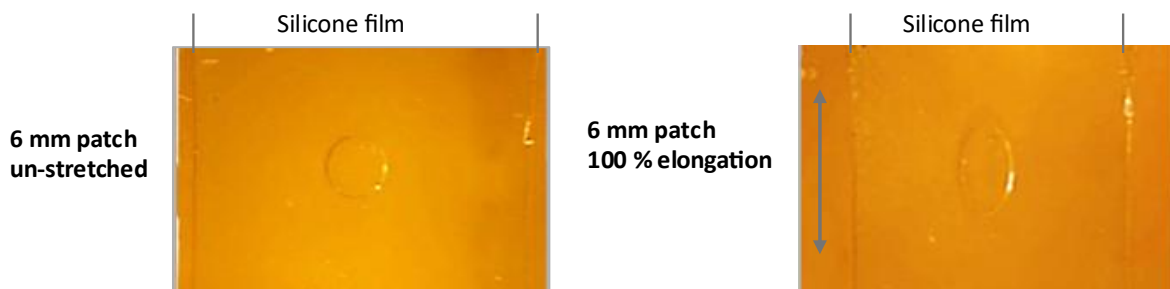


Figure 5.10. Adhesion test of 6 mm patch in un-stretched and 100 % stretched state, bonded to 60 μm silicone film with Silgel 612. Pad is of the same material as silicone film. No detachment of the patch was observed after repeated elongation.

Figure 5.10 shows an example adhesion test using a 6 mm patch on a 60 μm silicone film in both unstretched and 100 % stretched states. The patch remains securely attached under elongation, indicating good adhesion. This test was performed for all adhesives; the figure specifically shows results for Silgel 612.

The **room-temperature-curing** adhesive dried within one hour but needed a full day to complete crosslinking. As a result, this type is not considered further.

UV-curing adhesives typically offer short curing times, but in this case, both tested materials require over ten minutes to fully cure, despite using optimal wavelength and intensity. According to WACKER, this issue is often observed when bonding transparent silicone films. Another disadvantage of the UV-curing adhesives is that the curing process requires direct UV radiation and therefore not as many frames can be cured at the same time as is possible in heat curing applications. Additionally, due to the high viscosity, the adhesive had to be applied by stamping rather than dispensing, resulting in a relatively thick adhesive layer. This, combined with the minimal volume loss during curing, led to increased stiffness of the repair spot. Therefore, UV-curing adhesives are also excluded from further consideration at this stage.

The two remaining two-component **heat-curing adhesives**, Silgel 612 and TP 253L, each with a curing time of approximately 5 minutes, are well-suited for integration into a batch manufacturing process, as multiple frames can be cured simultaneously in an oven. Although neither material is marketed specifically as an adhesive - TP 253L being a silicone ink for pad printing and Silgel 612 a silicone rubber for encapsulating electronic components - both meet the necessary requirements.

Given their suitable application behavior, fast curing, and good adhesion, both are further evaluated for their mechanical impact on DEAs when used in the repair process. To assess this, force/displacement tests are performed on patched 60 μm silicone films (without electrodes), using 30 mm \times 30 mm samples each containing a single 6 mm patch. The samples are uniaxially stretched to a stretch ratio of $\lambda = 1.75$, and the force/displacement behavior is recorded and compared to that of unpatched samples.

Figure 5.11 (left) shows the experimental results as an average of three test samples for each configuration. For the patched samples, the patch is always glued to the same spot located in the middle of the three samples. A slight stiffening of the material can be observed for repaired samples. The use of TP253L also results in additional slight stiffening, which can be attributed to its higher shore hardness. Due to its longer pot life and easier handling during syringe or stamping application, Silgel 612 is selected for all repair processes.

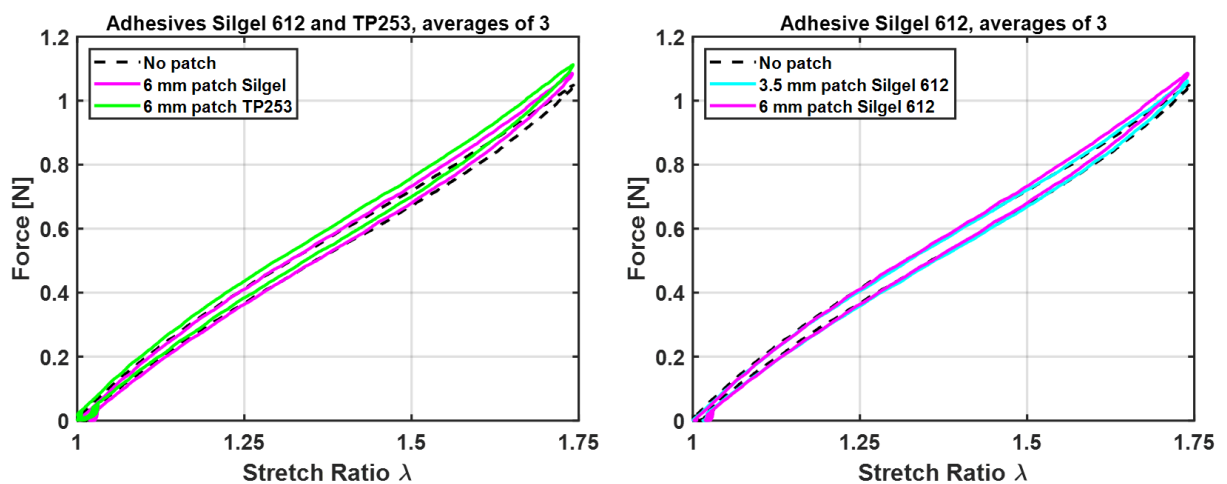


Figure 5.11. Comparison of the mechanical impact of adhesives Silgel 612 and TP253 for bonding 6 mm patches (left), and the effect of patch size (3.5 mm vs. 6 mm) using Silgel 612 on film stiffness during elongation (right).

Repair patches should ideally be made from the same material as the dielectric film to ensure matching mechanical properties and dielectric constant. To minimize the mechanical impact on the

film, the patch size should be kept as small as possible. Currently, the minimum patch size is limited by handling constraints. Initial experiments used 6 mm patches, as a stapler punch of this size was readily available. To reduce the patch size, a 3.5 mm diameter die-cutter is now used, producing clean-edged patches that are still manageable by hand.

To assess the impact of patch size on film stiffening, force/displacement tests are performed using the same adhesive - Silgel 612 - but different patch sizes. Each sample measured 30 mm x 30 mm. One patch has a diameter of 6 mm, covering approximately 3 % of the electrode area and the other patch has a diameter of 3.5 mm, covering approximately 1 % of the electrode area. The samples are uniaxially elongated to $\lambda = 1.75$ while the resulting force response is recorded. Figure 5.11 (right) presents a comparison of the average results from three samples for each patch size. Only a slight difference in stiffness is observed, suggesting that a single patch has minimal influence on the film's mechanical behavior. However, this effect becomes more relevant for smaller samples or when multiple repairs are required. To minimize this impact, 3.5 mm patches will be used for future repairs.

In another experiment, it was investigated whether dielectric strength could still be ensured when using a patch made from a thinner membrane than the actuator membrane, in order to further reduce mechanical impact. The hypothesis was that the adhesive—also made of PDMS—would contribute to insulating the breakdown site. However, this approach proved unsuccessful, as breakdown consistently occurred at the patch location. The dielectric behavior of the patch did not replicate that of a thicker, continuous membrane. This is likely due not only to the properties of the adhesive itself, but also to limitations in the repair method - such as inhomogeneous adhesive thickness and potential air entrapment during application, significantly reducing dielectric breakdown strength. This experiment led to the conclusion that the patch thickness should be equal to that of the actuator membrane.

5.3 Impact of repair patch on DEA performance

The impact of a repair patch on the mechanical and electro-mechanical properties of DEA samples is investigated and compared to those of unrepaired samples. A custom-designed test rig is used, enabling repeatable and controlled sample stretching while recording parameters such as force and displacement. The test rig design and operation are described in Chapter 2, Section 2.4.1 and in [46]. All tests presented in this section are performed using 60 μm thin silicone film type 192-1, supplied by Parker Hannifin GmbH & Co. KG.

Section 5.3.1 describes the sample design and the test procedure. Section 5.3.2 presents experimental results for actuation force and blocking force measurements calculated as difference between force output in actuated and not actuated state, comparing them to those of un-patched samples. Additionally, the increase in blocking force due to the patch process is demonstrated on a single sample to illustrate the effectiveness of the method.

The experimental conditions are chosen to reflect typical values found in actuator prototypes produced at iMSL. However, in this context, they primarily serve as illustrative examples of the testing methodology for the repair process. To detect any potential delamination or influence from the patches, the samples are stretched up to $\lambda = 1.75$. This represents a stretch at the upper end of the typical operating range for dielectric elastomer actuators.

The samples are actuated using electric fields of at least 80 V/ μm , as this is the lower threshold at which significant actuation occurs. The fields are increased up to 120 V/ μm . The electric field is calculated based on the film thickness in the maximally stretched state, assuming homogeneous

thickness distribution. Since these experiments are intended to demonstrate the test procedure, this assumption is considered acceptable.

5.3.1 Sample design and test procedure

The **test sample design**, screen printed on both sides of Parker 192-1 60 μm membrane attached to a metal carrier frame, is shown in Figure 5.12 (left). After the electrode is applied to one side of the film, the samples are tested in the breakdown box at 5400 V to ensure that the planned tests procedure can be carried out on patched and un-patched samples at least up to this breakdown field. In total, the tests are conducted with five unrepaired and five repaired samples each. Since not enough samples for patching experienced electrical breakdown at this voltage, the voltage was increased until breakdown occurred. The five samples were then repaired. The second electrode was then printed onto the opposite side of the film to manufacture one layer DEA.

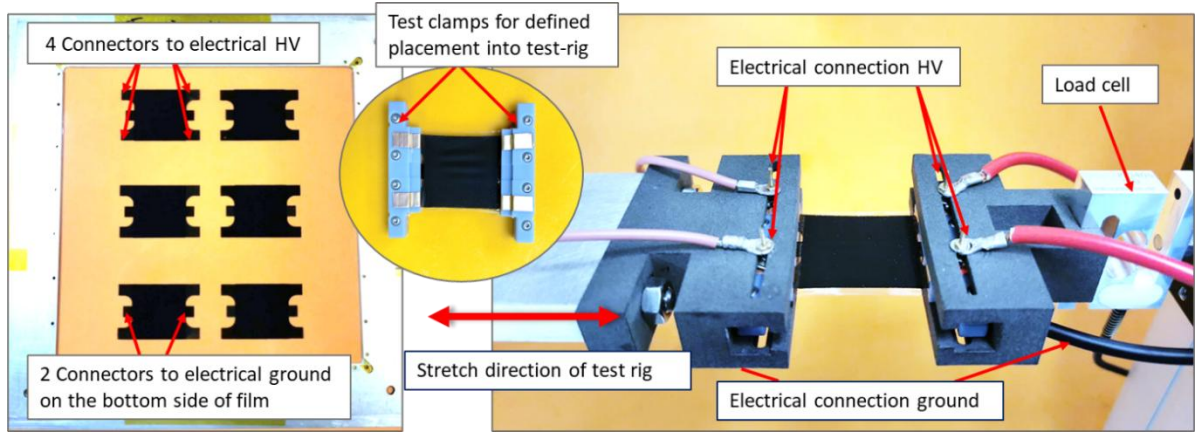


Figure 5.12. Test sample design with six electrodes screen printed on 60 μm thin silicone film attached to a carrier frame (left); test sample with 30 mm x 30 mm active area attached to test clamps (middle); test sample placed into custom build test rig (right)

An active electrode area of 30 mm x 30 mm is generated, which has four connectors for electrical high voltage connection on the top side of the film (designed for four-point-resistance measurements) and two connectors for electrical ground connection on the bottom side of the film. The connectors do not overlap. Each electrode is screwed between 3D- printed test clamps, which allow a repeatable and defined placement into the test-rig with simultaneous electrical connection, minimizing alignment errors. 2.5 mm unprinted area is left on both free sides of the DEA and 1 mm on each clamping side to avoid short-circuit during activation, so that the un-clamped membrane area is 35 mm x 32 mm, Figure 5.12 (middle).

When the samples are placed in the tester, Figure 5.12 (right), electrical connection is guaranteed by gold-plated spring contacts in the holding terminal that press on the copper strips of the clamps. In each case, a reliable electrical connection is verified through capacitance and resistance measurements using an LCR meter. The test rig allows elongation in a linear, sinusoidal, and cyclic manner as well as constant elongation over a constant time while at the same time recording the force.

Two different **test procedures** are conducted to evaluate the influence of the repaired spots on the DEA performance. In the first procedure, the influence of the patch on the stiffness of the DEA is examined by stretching the DEA while at the same time recording the force. The DEA is stretched cyclically from a stretch ratio $\lambda = 1.0$ to $\lambda = 1.75$ at a frequency of 0.1 Hz. This experiment is conducted at 0 V and additionally with constant voltage stimulation for both patched and un-patched samples. This way, information is gained about the influence of the patch on the stiffness as well as on the actuation performance of the DEA. The actuation force is calculated as the difference of the maximum force at $\lambda = 1.75$ of the not actuated state and actuated state.

In a second step, the influence on the blocking force is more thoroughly investigated by constant position measurements, in which the DEA is at a constant stretch $\lambda = 1.75$ and voltage is applied at a frequency of 1 Hz. The force difference between 0 V and max. voltage is defined as the blocking force.

Figure 5. (left) shows the stretch cycles used in the first test procedure, and an example of a 1 hertz voltage excitation for the second procedure is shown in Figure 5. (right). In the following, the electric field strength rather than the applied voltage is reported. The voltage shown in Figure 5. corresponds to an electric field of $80 \text{ V}/\mu\text{m}$ for a $60 \mu\text{m}$ thick membrane stretched to $\lambda = 1.75$ (calculated thickness assuming no necking: $34.3 \mu\text{m}$). This representation enables better comparability with literature values, especially when membrane thickness varies. Samples are tested from $0 \text{ V}/\mu\text{m}$ to $80 \text{ V}/\mu\text{m}$, subsequently increasing the maximal field in $5 \text{ V}/\mu\text{m}$ increments until breakdown occurs. The test sequence is summarized in Table 1.

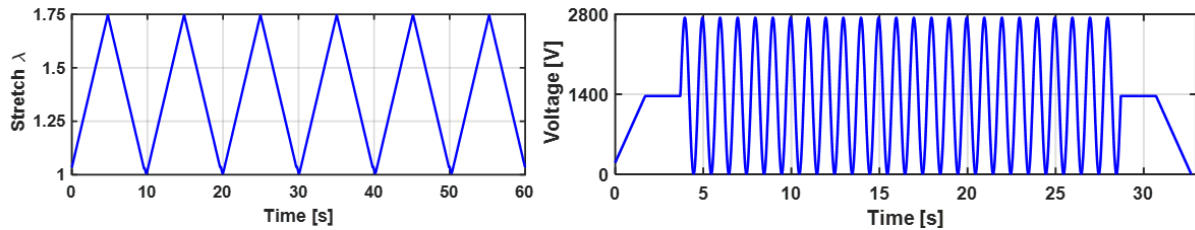


Figure 5.13. Stretch ratio over time at a frequency of 0.1 Hz from $\lambda = 1.0$ to $\lambda = 1.75$ for force/displacement measurements for actuation force (left) and example of voltage excitation of 1 hertz and electric field strength of $80 \text{ V}/\mu\text{m}$ for blocking force measurements

The same ten samples - five without repair patch and five patched samples - are tested for both procedures. The experiments start by stretching the samples six times before the actual measurement is carried out to minimize irreversible effects such as Mullins effect [136] occurring during the first few stretches, see Section 2.4.3. The measurements start with force/displacement cycles (6 cycles), immediately followed by constant position tests with 25 excitation cycles. This procedure is repeated with each $5 \text{ V}/\mu\text{m}$ - increment electric field strength.

The targeted breakdown field was $100 \text{ V}/\mu\text{m}$ for a minimum of three samples to be able to illustrate an average of three measurements. Out of the five samples without patch only three samples withstood $100 \text{ V}/\mu\text{m}$ during the force/displacement tests. Four out of the five patched samples withstood electrical fields $> 100 \text{ V}/\mu\text{m}$. None of the repaired samples broke at a repair spot.

Table 1. Test sequence for actuation force and blocking force measurements

		λ	Actuation		
			Field [V/ μm]	Frequency	cycles
1	Training	1 to 1.75	0	0.1 Hz	6
2	Force/Displacement	1 to 1.75	0	0.1 Hz	6
3	Force/Displacement	1 to 1.75	80	0.1 Hz	6
4	Blocking force	1.75	80	1 Hz	25
5	Force/Displacement	1 to 1.75	85	0.1 Hz	6
6	Blocking force	1.75	85	1 Hz	25
7	Force/Displacement	1 to 1.75	90	0.1 Hz	6
8	Blocking force	1.75	90	1 Hz	25

continued until breakdown with actuation field increase by 5 V/ μm

5.3.2 Experimental results for actuation force and blocking force measurements

This chapter starts with a comparison of the stiffness of un-patched and patched samples in Figure 5.. The curves show the average value of three DEA. Figure 5. (left) shows the force/displacement measurements for un-actuated DEA, Figure 5. (right) shows the results when the DEA is actuated with 100 V/ μm . The figures indicate only a very slight stiffening effect from the patch, whether the DEA is actuated or not. These results agree with the results shown in Figure 5.11, in which the stiffening effect of a patched and un-patched film on pure silicone film is compared.

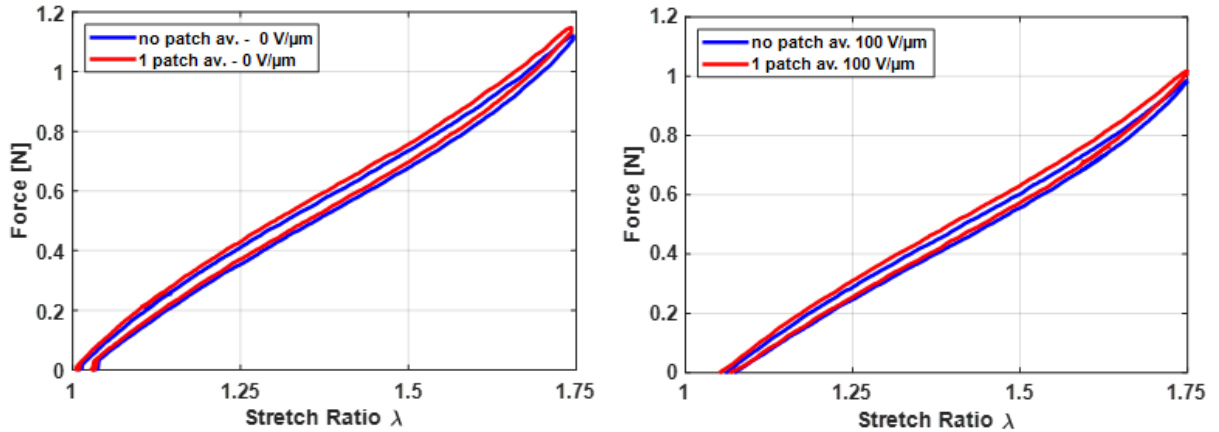


Figure 5.14. Comparison of stiffness and actuation force for un-patched and patched samples stretched to $\lambda = 1.75$. Each curve shows the average of three samples. Comparison without applied voltage (left) and when 100 V/ μm were applied.

Important for DEA, however, is not the stiffening of the membrane, but a possible reduction of the force gap between actuated and non-actuated samples.

For clearer comparison, the force/displacement curves for the activated and not activated DEA are shown separately for un-patched and patched samples in Figure 5.5. The force difference was evaluated for both conditions at $\lambda = 1.75$. The observed difference between patched and unpatched

samples is considered insignificant within the limits of measurement uncertainty, confirming that the stiffening effect due to a repair patch does not influence the actuation force. It is also important to point out that the repaired samples withstood multiple stretch- and voltage excitation cycles without breakdown until these tests were finished, demonstrating the durability of the repair process.

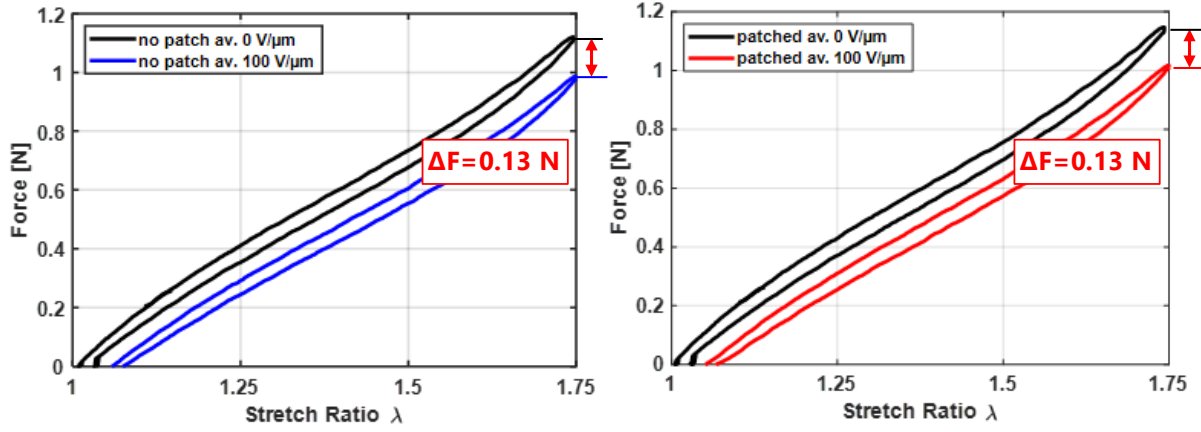


Figure 5.15 Comparison between actuation force of un-patched (left) and patched samples (right) and their calculated force difference between actuated and non-actuated state at $\lambda = 1.75$. Each curve shows the average of three samples.

After the effect of the patch under dynamic linear stretching with simultaneous DEA activation is presented, its influence on the blocking force is examined under constant stretch and periodic voltage excitation at 1 hertz across different electric field strengths. As summarized in Table 1, the tests alternated between constant-force measurements and constant-position experiments under voltage excitation.

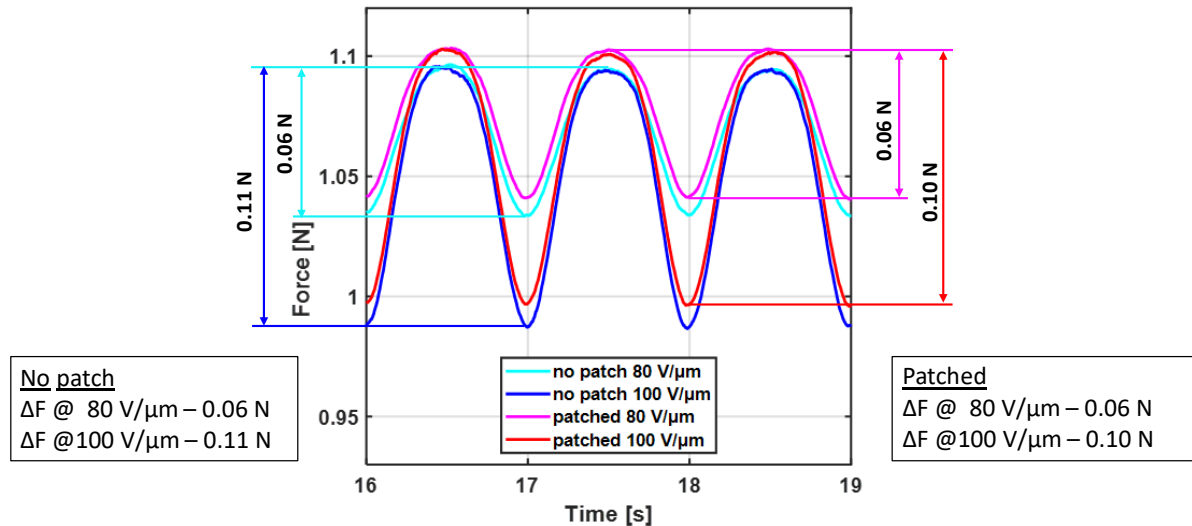


Figure 5.16. Blocking force vs. time for patched and unpatched samples with fixed elongation at $\lambda = 1.75$ and electric field excitation at 1 Hz with 80 V/ μm and 100 V/ μm amplitude. Three cycles - cycle 13 to 15 - out of 25 are depicted and blocking force values are included for each configuration. Curves represent the average of three for patched samples and average of two for unpatched samples due to breakdown of one sample before the test sequence was completed.

Figure 5. displays the blocking force results for both patched and unpatched samples at a fixed elongation of $\lambda = 1.75$. To improve visibility, only three out of the 25 voltage excitation cycles are shown. The curves correspond to electric field amplitudes of $80 \text{ V}/\mu\text{m}$ and $100 \text{ V}/\mu\text{m}$, applied using a sinusoidal waveform at 1 hertz. Blocking force values—calculated as the difference between the maximum force at 0 V and the minimum force at peak electric field—are also included in Figure 5..

For the patched samples, the curves represent the average of three measurements. For the unpatched group, only two samples are included in the average, as the third failed during the initial cycles of the constant-position test at $100 \text{ V}/\mu\text{m}$.

At an electric field of $80 \text{ V}/\mu\text{m}$, the patch has no observable effect on the blocking force. When the field is increased to $100 \text{ V}/\mu\text{m}$, the patched sample exhibits a slightly reduced blocking force compared to the unpatched sample.

The following measurements aim to demonstrate the potential increase in blocking force resulting from the repair process. They are performed on a randomly selected sample that experienced an early breakdown at 2820 V when tested in the breakdown box attached in un-stretched state on the carrier frame, corresponding to a breakdown field of $47 \text{ V}/\mu\text{m}$. The sample is repaired and re-tested in the breakdown box at 5400 V ($90 \text{ V}/\mu\text{m}$). The sample is then prepared with clamps for testing in the test rig, and the same test scenario as described above is performed until electric breakdown occurred at $125 \text{ V}/\mu\text{m}$. Figure 5.1 shows the results of the blocking force measurements at static elongation of $\lambda = 1.75$ applying four different fields, starting with the electric field of $47 \text{ V}/\mu\text{m}$ – the one when the initial breakdown occurred – and increasing the field up to $125 \text{ V}/\mu\text{m}$, when the sample broke electrically. For these measurements, the breakdown field of $47 \text{ V}/\mu\text{m}$, determined in the breakdown box for the unstretched state, is recalculated for the stretched state at $\lambda = 1.75$.

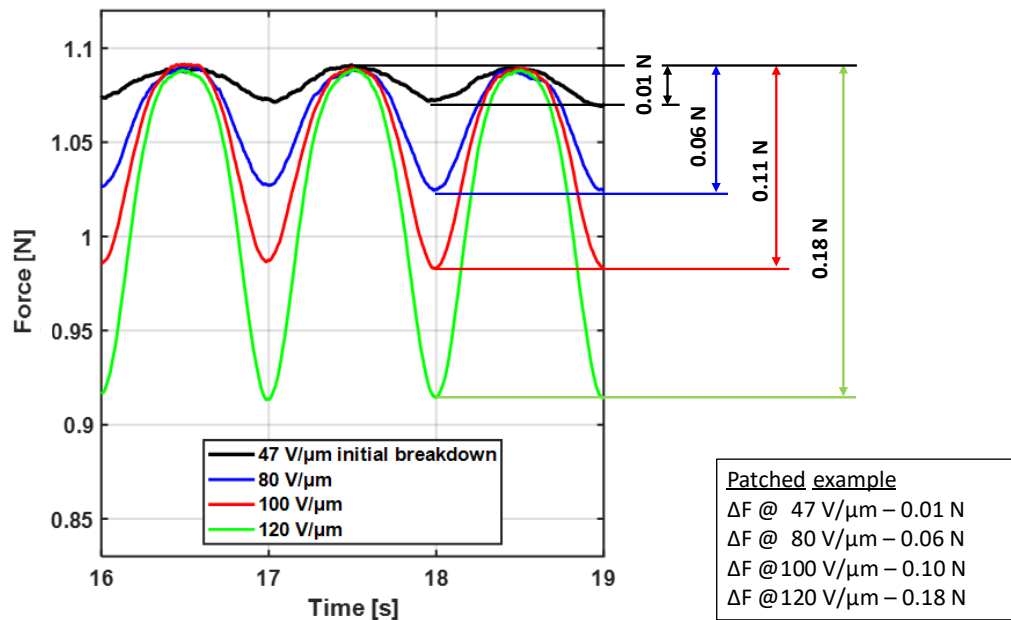


Figure 5.17. Blocking force vs. time shown for a patched DEA at a constant stretch of $\lambda = 1.75$. Excitation of electric field with sinusoidal signal at 1 Hz. Results shown for electric field at initial breakdown ($47 \text{ V}/\mu\text{m}$), $80 \text{ V}/\mu\text{m}$, $100 \text{ V}/\mu\text{m}$, and $120 \text{ V}/\mu\text{m}$. Cycle 13 to 15 out of 25 cycles are depicted and blocking force values are included for each configuration.

Figure 5.1 illustrates the influence of the electric field on the blocking force. These measurements demonstrate that pre-testing and subsequent repair can enable actuation that would otherwise not be possible without patching. The first curve shows the blocking force of the patched sample at an electric field of $47 \text{ V}/\mu\text{m}$, corresponding to the breakdown point in the breakdown box. At this field, the blocking force is only 0.01 N , which is too low for practical actuator applications, as the operating range of an actuator lies between the unactuated and actuated force curves (Section 2.4.3). Since the material behavior also exhibits a slight hysteresis, as shown for the same material in Figure 5., actuation is not possible under these conditions. With increasing electric field, the force difference increases quadratically according to Maxwell stress, reaching a value eighteen times higher at $120 \text{ V}/\mu\text{m}$. At $80 \text{ V}/\mu\text{m}$, the blocking force is already within a range that allows for feasible actuator design.

5.4 Impact of multiple repair patches on the performance of the DEA

The preceding chapters described the repair process in detail and analyzed the effects of a repair patch on dielectric performance. It was demonstrated that patching can substantially increase the breakdown field by mitigating locally weak regions. This raises the question: if a single repair enhances the electrical breakdown field, could multiple repairs lead to further improvements? Moreover, does the breakdown field increase consistently with the number of repairs, or are there inherent limitations to this approach?

Section 5.3 demonstrated that the electrical breakdown field can be successfully increased by repairing a premature breakdown spot in a DEA. This section investigates the extent to which the breakdown field can be further enhanced through multiple consecutive repairs. The primary limitation of this enhancement is most likely the material-specific maximum electrical breakdown field of the silicone thin film. Once early breakdown spots are repaired and this limit is approached, additional repairs become ineffective in further increasing the electrical breakdown strength.

To determine how many repair cycles consistently improve the breakdown field, two different silicone thin films are tested and repaired until improvement is no longer observed. One silicone film is the Parker Hannifin $60 \mu\text{m}$ thin film No. 192-1, which is also used in Section 5.3, the other one a $50 \mu\text{m}$ thin film Elastosil 2030/50 5420-01 provided by Wacker Chemical Corporation. Wacker specifies the maximum electrical breakdown field in its data sheet between $80 \text{ V}/\mu\text{m}$ and $100 \text{ V}/\mu\text{m}$ [106]. No data sheet is available for the Parker material.

For each material, 24 electrodes are screen printed on one side of the film with the DEA electrode design depicted in Figure 5.12. The electrodes are then placed into the breakdown box, Figure 5.6, and voltage applied until breakdown. The location of the breakdown spots and its breakdown voltage is recorded and the sample repaired. This procedure is repeated, until each DEA is repaired ten times.

An example of the local distribution of repair points for Wacker Elastosil 2030/50 5420-01 is shown in Figure 5.18. The schematic on the left of Figure 5.19 illustrates the locations of the patched breakdown spots, while the right side presents photographs of the six repaired electrodes. In all electrodes, a clustering of breakdown sites can be observed - likely caused by local manufacturing inhomogeneities that extend over an area rather than being confined to isolated points. Notably, the patches on electrode 680E are aligned along a vertical line, suggesting imperfections introduced along the film roll during the production process

Frame 680

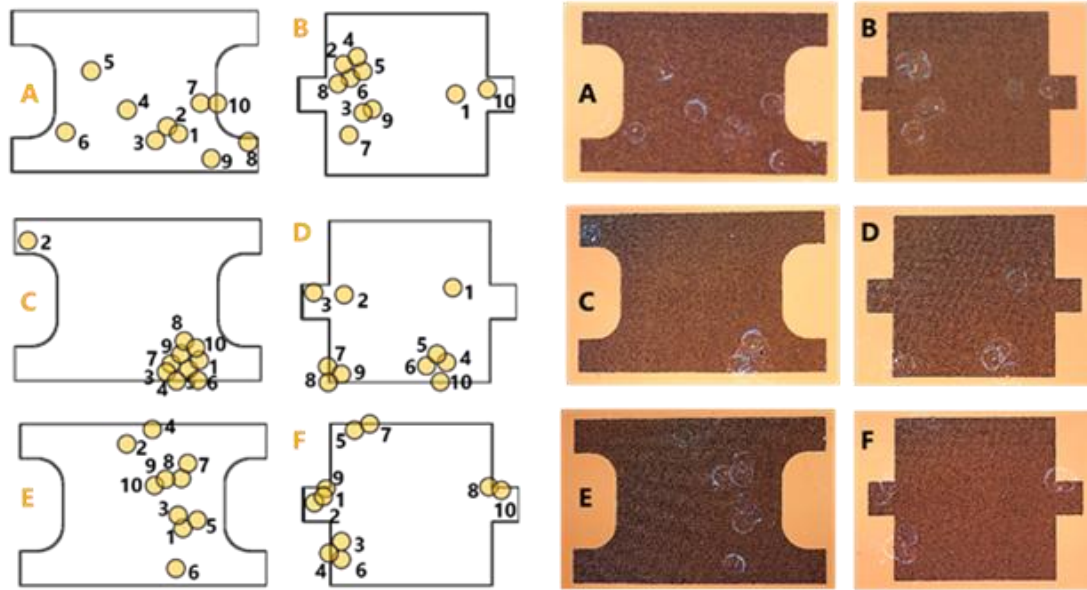


Figure 5.18. Wacker Local distribution of ten consecutively repaired breakdown spots for Wacker Elastosil 2030/50 5420-01 silicone film. Schematic of repaired points (left) and photographs of six repaired electrodes on Frame 680

Figure 5.19 shows an example of the local distribution of repair points for a 60 μm thick silicone film from Parker No. 192-1. Here, breakdown spots are more homogeneously distributed over the DEA.

Frame 643

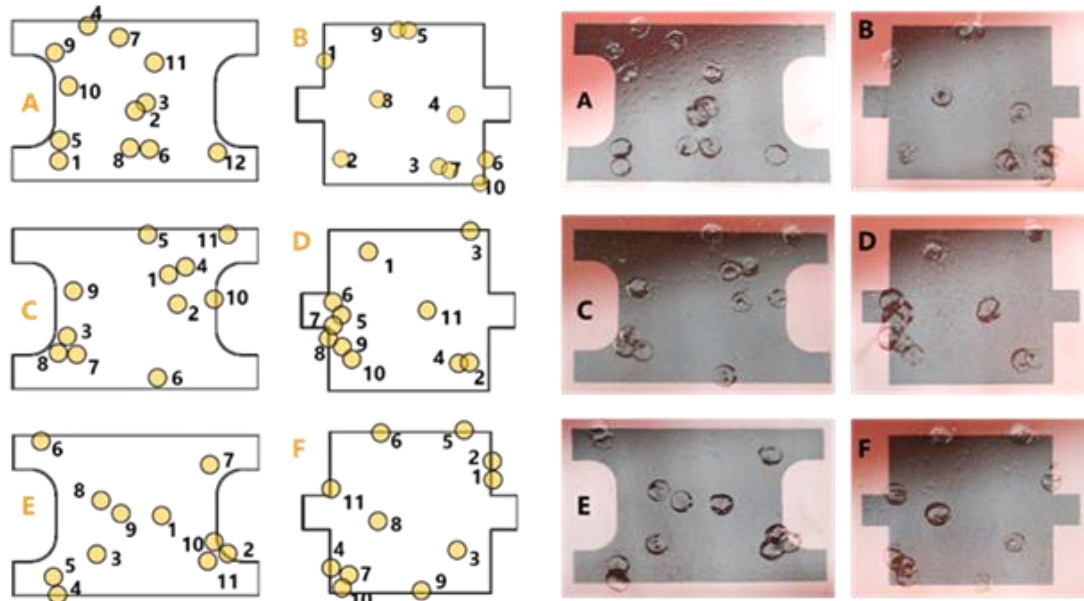


Figure 5.19. Local distribution of ten consecutively repaired breakdown spots for Parker 192-1 silicone film. Schematic of repaired points (left) and photographs of six repaired electrodes on Frame 643

Figure 5.20 presents the breakdown field as a function of the number of breakdown events for both silicone films. Following each breakdown, the DEA was repaired before conducting the subsequent test. For each film, data from 22 samples are shown, comprising up to ten consecutive breakdown tests and their corresponding breakdown field values. The left panel of Figure 5.20 displays results for Wacker Elastosil 2030/50, while the right panel shows those for Parker 192-1.

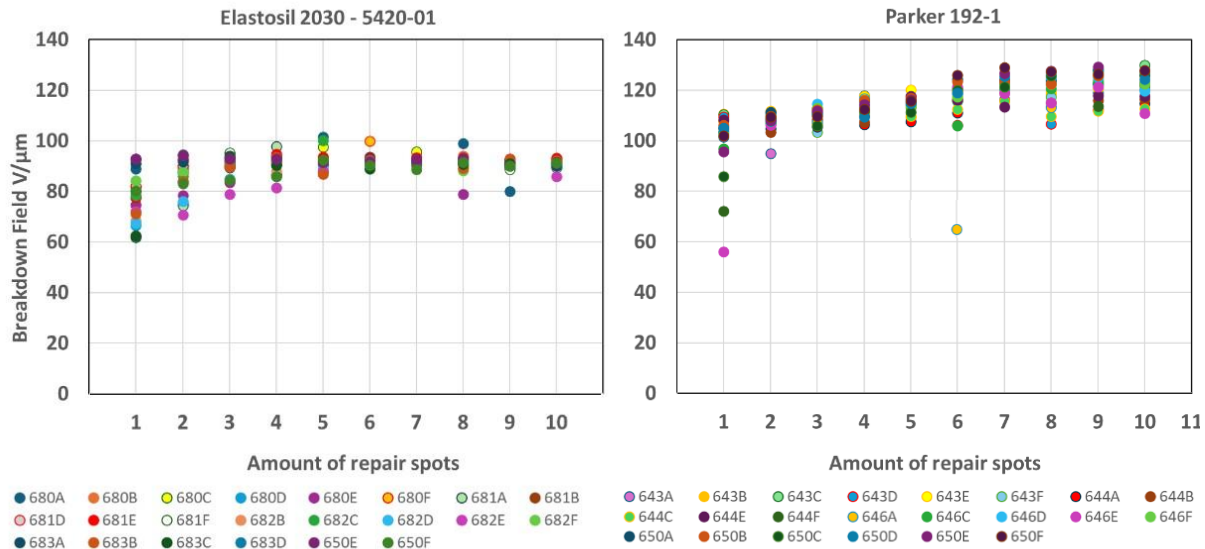


Figure 5.20. Electric breakdown field over number of repaired spots for 50 μm thick Wacker Elastosil 2030 - 5420-01 and 60 μm thick Parker 192-1. Each breakdown spot is repaired before the next test. 22 samples are tested for each film

The first repair achieves the highest increase in the breakdown field for both films, because the variation in breakdown events is largest in the first step. After the DEA are repaired the second time, the breakdown range decreases to between 10 V/ μm and 20 V/ μm .

The maximal average electric breakdown field for Wacker Elastosil is 90 V/ μm - after five repairs -, suggesting that this is the overall maximum breakdown field.

After five repairs, the breakdown field decreases again. This phenomenon is most likely caused by the distribution of defects, which are not evenly spread across the DEA but instead cluster locally (Figure 5.18). During the repair process, multiple patches are applied on top of one another, increasing the total repaired area with each additional patch. When the sample is retested, the patched side faces the ground plate of the breakdown box. Due to its greater local thickness, the application of voltage causes the electrode and ground plate to attract, leading to localized thinning of the film at the interface between patched and unpatched regions. This, in turn, produces local electric field intensification, which can trigger additional breakdowns at the interface. Figure 5.21 illustrates this accumulation of repair patches.



Figure 5.21. Example of multiple localized breakdowns and accumulation of repair pads

The breakdown fields of the Parker 192-1 thin film also improve up to four repair spots. Further repairs do not lead to a significant increase in the breakdown field but instead result in increased variation. An average maximum breakdown field of $120 \text{ V}/\mu\text{m}$ is reached, which likely corresponds to the specific breakdown field of this material. Although breakdowns are more evenly distributed across many DEAs, this material also exhibits localized clustering of defect sites. At the sixth test, sample 646A broke at a breakdown field significantly lower than on the fifth one. In this case, the hole was not patched but accidentally the patch was attached next to the breakdown spot.

Figure 5.20 demonstrates how different materials can vary significantly in both their maximum breakdown field and the distribution and presence of weak spots. It is important to note that this Wacker material was known to be of lower quality compared to the previously tested materials, as it was produced on a new manufacturing line. Nevertheless, it was intentionally included in this study to highlight the importance of quality assessment through breakdown and repair testing, as material quality can vary substantially between production batches or manufacturing processes.

The investigations demonstrate that repeated repairs improve breakdown performance; however, this process does not result in unlimited enhancement. After approximately four repair cycles, no further improvement in breakdown behavior is observed, likely due to the material reaching its intrinsic breakdown strength. This raises two key questions: can a DEA still elongate and function after ten repair cycles, and how does actuation performance compare to that of DEAs patched only up to the recommended four times?

To investigate this, a second electrode is applied to four of the DEA of the Parker 192-1 material that had undergone ten repairs. To verify that the patches could reliably withstand $\lambda = 1.75$, one of these samples is stretched up to $\lambda = 2$ and photographs are taken in both unstretched and stretched states to assess patch behavior and adhesion to the film, Figure 5.22.

Subsequently, the remaining three samples are tested using the setup and procedure described in Section 5.3. Force/displacement measurements at a stretch ratio of $\lambda = 1.75$ under different voltage levels, from which the actuation force is calculated, are shown in Figure 5.23 for the average of the three samples.

Figure 5.22 shows underlit images of an unstretched and a stretched sample. The right-hand image highlights an area where multiple patches were layered. The photos confirm that elongation remains possible even with multiple overlapping patches, and that the patches remain securely bonded to the film under strain.

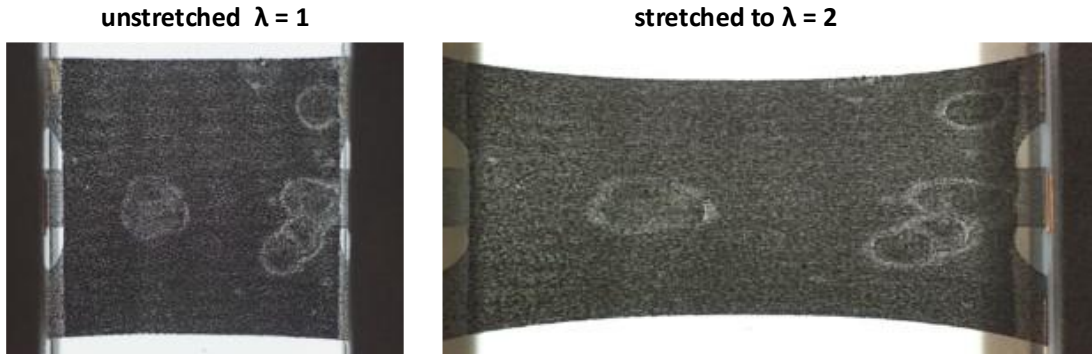


Figure 5.22. Underlit photos of unstretched (left) and 100 % stretched sample (right) after ten repair cycles. Photos illustrate that stretching is possible even after multiple repairs, without the patches detaching.

Figure 5.23 presents force/displacement measurements at 0 V/ μm , 90 V/ μm , and 120 V/ μm . The actuation force is calculated as the difference between the maximum force at $\lambda = 1.75$ in the actuated and non-actuated states. The results show that elongation and actuation is still possible when samples are patched ten times, even though up to 10 % of the actuated area is covered with patches.

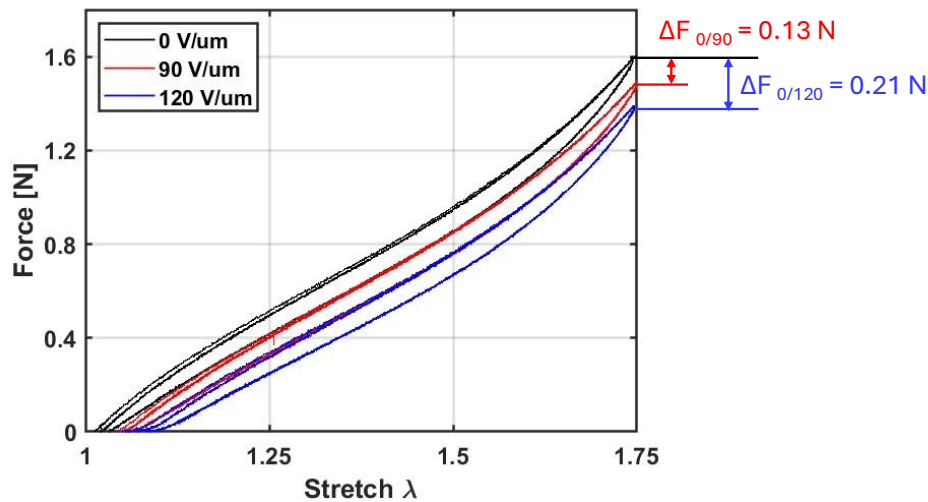


Figure 5.23. Force/displacement measurements for DEA (Parker 192-1) after ten repair cycles for the average of three samples and results of the actuation force at 90 V/ μm and 120 V/ μm , stretch cycle @ 0.1 Hz

The results presented above confirm that actuation remains possible in samples that have undergone ten repair cycles. This finding is significant, as it represents a practical upper limit for the number of repairs - well beyond the recommended number. Consequently, if actuation is achievable after ten patches, it can be assumed to remain viable with fewer. However, it is essential to compare the actuation performance of these extensively repaired samples to that of DEAs repaired only up to the recommended four times, as well as to unpatched samples, since these are more representative of those used in practical applications.

To address this, a set of samples is manufactured and repaired four times before applying the second electrode. In addition, a second set of unpatched samples that successfully withstood an electric field of 100 V/ μm in the breakdown box is also prepared with a second electrode. For both sets

force/displacement and blocking force measurements are performed using the same setup and procedure as described previously.

Using the results from the force/displacement measurements, the actuation force is calculated as the difference between the maximum force at $\lambda = 1.75$ in the actuated and non-actuated state. This calculation was carried out in $10 \text{ V}/\mu\text{m}$ increments from $80 \text{ V}/\mu\text{m}$ to $120 \text{ V}/\mu\text{m}$ for the three different patch conditions: unpatched, four patches, and ten patches. Figure 5.24 summarizes the average results for three samples per condition. In the case of the unpatched samples, a total of seven were tested to obtain three that could be actuated up to $120 \text{ V}/\mu\text{m}$ without experiencing electrical breakdown.

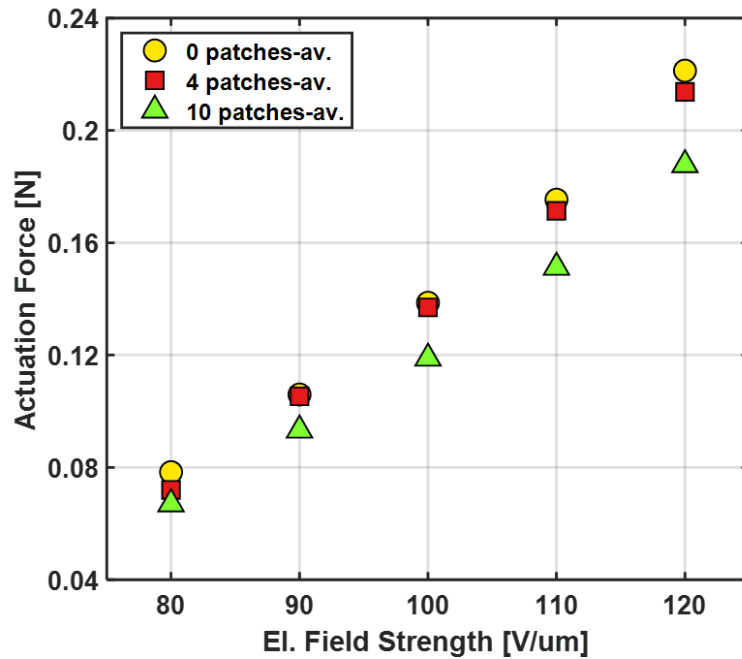


Figure 5.24. Results of calculated actuation force at $\lambda = 1.75$ as difference between maximum force without actuation and when actuated with electric fields from $80 \text{ V}/\mu\text{m}$ to $120 \text{ V}/\mu\text{m}$ for different actuation fields for DEA (Parker 192-1) repaired with no patch, four patches and ten patches. Results are shown as average of three samples for each condition.

The results in Figure 5.24 show that the influence of four patches has no significant effect on actuation force up to an electric field strength of $100 \text{ V}/\mu\text{m}$. At $120 \text{ V}/\mu\text{m}$, however, the actuation force of samples with four patches is lower than that of unpatched samples. Since this field strength exceeds the typical operating range of silicone DEAs—usually around $90 \text{ V}/\mu\text{m}$ —this reduction is not considered critical for most applications. In contrast, samples with ten patches consistently exhibit reduced actuation force across all tested field strengths. In these samples, nearly 10 % of the electrode area is covered by patches, resulting in reduced capacitance and, consequently, reduced actuation performance.

These findings suggest that the number of repair cycles should ideally be limited to four, or to approximately 4 % of the active electrode area. Nevertheless, even when a notable reduction in actuation force occurs due to extensive patching, repairs may still be justified in multilayer systems, where due to the frame stacking of multiple DEA on one frame, cumulative output of multiple stacked layers compensates for losses in individual actuators.

5.5 Performance of patched DEA in practical applications

Section 5.5 presents three examples of patched DEA, which are integrated into applications sustaining working operations over millions of cycles, illustrating that due to a test and repair process robust and long-lasting DEA can be manufactured. While the previous chapter focused on the repair method and its evaluation using rectangular or strip-shaped DEAs, the technique is not limited to this geometry. It is equally applicable to other DEA configurations, such as circular and rolled designs. The first application features rolled DEA, the second application circular DEA, and the third application circular and strip DEA.

The manufacturing and repair of the actuators followed the procedures outlined in the preceding chapters. The application concepts, design, and assembly were carried out by other PhD students at the iMSL and are kindly made available for this work.

Locomoting DE-Tensegrity Soft Robot

The *Locomoting DE-Tensegrity Soft Robot* by Julian Kunze consists of eight rolled DEA (RDEA), five of them patched, Figure 5.25. The robot conducts a forward movement by actuation of the RDEA in resonance frequency at 43 Hz. The robot won Second place at the “25th Annual EAP-in-Action Hardware Competition”, which was part of the SPIE Smart Structures - EAPAD conference. It has been operated successfully for **over three million cycles** and is still operating.

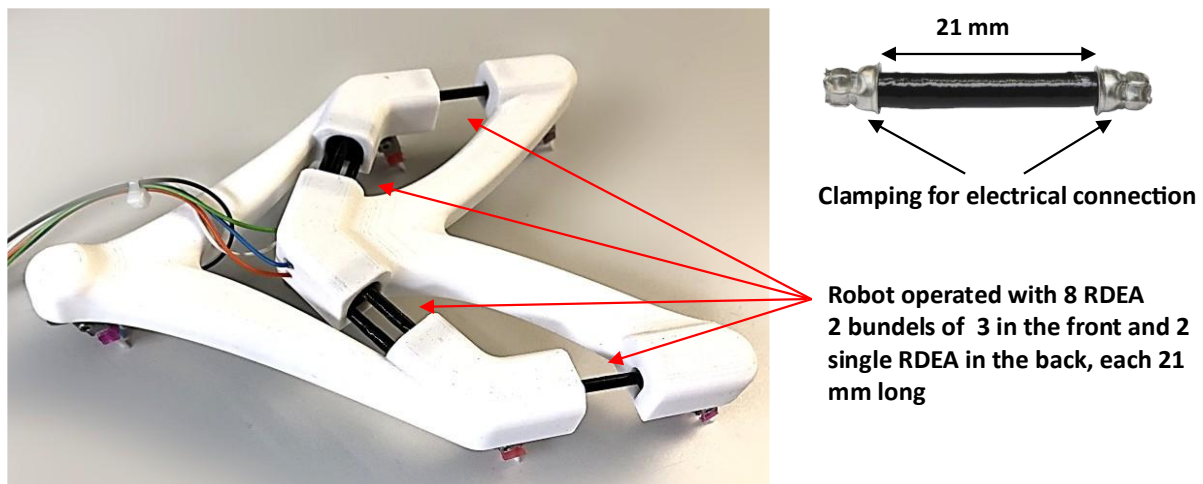


Figure 5.25. Locomoting DE Tensegrity Soft Robot by Julian Kunze actuated by 8 patched and rolled DEA, acutated in resonance frequency at 43 Hz

DEA technology implemented in Incredible Machine

Two DEA systems were designed and implemented as part of the 'Incredible Machine', showcased by Festo GmbH at HANNOVER MESSE 2025 in celebration of the company's 100th anniversary [157].

One system was designed to use the stroke generated during actuation to drive a gearbox that preloads a spring. Once fully tensioned, the spring launches a ping-pong ball into the air. This system consists of 16 circular DEAs, operated at a frequency of 30 Hz.

The second system uses a 24-layer strip DEA to actuate a gripper that catches the ball in mid-air. This actuator is only triggered periodically after the ball is launched. The DEA in both systems were tested and underwent repairs. An image of the system is shown in Figure 5.26 (left), with a circular DEA featuring three repair sites shown on the right.

The DEA system driving the gearbox has already **completed over eighty million operating cycles**.

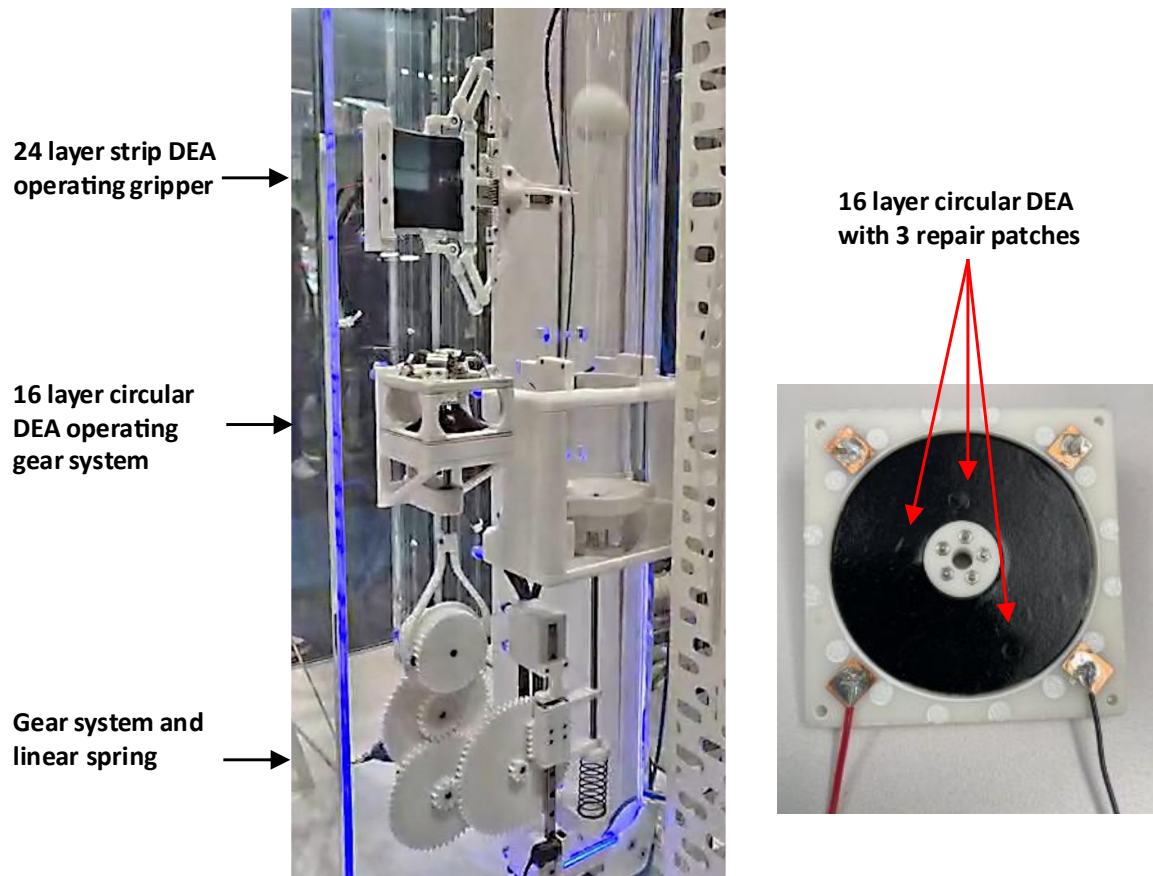


Figure 5.26. Strip DEA and circular DEA as part of the "Incredible Machine" by Festo GmbH for the company's 100th anniversary (left) and photo of 16 layer circular DEA system with three repair patches (right)

DEA Vacuum Pump

The *DEA Vacuum Pump* by Matthias Baltes consists of 64 circular DEA, layered in four stacks à 16 DEA, Figure 5.27. Each DEA is separately tested and repaired with a total of 18 repair patches in the 64 DEA stack. The DEA pump operates at 80 Hz. It won second place at the “Hardware Challenge” at the SMASIS 2024 conference and was finalist at the SPIE 2024 hardware competition “EAP in Action”. Up until now it has been operated **over fifteen million cycles** and is still operating.

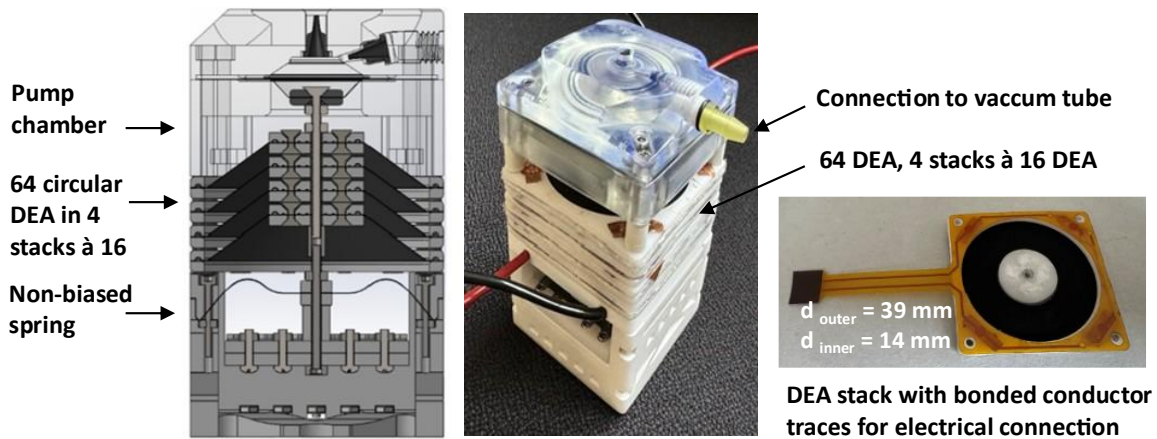


Figure 5.27. DEA Vacuum Pump by Matthias Baltes consisting of 64 tested and repaired DEA as schematic illustration (left), and photo (middle). A photo of a single DEA stack composed of 16 DEA, clamped between two frames, attached with conductor traces for electrical connection, is shown on the right.¹⁰¹

6. Conclusion and Outlook

This thesis contributes to the advancement of dielectric elastomer actuator (DEA) technology, transitioning it from laboratory-scale demonstrations toward robust and reliable operation for future commercial applicability. A DEA consists of two key components - the dielectric membrane and the compliant electrodes. This work systematically investigates the parameters affecting DEA performance for each component with a focus on manufacturing processes, reliability, and operational efficiency. Furthermore, the thesis introduces a novel patent-pending repair method for DEA. Although the operational parameters can be optimized to enable reliable performance, commercially available dielectric membrane material may still contain intrinsic defects arising from complex fabrication processes, which can ultimately lead to system failure. The developed repair process has been successfully implemented in several DEA prototypes and could be shown to enable reliable operation over millions of cycles.

One of the core objectives of the work is the development and scientific evaluation of a scalable and industry-relevant process for the application of compliant electrodes onto low-adhesion silicone membranes. The systematic variation of screen-printing parameters such as mesh size and number of consecutive layers as well as the electrode configurations provided valuable insights into their impact on electromechanical performance.

The findings indicate that for sensor applications a coarser mesh or a two- or three-layer print with the lowest electrical resistance is advisable. For actuator applications, the mesh and print scenario need to be individually adjusted to the DEA application. While a thin electrode layer has the lowest impact on the mechanical hysteresis and stiffening of the DEA, its higher resistance can be problematic in high frequency applications, where fast charging times and low currents are required. In this case, multi-layer prints are preferable.

A further emphasis of this thesis is the analysis of parameters that influence the dielectric breakdown behavior of DEA. While higher voltages enable more efficient actuation, they also increase the risk of dielectric breakdown, which represents a fundamental performance limit. Given the critical role of breakdown voltage in the design and reliable operation of DEA systems, a thorough understanding of the factors affecting it is essential.

Using a novel automated breakdown tester, this work presents an in-depth investigation of the influence of environmental conditions - such as temperature and humidity - as well as application parameters like pre-stretch on the electrical breakdown behavior of silicone-based DEA films. Since technical applications require the presence of electrodes on the film, these experiments were not only conducted on pure silicone films but also on films with electrodes of different compositions and manufacturing methods.

A key finding of this thesis is that the presence of electrodes on silicone membranes significantly affects the breakdown voltage, a critical parameter in DEA design. A collaborative investigation with two other research groups systematically examined various electrode types, including sputtered gold and nickel material, as well as carbon black-based electrodes applied via screen printing.

Despite their superior breakdown strength, sputtered electrodes are unsuitable for practical DEA use without pre-stretch and relaxation steps, as they lose conductivity under strain. Therefore, further studies focused on carbon black-based electrodes. To systematically assess the impact of electrode composition, each constituent—solvent, PDMS, and carbon black—was examined separately.

While pure solvents had negligible effects, their combination with carbon black consistently reduced breakdown voltage, indicating a synergistic effect. PDMS concentration was then varied between 0 % and 90 %, revealing a clear trend: higher PDMS content led to improved breakdown performance. Finally, the impact of carbon black morphology was investigated. Electrodes manufactured with finely milled carbon black exhibited higher breakdown voltages compared to those using coarsely ground particles.

Above results provide a comprehensive understanding of the factors influencing electrical breakdown, enabling the design and manufacturing of DEA systems that can operate reliably within a given environment.

Despite the optimization of relevant parameters, premature breakdown can still occur due to inhomogeneities in the film. These failures reflect the early developmental stage of industrial silicone thin film manufacturing for dielectric elastomer applications and present a major obstacle to reliable large-scale DEA production. To address this issue, an innovative patent-pending test-and-repair method was developed to ensure the operational reliability of future DEA systems while simultaneously enhancing material yield and minimizing production waste.

The process consists of a sequence of three operational steps:

In a first step, a carrier frame with several screen-printed electrodes on one side of a silicone film is placed inside a specifically developed breakdown box. This box is designed to safely and reliably test dielectric elastomer actuators under high-voltage conditions up to the required breakdown field strength. If the electrodes withstand this voltage without failure, they are approved for further processing. However, if an electric breakdown occurs, the corresponding DEAs are subjected to a second processing step.

In a second step, the frame is removed, and breakdown sites are visually identified on the film side opposite the electrodes using a camera-based automatic procedure. An adhesive is applied to the damaged area using a dispenser and a stamp, followed by the placement of a silicone repair patch and curing of the repair spot. Both, adhesive and patch, are selected to match the chemical, electrical, and mechanical properties of the film.

In a third step, the repaired DEAs are returned to the breakdown box and subjected to the required test voltage again. If further breakdowns are detected, the second step is repeated.

After successfully implementing the repair method, it was essential to determine whether—and to what extent—the repair affects the performance of the DEA. The findings indicate that one or two repair patches do not adversely affect DEA performance. Moreover, since non-repaired DEAs often fail under high voltages, repaired samples show a significantly enhanced actuation potential.

The goal of this thesis was a contribution to the advancement of dielectric elastomer actuator technology toward commercial applicability through a thorough understanding of the effects of production processes and parameters necessary to ensure reliable and robust operation.

This work has led to the development of several prototypes that could be shown to operate reliably over millions of cycles without failure at trade shows and exhibitions, indicating that an initial commercialization of the technology is within reach.

However, additional systematic studies of both individual DEA and complete actuator systems under long-term operation and varying environmental conditions are still necessary. High-cycle fatigue testing of DEAs can reveal the influence of different electrode materials, while testing of complete DEA systems can additionally verify system integration, functionality, and potentially also the reliability of the associated electronics under long-term operation.

The repair process introduced in this thesis has proven to be highly successful in enabling robust actuator operation. For a successful integration into a future manufacturing workflow, the next step should be the automation of this process. Since the fabrication of DEA - from pre-stretching to the stacking process - can be carried out on standardized carrier frames, such automation within a batch process is feasible and has the potential to significantly reduce overall production time.

For this purpose, DEAs printed with electrodes on one side and crosslinked must be fed into a testing device, where they are subjected to high voltage. Breakdown sites can then be detected using a camera system and automatically be logged in a database. In the subsequent repair station, the information retrieved from the database enables automated application of adhesive followed by a repair patch, for instance using a pad-printing system.

To support this procedure, the development of an automated transport and handling system would be highly beneficial. Such a system would connect the individual stations - from the screen printer and crosslinking units to the testing and repair stations - and would return the frames, after patching and curing, to the testing device for quality control.

In addition, further developments are particularly required in the preparation and execution of the repair processes. One promising approach could involve a punching process for the production of standardized prefabricated repair patches, followed by gripping and transporting the patches to the repair site with automated vacuum tools.

It is also advisable to establish a continuously updated database capturing all relevant data on elastomer films, electrode compositions, manufacturing parameters, test and breakdown voltages, and repair frequencies. This comprehensive dataset would enable model-based optimization and predictive analysis of process durations across the entire manufacturing and repair workflow.

Although DEA fabrication is already feasible today, the implementation of these steps could substantially improve the performance of the manufacturing process and accelerate the transition toward large-scale production.

.

References

- [1] G. Rizzello, "A Review of Cooperative Actuator and Sensor Systems Based on Dielectric Elastomer Transducers", *Actuators* (vol. 12, no. 2, p. 46), Jan. 2023, doi: 10.3390/act12020046.
- [2] H. Böse and J. Ehrlich, "Dielectric Elastomer Sensors with Advanced Designs and Their Applications", *Actuators* (vol. 12, no. 3, p. 115), Mar. 2023, doi: 10.3390/act12030115.
- [3] R. Pelrine, R. D. Kornbluh, and Q. Pei, "Dielectric elastomers: past, present, and potential future", *Electroactive Polymer Actuators and Devices (EAPAD) XX*, (Vol. 10594, pp. 15–22). SPIE, Mar. 2018, doi: 10.1117/12.2302815.
- [4] G. Moretti, S. Rosset, R. Vertechy, I. Anderson, and M. Fontana, "A Review of Dielectric Elastomer Generator Systems", *Advanced Intelligent Systems* (vol. 2, no. 10), Oct. 2020, doi: 10.1002/aisy.202000125.
- [5] M. Hill, G. Rizzello, and S. Seelecke, "Development and experimental characterization of a pneumatic valve actuated by a dielectric elastomer membrane", *Smart Materials and Structures*, (vol. 26, no. 8), 2017, doi: 10.1088/1361-665X/aa746d.
- [6] M. Giousouf and G. Kovacs, "Dielectric elastomer actuators used for pneumatic valve technology", *Smart Materials and Structures* (vol. 22, no. 10), Oct. 2013, doi: 10.1088/0964-1726/22/10/104010.
- [7] C. Tang, B. Du, S. Jiang, Z. Wang, X. J. Liu, and H. Zhao, "A Review on High-Frequency Dielectric Elastomer Actuators: Materials, Dynamics, and Applications", *Advanced Intelligent Systems* (vol. 6, no. 2), Feb. 2024, doi: 10.1002/aisy.202300047.
- [8] C. Cao, X. Gao, and A. T. Conn, "A Magnetically Coupled Dielectric Elastomer Pump for Soft Robotics", *Advanced Material Technologies*, (vol. 4, no. 8), Aug. 2019, doi: 10.1002/admt.201900128.
- [9] L. Pniak, M. Almanza, Y. Civet, and Y. Perriard, "Ultrahigh-Voltage Switch for Bidirectional DC-DC Converter Driving Dielectric Elastomer Actuator", *IEEE Transactions on Power Electronics*, (vol. 35, no. 12, pp. 13172–13181), Dec. 2020, doi: 10.1109/TPEL.2020.2995047.
- [10] J. Yi, L. Ciarella, S. Rosset, K. Wilson, I. Anderson, A. Richter, and E.F.M. Vorrath, "A piezoresistive dielectric elastomer switch consisting of inkjet-printed carbon black", *Chemical Engineering Journal*, (vol. 500), Nov. 2024, doi: 10.1016/j.cej.2024.156718.
- [11] Y. Wang, X. Ma, Y. Jiang, W. Zang, P. Cao, M. Tian, N. Ning, and L. Zhang, "Dielectric elastomer actuators for artificial muscles: A comprehensive review of soft robot explorations", *Resources Chemicals and Materials*, (vol. 1, no. 3, pp. 308–324), Sep. 2022, doi: 10.1016/j.recm.2022.09.001.
- [12] Y. Guo, L. Liu, Y. Liu, and J. Leng, "Review of Dielectric Elastomer Actuators and Their Applications in Soft Robots", *Advanced Intelligent Systems*, (vol. 3, no. 10), Oct. 2021, doi: 10.1002/aisy.202000282.
- [13] J. H. Youn, S.M. Jeong, G. Hwang, H. Kim, K. Hyeon, J. Park, and K.U. Kyung, "Dielectric elastomer actuator for soft robotics applications and challenges", *Applied Sciences*, (vol. 10, no. 2), Jan. 2020, doi: 10.3390/app10020640.
- [14] M. Baltes, J. Kunze, J. Prechtel, S. Seelecke, and G. Rizzello, "A bi-stable soft robotic bendable module driven by silicone dielectric elastomer actuators: design, characterization, and parameter study," *Smart Materials and Structures*, (vol. 31, no. 11), Nov. 2022, doi: 10.1088/1361-665X/ac96df.

References

- [15] H. Zhao, A. M. Hussain, A. Israr, D. M. Vogt, M. Duduta, D. R. Clarke, and R. J. Wood, "A Wearable Soft Haptic Communicator Based on Dielectric Elastomer Actuators", *Soft Robotics*, (vol. 7, no. 4, pp. 451–461), Aug. 2020, doi: 10.1089/soro.2019.0113.
- [16] X. Ji, X. Liu, V. Cacucciolo, Y. Civet, A. El Haitami, S. Cantin, Y. Perriard, and H. Shea, "Untethered Feel-Through Haptics Using 18- μ m Thick Dielectric Elastomer Actuators", *Advanced Functional Materials*, (vol. 31, no. 39,) Sep. 2021, doi: 10.1002/adfm.202006639.
- [17] S. Gratz-Kelly, T. Krüger, G. Rizzello, S. Seelecke, and G. Moretti, "An audio-tactile interface based on dielectric elastomer actuators", *Smart Materials and Structures*, (vol. 32, no. 3), Mar. 2023, doi: 10.1088/1361-665X/acb6da.
- [18] S. Gratz-Kelly, D. Philippi, B. Fasolt, S. Nalbach, and P. Motzki, "Gesture and force sensing based on dielectric elastomers for intelligent gloves in the digital production", *Tm - Technisches Messen*, (vol. 91, no. 4), Mar. 2024, doi: 10.1515/teme-2024-0003.
- [19] Y. Chen, Y. Yang, M. Li, E. Chen, W. Mu, R. Fischer, and R. Yin, "Wearable Actuators: An Overview", *Textiles*, (vol. 1, no. 2), Sep. 2021, doi: 10.3390/textiles1020015.
- [20] M. Lidka, A. D. Price, and A. L. Trejos, "Development and Evaluation of Dielectric Elastomer Actuators for Assistive Wearable Devices", *2018 IEEE Canadian Conference on Electrical & Computer Engineering (CCECE)*. IEEE, 2018, (pp. 1–4), May 2018, doi: 10.1109/CCECE.2018.8447581.
- [21] G. L. Novelli, G. G. Vargas, and R. M. Andrade, "Dielectric elastomer actuators as artificial muscles for wearable robots", *Journal of Intelligent Material Systems and Structures*, (vol. 34, no. 9, pp. 1007–1025), May 2023, doi: 10.1177/1045389X221128567.
- [22] X. Ji, X. Liu, V. Cacucciolo, M. Imboden, Y. Civet, A. El Haitami, S. Cantin, Y. Perriard, and H. Shea, "An autonomous untethered fast soft robotic insect driven by low-voltage dielectric elastomer actuators", *Science Robotics*, (vol. 4, no. 37), Dec. 2019, doi: 10.1126/scirobotics.aaz6451.
- [23] S. Hau, G. Rizzello, and S. Seelecke, "A novel dielectric elastomer membrane actuator concept for high-force applications", *Extreme Mechanics Letters*, (vol. 23, pp. 24–28), Sep. 2018, doi: 10.1016/j.eml.2018.07.002.
- [24] Y. Chen, L. Agostini, G. Moretti, M. Fontana, and R. Vertechy, "Dielectric elastomer materials for large-strain actuation and energy harvesting: A comparison between styrenic rubber, natural rubber and acrylic elastomer", *Smart Materials and Structures*, (vol. 28, no. 11), Oct. 2019, doi: 10.1088/1361-665X/ab3b32.
- [25] L. J. Yin, Y. Zhao, J. Zhu, M. Yang, H. Zhao, J. Y. Pei, S. L. Zhong, and Z. M. Dang, "Soft, tough, and fast polyacrylate dielectric elastomer for non-magnetic motor", *Nature Communications*, (vol. 12, no. 1), Dec. 2021, doi: 10.1038/s41467-021-24851-w.
- [26] Y. Zhao, Q. Y. Feng, Y. K. Xie, Z. L. Zhang, L. J. Yin, and Z. M. Dang, "Advanced Acrylate Dielectric Elastomers with Large Actuation Strains at Very Low Electric Field", *ACS Applied Polymer Materials*, (vol. 4, no. 12, pp. 8892–8899), Dec. 2022, doi: 10.1021/acsapm.2c01293.
- [27] W. Z. Dong, Y. Zhao, L. J. Yin, and Z. M. Dang, "Fabrication and actuation characterization of a new UV curing acrylic dielectric elastomer", *IET Nanodielectrics*, (vol. 5, no. 2, pp. 104–111), Jun. 2022, doi: 10.1049/nde2.12035.
- [28] G. Kofod, P. Sommer-Larsen, R. Kornbluh, and R. Pelrine, "Actuation response of polyacrylate dielectric elastomers," *Journal of intelligent material systems and structures*, (vol. 14, no. 12, pp. 787–793), Dec. 2003, doi: 10.1177/104538903039260.

References

- [29] T. Chen, J. Qiu, K. Zhu, and J. Li, "Electro-mechanical performance of polyurethane dielectric elastomer flexible micro-actuator composite modified with titanium dioxide-graphene hybrid fillers", *Materials and Design*, (vol. 90, pp. 1069–1076), 2016, doi: 10.1016/j.matdes.2015.11.068.
- [30] C. Zhang, W. Wei, H. Sun, and Q. Zhu, "Study on the properties of different dielectric elastomers applying to actuators", (vol. 329), Oct. 2021, doi: 10.1016/j.sna.2021.112806.
- [31] L. Maffli, S. Rosset, M. Ghilardi, F. Carpi, and H. Shea, "Ultrafast all-polymer electrically tunable silicone lenses", *Advanced Functional Materials*, (vol. 25, no. 11, pp. 1656–1665), Jan. 2015, doi: 10.1002/adfm.201403942.
- [32] E. Jewell, S. Hamblyn, T. Claypole, and D. Gethin, "Deposition of high conductivity low silver content materials by screen printing", *Coatings*, (vol. 5, no. 2, pp. 172–185), Jun. 2015, doi: 10.3390/coatings5020172.
- [33] J. Hubertus, J. Neu, S. Croce, G. Rizzello, S. Seelecke, and G. Schultes, "Nanoscale Nickel-Based Thin Films as Highly Conductive Electrodes for Dielectric Elastomer Applications with Extremely High Stretchability up to 200%", *ACS Applied Material Interfaces*, (vol. 13, no. 33, pp. 39894–39904), Aug. 2021, doi: 10.1021/acsami.1c10686.
- [34] D. Pantea, H. Darmstadt, S. Kaliaguine, and C. Roy, "Electrical conductivity of conductive carbon blacks: Influence of surface chemistry and topology", *Applied Surface Science*, (vol. 217, no. 1–4, pp. 181–193), Jul. 2003, doi: 10.1016/S0169-4332(03)00550-6.
- [35] H. Shivashankar, R. Sangamesh, and S. M. Kulkarni, "Processing and investigation of mechanical characteristics on the polydimethylsiloxane/carbon black composites", *Materials Research Express*, (vol. 6, no. 10), Aug. 2019, doi: 10.1088/2053-1591/ab3b7e.
- [36] T. P. Willian, B. Fasolt, P. Motzki, G. Rizzello, and S. Seelecke, "Effects of Electrode Materials and Compositions on the Resistance Behavior of Dielectric Elastomer Transducers", *Polymers*, (vol. 15, no. 2), Jan. 2023, doi: 10.3390/polym15020310.
- [37] E. Hajiesmaili and D. R. Clarke, "Dielectric elastomer actuators," *Journal of Applied Physics*, (vol. 129, no. 15), Apr. 2021, doi: 10.1063/5.0043959.
- [38] E. Cakmak, X. Fang, O. Yildiz, P. D. Bradford, and T. K. Ghosh, "Carbon nanotube sheet electrodes for anisotropic actuation of dielectric elastomers," *Carbon*, (vol. 89, pp. 113–120), Aug. 2015, doi: 10.1016/j.carbon.2015.03.011.
- [39] H. Stoyanov, P. Brochu, X. Niu, C. Lai, S. Yun, and Q. Pei, "Long lifetime, fault-tolerant freestanding actuators based on a silicone dielectric elastomer and self-clearing carbon nanotube compliant electrodes", *RSC Advances*, (vol. 3, no. 7, pp. 2272–2278), Feb. 2013, doi: 10.1039/c2ra22380e.
- [40] J. E. Q. Quinsaat, I. Burda, R. Krämer, D. Häflinger, F. A. Nüesch, M. Dascalu, and D. M. Opris, "Conductive silicone elastomers electrodes processable by screen printing", *Scientific reports*, (vol. 9, no. 1), Dec. 2019, doi: 10.1038/s41598-019-49939-8.
- [41] E. Kim, J.C. Lai, L. Michalek, W. Wang, C. Xu, H. Lyu, W. Yu, H. Park, Y. Tomo, S. E. Rood, B. Lee, J. Park, B. Park, S. Wei, C. Zhao, and Z. Bao, "A Transparent, Patternable, and Stretchable Conducting Polymer Solid Electrode for Dielectric Elastomer Actuators", *Advanced Functional Materials*, (vol. 35, no. 1), 2025, doi: 10.1002/adfm.202411880.
- [42] A. Wiranata, M. Kanno, N. Chiya, H. Okabe, T. Horii, T. Fujie, N. Hosoya, and S. Maeda, "High-Frequency, low-voltage oscillations of dielectric elastomer actuators", *Applied Physics Express*, (vol. 15, no. 1), Jan. 2022, doi: 10.35848/1882-0786/ac3d41.

- [43] M. Shrestha, L. Depari, and E. H. T. Teo, "Printable transparent conductive ink for dielectric elastomer-based tunable acoustic absorber", *FLEPS 2024 - IEEE International Conference on Flexible and Printable Sensors and Systems*, (pp 1–4), 2024. doi: 10.1109/FLEPS61194.2024.10604244.
- [44] H. Shigemune, S. Sugano, J. Nishitani, M. Yamauchi, N. Hosoya, S. Hashimoto, and S. Maeda, "Dielectric elastomer actuators with carbon nanotube electrodes painted with a soft brush", *Actuators*, (vol. 7, no. 3), Sep. 2018, doi: 10.3390/act7030051.
- [45] T. P. Willian, S. Pohl, D. Bruch, G. Rizzello, P. Motzki, G. Kickelbick, and S. Seelecke, "Effects of Solvents on the Material Properties of Screen-Printed Electrodes and a Polydimethylsiloxane Dielectric for Dielectric Elastomer Transducers", *Advanced Engineering Materials*, (vol. 26, no. 10), May 2024, doi: 10.1002/adem.202301736.
- [46] M. Hodgins and S. Seelecke, "Systematic experimental study of pure shear type dielectric elastomer membranes with different electrode and film thicknesses", *Smart Materials and Structures*, (vol. 25, no. 9), Aug. 2016, doi: 10.1088/0964-1726/25/9/095001.
- [47] S. Schlatter, G. Grasso, S. Rosset, and H. Shea, "Inkjet Printing of Complex Soft Machines with Densely Integrated Electrostatic Actuators", *Advanced Intelligent Systems*, (vol. 2, no. 11), Nov. 2020, doi: 10.1002/aisy.202000136.
- [48] O. Cabuk, M. Wegener, B. Gruber, S.-O. Seidel, and J. Maas, "Inkjet printing and characterization of applied electrodes for dielectric elastomer transducer", *Electroactive Polymer Actuators and Devices (EAPAD) XXII*, (vol. 11375, pp. 173–185) SPIE, Jun. 2020, doi: 10.1117/12.2558545.
- [49] S. Rosset, O. A. Ararom, S. Schlatter, and H. R. Shea, "Fabrication process of silicone-based dielectric elastomer actuators", *Journal of Visualized Experiments*, (vol. 2016, no. 108), Feb. 2016, doi: 10.3791/53423.
- [50] S. Holzer, A. Walter, S. Konstantinidi, T. Martinez, Y. Civet, and Y. Perriard, "SPIE Smart Structures + Nondestructive Evaluation: Carbon based printed electrodes for DEAs: study of pad, inkjet and stencil printing," *Electroactive Polymer Actuators and Devices (EAPAD) XXVI*, (vol. 12945, pp.267–275), SPIE, Mar. 2024, doi: <https://doi.org/10.1117/12.3010530>.
- [51] P. Lotz, M. Matysek, and H. F. Schlaak, "Fabrication and application of miniaturized dielectric elastomer stack actuators", *IEEE/ASME Transactions on Mechatronics*, (vol. 16, no. 1, pp. 58–66), Feb. 2011, doi: 10.1109/TMECH.2010.2090164.
- [52] A. J. Cohen, M. Kollosche, M. C. Yuen, D. Y. Lee, D. R. Clarke, and R. J. Wood, "Batch-Sprayed and Stamp-Transferred Electrodes: A New Paradigm for Scalable Fabrication of Multilayer Dielectric Elastomer Actuators", *Advanced Functional Materials*, (vol. 32, no. 43), Oct. 2022, doi: 10.1002/adfm.202205394.
- [53] C. Zhang, Y. Li, C. Wang, S. Lu, J. Zhao, J. Gao, S. Wang, and A. Luo, "Research on spraying process of flexible electrode for dielectric elastomer sensors," *Journal of Materials Science: Materials in Electronics*, (vol. 33, no. 24, pp. 19307–19319), Aug. 2022, doi: 10.1007/s10854-022-08769-7.
- [54] M. Iacob, A. Verma, T. Buchner, Y. Sheima, R. Katschmann, and D. M. Opris, "Slot-Die Coating of an On-the-Shelf Polymer with Increased Dielectric Permittivity for Stack Actuators," *ACS Applied Polymer Materials*, (vol. 4, no. 1, pp. 150–157), Jan. 2022, doi: 10.1021/acsapm.1c01135.
- [55] Z. Li, M. Sheng, M. Wang, P. Dong, B. Li, and H. Chen, "Stacked dielectric elastomer actuator (SDEA): Casting process, modeling and active vibration isolation", *Smart Materials and Structures*, (vol. 27, no. 7), Jun. 2018, doi: 10.1088/1361-665X/aabea5.

References

- [56] J. Hubertus, B. Fasolt, P. Linnebach, S. Seelecke, and G. Schultes, "Electromechanical evaluation of sub-micron NiCr-carbon thin films as highly conductive and compliant electrodes for dielectric elastomers", *Sensors and Actuators A: Physical*, (vol. 315, Nov. 2020), doi: 10.1016/j.sna.2020.112243.
- [57] J. Hubertus, S. Croce, J. Neu, S. Seelecke, G. Rizzello, and G. Schultes, "Laser Structuring of Thin Metal Films of Compliant Electrodes on Dielectric Elastomers," *Advanced Functional Materials*, (vol. 33, no. 16), Apr. 2023, doi: 10.1002/adfm.202214176.
- [58] F. Carpi, D. De Rossi, R. Pelrine, R. Kornbluh, and P. Sommer-Larsen, "Dielectric elastomers as electromechanical transducers: Fundamentals, material devices, models and applications of an emerging electroactive polymer technology", *Elsevier*, (vol. 1.), 2008. ISBN: 978-0-08-047488-5
- [59] L. Yu, S. Vudayagiri, L. A. Jensen, and A. L. Skov, "Temperature dependence of dielectric breakdown of silicone-based dielectric elastomers", *International Journal of Smart and Nano Materials*, (vol. 11, no. 2, pp. 129–146), Apr. 2020, doi: 10.1080/19475411.2020.1768605.
- [60] F. B. Albuquerque and H. Shea, "Influence of humidity, temperature and prestretch on the dielectric breakdown strength of silicone elastomer membranes for DEAs", *Smart Materials and Structures*, (vol. 29, no. 10), Oct. 2020, doi: 10.1088/1361-665X/aba5e3.
- [61] F. Förster-Zügel, T. Grotepaß, and H. F. Schlaak, "Characterization of the dielectric breakdown field strength of PDMS thin films: thickness dependence and electrode shape," *Electroactive Polymer Actuators and Devices (EAPAD) 2015*, SPIE, (Vol. 9430, pp. 84–92), Apr. 2015, doi: 10.1117/12.2084504.
- [62] D. Gatti, H. Haus, M. Matysek, B. Frohnäpfel, C. Tropea, and H. F. Schlaak, "The dielectric breakdown limit of silicone dielectric elastomer actuators", *Applied Physics Letters*, (vol. 104, no. 5), Feb. 2014, doi: 10.1063/1.4863816.
- [63] B. Chen, M. Kollasche, M. Stewart, J. Busfield, and F. Carpi, "Electrical breakdown of dielectric elastomers: influence of compression, electrode's curvature and environmental humidity", *Electroactive Polymer Actuators and Devices (EAPAD) 2016*, SPIE, (vol. 9798, pp. 76–85), Apr. 2016, doi: 10.1117/12.2218603.
- [64] S. Zakaria, P. H. F. Morshuis, M. Y. Benslimane, L. Yu, and A. L. Skov, "The electrical breakdown strength of pre-stretched elastomers, with and without sample volume conservation", *Smart Materials and Structures*, (vol. 24, no. 5), May 2015, doi: 10.1088/0964-1726/24/5/055009.
- [65] T. Vu-Cong, C. Jean-Mistral, and A. Sylvestre, "Impact of the nature of the compliant electrodes on the dielectric constant of acrylic and silicone electroactive polymers", *Smart Materials and Structures*, (vol. 21, no. 10), Oct. 2012, doi: 10.1088/0964-1726/21/10/105036.
- [66] J. Zhang, L. Liu, and H. Chen, "Electromechanical properties of soft dissipative dielectric elastomer actuators influenced by electrode thickness and conductivity", *Journal of Applied Physics*, (vol. 127, no. 18), May 2020, doi: 10.1063/5.0001580.
- [67] P. Khodaparast, S. R. Ghaffarian, and M. R. Khosroshahi, "Effect of Different Electrode Materials on the Performance of Smart Composite Actuators Based on Dielectric Elastomers", *Key Engineering Materials*, (vol. 334, pp. 985–988), Mar. 2007, doi: 10.4028/www.scientific.net/kem.334-335.985.
- [68] D. P. Muffoletto, A. M. Martinez, K. M. Burke, and J. L. Zirnheld, "Electrode composition and partial discharges and their role in the breakdown of dielectric elastomer films", *IEEE Transactions on Dielectrics and Electrical Insulation*, (vol. 22, no. 4, pp. 1756–1762), Aug. 2015, doi: 10.1109/TDEI.2015.004988.

References

- [69] S. Chiba, M. Waki, M. Takeshita, and K. Ohyama, "Examination of factors to improve the performance of dielectric elastomer transducers and their applications", *Smart Materials and Structures*, (vol. 33, no. 6), Jun. 2024, doi: 10.1088/1361-665X/ad4759.
- [70] L. Sohlbach, S. Bhatta, F. Perez-Peña, and K. Schmidt, "A Portable Real-Time Test Bench for Dielectric Elastomer Actuators", *Machines*, (vol. 11, no. 3), Mar. 2023, doi: 10.3390/machines11030380.
- [71] H. Wang and L. Yang, "Effects of effective voltages, electrode types and stretching states on electrical properties and actuation characteristics of dielectric elastomer materials", *Polymer Testing*, (vol. 120), Mar. 2023, doi: 10.1016/j.polymertesting.2023.107939.
- [72] X. Liu, Y. Xing, W. Sun, Z. Zhang, S. Guan, and B. Li, "Investigation of the Dynamic Breakdown of a Dielectric Elastomer Actuator Under Cyclic Voltage Excitation," *Frontiers in robotics and AI*, (vol. 8), Apr. 2021, doi: 10.3389/frobt.2021.672154.
- [73] F. Beco Albuquerque, "Lifetime of dielectric elastomer actuators under DC electric fields", Doctoral dissertation 2022, EPFL, Lausanne, doi: doi.org/10.5075/epfl-thesis-10457.
- [74] J. E. Mark, "Polymer Data Handbook", (vol. 1), *Oxford University Press, Inc.*, 1999. ISBN: 9780197704172.
- [75] B. Wang and S. Krause, "Properties of Dimethylsiloxane Microphases in Phase-Separated Dimethylsiloxane Block Copolymers", *Macromolecules*, (vol. 20, no. 2, pp. 2201–2208), Jan. 1987, doi: <https://doi.org/10.1021/ma00168a700>.
- [76] W. C. Röntgen, "Ueber die durch Electricität bewirkten Form- und Volumenänderungen von dielektrischen Körpern", *Annalen der Physik*, (vol. 247, no. 13, pp. 771–786), 1880, doi: 10.1002/andp.18802471304.
- [77] B. Fasolt and S. Seelecke, "Influence of silicone oil content in electrodes on longevity of dielectric elastomer transducers (DET)," *International conference on Electromechanically Active Poymer (EP) transducers & artificial muscels*, Jun. 2017.
- [78] R. Pelrine, P. Sommer-Larsen, R. D. Kornbluh, R. Heydt, G. Kofod, Q. Pei, and P. Gravesen, "Applications of Dielectric Elastomer Actuator," *Smart Structures and Materials 2001: Electroactive Polymer Actuators and Devices*, SPIE, (vol. 4329, pp. 335–349), Jul. 2001, <http://www.erg.sri.cornlautomation/actuators.html>.
- [79] J. Biggs, K. Danielmeier, J. Hitzbleck, J. Krause, T. Kridl, S. Nowak, E. Orselli, X. Quan, D. Schapeler, W. Sutherland, J. Wagner, "Elektroaktive Polymere: Entwicklungen und Perspektiven dielektrischer Elastomere", *Angewandte Chemie*, (vol. 125, no. 36, pp. 9581–9595), Sep. 2013, doi: 10.1002/ange.201301918.
- [80] R. E. Pelrine, R. D. Kornbluh, and J. P. Joseph, "Electrostriction of polymer dielectrics with compliant electrodes as a means of actuation", *Sensors and Actuators A*, (vol. 64, no. 64, pp. 77–85), 1998, doi: doi.org/10.1016/S0924-4247(97)01657-9.
- [81] S. Chiba and M. Waki, "Innovative power generator using dielectric elastomers (creating the foundations of an environmentally sustainable society)", *Sustainable Chemistry and Pharmacy*, (vol. 15), Mar. 2020, doi: 10.1016/j.scp.2019.100205.
- [82] S. Nalbach, "Intelligente Antriebssysteme für dynamische Anwendungen auf Basis dielektrischer Elastomere," Doctoral dissertation 2016, Universität des Saarlandes, 2023.
- [83] M. Hill, G. Rizzello, and S. Seelecke, "Development and experimental characterization of a pneumatic valve actuated by a dielectric elastomer membrane", *Smart Materials and Structures*, (vol. 26, no. 8), 2017, doi: 10.1088/1361-665X/aa746d.

References

- [84] G. Rizzello, P. Loew, L. Agostini, M. Fontana, and S. Seelecke, "A lumped parameter model for strip-shaped dielectric elastomer membrane transducers with arbitrary aspect ratio", *Smart Materials and Structures*, (vo. 29, no. 11, pp. 115030), 2020, doi: 10.1088/1361-665X/abb09e.
- [85] J. Kunze, J. Prechtel, D. Bruch, B. Fasolt, S. Nalbach, P. Motzki, S. Seelecke, and G. Rizzello, "Design, manufacturing, and characterization of thin, core-free, rolled dielectric elastomer actuators", *Actuators*, (vol. 10, no. 4), Apr. 2021, doi: 10.3390/act10040069.
- [86] J. Cheng, Z. Jia, and T. Li, "Dielectric-elastomer-based capacitive force sensing with tunable and enhanced sensitivity," *Extreme Mechanics Letters*, (vol. 21, pp. 49–56), May 2018, doi: 10.1016/j.eml.2018.03.004.
- [87] A. Tairych and I. A. Anderson, "Capacitive stretch sensing for robotic skins", *Soft Robotics*, (vol. 6, no. 3, pp. 389–398), Jun. 2019, doi: 10.1089/soro.2018.0055.
- [88] J. T. Dunn, S. Ellis, R. Briese, T. Orstad, T. Lambert, J. Page, M. Calvo, and T. Skwiot, "Electroactive Polymer Pressure Sensor," Patent EP 26410602A2, Dec. 24, 2012.
- [89] D. McCoul and Q. Pei, "Tubular dielectric elastomer actuator for active fluidic control", *Smart Materials and Structures*, (vol. 24, no. 10), Sep. 2015, doi: 10.1088/0964-1726/24/10/105016.
- [90] S. Xu, Y. Chen, N.-S. P. Hyun, K. P. Becker, and R. J. Wood, "A dynamic electrically driven soft valve for control of soft hydraulic actuators", *Proceedings of the National Academy of Sciences*, (vol. 118, no. 34), Aug. 2021, <https://doi.org/10.1073/pnas.2103198118>.
- [91] F. A. Mohd Ghazali, C. K. Mah, A. AbuZaiter, P. S. Chee, and M. S. Mohamed Ali, "Soft dielectric elastomer actuator micropump", *Sensors and Actuators A: Physical*, (vol. 263, pp. 276–284), Aug. 2017, doi: 10.1016/j.sna.2017.06.018.
- [92] G. Kovacs, L. Düring, S. Michel, and G. Terrasi, "Stacked dielectric elastomer actuator for tensile force transmission", *Sensors and Actuators A: Physical*, (vol. 155, no. 2, pp. 299–307), Oct. 2009, doi: 10.1016/j.sna.2009.08.027.
- [93] D. Bruch, "Multifunctional Test Rig for Accelerated Assessment of Electromechanical Characteristics and Failure Mechanisms of Dielectric Elastomer Transducers," Doctoral dissertation 2024, Universität des Saarlandes, Saarbrücken, doi: <http://dx.doi.org/10.22028/D291-42513>.
- [94] R. Peirine, R. Kornbluh, J. Eckerle, P. Jeuck, S. Oh, Q. Pei, and S. Stanford, "Dielectric Elastomers: Generator Mode Fundamentals and Applications," *8th Annual International Symposium on Smart Structures and Materials, SPIE*, (pp. 148–156), Mar. 2001, <https://doi.org/10.1117/12.432640>.
- [95] S. Chiba, "Power Generation Using Dielectric Elastomers." Available: <https://encyclopedia.pub/entry/11449> (accessed on May 20, 2025).
- [96] R. Baumgartner, C. Keplinger, R. Kaltseis, R. Schwödiauer, and S. Bauer, "Dielectric elastomers: from the beginning of modern science to applications in actuators and energy harvesters", *Electroactive Polymer Actuators and Devices (EAPAD) 2011, SPIE*, (pp. 34–39), Mar. 2011, doi: 10.1117/12.880289.
- [97] P. Brochu and Q. Pei, "Advances in dielectric elastomers for actuators and artificial muscles", *Macromolecular Rapid Communications*, (vol. 31, no. 1, pp. 10–36), Jan. 2010, doi: 10.1002/marc.200900425.
- [98] R. Pelrine, R. Kornbluh, Q. Pei, and J. Joseph, "High-Speed Electrically Actuated Elastomers with Strain Greater Than 100%," *Science*, (vol. 287, no. 5454, pp. 836–839), 2000, doi: 10.1126/science.287.5454.836.

References

- [99] G. M. Santos, G. M. S. Tavares, G. De Gasperi, and G. R. Bau, "Mechanical evaluation of the resistance of elastic bands Avaliação mecânica da resistência de faixas elásticas", *Brazilian Journal of Physical Therapy*, (no. 13, pp. 521–526), Sep. 2009, <https://doi.org/10.1590/S1413-35552009000600009>.
- [100] G. Moretti, L. Sarina, L. Agostini, R. Vertechy, G. Berselli, and M. Fontana, "Styrenic-rubber dielectric elastomer actuator with inherent stiffness compensation", *Actuators*, (vol. 9, no. 2), Jun. 2020, doi: 10.3390/ACT9020044.
- [101] S. Chiba, M. Waki, M. Takeshita, and K. Ohyama, "Examination of factors to improve the performance of dielectric elastomer transducers and their applications", *Smart Materials and Structures*, (vol. 33, no. 6), Jun. 2024, doi: 10.1088/1361-665X/ad4759.
- [102] S. Chiba, M. Waki, C. Jiang, M. Takshita, M. Uejima, K. Arakawa, and K. Ohyama, "The possibility of a high-efficiency wave power generation system using dielectric elastomers", *Energies*, (vol. 11, no. 12), 2021, doi: 10.3390/en14123414.
- [103] X. Zhao and Z. Suo, "Method to analyze electromechanical stability of dielectric elastomers", *Applied Physics Letters*, (vol. 91, no. 6), 2007, doi: 10.1063/1.2768641.
- [104] L. Zhao, J. C. Su, and C. L. Liu, "Review of developments on polymers' breakdown characteristics and mechanisms on a nanosecond time scale", *AIP Advances*, (vol. 10, no. 3), Mar. 2020, doi: 10.1063/1.5110273.
- [105] J. Zhang, J. Sheng, X. Liu, L. Liu, J. Zhao, and H. Chen, "Temperature effect on electromechanical properties of polyacrylic dielectric elastomer: an experimental study", *Smart Materials and Structures*, (vol. 29, no. 4), Mar. 2020, doi: 10.1088/1361-665X/ab79b7.
- [106] Wacker Chemical Corporation, "Datenblätter Elastosil Film 2030 250/20," 2025. Available: www.wacker.com, (accessed on June 20, 2024)
- [107] J. E. Mark, "Some interesting things about polysiloxanes," *Accounts of chemical research*, (vol. 37, no. 12, pp. 946–953), Dec. 2004, doi: 10.1021/ar030279z.
- [108] J. E. Mark, "Rubber Elasticity." Available: <https://pubs.acs.org/sharingguidelines>, (accessed on March 10, 2025)
- [109] F. Carpi, P. Chiarelli, A. Mazzoldi, and D. De Rossi, "Electromechanical characterisation of dielectric elastomer planar actuators: Comparative evaluation of different electrode materials and different counterloads", *Sensors and Actuators A: Physical*, (vol. 107, no. 1, pp. 85–95), Oct. 2003, doi: 10.1016/S0924-4247(03)00257-7.
- [110] M. Mehnert and P. Steinmann, "On the influence of the compliant electrodes on the mechanical behavior of VHB 4905", *Computational Materials Science*, (vol. 160, pp. 287–294), Apr. 2019, doi: 10.1016/j.commatsci.2019.01.011.
- [111] K. E. Polmanteer, "Current perspectives on silicone rubber technology", *Rubber Chemistry and technology*, (vol. 54, no. 5, pp. 1051–1080), 1981.
- [112] P. R. Dvornic, J. D. Jovanovic, and M. N. Govedarica, "On the critical molecular chain length of polydimethylsiloxane," *Journal of applied polymer science*, (vol. 49, no. 9, pp. 1497–1507), 1993, doi: 10.1002/app.1993.070490901.
- [113] F. De Buyl, "Silicone sealants and structural adhesives," *International Journal of Adhesion and Adhesives*, (vol. 21, no. 5, pp. 411–422), 2001, doi: 10.1016/S0143-7496(01)00018-5.
- [114] M. J. Owen and S. Emeritus, "Why Silicones Behave Funny," *Chimie nouvelle*, (no. 85, pp. 27–33), 2004.

- [115] H. Zhang and A. Cloud, "The Permeability characteristics of silicone Rubber," *Global Advances in Material and Process Engineering*, (pp. 72–75), 2006, https://cdn.thomasnet.com/kc/2650/doc/0000102048_70_83571.pdf
- [116] K. S. Chang, Y. C. Chung, T. H. Yang, S. J. Lue, K. L. Tung, and Y. F. Lin, "Free volume and alcohol transport properties of PDMS membranes: Insights of nano-structure and interfacial affinity from molecular modeling", *Journal of membrane science*, (vol. 417–418, pp. 119–130), Nov. 2012, doi: 10.1016/j.memsci.2012.06.019.
- [117] Z. Wang, Z. D. Jia, M. H. Fang, and Z. C. Guan, "Absorption and permeation of water and aqueous solutions of high-Temperature vulcanized silicone rubber", *IEEE Transactions on Dielectrics and Electrical Insulation*, (vol. 22, no. 6, pp. 3357–3365), Dec. 2015, doi: 10.1109/TDEI.2015.005192.
- [118] Y. Yang, Z. Wang, X. Peng, Z. Huang, and P. Fang, "Influence of Crosslinking Extent on Free Volumes of Silicone Rubber and Water Diffusion after Corona Discharge," *Materials*, (vol. 15, no. 19), Oct. 2022, doi: 10.3390/ma15196833.
- [119] M. Leda, "Dielectric breakdown process of polymers", *IEEE Transactions on Electrical Insulation*, (no. 3, pp. 206–224), Jun. 1980, doi: 10.1109/TEI.1980.298314.
- [120] R. V. Mateiu, L. Yu, and A. L. Skov, "Electrical breakdown phenomena of dielectric elastomers", *Electroactive Polymer Actuators and Devices (EAPAD)*, SPIE, (pp. 403–411), Apr. 2017, doi: 10.1117/12.2258719.
- [121] J. Wang, G. Li, Z. Zhang, Q. Huang, B. Niu, Y. Zhang, and D. Long, "Detailed insights of polydimethylsiloxane (PDMS) degradation mechanism via ReaxFF MD and experiments", *Chemical Engineering Journal*, (vol. 488), May 2024, doi: 10.1016/j.cej.2024.150728.
- [122] S. Li, G. Yin, G. Chen, J. Li, S. Bai, L. Zhong, Y. Zhang, and Q. Lei, "Short-term Breakdown and Long-term Failure in Nanodielectrics: A Review", *IEEE Transactions on Dielectrics and Electrical Insulation*, (vol. 17, no. 5, pp. 1523–1535), 2010, doi: 10.1109/TDEI.2010.5595554.
- [123] J. C. Fothergill, "Ageing, Space Charge and Nanodielectrics: Ten Things We Don't Know About Dielectrics", *IEEE International Conference on Solid Dielectrics*, (pp. 1–10), 2007, doi: 10.1109/ICSD.2007.4290739
- [124] M. Leda, M. Nagao, and M. Hikita, "High-field Conduction and Breakdown in Insulating Polymers Present Situation and Future Prospects", *IEEE transactions on dielectrics and electrical insulation*, (vol. 1, no. 5, pp. 934–945), 2004, doi: 10.1109/94.326660.
- [125] L. A. . Dissado and J. C. . Fothergill, *Electrical degradation and breakdown in polymers*, (vol. 9.) Institution of Engineering and Technology, 1992, ISBN: 0 86341 196 7.
- [126] Y. Zhang, Y. Zhou, L. Zhang, Z. Zhou, and Q. Nie, "Electrical trees and their growth in silicone rubber at various voltage frequencies", *Energies*, (vol. 11, no. 2), Feb. 2018, doi: 10.3390/en11020327.
- [127] Y. Sun, C. Bealing, S. Boggs, and R. Ramprasad, "50+ Years of Intrinsic Breakdown", *IEEE Electrical Insulation Magazine*, (vol. 29, no. 2, pp. 8–15), Mar. 2013, doi: 10.1109/MEI.2013.6457595.
- [128] L. Zhao, J. C. Su, and C. L. Liu, "Review of developments on polymers' breakdown characteristics and mechanisms on a nanosecond time scale", *AIP Advances*, (vol. 10, no. 3), Mar. 2020, doi: 10.1063/1.5110273.
- [129] X. Zhao and Z. Suo, "Method to analyze electromechanical stability of dielectric elastomers", *Applied Physics Letters*, (vol. 91, no. 6), 2007, <https://doi.org/10.1063/1.2768641>.

- [130] J. Li, Z. Wang, and J. Zhou, "Mechanics of Surface Instabilities in Soft Dielectrics Subject to Electromechanical Loading," *Polymers*, (vol. 16, no. 24, p. 3612), Dec. 2024, doi: 10.3390/polym16243612.
- [131] B. Fasolt, F. Welsch, S. Nalbach, S. Seelecke, and G. Rizzello, "The beauty of breakdown," *International conference on Electromechanically Active Polymer (EAP) transducers & artificial muscle*, EuroEAP 2021, Jun. 2021.
- [132] F. Carpi *et al.*, "Standards for dielectric elastomer transducers", *Smart Materials and Structures*, (vol. 24, no. 10), Sep. 2015, doi: 10.1088/0964-1726/24/10/105025.
- [133] M. Kollosche and G. Kofod, "Electrical failure in blends of chemically identical, soft thermoplastic elastomers with different elastic stiffness", *Applied Physics Letters*, (vol. 96, no. 7), 2010, doi: 10.1063/1.3319513.
- [134] M. Hodgins, "Design of diaphragm dielectric elastomer actuators (DEAS) and experimental characterization and experimental characterization techniques", Doctoral dissertation 2016, Universität des Saarlandes, 2016.
- [135] F. Forster-Zügel, L. Braisz, and H. F. Schlaak, "Characterization of the dielectric breakdown strength of thin elastic films in various ambient media," *IEEE International Conference on Dielectrics (ICD)*, (vol. 1, pp. 569–572), Mar. 2016. doi: 10.1109/ICD.2016.7547668.
- [136] J. Diani, B. Fayolle, and P. Gilormini, "A review on the Mullins effect", *European Polymer Journal*, (vol. 45, no. 3, pp. 601–612), Mar. 2009. doi: 10.1016/j.eurpolymj.2008.11.017.
- [137] D. Kühnel, F. Beco Albuquerque, V. Py, and H. Shea, "Automated test setup to quantify the lifetime of dielectric elastomer actuators under a wide range of operating conditions", *Smart Materials and Structures*, (vol. 30, no. 6), Jun. 2021, doi: 10.1088/1361-665X/abfb85.
- [138] B. Fasolt, B. Holz, D. Bruch, P. Motzki, and S. Seelecke, "Influence of silicone content in the electrode matrix on the failure of DE actuators", *International conference on Soft Transducers and Electromechanically Active Polymers*, EuroEAP 2025, Jun. 2025.
- [139] M. Hill, "Entwicklung bauraumoptimierter dielektrischer Elastomer-Aktoren und eines Prüfstandes zur Charakterisierung ihres Ermüdungsverhaltens", Doctoral dissertation 2018, Universität des Saarlandes, 2018.
- [140] Coates Screen Inks Gmbh, "Grundkurs Siebdruck Seminar", *Sun Chemical/Coates Screen, Nürnberg*, Jan. 2014
- [141] B. Fasolt, F. Beco Albuquerque, J. Hubertus, G. Schultes, H. Shea, and S. Seelecke, "Influence of environmental conditions and manufacturing methods on the electrical breakdown of DE thin films", *International conference on Electromechanically Active Polymer (EAP) transducers & artificial muscles*, EuroEAP, Jun. 2022.
- [142] Lechler USA, "Spray Facts on Viscosity", <https://www.lechlerusa.com/en/resources/spray-facts/viscosity#>, (accessed on Dec. 10, 2024).
- [143] C. Baechler, S. Gardin, H. Abuhimd, and G. Kovacs, "Inkjet printed multiwall carbon nanotube electrodes for dielectric elastomer actuators", *Smart Materials and Structures*, (vol. 25, no. 5), 2016, doi: 10.1088/0964-1726/25/5/055009.
- [144] J. Yi, F. Babick, C. Strobel, S. Rosset, L. Ciarella, D. Borin, K Wilson, I. Anderson, A. Richter and E.-F. M. Henke, "Characterizations and Inkjet Printing of Carbon Black Electrodes for Dielectric Elastomer Actuators", *ACS Applied Material Interfaces*, (vol. 15, no. 35, pp. 41992–42003), Sep. 2023, doi: 10.1021/acsami.3c05444.
- [145] A. Poulin, S. Rosset, and H. R. Shea, "Printing low-voltage dielectric elastomer actuators", *Applied Physics Letters*, (vol. 107, no. 24), Dec. 2015, doi: 10.1063/1.4937735.

References

- [146] S. Rosset and H. R. Shea, "Flexible and stretchable electrodes for dielectric elastomer actuators," *Applied Physics A*, (vol. 110, no. 2, pp. 281–307), Feb. 2013, doi: 10.1007/s00339-012-7402-8.
- [147] Angstrom Engineering, "Magnetron Sputtering," <https://angstromengineering.com/tech/magnetron-sputtering/>, (accessed on Feb 15, 2024).
- [148] F. Förster-Zügel, S. Solano-Arana, F. Klug, and H. F. Schlaak, "Dielectric breakdown strength measurements with silicone-based single-layer dielectric elastomer transducers", *Smart Materials and Structures*, (vol. 28, no. 7), Jun. 2019, doi: 10.1088/1361-665X/ab1ebf.
- [149] O. Perera, R. Liyanapathirana, G. Gargiulo, and U. Gunawardana, "A Review of Soft Robotic Actuators and Their Applications in Bioengineering, with an Emphasis on HASEL Actuators' Future Potential," *Actuators*, (vol. 13, no. 12, p. 524), doi: 10.3390/act13120524.
- [150] M. Okagawa and T. Chiba, "Backing material for polymer actuator and polymer actuator", translated from Japanese, Patent JP 2019169659A I," Mar. 10, 2019
- [151] Y. Zhang, C. Ellingford, R. Zhang, J. Roscow, M. Hopkins, P. Keogh, T. McNally, C. Bowen, and C. Wan., "Electrical and Mechanical Self-Healing in High-Performance Dielectric Elastomer Actuator Materials," *Advanced Functional Materials*, (vol. 29, no. 15), Apr. 2019, doi: 10.1002/adfm.201808431.
- [152] R-P. Nie, H. Lin, Y. Li, H-D. Huang, D-X. Yan, K. Dai, J. Lei, and Z-M. Li, "Dynamic chemical bonds design strategy for fabricating fast room-temperature healable dielectric elastomer with significantly improved actuation performance", *Chemical Engineering Journal*, (vol. 439), Jul. 2022, doi: 10.1016/j.cej.2022.135683.
- [153] J. von Szczepanski, P. M. Danner, and D. M. Opris, "Self-Healable, Self-Repairable, and Recyclable Electrically Responsive Artificial Muscles," *Advanced Science*, (vol. 9, no. 22), Aug. 2022, doi: 10.1002/advs.202202153.
- [154] S. Hunt, T. G. McKay, and I. A. Anderson, "A self-healing dielectric elastomer actuator", *Applied Physics Letters*, (vol. 104, no. 11), Mar. 2014, doi: 10.1063/1.4869294.
- [155] S. Kim, Y-H. Hsiao, Y. Lee, W. Zhu, Z. Ren, F. Niroui, and Y. Chen, "Laser-assisted failure recovery for dielectric elastomer actuators in aerial robots," *Science Robotics*, (vol. 8, no.76), doi: 10.1126/scirobotics.adf4278
- [156] E. Taine, P. Jean, and R. Boulard, "Electroactive polymer device and method for manufacturing such an electroactive polymer device", Patent WO 2020064872A1 I, Apr. 02, 2020
- [157] Festo GmbH, Germany. *Incredible Machine, Festo 100th anniversary Hannover Messe, 2025*, available: https://www.festo.com/de/en/e/about-festo/incredible-machine-id_2073685/, (accessed May 15, 2025)

List of abbreviations

CB	Carbon black
DE	Dielectric elastomer(s)
DEA	Dielectric elastomer actuator(s)
DEG	Dielectric elastomer generator(s)
DES	Dielectric elastomer sensor(s)
DET	Dielectric elastomer transducer(s)
PDMS	Polydimethylsiloxan

Table of figures

Figure 2.1. Polar molecules in dielectric elastomer	5
Figure 2.2. Examples of DET designs	6
Figure 2.3. Working principle of DES in the un-stretched state and stretched state	7
Figure 2.4. Stretch sensor for a respiration-monitoring functional shirt and pressure sensor for gait analysis	8
Figure 2.5. Working principle of DEA when no voltage is applied , and when high voltage is applied leading to area increases and simultaneous thickness decrease	8
Figure 2.6. Images of a strip DEA pre-stretched by 75%, held in a fixed position and actuated under various constant electric fields	9
Figure 2.7. Multiple DET layers assembled in stacks that operate through thickness reduction.....	10
Figure 2.8. Actuation principle of typical DEA utilizing surface area expansion	10
Figure 2.9. 16 DE layer high-force circular DEA and biased strip in plane actuator	11
Figure 2.10. The four phases of the working cycle of a DE generator	12
Figure 2.11. Pilot project of DEG for wave generator harvesting	13
Figure 2.12. Molecular structure of PDMS.....	18
Figure 2.13. Design of gold contacts – flat and spherical - used for voltage application and images captured at intervals from 1 minute to 24 hours after breakdown.....	21
Figure 2.14. Conceptual sketch of the automated test rig including data acquisition system.....	22
Figure 2.15. 3D model of the test rig with labeled components and sensors	22
Figure 2.16. Standardized procedure for samples preparation	24

Table of figures

Figure 2.17. Example measurements relevant for the design of a DES.....	25
Figure 2.18. Representative measurements without applied electrodes relevant for DET design.....	27
Figure 2.19. Representative measurements with applied electrodes relevant for DET design.....	28
Figure 3.1. Semi- automatic screen printer setup with mesh, bars, and printed silicone film at the iMSL lab.....	32
Figure 3.2. From mesh screen preparation to printed design	33
Figure 3.3. Illustration of electrical breakdown setup by Yu et al.	36
Figure 3.4. Schematic of a test stand for dielectric breakdown field strength by Gatti et al.....	37
Figure 3.5 Experimental measurement setup for the characterization of the dielectric breakdown field strength of thin elastic films in various ambient media designed by Förster-Zügel et al.	38
Figure 3.6. Schematic breakdown test setup for single-layer DET samples clamped between two frames by Förster-Zügel et al.	39
Figure 3.7. Schematic of the breakdown tester developed by Beco Albuquerque et al.	40
Figure 4.1. Example of two breakdown spots formed during electrical breakdown on Wacker Elastosil 2030 film.	56
Figure 5.1. Main process steps for repair method and quality control	99
Figure 5.2. 300 mm repaired circular DEA used for large-stroke actuation and investigation of vibration modes in loudspeaker applications.....	100
Figure 5.3. Photograph of a deflected multilayer DEA consisting of three stacks of seven single-layer DEA.	100
Figure 5.4. Example of carrier frame placement when frames are stacked.....	101
Figure 5.5. Premature breakdown spots in four single-layer frames with nine DEA each	102
Figure 5.6. Test setup for breakdown experiments.....	104
Figure 5.7. Illustration of the LabVIEW program interface.....	105
Figure 5.8. Illustration of a repair station.	106
Figure 5.9. Repair procedure after DEA breakdown.....	107
Figure 5.10. Adhesion test of 6 mm patch in un-stretched and 100 % stretched state.	108
Figure 5.11. Comparison of the mechanical impact of adhesives Silgel 612 and TP253 for bonding 6 mm patches.	109
Figure 5.12. Test sample design with six electrodes.....	111
Figure 5.13. Stretch ratio over time for force/displacement measurements for actuation force and example of voltage excitation for blocking force measurements.....	112
Figure 5.14. Comparison of stiffness and actuation force for un-patched and patched samples.....	113

Table of figures

Figure 5.15. Comparison between actuation force of un-patched and patched samples and their calculated force difference between actuated and non-actuated state	114
Figure 5.16. Blocking force vs. time for patched and unpatched samples.	114
Figure 5.17. Blocking force vs. time for a patched DEA at a constant stretch of $\lambda = 1.75$	115
Figure 5.18. Local distribution of ten consecutively repaired breakdown spots for Wacker Elastosil 2030/50 5420-01 silicone film	117
Figure 5.19. Local distribution of ten consecutively repaired breakdown spots for Parker 192-1 silicone film	117
Figure 5.20. Electric breakdown field over number of repaired spots	118
Figure 5.21. Example of multiple localized breakdowns and accumulation of repair pads	119
Figure 5.22. Underlit photos of unstretched and 100 % stretched sample after ten repair cycles.....	120
Figure 5.23. Force/displacement measurements for Parker 192-1 after ten repair cycles.....	120
Figure 5.24. Results of calculated actuation force at $\lambda = 1.75$ as difference between maximum force without actuation and when actuated with electric fields from 80 V/ μm to 120 V/ μm	121
Figure 5.25. Locomoting DE Tensegrity Soft Robot by Julian Kunze	122
Figure 5.26. Strip DEA and circular DEA as part of the "Incredible Machine" by Festo GmbH for the company's 100th anniversary	123
Figure 5.27. DEA Vacuum Pump by Matthias Baltes consisting of 64 tested and repaired DEA.....	124

Author's publications

Journal publications

S. Gratz-Kelly, D. Philippi, **B. Fasolt**, S. Nalbach, and P. Motzki, "Gesture and force sensing based on dielectric elastomers for intelligent gloves in the digital production", *Tm - Technisches Messen*, (vol. 91, no. 4), Mar. 2024, doi: 10.1515/teme-2024-0003.

B. Fasolt, F. B. Albuquerque, J. Hubertus, G. Schultes, H. Shea, H., and S. Seelecke, "Electrode impact on the electrical breakdown of dielectric elastomer thin films", *Polymers*, (vol. 15, no. 20, pp. 4071), 2023, <https://doi.org/10.3390/polym15204071>.

T. P. Willian, **B. Fasolt**, P. Motzki, G. Rizzello, and S. Seelecke, "Effects of Electrode Materials and Compositions on the Resistance Behavior of Dielectric Elastomer Transducers", *Polymers*, (vol. 15, no. 2), Jan. 2023, doi: 10.3390/polym15020310.

J. Kunze, J. Prechtel, D. Bruch, **B. Fasolt**, S. Nalbach, P. Motzki, S. Seelecke, and G. Rizzello, "Design, manufacturing, and characterization of thin, core-free, rolled dielectric elastomer actuators", *Actuators*, (vol. 10, no. 4), Apr. 2021, doi: 10.3390/act10040069.

J. Hubertus, **B. Fasolt**, P. Linnebach, S. Seelecke, and G. Schultes, "Electromechanical evaluation of sub-micron NiCr-carbon thin films as highly conductive and compliant electrodes for dielectric elastomers", *Sensors and Actuators A: Physical*, (vol. 315), Nov. 2020, doi: 10.1016/j.sna.2020.112243.

B. Fasolt, F. Welsch, M. Jank, and S. Seelecke, "Effect of actuation parameters and environment on the breakdown voltage of silicone dielectric elastomer films", *Smart Materials and Structures*, (vol. 28, no. 9, pp. 094002), 2019, doi: 10.1088/1361-665X/ab2f34.

B. Fasolt, M. Hodgins, G. Rizzello, and S. Seelecke, "Effect of screen printing parameters on sensor and actuator performance of dielectric elastomer (DE) membranes", *Sensors and Actuators A: Physical*, (vol. 265, pp. 10-19), 2017, <https://doi.org/10.1016/j.sna.2017.08.028>.

B. Fasolt, „Sicherung eines Gebäudekomplexes gegen den Eintritt von Deponiegas“, *Müll und Abfall*, (vol. 30, no. 8, pp. 519-522), 1998.

B. Fasolt, and J. Schneider, (1994). „Emissionsstrombestimmung von Deponiegas aus Mülldeponien durch Konzentrationsmessungen in der Abdeckschicht“, *Müll und Abfall*, (vol. 26, no. 11, pp. 721-728), 1994.

Patent pending

Zentrum für Mechatronik und Automatisierungstechnik gGmbH: „Verfahren zum Reparieren von dielektrischen Elastomeren nach elektrischem Durchbruch oder mechanischer Beschädigung“. Erfinder: Bettina Fasolt, Tobias Willian, Stefan Seelecke, Aurel Weller. Anmeldung 27.05.2023; Patentantrag: UDS4630DE

Conference proceedings

T. Weber, **B. Fasolt**, T. Willian, D. Bruch, S. Nalbach, and P. Motzki, "ADEPT: automated dielectric elastomer actuator performance-tester", *Electroactive Polymer Actuators, Sensors, and Devices (EAPAD) 2025*, (vol. 13431, pp. 173-180), SPIE, May 2025, <https://doi.org/10.1117/12.3051016>.

S. Croce, J. Neu, J. Hubertus, G. Schultes, S. Seelecke, **B. Fasolt**, and G. Rizzello, (2024, May). "Self-sensing investigation of a dielectric elastomer actuator array", *Electroactive Polymer Actuators and Devices (EAPAD) XXVI*, (vol. 12945, pp. 58-69), SPIE, May 2025, <https://doi.org/10.1117/12.3010487>.

B. Fasolt, T. Willian, A. Weller, D. Bruch, S. Seelecke, and P. Motzki, "Yield increase of DE actuators using novel repair process", *Electroactive Polymer Actuators and Devices (EAPAD) XXV*, (vol. 12945, pp. 97-106), SPIE, May 2024, <https://doi.org/10.1117/12.3010741>.

F. Welsch, **B. Fasolt**, and S. Seelecke, "Dielectric breakdown test setup for dielectric elastomers: design and validation", *Electroactive Polymer Actuators and Devices (EAPAD) XX*, (vol. 10594, pp. 260-268). SPIE, March 2018, <https://doi.org/10.1117/12.2296995>.

B. Fasolt, M. Hodgins, and S. Seelecke, "Characterization of screen-printed electrodes for dielectric elastomer (DE) membranes: influence of screen dimensions and electrode thickness on actuator performance", *Electroactive Polymer Actuators and Devices (EAPAD) 2016*, (vol. 9798, pp. 662-672). SPIE, <https://doi.org/10.1117/12.2222095>.

B. Fasolt, D. Palmacci, A. Ramthun, and J. Schneider, (1999) "Development of a new Containment Concept for Landfills with low Gas Production", *Sardinia 99, Seventh International Landfill Symposium*, Oct. 1999.

Award and invited key note presentation

Best Poster Award EuroEAP 2025 (2025, June 10-12), **B. Fasolt**, B. Holz, D. Bruch, P. Motzki, and S. Seelecke, "Influence of silicone content in the electrode matrix on the failure of DE actuators", *13th international conference on Soft Transducers and Electromechanically Active Polymers*, Linz, Austria

Bettina Fasolt, "Dielectric elastomers - from manufacturing to application", Invited Talk, *International Conference on Smart Materials, Scientex*, Vienna 2021, Wien, Austria

Statement of contributions to the included publications

Fakultät NT

Kumulative Form der Dissertationsschrift

Titel: Effect of screen printing parameters on sensor and actuator performance of dielectric elastomer (DE) membranes

Authors: Bettina Fasolt¹, Micah Hodgins², Gianluca Rizzello², Stefan Seelecke^{1,2}

¹ Center for Mechatronics and Automation Technologies (ZeMA), Saarbrücken, Germany

² Department of Systems Engineering, Department of Materials Science & Engineering, Saarland University, Saarbrücken, Germany

Journal: Sensors and Actuators A: Physical

Publisher: Elsevier

Quality: Peer Reviewed Journal


Status: Published October, 2017

Beitrag an der Veröffentlichung und Unterschrift

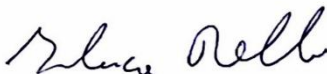
Bettina Fasolt Conceptualization; methodology; manufacturing of samples; sample preparation; formal analysis; investigations and conducting of tests; validation; writing; review and editing

Date/Signature: 6.5.25 

Micah Hodgins Methodology; design and building of test rig, programming for test procedure; formal analysis, review and editing

Date/Signature: 3/3/2025 

Gianluca Rizzello Methodology; review and editing

Date/Signature: 8.5.2025 

Stefan Seelecke Conceptualization, methodology, review and editing; supervision

Date/Signature: 30.5.25 

Fakultät NT

Kumulative Form der Dissertationsschrift

Titel: Dielectric breakdown test setup for dielectric elastomers: Design and validation

Authors: Felix Welsch¹, Bettina Fasolt², Stefan Seelecke^{1,2}

- ¹ Intelligent Materials Systems lab, Department of Systems Engineering, Department of Materials Science and Engineering, Saarland University, Saarbruecken, Germany
- ² Intelligent Materials Systems Lab, Center for Mechatronics and Automation Technologies (ZeMA) gGmbH, Saarbruecken, Germany

Journal: Proceedings of SPIE 10594, Electroactive Polymer Actuators and Devices (EAPAD) XX

Event: SPIE Smart Structures and Materials + Nondestructive Evaluation and Health Monitoring 2018, Denver, Colorado, United States

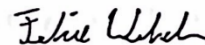
Quality: Conference Paper

Status: Published March, 2018

Beitrag an der Veröffentlichung und Unterschrift

Felix Welsch Conceptualization; methodology; design and building of test rig, programming of test procedure; writing; review and editing

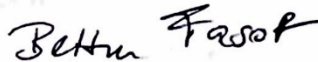
Date/Signature: Sulzbach, den 13.03.2025



Bettina Fasolt Conceptualization; methodology; manufacturing of samples; sample preparation; investigations and conducting of tests; evaluation of results; writing; review and editing

Date/Signature:

6.5.25



Stefan Seelecke Conceptualization, methodology, review and editing; supervision

Date/Signature:

30.5.25



Fakultät NT

Kumulative Form der Dissertationsschrift

Titel: Effect of actuation parameters and environment on the breakdown voltage of silicone dielectric elastomer films

Authors: Bettina Fasolt¹, Felix Welsch², Marius Jank², Stefan Seelecke^{1,2}

¹ Intelligent Materials Systems Lab, Center for Mechatronics and Automation Technologies (ZeMA) gGmbH, Saarbrücken, Germany

² Intelligent Materials Systems Lab, Department of Systems Engineering, Department of Materials Science & Engineering, Saarland University, Saarbrücken, Germany

Journal: Smart Materials and Structures

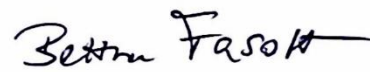
Publisher: IOP Publishing

Quality: Peer Reviewed Journal

Status: Published August, 2019

Beitrag an der Veröffentlichung und Unterschrift


Bettina Fasolt Conceptualization; methodology; manufacturing of samples; sample preparation; investigations and conducting of tests; evaluation of results; validation; writing; review and editing

Date/Signature: 6.5.25 

Felix Welsch Design and building of test rig; programming for test procedure; review and editing

Date/Signature: Sulzbach, den 13.03.2025 

Marius Jank Design and building of stretcher; programming of stretcher; sample preparation; photos and illustrations;

Date/Signature: 17.03.2025 

Stefan Seelecke Conceptualization, methodology, review and editing; supervision

Date/Signature: 30.5.25 

Fakultät NT

Kumulative Form der Dissertationsschrift

Titel: Electrode Impact on the Electrical Breakdown of Dielectric Elastomer Thin Films

Authors: Bettina Fasolt^{1,2}, Fabio Beco Albuquerque³, Jonas Hubertus⁴, Günter Schultes⁴, Herbert Shea³, Stefan Seelecke²

- 1 Intelligent Materials Systems Lab, Center for Mechatronics and Automation Technologies (ZeMA) gGmbH, Saarbrücken, Germany
- 2 Intelligent Materials Systems Lab, Department of Systems Engineering, Department of Materials Science & Engineering, Saarland University, Saarbrücken, Germany
- 3 LMTS Soft Transducers Laboratory, EPFL Ecole Polytechnique Fédérale de Lausanne, Neuchâtel, Switzerland
- 4 Sensors and Thin Film Group, University of Applied Sciences, Saarbrücken, Germany

Journal: Polymers

Publisher: MDPI

Quality: Peer Reviewed Journal

Status: Published October, 2023

Beitrag an der Veröffentlichung und Unterschrift


Bettina Fasolt Conceptualization; methodology; sample preparation (no electrode, screen-printed electrodes, all samples for additional tests); formal analysis; investigations and conducting of tests; validation; writing; review and editing

Date/Signature: 6.5.25 


Fabio Beco Albuquerque Methodology; sample preparation – sputtered gold, pad printed, and inkjet printed electrodes; writing section about manufacturing of these electrodes, review and editing,

Date/Signature: 09.03.2025, Fabio Beco Albuquerque 

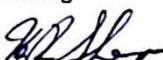
Jonas Hubertus Methodology; sample preparation – sputtered nickel; writing section about manufacturing of these electrodes, review and editing

Date/Signature: 18.03.2025 

Günter Schultes Methodology; review and editing

Date/Signature: 24.3.2025 

Herbert Shea Methodology; review and editing

Date/Signature: 13-3-2025 

Stefan Seelecke Conceptualization, methodology, review and editing; supervision

Date/Signature: 30.5.25 